Detonation Initiation and Propagation

Within Gas layers in Water-Filled Piping.

R. Akbar and J. E. Shepherd

Graduate Aeronautical Laboratories
California Institute of Technology
Pasadena, CA 91125

Explosion Dynamics Laboratory Report FM2010.003

June 24, 2010
Revision of August 22, 2010

Sponsor: US Department of Energy, Office of River Protection, Hanford, WA.

Abstract

We report on a series of 24 tests carried out in the Explosion Dynamics Laboratory, California Institute of Technology. These tests examined transition to detonation in gas layers of hydrogen-nitrous oxide mixtures within liquid-filled channels and tubes. This work was carried out for the US Department of Energy, Office of River Protection at Richland, WA in support of the Hydrogen in Piping and Ancillary Vessels (HPAV) program that is developing criteria and methods for evaluating hydrogen hazards in the Waste Treatment Plant (WTP) under construction at the Hanford Site.

There were two questions that these tests were designed to address. First, does a layer of liquid waste within the piping system containing an explosive gas mixture inhibit or promote transition to detonation? Second, what is the effect on the peak strains of having the piping system partially filled with gas and partially with waste? A series of 21 experiments were carried out to visualize explosions in a rectangular channel (nominally 2 in high, 3 in wide, and 60 in long) with transparent sides. A series of three experiments were carried out to measure strains in a 60-in long section of 2-in, Schedule 40 pipe. In 10 of the tests, a layer of water (the test fixtures were oriented with the axis horizontal) was introduced under the gas mixture to simulate low-viscosity waste in the WTP.

The gas initial conditions were a 30/70 H_2-N_2O mixture at 1 atm initial pressure and 300 K. The mixtures were deliberately ignited with a spark discharge and in selected cases, transition to detonation was promoted with a wire coil (Shchelkin spiral). Measurements included visual observations with high-speed video, as well as pressure and strain recorded using a high-speed (1 MHz recording speed) digital data acquisition system and calibrated signal conditioners for all instruments. The testing was carried out under a Quality Assurance plan based on ANSI/ASQ Z1.13-1999 which was determined by the DOE after surveillance visits to meet the requirements of the ASME standard NQA-1, Subpart 4.2 and the data was approved by the DOE for use in supporting development of methods and criteria by which HPAV is evaluated. The digital data and documentation of the tests are available on the CIT Explosion Dynamics Laboratory web site http://www.galcit.caltech.edu/EDL/data-hanford/.

The visualization tests demonstrated that transition-to-detonation and detonation propagation can occur in thin (3 to 6 mm, 1/8 to 1/4 in) gas (0.3H2 +0.7N2O) layers above a water layer within a channel or pipe with a 2-in nominal height or diameter. The implications is that the combustion process during both deflagration and detonation occurs much more quickly than lofting and heat transfer to the liquid spray from the combustion products above a horizontal liquid layer. The strain measurement tests showed that transition to high-speed combustion are possible in lenticular gas volumes with maximum gas layer heights of 9 mm (3/8-in). The peak strains were substantially reduced in comparison to tests in the same fixture without water. The explosion propagation in a 60-in long bubble either did not develop into a near-CJ detonation or else the interaction with the water surface resulted in lowering the combustion wave speed and peak pressure. We believe that this is a significant factor in the reduction of the peak strains.

It is not clear if water enhances or inhibits transition to detonation. Previous experience indicates that there is substantial variability in the transition location even for repeated tests under a nominal fixed set of conditions. The fixtures used in the present test also

have have features like joints and protuberances that promote transition so it is difficult to isolate the effect of water. Previous experience also indicates that tube diameter or channel height has a strong influence on DDT for gas-filled tubes or channels. Up to the point where significant boundary layer effects and quenching begin to play a role, DDT distance decreases with decreasing tube diameter or layer height. Without making direct comparisons of the explosion of a given thickness gas layer with and without a water boundary, we are unable to isolate the effect of the water surface in the transition process.

Despite the limitations of the present testing we can draw some definite conclusions.

1. Flame acceleration resulting in transition to detonation (DDT) is possible with a 60-in segment of 2-in pipe or a 2 × 3 in rectangular channel filled with a 30/70 H_2-N_2O gas mixture.

2. High speed explosions and shock waves are possible within 30/70 H_2-N−2O gas layer greater than 1/4-in in height above water in a horizontal 2-in Schedule 40 piping section less than 60-in long.

3. A very limited amount of dispersion of the water ahead of and immediately behind the combustion front was observed. Based on this, we speculate that our results will be valid not only for waste with water-like rheology but for more viscous waste with non-zero yield stress.

4. The strains created by the explosion of a 9-10 mm layer of gas above a water layer in a 2-in pipe were up to a factor of 4 smaller than those observed in a pipe completely filled with the same gas mixture. Both the change in explosion mode and dynamics of the gas-liquid interaction appeared to be factors.

Contents

List of Figures

List of Tables

1 Introduction

The present study is part of a multi-institution, multi-year effort to assess potential explosion hazards in the Waste Treatment Plant (WTP) being constructed at Hanford, WA. The plant will dispose of radioactive waste by converting it to glass which will require pumping the waste through an enormous complex of piping and vessels. One of the potential explosion hazards is the build-up of explosive gas pockets or bubbles generated by radiolysis in waste trapped in the piping during a plant upset or power outage that is not immediately recovered. Previous studies in our laboratory Liang et al. (2006), Shepherd and Akbar (2009a,b) and at SwRI SwRI (2009) have concentrated on combustion tests in pipes that have been filled with explosive gas. In an evaluation of the safety approach conducted in 2009, the HPAV Assessment Team (Hildebrant and McCoy, 2009) identified fully gas-filled pipes as an unrealistic and highly conservative assumption about potential explosion hazards in the WTP. A more realistic situation for a horizontal pipe run is that it is wholly or partly filled with liquid waste and a bubble of explosive gas may form above the waste due to radiolysis.

Although a more realistic approach is desirable for many reasons, the HPAV Assessment Team identified as a technical risk the lack of data on the combustion behavior in bubbles or layers of gas above a waste layer. In particular, there was a concern about the lack of knowledge regarding:

> DDT limits for small gas volumes with more realistic gas compositions based on the MAR study recommendations, and with more realistic gas pocket geometries. (Hildebrant and McCoy, 2009)

To address this concern, we have examined the behavior of explosions in a gas volume above a liquid layer in a rectangular channel as well as a circular pipe. A series of 24 tests were carried out in the Explosion Dynamics Laboratory, California Institute of Technology, to examine the transition to detonation in gas layers of hydrogen-nitrous oxide mixtures within liquid-filled channels and tubes. This work was carried out for the US Department of Energy, Office of River Protection at Richland, WA in support of the Hydrogen in Piping and Ancillary Vessels (HPAV) program that is developing criteria and methods for evaluating hydrogen hazards in the Waste Treatment Plant (WTP) under construction at the Hanford Site.

There were two questions that these tests were designed to address. First, does a horizontal layer of liquid waste within a horizontal segment of a piping system containing an explosive gas mixture inhibit or promote transition to detonation? Second, what is the effect on the peak strains of having the piping system partially filled with gas and partially with waste?

A series of experiments with three test fixture configurations were carried out to address these questions. These experiments are a continuation of previous work done in our laboratory on piping system response to detonations; the work is described in detail in two reports, Shepherd and Akbar (2009a,b).

Testing was carried out using the facility and procedures briefly described in Section 2. A total of 21 visualization experiments were carried out in a rectangular channel geometry 2 in x 3 in by 60 in with transparent sides. High-speed video and pressure measurements were used to observe the combustion process and interaction of the gas explosion with the liquid layer. The first 15 tests were carried out with the visualization section connected to a

2-in piping segment (SS1-2 used in previous testing) that was approximately 73-in long and terminating in a 90-deg 3D bend. This is referred to as configuration D1 and results of those tests are described in Section 3. Shots 16-21 were carried out with only the visualization chamber (SS1-2 was disconnected) and ignition on the top of the east end of the chamber. This is referred to as configuration D2 and the results are presented in Section 4.

A total of three experiments were carried out in a 60-in long 2-in Schedule 40 pipe instrumented with strain and pressure gages. A horizontal layer of water (the channels and pipes were oriented with the long axis horizontal) was used to simulate low-viscosity liquid waste in 10 of the tests. The gas mixture in all cases was a 30/70 H_2-N_2O mixture at 1 atm initial pressure and 300 K. This is referred to as configuration D4 and the results are presented in Section 5.

This report describes the facility, each of the experimental fixtures (D1, D2, and D4) that were used, and gives a discussion of the results obtained for each test. The details of the test fixtures, the raw data plots from each test, and supplementary information is provided in the Appendices. The digital data and documentation of the tests are available on the CIT Explosion Dynamics Laboratory web site http://www.galcit.caltech.edu/EDL/data-hanford/.

2 Facility, Test Procedures and Conditions

The experiments were carried out in the Explosion Dynamics Laboratory laboratory in Room 19 of the Guggenheim Building complex at the California Institute of Technology, Pasadena CA. The laboratory facility and test procedures are documented in the report on previous testing done for the HPAV program (Shepherd and Akbar, 2009b). The laboratory safety features, plumbing, vacuum systems, and data acquisition system were identical to that described in Shepherd and Akbar (2009b).

The gas initial conditions were a 30/70 H_2-N_2O mixture at 1 atm initial pressure and 300 K. Gases were introduced into the test chambers using the method of partial pressures after evacuating and leak checking. The gas components were thoroughly mixed by circulation through the test chamber using a bellows pump. If water was used in the test, it was introduced after the gas was mixed. The pressure and temperature in the test chamber were monitored by calibrated instruments. In tests with a water layer, the gases were introduced and mixed before the water was introduced slowly at the bottom of the chamber. The pressure of the gas mixture was adjusted based on the computed volume and desired final water level so that the final pressure was nominally 1 atm after filling with water. The arrangement of valves, pumps, and instruments used to control the gases are shown in Figs. 1 and 2.

The mixtures were deliberately ignited with a spark discharge and in selected cases, transition to detonation was promoted with a wire coil (Shchelkin spiral). The details of the spark discharge circuit are given in Shepherd and Akbar (2009b). A special miniature spark plug was used in tests with small layers of water. This spark plug, unlike the one described in Shepherd and Akbar (2009b) and mounted in the end flanges, was mounted in a port on the top of test chamber and slightly recessed to avoid being shorted out with water.

Measurements included visual observations with high-speed video (Phantom v7.10) camera, as well as pressure and strain recorded using a high-speed (1 MHz recording speed) digital data acquisition system and calibrated signal conditioners for all instruments. A schematic of the data acquisition system and timing circuit arrangement is shown on Fig. 3; complete details are given in Shepherd and Akbar (2009b).

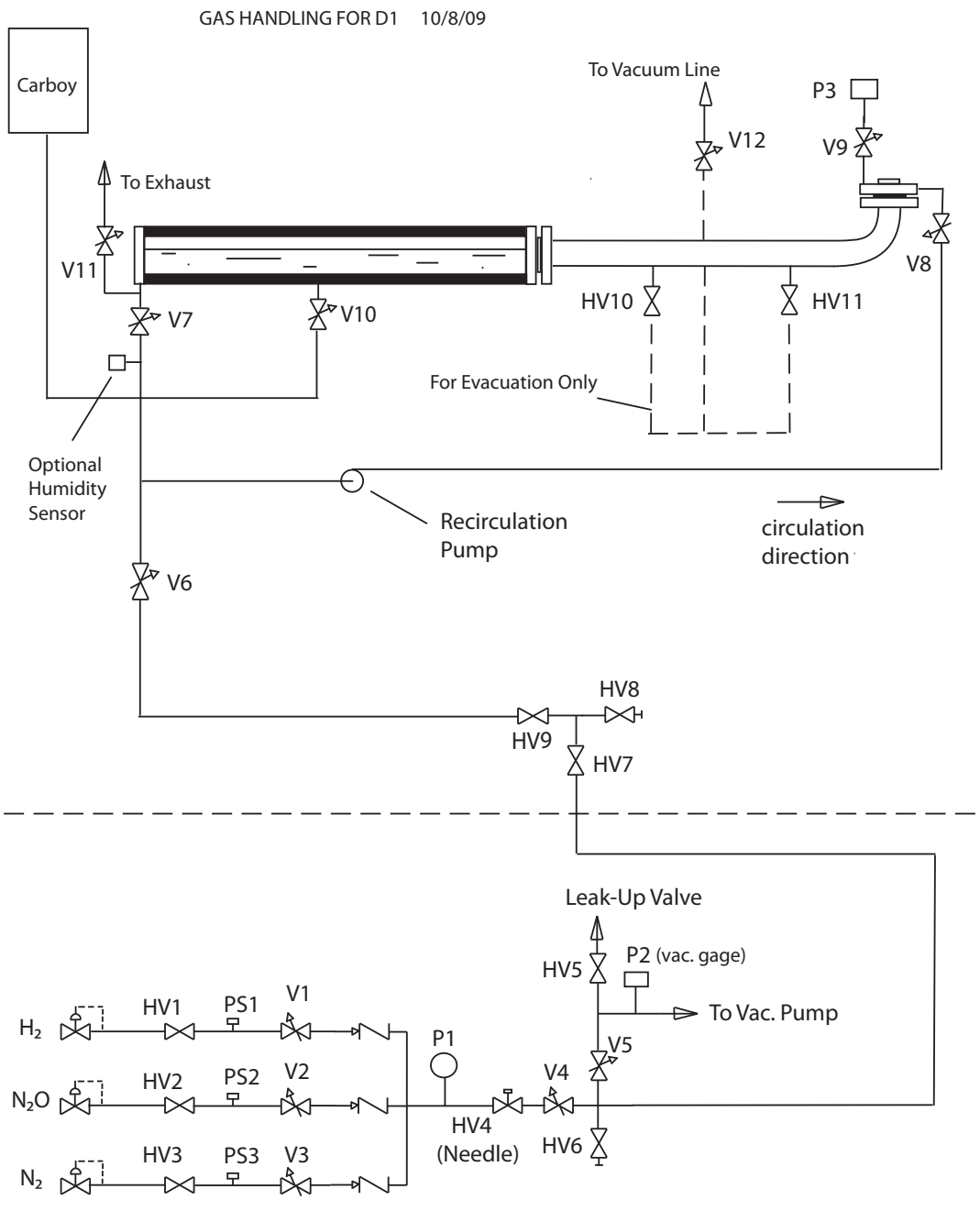

Figure 1: Plumbing diagram for D1 testing.

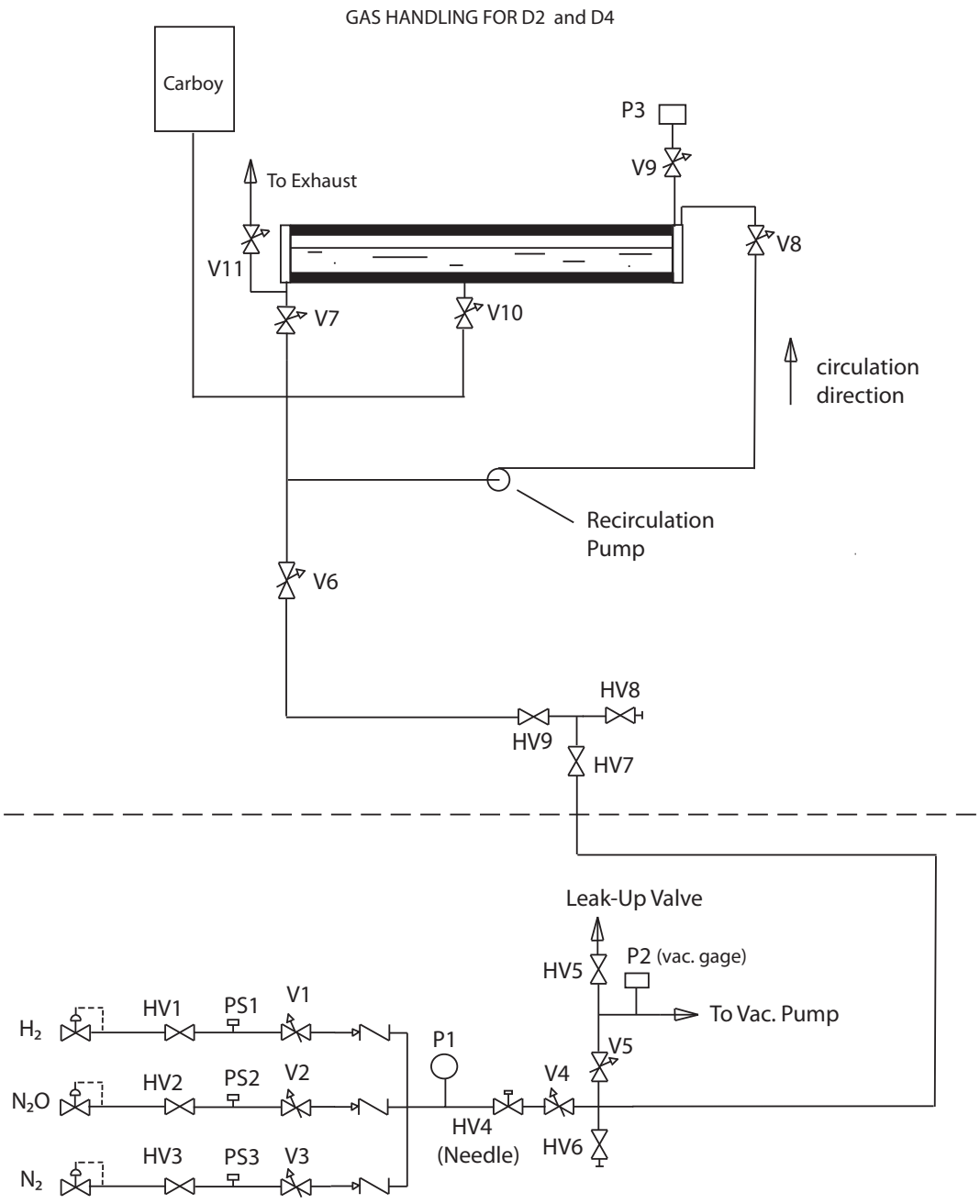

Figure 2: Plumbing diagram for D2 and D4 testing.

2.1 QA Program

The testing was carried out under a Quality Assurance plan based on ANSI/ASQ Z1.13-1999 which was determined by the DOE after surveillance visits to meet the requirements of the

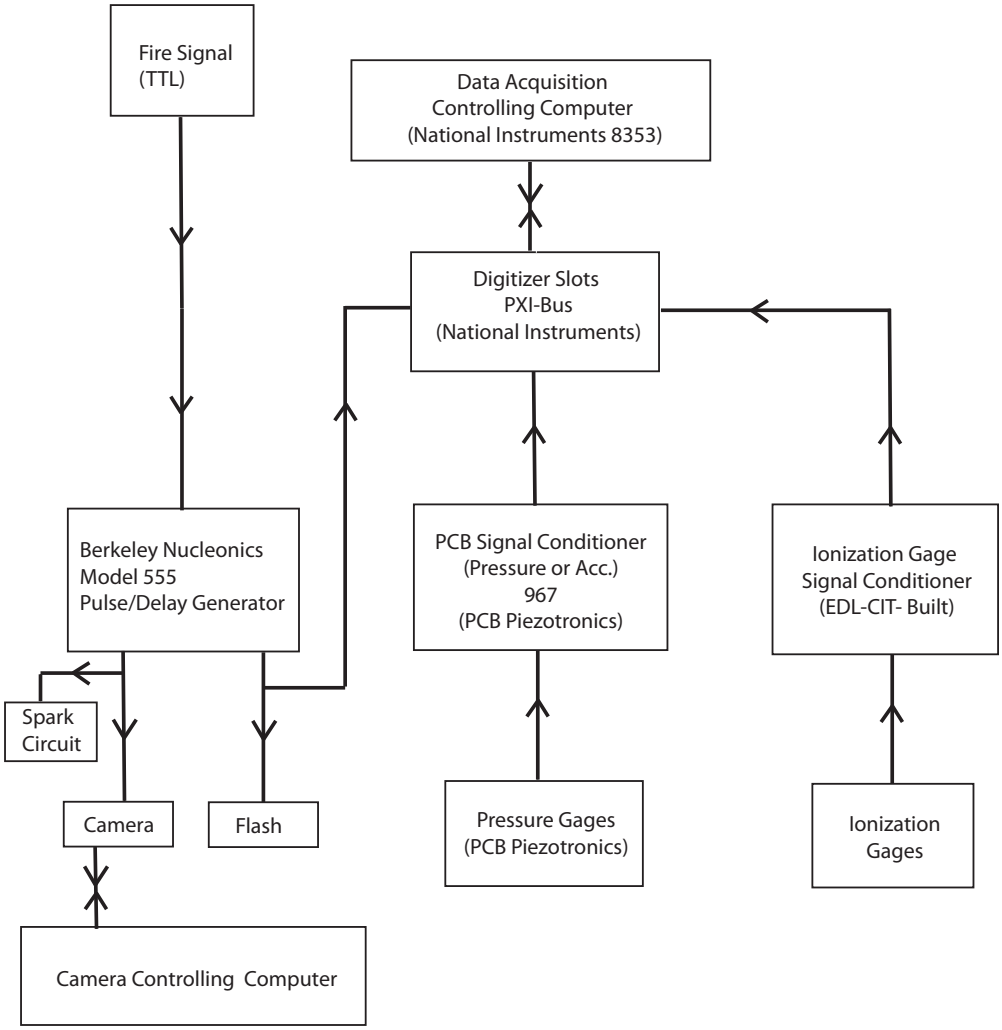

Figure 3: Data acquisition system schematic. Flash lamps were used for D1 testing only.

ASME standard NQA-1, Subpart 4.2 and the data was approved by the DOE for use in supporting development of methods and criteria by which HPAV is evaluated. A complete description of the QA program is given in Appendices to Shepherd and Akbar (2009b). In

addition to visits in 2008 and 2009 during the previous HPAV testing program, the DOE conducted surveillance of the facility and QA program on Nov. 10-13, 2009. The surveillance report is reproduced in Appendix I. There were no findings of deficiency during these visits and on the basis of our successful QA program, the DOE has directed that our data may be used in supporting development of methods and criteria by which HPAV is evaluated. The letter of authorization is reproduced at the end of Appendix I.

2.2 Test Conditions

All tests used a nominal mixture of $0.3H_2$ and $0.7N_2O$ with a starting pressure (after any water was added) of nominally 760 Torr. The initial temperature was the ambient temperature in the laboratory, about 27°C. The details of each test and digital data is available on the CIT Explosion Dynamics Laboratory web site http://www.galcit.caltech.edu/EDL/data-hanford/. The configuration refers to the test chamber, D1 is the visualization section with the addition of the SS1-2 segment attached to the east flange. The notation "open", "midway", "midway - 0.5", "midway + 0.5" refers to the type of blockage element (see Fig. 7 in the next section) placed between the visualization test chamber and the SS1-2 segment. D-2 is just the visualization test section. D-4 is a 60-in segment of 2-in schedule 40 pipe with instrumentation ports and strain gages.

Table 1: List of tests and conditions.

Shot	T_o (°C)	P_o (Torr)	Date and Time	Configuration	Water (in)	Notes
1	26.8	758.1	10122009 034112 PM	D1 open	None	Spark plug and spiral in E flange of SS1-2
2	27	757.1	10282009 120557 PM	D1 open	None	Spark plug and spiral in E flange of SS1-2
3	26.8	757.5	11022009 030250 PM	D1 - midway	None	Spark plug and spiral in E flange of SS1-2
4	26.4	756.8	11052009 025534 PM	D1 - midway	None	Spark plug and spiral in E flange of SS1-2
5	26.8	756.9	11112009 034434 PM	D1 - midway + 0.5	None	Spark plug and spiral in E flange of SS1-2
6	27	756.7	11162009 113727 PM	D1 - midway + 0.5	None	Spark plug and spiral in E flange of SS1-2
7	27	756.5	11232009 031045 PM	D1 - midway - 0.5	None	DDT, spark plug in W flange
8	26.8	756.7	11242009 011030 PM	D1 - midway - 0.5	None	DDT, spark plug in W flange
9	27.2	760.8	11242009 045349 PM	D1 - midway - 0.5	0.25	DDT, spark plug in W flange
10	26.6	759.8	12042009 020545 PM	D1 - midway + 0.5	None	DDT, spark plug in W flange
11	26.6	759.8	12092009 114202 AM	D1 - midway + 0.5	0.375-0.50	DDT, spark plug in W flange
12	27.3	760.5	12142009 025436 PM	D1 - midway + 0.5	0.375-0.5	DDT, spark plug in W flange, video lost, liquid supply valve moved
13	27.8	761.1	12162009 114839 AM	D1 - midway + 0.5	0.375-0.5	DDT/ Flame Acc., spark plug in W flange,liquid supply valve moved
14	25.2	759.4	02022010 092802 PM	D1 - open	None	Full Field Image DDT/ Flame Acc.
15	25.5	756.1	02172010 063433 PM	D1 - open	None	Liquid Feed Valve removed
16	26.6	754.4	02232010 100307 AM	D2	None	DDT, spark plug in W flange
17	26.1	754.3	02242010 125822 AM	D2	None	DDT, mini-spark plug in 8T
18	26.1	761.0	02252010 040511 AM	D2	1.35-1.375	DDT, mini-spark plug in 8T
19	26.4	760.4	03022010 120440 PM	D2	1.55-1.65	DDT, mini-spark plug in 8T
20	26.8	758.5	03052010 124637 PM	D2	1.85-1.90	rapid flame, DDT(?), mini-spark plug in 8T
21	27	755.3	03082010 031118 PM	D2	1.73-1.75	DDT, mini-spark plug in 8T, video close-up
22	27.4	753.6	03262010 065351 PM	D4	None	DDT, mini-spark plug in top port, E end
23	26.7	763.1	03282010 055157 PM	D4	1.7-1.8	Rapid flame, mini-spark plug in top port, E end, gas layer 0.23-0.33 in
24	27.2	761	03302010 013829 AM	D4	1.53-1.60	Rapid flame/DDT, mini-spark plug in top port, E end, gas layer 0.43-0.50 in

3 D1 Testing Results

This series consisted of a total of 15 shots. The first 6 shots were tests with detonation initiated at the east end outside the visualization section and used to shakedown the facility operation. No results are given from these tests since they do address the issue of DDT that this program was focused on. Following the shakedown shots, the ignition was moved to the west end of the visualization section and 9 shots were carried out with DDT occurring within the visualization section. Of these 9 tests, 4 were carried out with a water layer within the visualization section.

D1 testing was carried out in a combination of the visualization test section and a section (SS1-2) of 2-in schedule 40 pipe that was used in the previous testing. The components were mounted on Uni-strut attached to the north wall of the facility as shown in Figs. 4. The high-speed video camera was mounted on the south wall of the facility and located behind a polycarbonate shield, Fig. 5.

The visualization section was constructed (see the engineering drawings in Appendix A) from two sections of 3-in by 6 lb/ft structural channel welded to end plates (Fig. 6) that mated to the gas handling flanges with a bolt circle that corresponded to the 300 lb, 2-in Schedule 40 pipe flanges used in the previous testing (Shepherd and Akbar, 2009b).

The channel side surfaces were machined flat to seal to the 1-in thick polycarbonate windows that were attached with 18 lengths of 5/8 threaded rod and nuts with reinforcing plates and blocks to limit the bending of the windows due to the explosion pressure. Bowing of the top and bottom channels in the vertical direction was observed due to pressure differences created by the evacuation of the chamber and the explosion pressure. To limit the deflection during the explosion, four heavy-duty C clamps were used to restrain the channels from bowing away from each other. A steel backing plate and three vertical steel blocks (one and each side and at the middle) clamped the windows to the C-channel with 18 threaded rods that passed through the holes in the plate, support block, windows, and channels. Reinforcing bosses were welded onto the channel interior surface and machined to accept 9/16-18 UNF SAE J1926 plugs that were used to mount the instrumentation. The location of the instrumentation ports is described in Appendix F, Fig. 87.

The visualization section was attached at the east end to SS1-2, an approximately 72 in long straight section of 2-in Schedule 40 pipe that terminates in a short 90-deg bend as shown in Fig. 4. See Shepherd and Akbar (2009b) and the drawings reproduced in Appendix A for more complete specifications of the SS1-2 section. The blockage elements are shown in Fig. 8 and the dimensions are schematically indicated in Fig. 7. The nominal inner diameter of SS1-2 is 2.03 in (51.6 mm) for the 2-in, schedule 40 pipe and the visualization section had a rectangular cross-section of 2 $\times$ 3 in. This resulted in a change in the cross-sectional area and a disturbance to the flow at the connection between the visualization section and SS1-2. The extent of the disturbance depended on the blockage element that was used as well as the construction of the test section, Fig. 6.

Gas handling plumbing (Fig. 1 was connected at each end of test fixture. The gas mixtures was introduced by the method of partial pressures after evacuating the test chamber. A bellows pump was used to thoroughly mix the gases prior to initiating combustion with the sparkplug. In cases where water was introduced into the test section, a port at the bottom of the visualization section was connected through a valve to an elevated carboy that contained

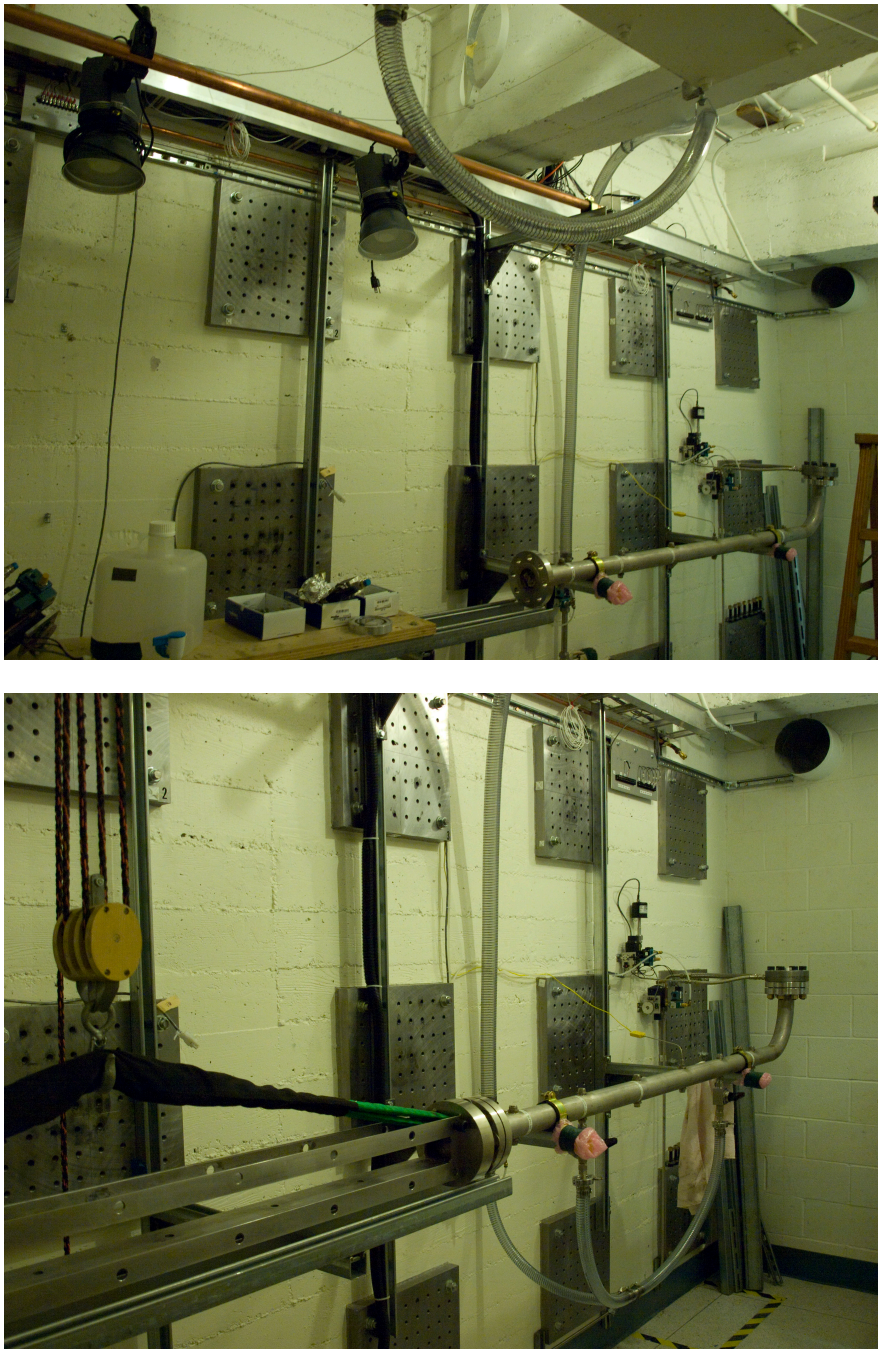

Figure 4: Views of the process of installing D1 into test cell in room 19A.

the water. Water was allowed to flow into the visualization section under gravity, the desired depth could be determined by the visualization video, and the gas mixture was vented to maintained the desired final pressure.

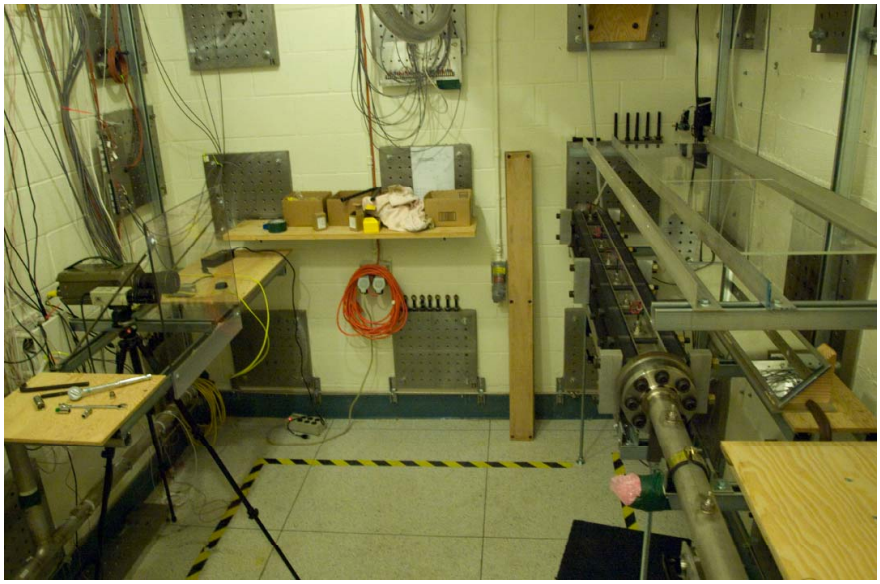

Figure 5: View of D1 and high-speed video camera installation.

3.1 Shots 1-6

A total of 6 shots of promptly initiated detonation (D1 configuration) were performed both as a baseline to obtain the effect of blockage as well as to explore imaging limitations. These shots used the Shchelkin spiral and spark ignition on the east end of SS1-2 to have "direct initiation" of a detonation which then propagated through the blockage element into the visualization section, Fig. 9. We report pressure data only from these tests since the video data yielded only a limited amount of information. We did learn from the video that small features like the ion probes mounts, which protruded about 1/6-in into the test section, created substantial luminosity revealing a turbulent wake behind the probe. Turbulent from within the chamber could also be observed after the detonation passage and the reflected shock wave could be visualized interacting with the side-wall boundary layers in some cases. From the luminosity observations, the detonations and reflected shock waves appeared to planar and propagating normal to the walls except just (2-3 diameters) downstream of the blockage element and immediately following reflection of the detonation from the end wall. In shot 1, the luminosity appeared to show an oblique shock in the boundary layer running ahead of the main reflected shock. After the shock propagated 5-10 channel heights from the end wall, the oblique shock was overtaken and a nearly planar configuration was observed.

The first shot used a gasket material for sealing the windows to the visualization test section. The first shot with gaskets was successful but gasket movement was substantial. Re-positioning the gasket after the shot and getting a pressure/vacuum seal was problematic. These difficulties in sealing the windows with the gasket design lead to a redesign of the sealing to use O-rings mounted in groves machined in the polycarbonate windows. This was a significant improvement in reliability and ease in testing. A change in speed was observed when the detonation diffracted through the blockage element, a lower pressure and multiple peaks are observed on P3 in those cases. The smaller blockage element (midway - 0.5) had

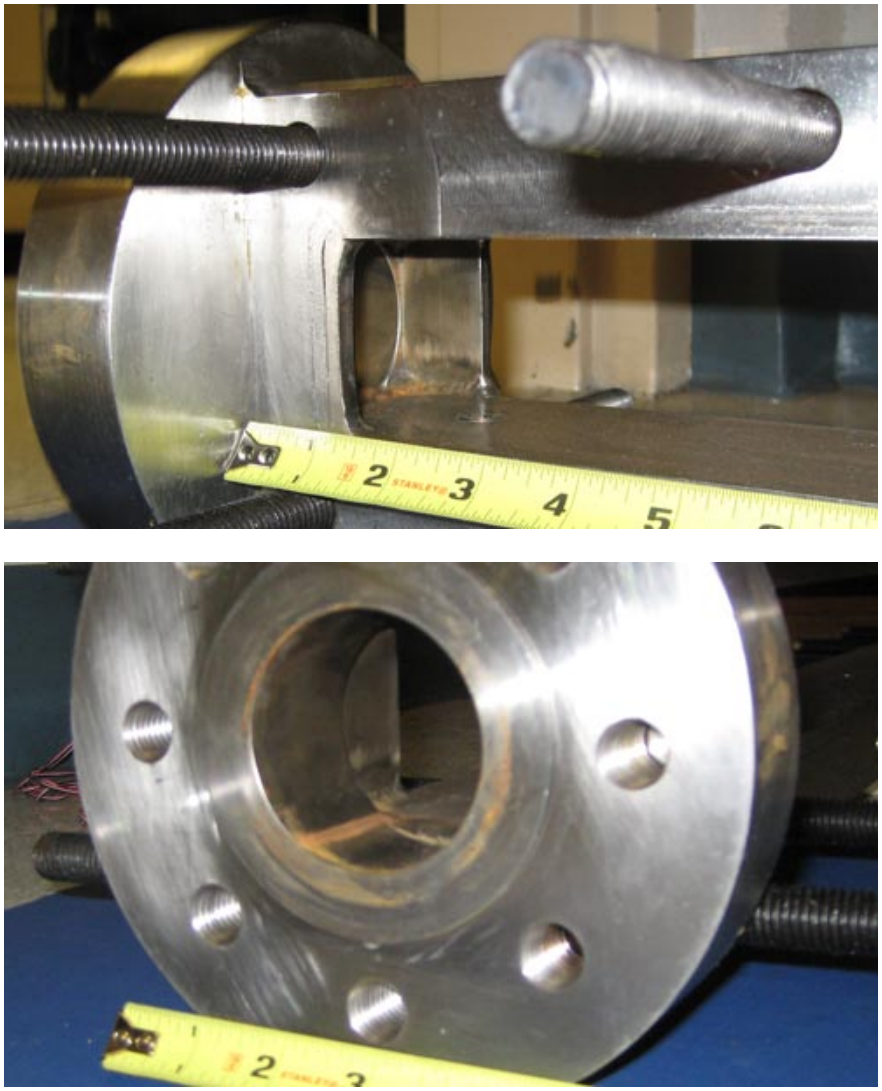

Figure 6: Views of end plates showing welds attaching C-channel and transition from rectangular to round cross section.

relatively little effect after 2-3 diameters of propagation downstream of the blockage element, the pressure histories (Figs. 10, 11, and 12) and peak pressure amplitude were little changed on gages P4, P5, P6 and P7 between shots 1 and 2 (no blockage) and 3 and 4 (midway - 0.5 blockage). Careful examination of the arrival time data (see Section 3.3) for shots 5 and 6 (midway + 0.5 blockage) reveals that although the peak pressure was relatively unchanged downstream of the blockage, the wave slowed down substantially and was still accelerating when it reached P7. A reflected shock wave created by the incident detonation interacting with the blockage is visible on P1 and P2 in shots 3-6. In shots 1-6, a strong reflected shock wave can be observed on gage P7, and subsequently on P6-P3 as it propagates from W to E.

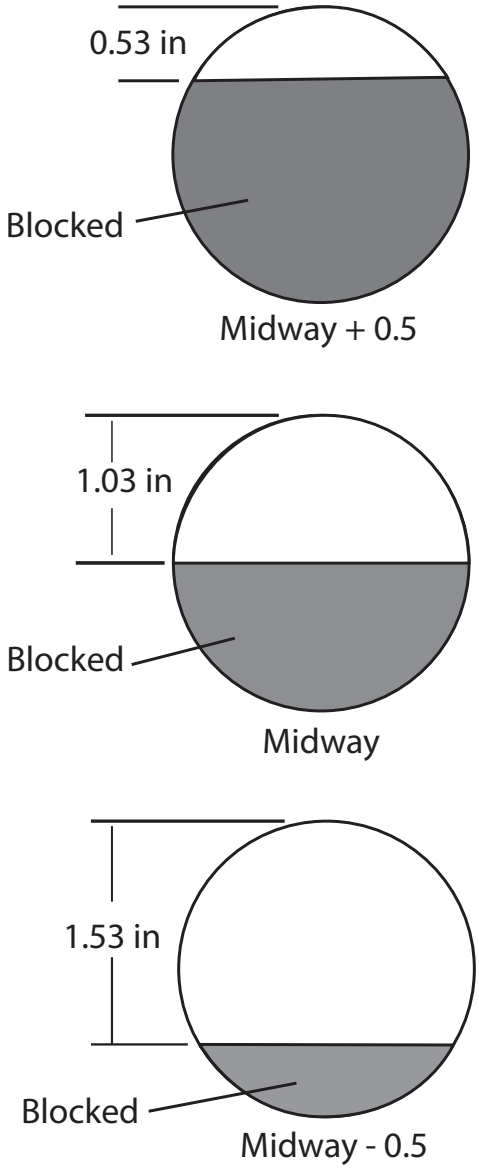

Figure 7: Key to blockage insert notation and vertical dimension of open area.

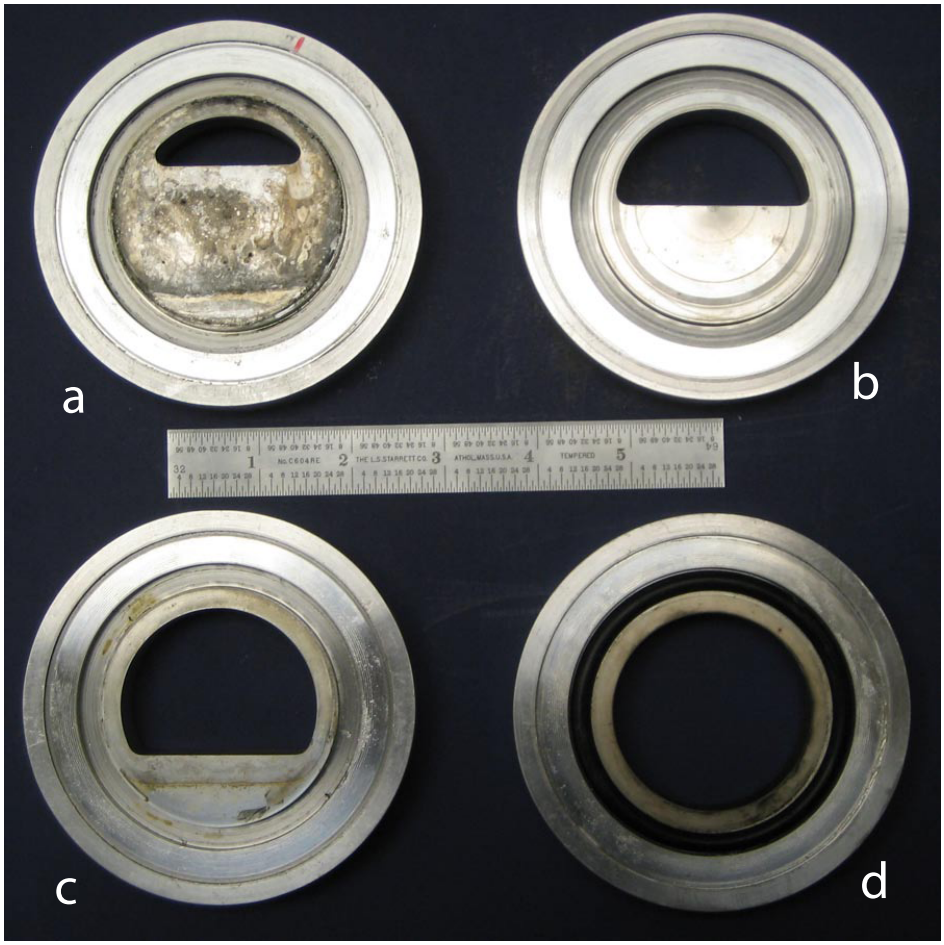

Figure 8: Photographs of the four blockage inserts used in the D1 tests. a) Midway + 0.5 b) midway c) midway - 0.5 d) open.

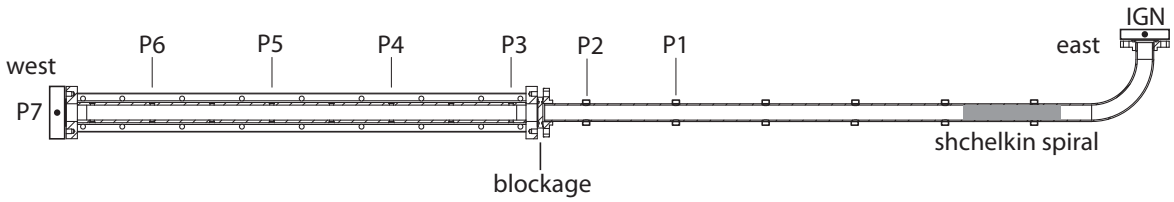

Figure 9: Location of sensors in shots 1-6.

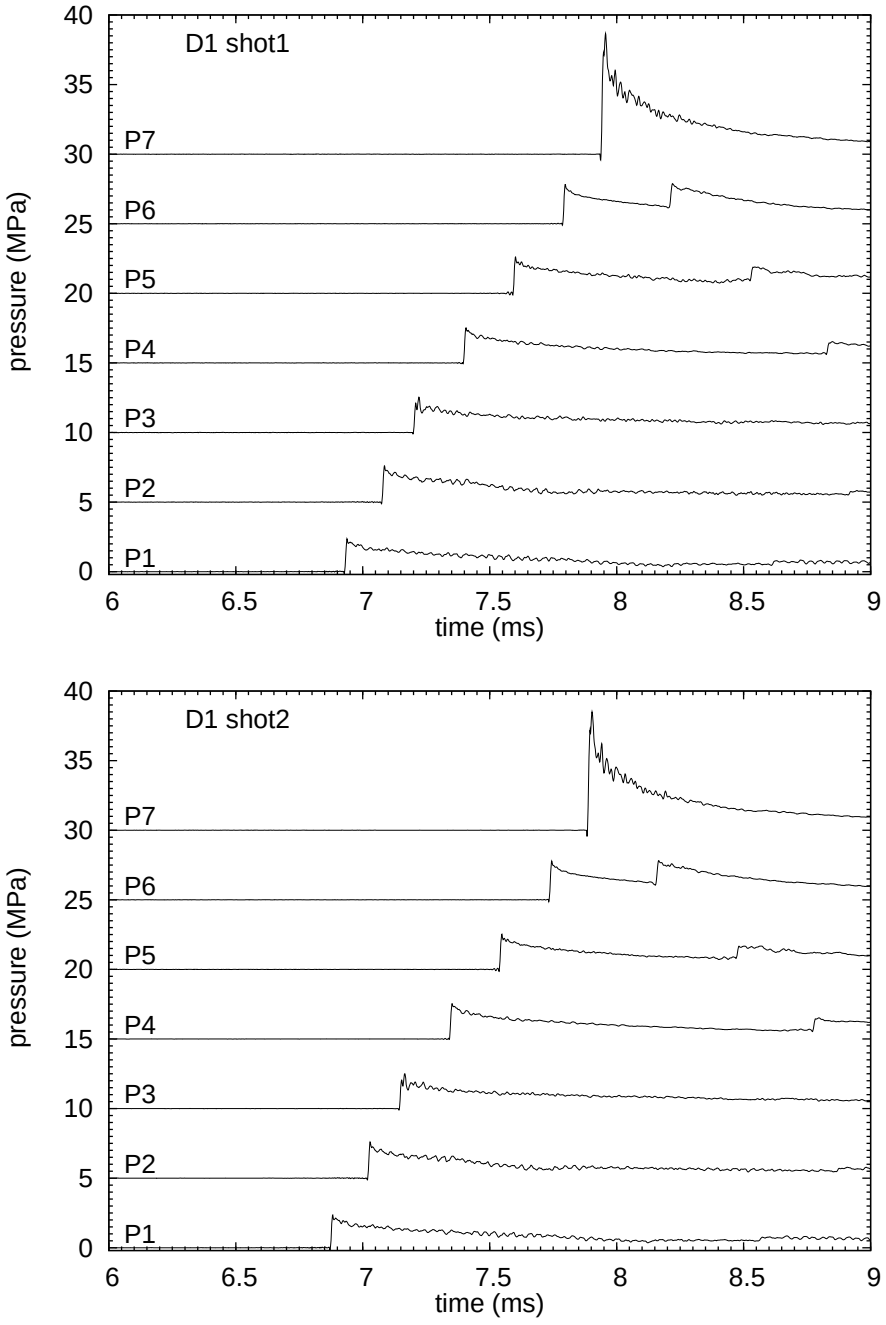

Figure 10: Shot 1 and 2 filtered and baseline corrected pressure-time histories showing detonation propagation in SS1-2 and visualization test section, no blockage.

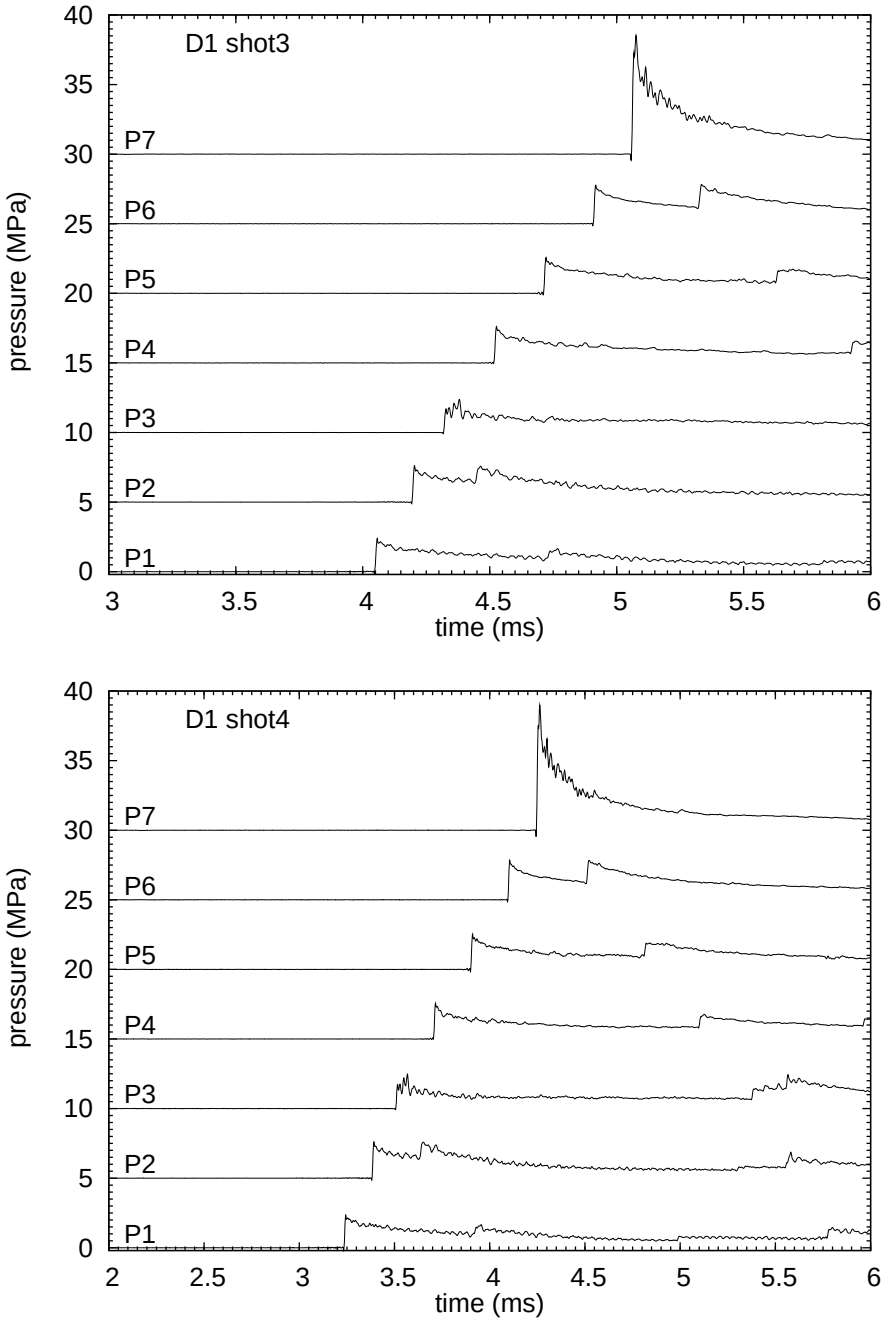

Figure 11: Shot 3 and 4 filtered and baseline corrected pressure-time histories showing detonation propagation in SS1-2 and visualization test section, midway - 0.5 blockage.

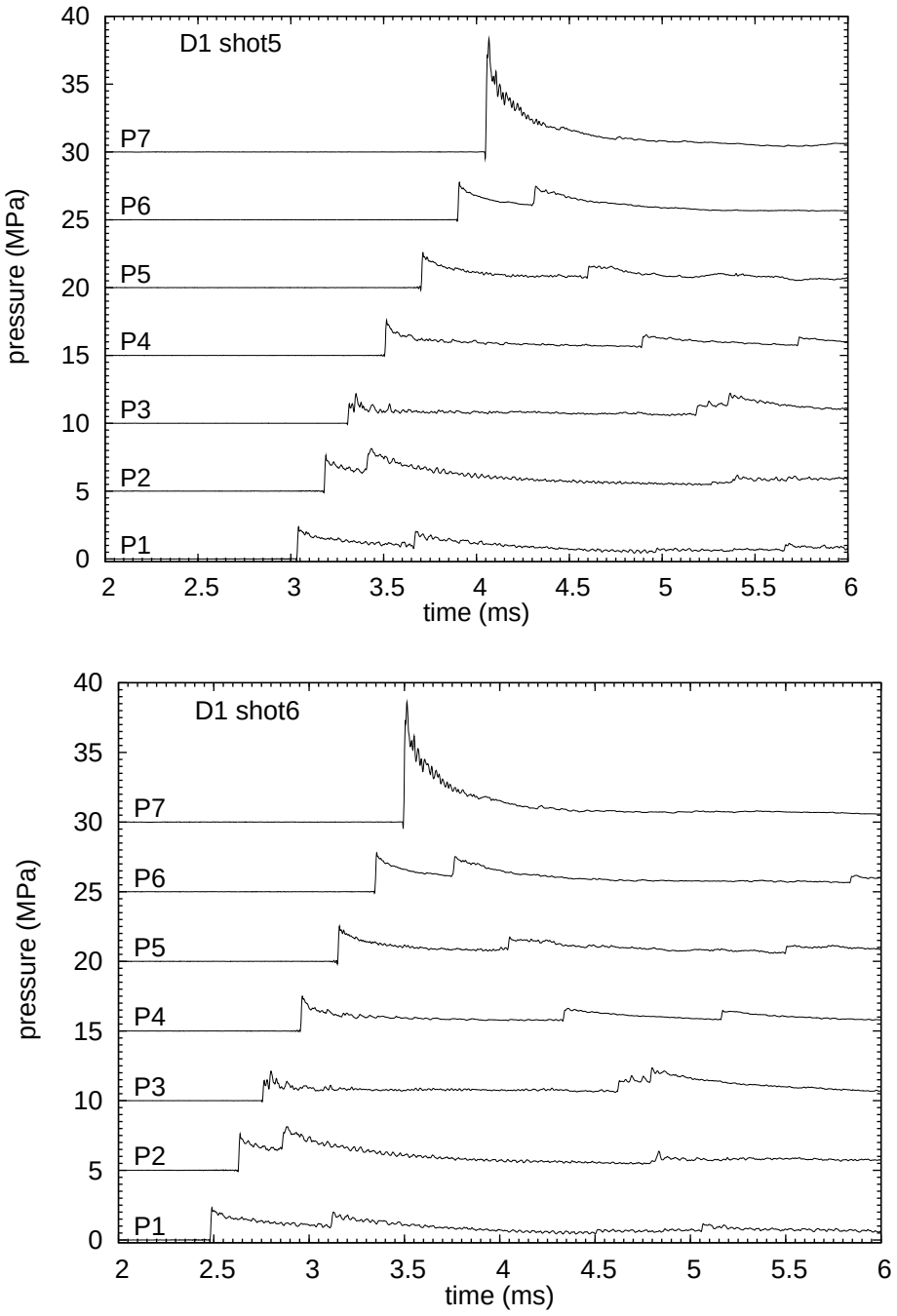

Figure 12: Shot 5 and 6 filtered and baseline corrected pressure-time histories showing detonation propagation in SS1-2 and visualization test section, midway + 0.5 blockage.

3.2 Shots 7-15

For these tests, the spark ignition was switched to the visualization section west end for DDT shots within test section. A blockage element was used in some tests to partially isolate the visualization section from SS1-2. This enabled a test with DDT entirely within the visualization section without making any plumbing changes. The location of the instrumentation in shown in Fig. 13 and dimensions are given in Appendix F.

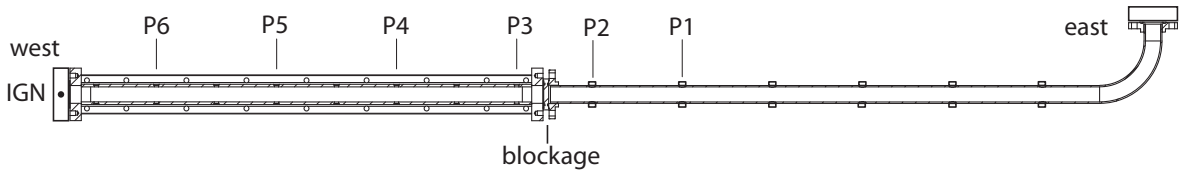

Figure 13: Location of sensors in shots 7–11.

3.2.1 Shot 7

This test was carried out without water and the midway-0.5 blockage insert. Flame acceleration resulted in DDT near the end of the test section. Flame acceleration appeared to be promoted by the protrusion of the ion gages into the test chamber. The video from this shot was very low contrast and is not reproduced here. The imaging does show that DDT appears to originate at 6.215 ms near the location of the ion probe in 8T, just upstream of P3. This is consistent with the pressure signals shown in Fig. 14.

3.2.2 Shot 8

The ion gages were removed and the conditions of shot 7 were repeated. The result was flame acceleration followed by DDT near the end of the test section occurred. Flame acceleration may have been enhanced by a transverse burnt gas jet from the plumbing line at location 10B but transition did not take place until right at the end of the test section. The video (Table 2) shows that detonation appears at both the top and bottom of the channel near the weldments almost simultaneously near 6.215 ms, Fig. 16.

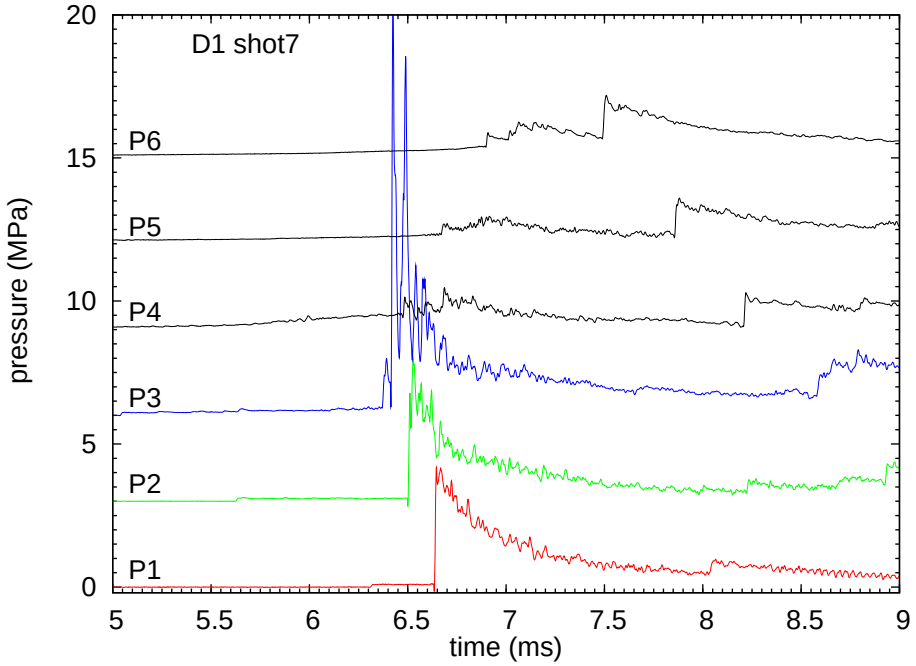

Figure 14: Shot 7 filtered and baseline corrected pressure-time histories showing DDT event.

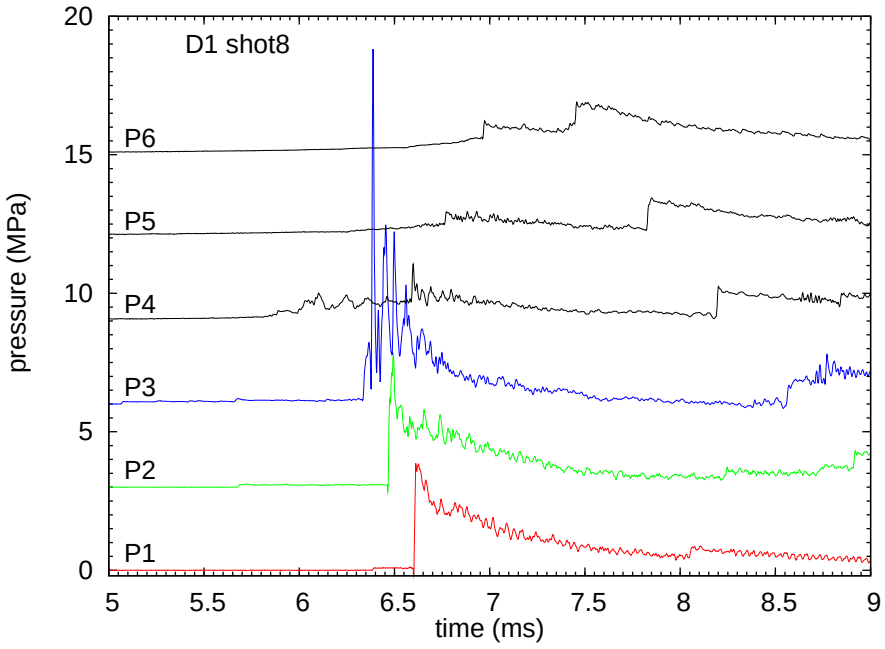

Figure 15: Shot 8 filtered and baseline corrected pressure-time histories showing DDT event.

Table 2: Video settings for shot 8

horizontal field of view	∼30-40 in
	includes part of SS1-2
exposure time	9.37 microsecond
interframe time 18.18 microsecond	
DDT time	6.215 ms, 341 frame
	detonation bubble appears near top and bottom of channel end
wave reaches end of channel	6.215 ms, 341 frame
	Immediately after DDT
visible flame	4.379 ms, 240 frame
resolution	912 × 128
Notes:	No backlight - luminosity only
	low contrast but useable
	Jet from fill line at 10B visble at 5.631 ms, 310 frame

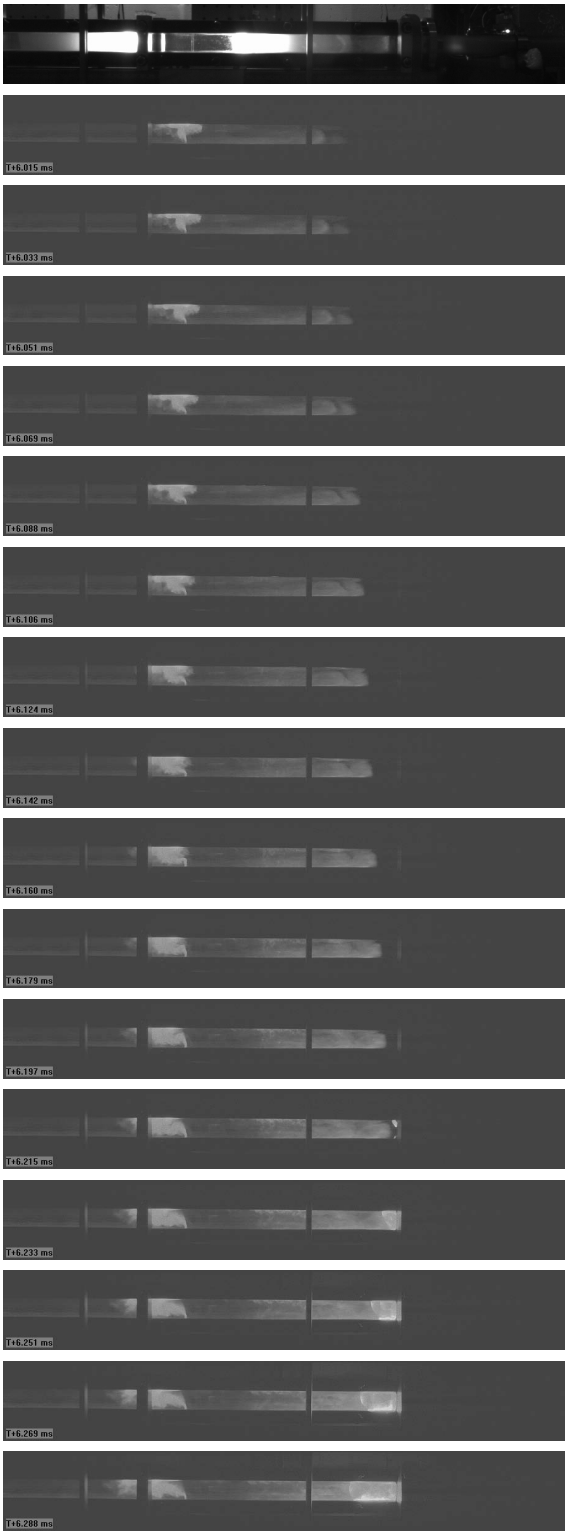

Figure 16: Sequential frames between 6.015 and 6.288 ms from the visualization of the DDT event in shot 8. Time increases from top to bottom. Above the sequence is a image of the test section taken immediately prior to the shot.

3.2.3 Shot 9

This test used a water layer of approximately 0.25 in height and the midway-0.5 blockage insert. The water layer served to cover the opening for plumbing line and a test of liquid layer interaction with the detonation. Transition from deflagration to detonation occurred close to the end of the test section with over 15 MPa on P3, Fig. 17. The side supporting bars at the end of the test section may provide a transition trigger due to shock reflection, which occurs right the end of the visualization section, Fig. 18. However, this is only possible if enough flame acceleration has occurred within the section to create a sufficiently strong shock. The effects of the flow induced by flame acceleration creates motion of the surface of the water, which appears perturbed and possibly provides an acceleration mechanism. The video recording had a long exposure time in this test, Table 3, so details are difficult to see.

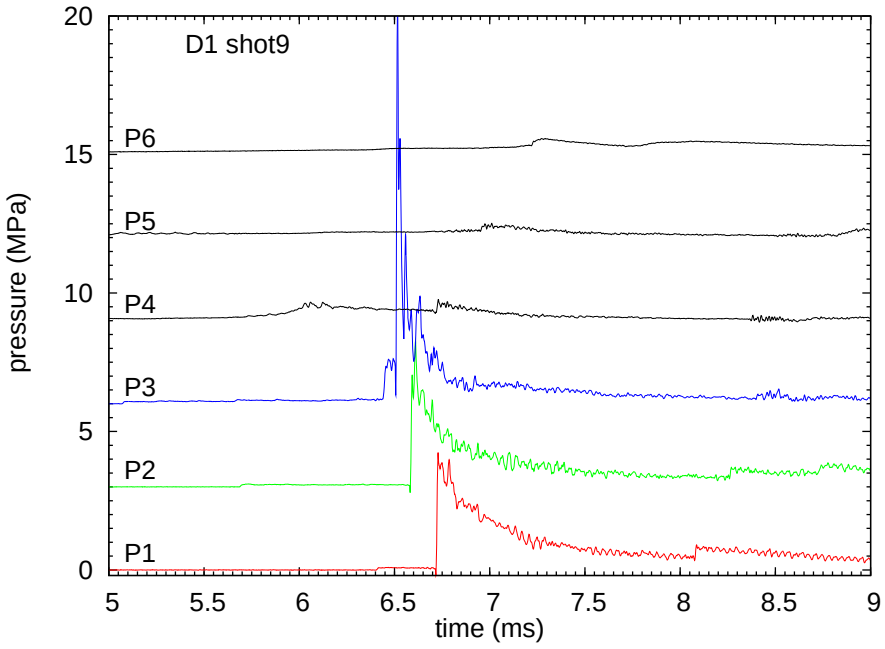

Figure 17: Shot 9 filtered and baseline corrected pressure-time histories showing DDT event.

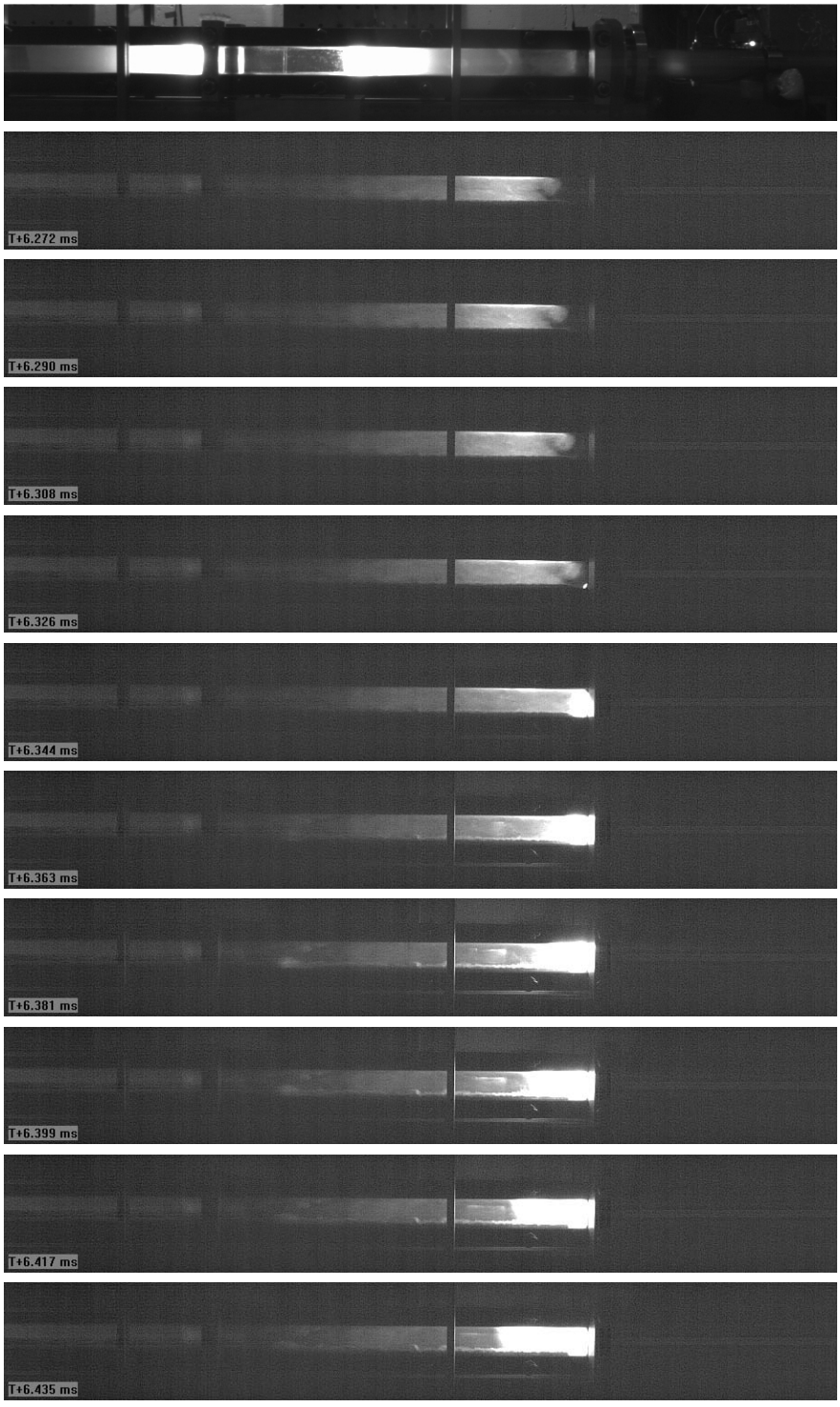

Figure 18: Sequential frames between 6.272 and 6.435 ms from the visualization of the DDT event in shot 9. Time increases from top to bottom. Above the sequence is a image of the test section taken immediately prior to the shot.

Table 3: Video settings for shot 9

horizontal field of view	∼30 in
exposure time	9.37 microsecond
interframe time	18.18 microsecond
DDT time	6.326 ms, 348 frame
	detonation bubble appears end near weldment
wave reaches end of channel	6.326 ms, 348 frame
visible flame	5.272, ms 290 frame
	limited by editing of cine
resolution	912×128
Notes:	No back light - self-luminosity only

3.2.4 Shots 10 and 11

These tests used the "midway+0.5" blockage element and ignition on the W flange. The instrumentation configuration was the same as in shot 9. In shot 10, there was no water and in shot 11, a layer of water 0.375-0.5 in high was located within the visualization test section. In the shot 10 without a water layer, the DDT occurs at 6.270 ms; in shot 11 with a 0.25 in water layer, transition occurs at 5.094 ms. It is not clear if this 20% difference is significant since DDT run-up length is a property that shows substantial shot-to-shot variation.

Table 4: Video settings for shot 10 and 11

shot 10

horizontal field of view	30-40 in
exposure time	3.93 microsecond
interframe time	18.18 microsecond
DDT time	6.270 ms, 344 frame
	detonation bubble appears at bottom close to end
wave reaches end of channel	6.342 ms, 348 frame
	camera saturated
visible flame	4.616, ms 253 frame
	Flame visible propagating along bottom from ignition end
resolution	912×128
Notes:	No back light - self-luminosity only

shot 11

horizontal field of view	30-40 in
exposure time	3.91 microsecond
interframe time	18.18 microsecond
DDT time	5.094 ms, 280 frame
	detonation bubble appears at bottom between P3 and P9
wave reaches end of channel	5.185 ms, 285 frame
	camera saturated
visible flame	4.257, ms 234 frame
resolution	912×128
Notes:	No back light - self-luminosity only

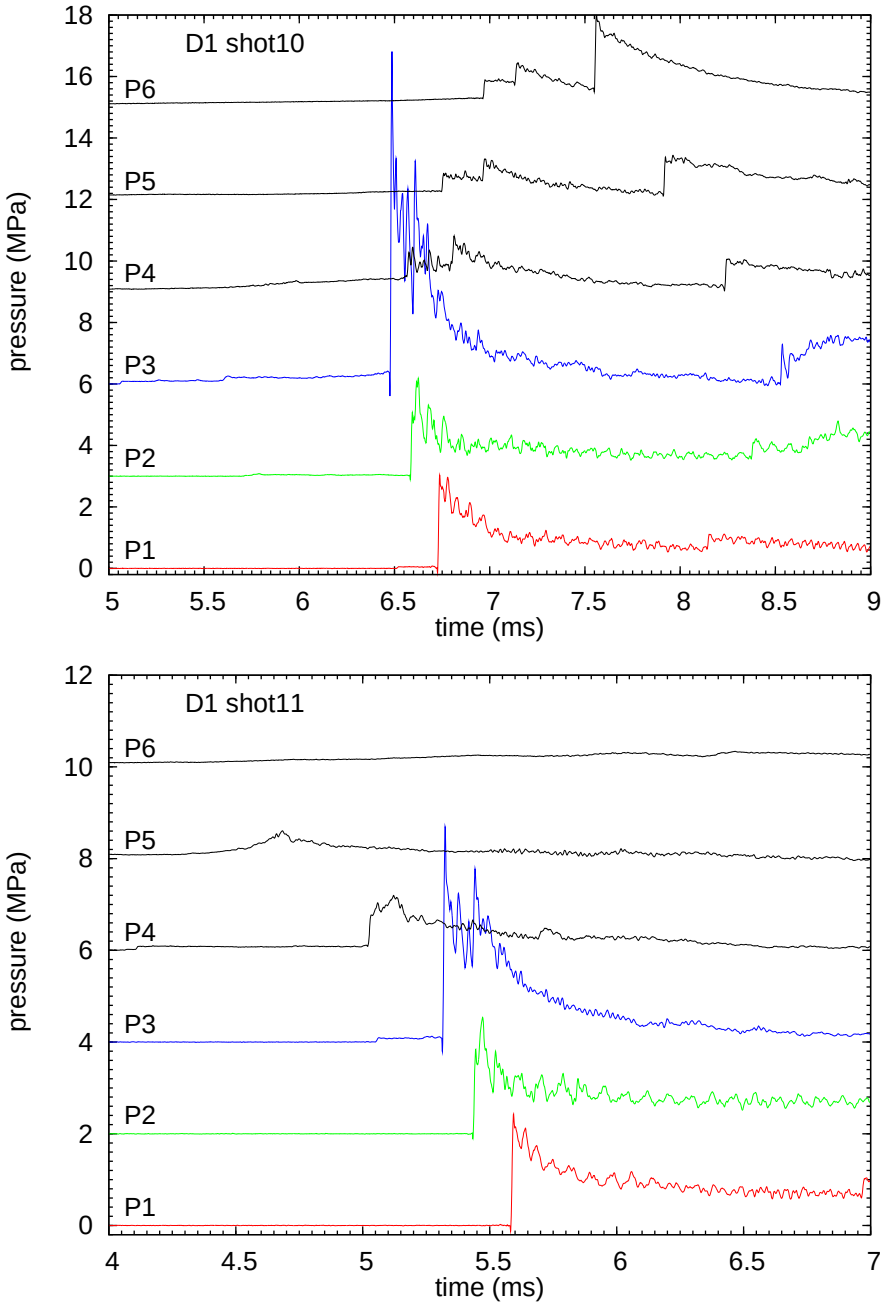

Figure 19: Shot 10 and 11 filtered and baseline corrected pressure-time histories showing DDT event.

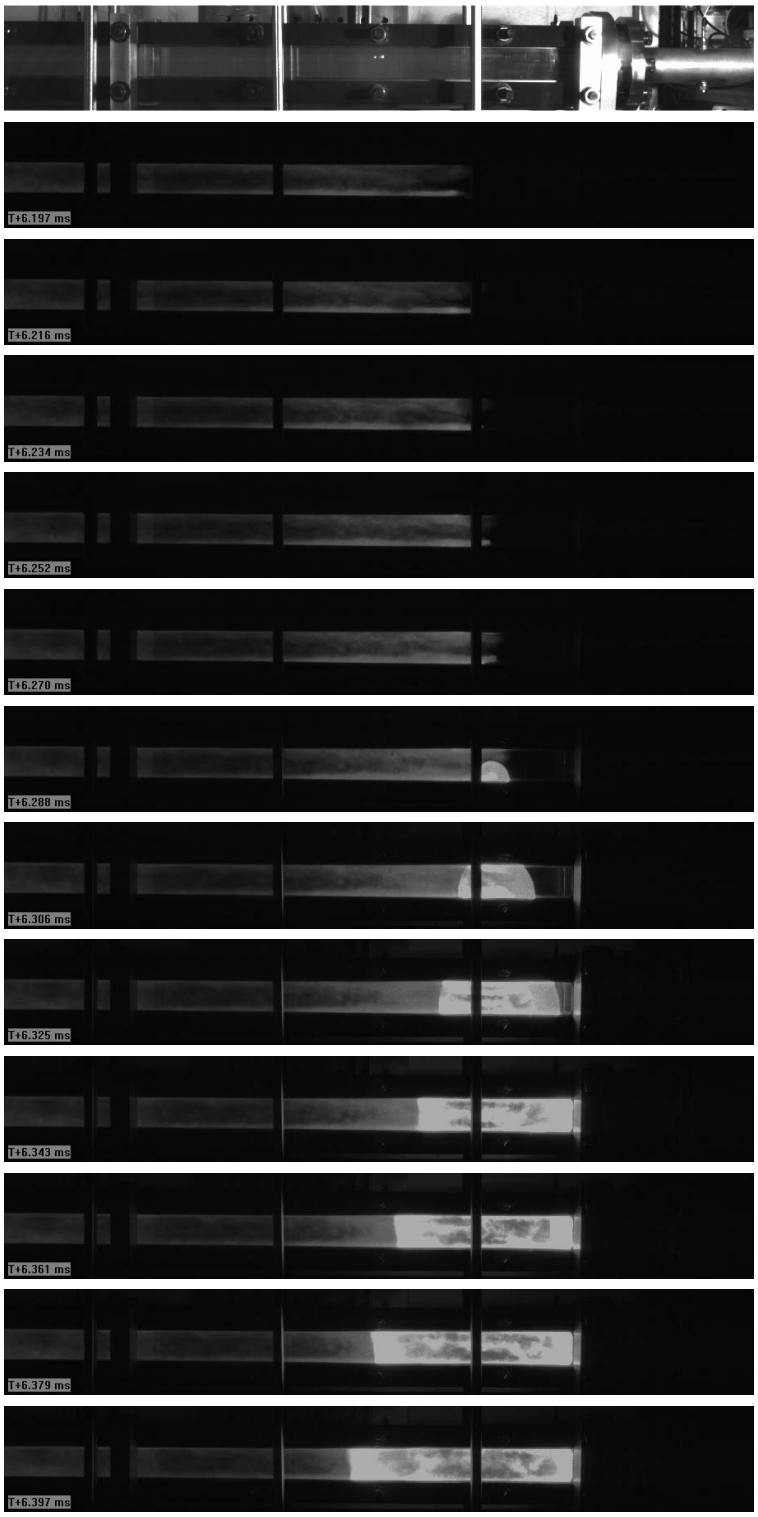

Figure 20: Sequential frames between 6.197 and 6.397 ms from the visualization of the DDT event in shot 10. Time increases from top to bottom. Above the sequence is a image of the test section taken immediately prior to the shot.

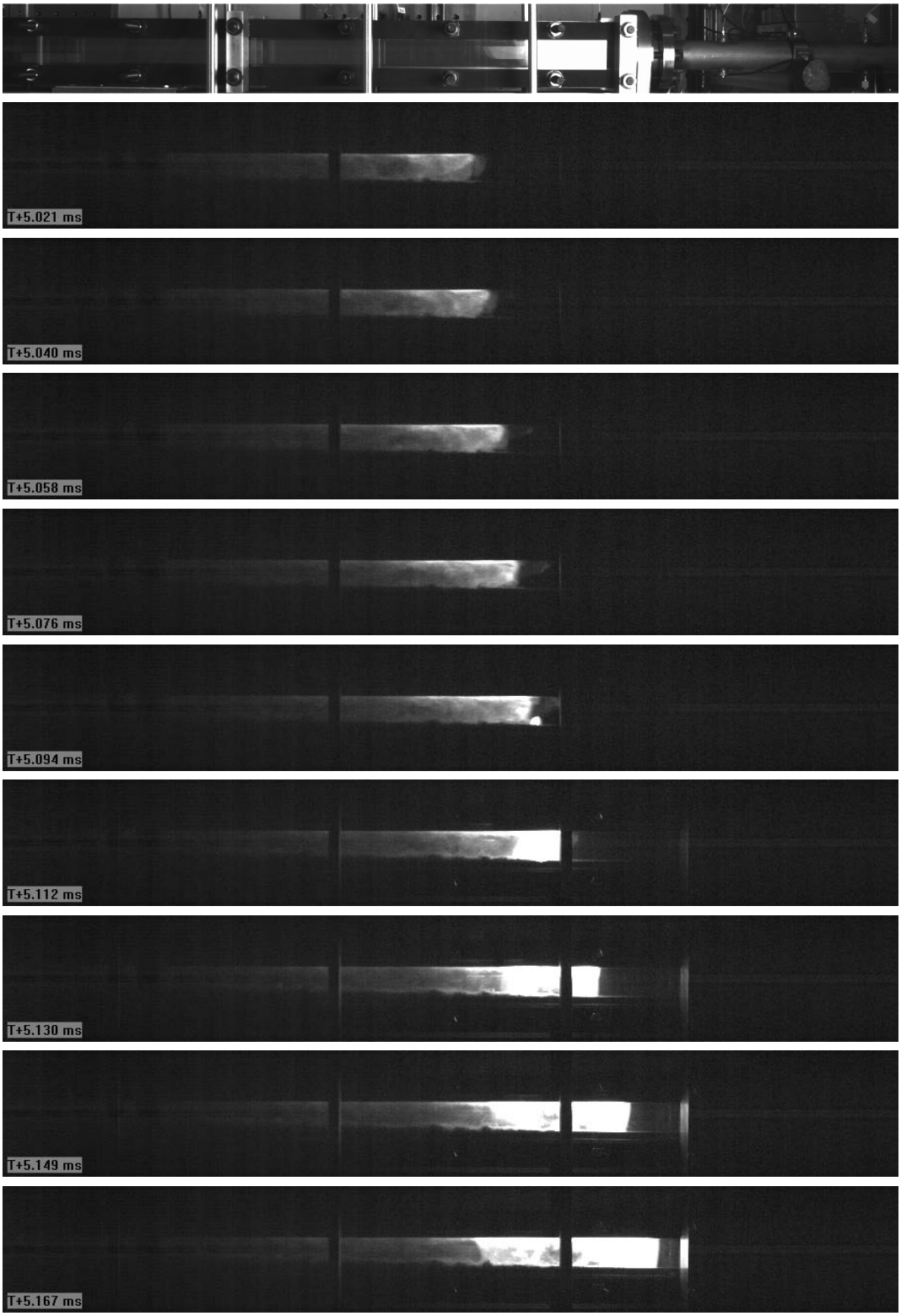

Figure 21: Sequential frames between 5.021 and 5.167 ms from the visualization of the DDT event in shot 11. Time increases from top to bottom. Above the sequence is a image of the test section taken immediately prior to the shot.

3.2.5 Shots 12 and 13

In shots 12-13, two effects were investigated that we speculated played a role in the DDT process.

1. The relevance of splashing that occurs during the filling process to DDT promotion. This was motivated by observation that drops collect close to the fill tube outlet and can be seen on the sides of the test section. These droplets may generate promote transition to detonation through the generation of turbulence and acoustic waves in the flow.

2. The generation of stress waves in the channels and windows causing significant structural motion that may feedback into the DDT process.

These tests used the "midway+0.5" blockage element, ignition on the W flange, and a layer of water 0.375-0.5 in high within the visualization test section. Strain gages were added on the windows and the top C-channel to measure strains and pressure simultaneously. The locations of the strain gages are shown in Fig. 23 and Fig. 22. Gages S11 (window), S12 (C-channel vertical) and S13 (C-channel horizontal) are about 2 in east of port 9T, gage S14 is aligned with port 8T and gage S15 is aligned with port 9T. The water depth was approximately the same in both tests, about 0.40–0.50 in.

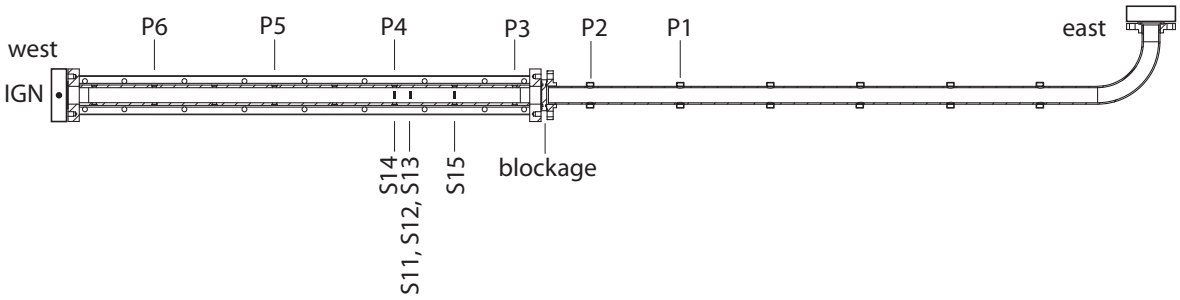

Figure 22: Location of sensors in shots 12 and 13.

Comparing the pressure (Fig. 24) and strain histories (Fig. 25), we see that the strain signal occurs simultaneously with the onset of detonation at about 5.76 ms, see discussion of the video below. Transition occurs close to gage P3, which has pressure peak of about 9 MPa at 5.93 Ms. The pressure histories are quantitatively and qualitatively almost identical for these two tests.

The video (see Table 5) of shot 13 shows water droplets being stripped off the wall by the flow in front of the flame in Fig. 26 and some disturbance of the water free surface by the flow created by the flame prior to detonation. The onset of detonation in Fig. 27 appears to be on the upper surface of the channel and wave fronts can be observed propagating upstream and downstream following the DDT event. Once the detonation takes place the dispersion of the water greatly increases.

Table 5: Video settings for shot 13

horizontal field of view	∼30 in
exposure time	3.91 microsecond
interframe time	18.8 microsecond
DDT time	5.726 ms, 315 frame
	detonation bubble appears at top of channel
wave reaches end of channel	5.780 ms, 318 frame
visible flame	5.471, ms 301 frame
	visible stripping of droplets on side walls
resolution	912×128
Notes:	back light and self-luminosity

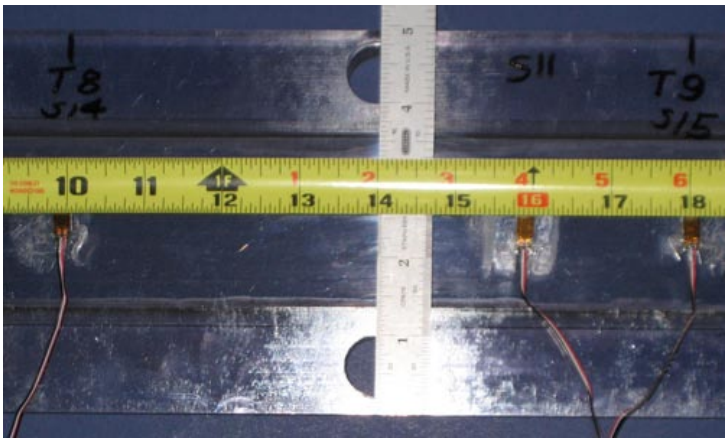

a

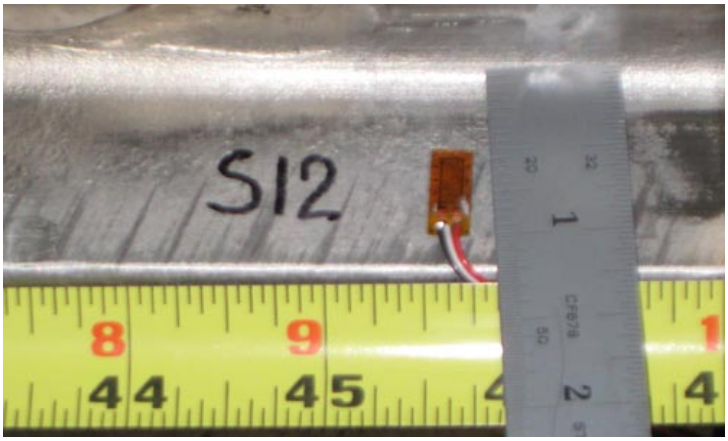

b

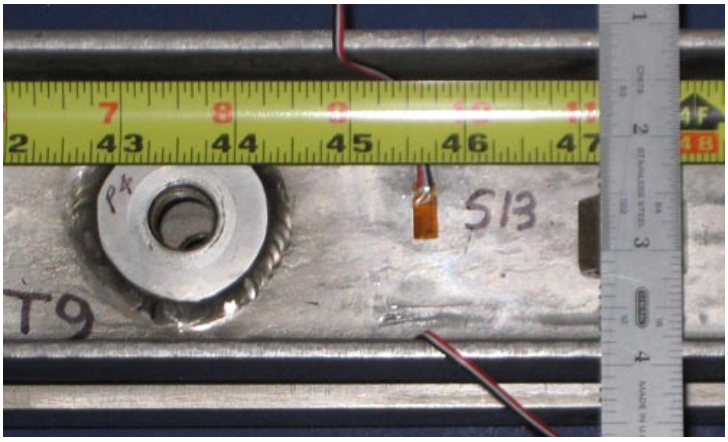

c

Figure 23: Photographs of strain gages used in shots 12-13. a) gages mounted on outside of window, only S11 was used in shot 12, S14 and S15 were added for shot 14. Measurements are from the E end of the window. b) S12 in mounted on the inside vertical portion of the C-section. c) S13 is mounted on the inside horizontal portion of the C-section. Measurements in b) and c) are from the outside of the W end plate of the visualization section.

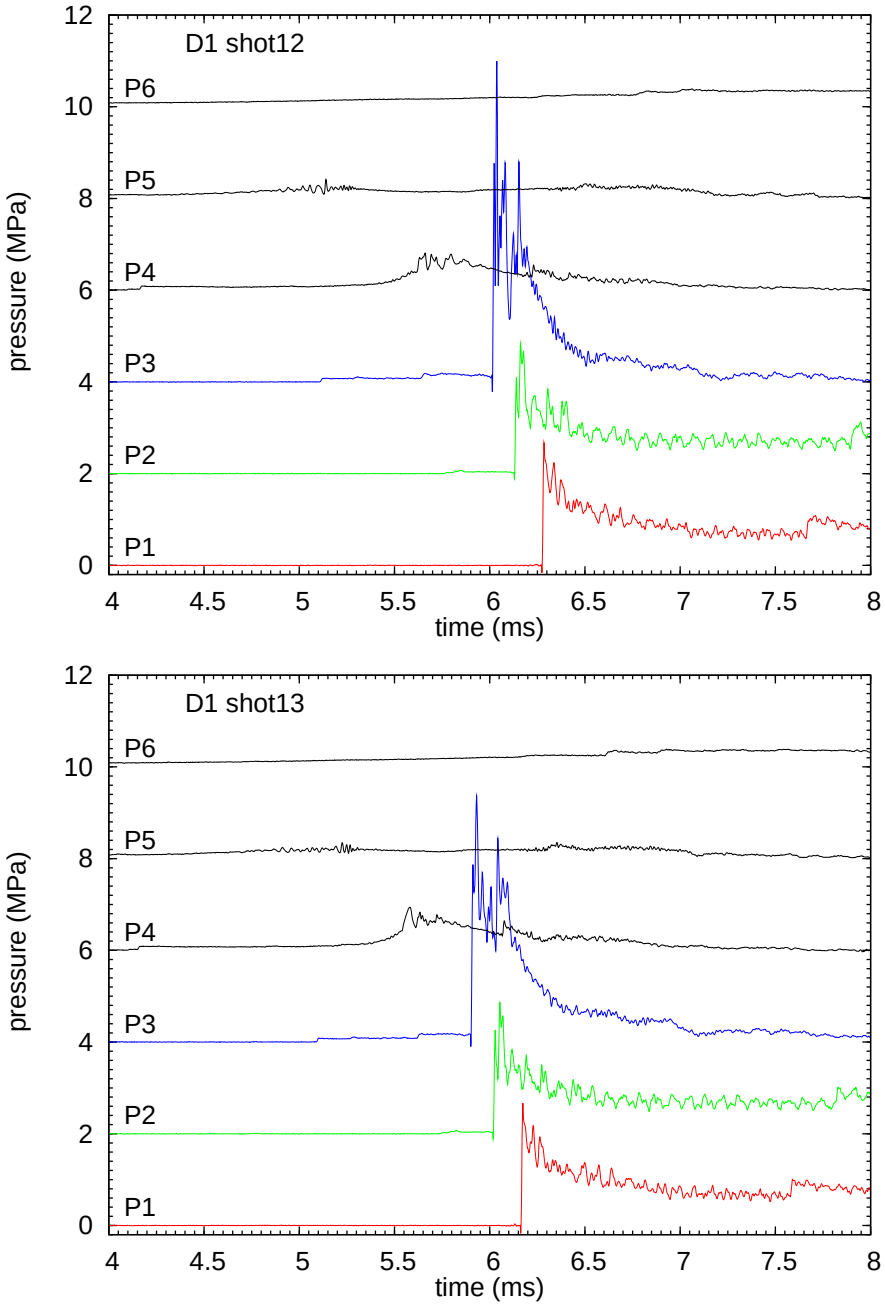

Figure 24: Shot 12 and 13 filtered and baseline corrected pressure-time histories showing DDT event.

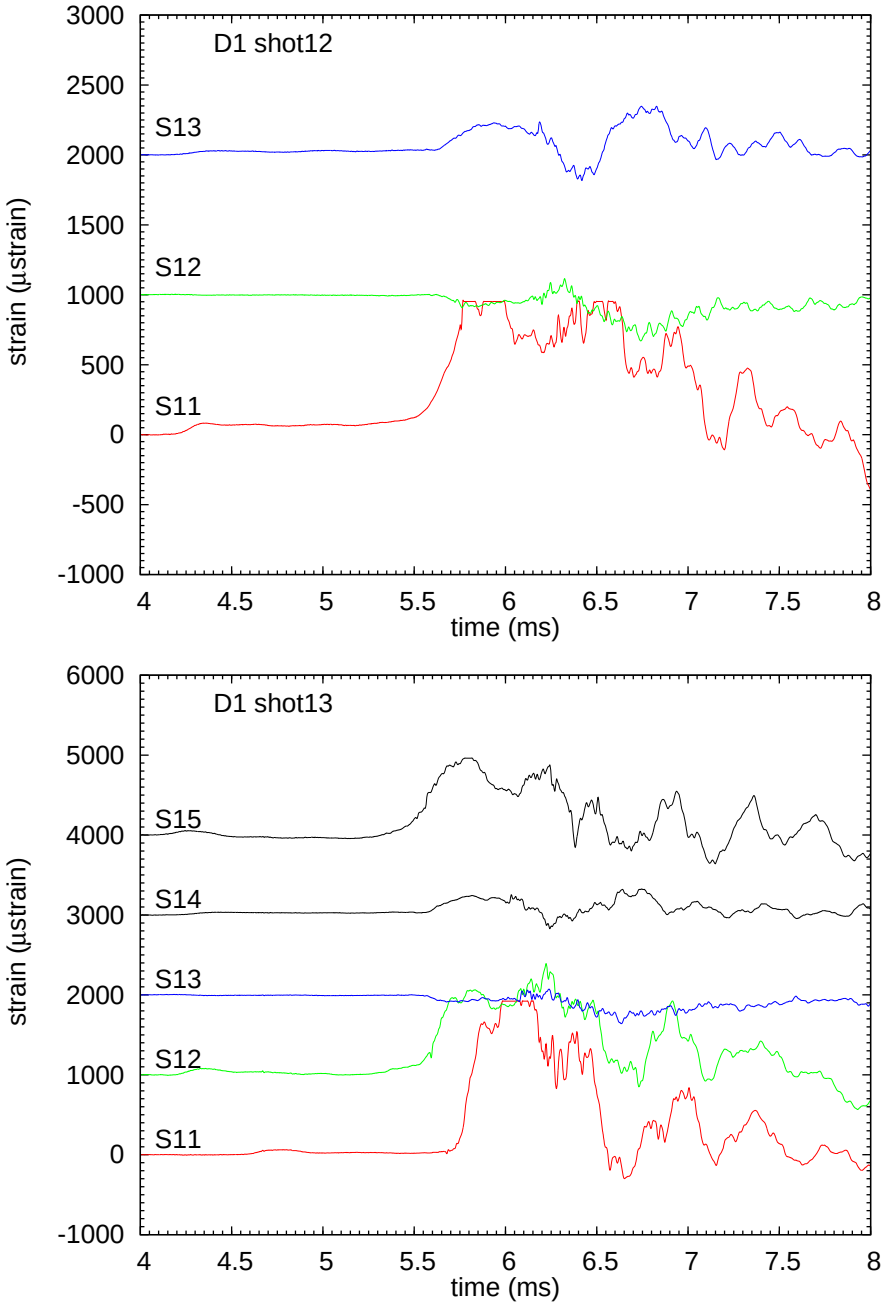

Figure 25: Shot 12 and 13 filtered and baseline corrected strain-time histories showing DDT event.

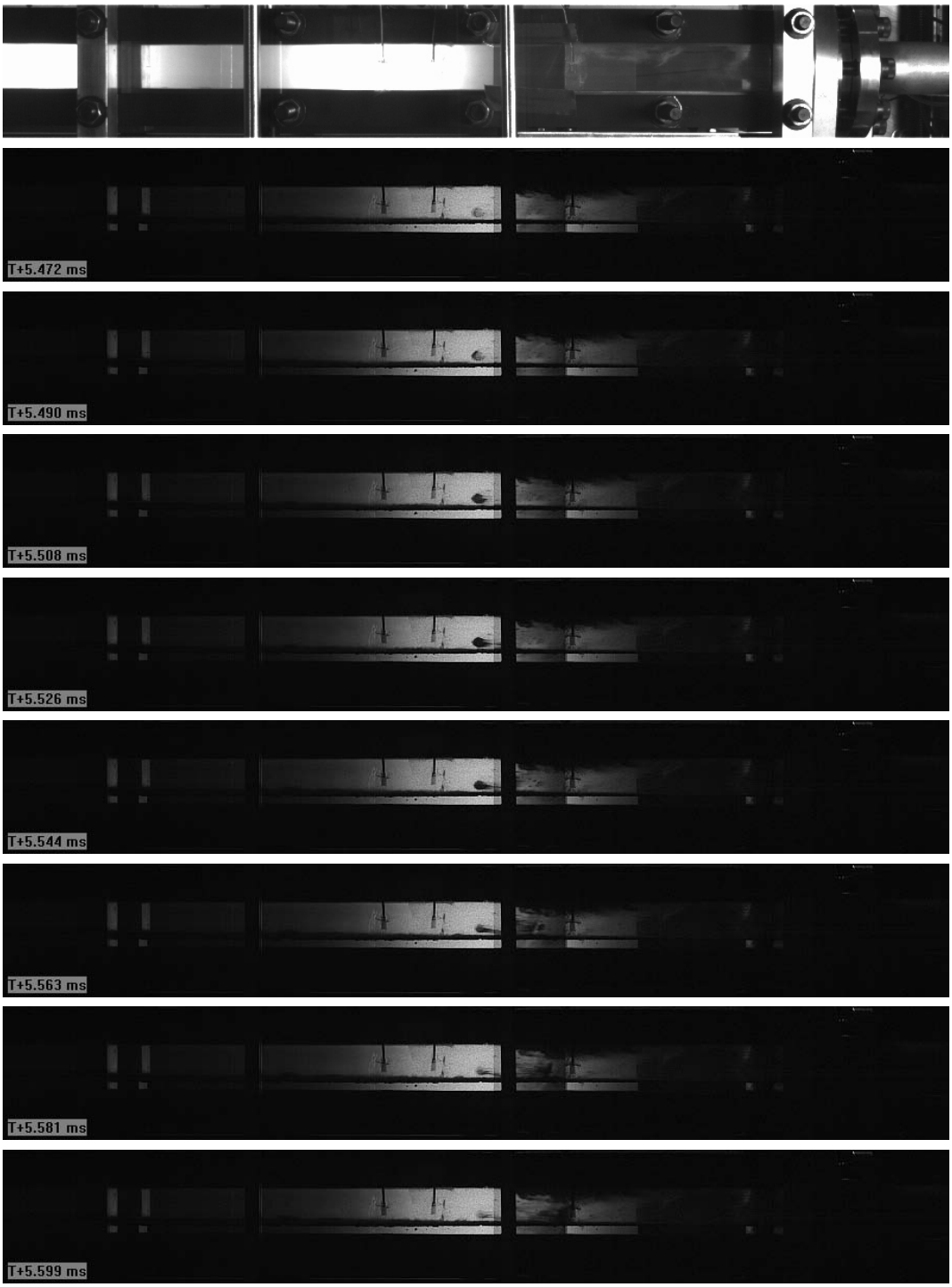

Figure 26: Sequential frames between 5.472 and 5.599 ms from the visualization of flow-droplet interaction in shot 13. Time increases from top to bottom. Above the sequence is a image of the test section taken immediately prior to the shot.

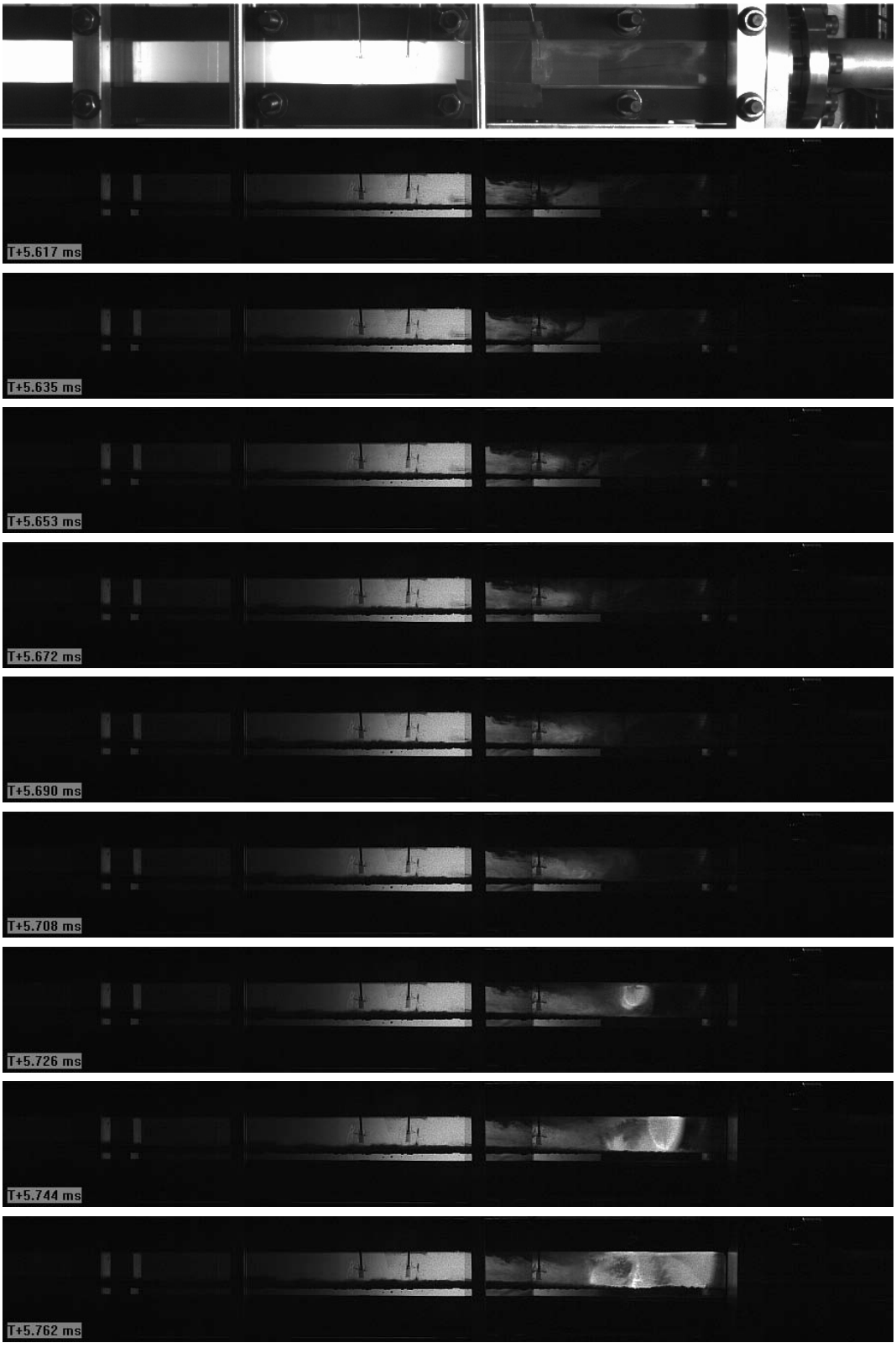

Figure 27: Sequential frames between 5.617 and 5.762 ms from the visualization of the DDT event in shot 13. Time increases from top to bottom. Above the sequence is a image of the test section taken immediately prior to the shot.

3.2.6 Shots 14 and 15

Shots 14 and 15 were carried out with a fully open spacer, Fig. 8d, connecting the visualization section with SS1-2. The conditions for the two tests were identical but the liguid feed line, which slightly protruded into the visualization section at port 8B, was removed in test 15. The transition occurred slightly later in test 15 compared to test 14 but the change is small (the transition distance is displaced downstream by several inches at most) compared to the total transition distance and it is not clear if transition in shot 14 can be attributed entirely to the disturbance caused by the fitting at P8.

Ignition was at the west end with the spark plug, the Shchelkin spiral was left in SS1-2 but only two pressure transducers (P1, P2) recorded data in this section. There was no water layer present so these tests examined just the influence of blockage on DDT within the visualization section. The results can be compared with earlier tests with water and various extents of blockage, as well the subsequent tests D2 with the visualization section alone. The instrumentation locations are shown in Fig. 28 and the distances are given in Appendix F

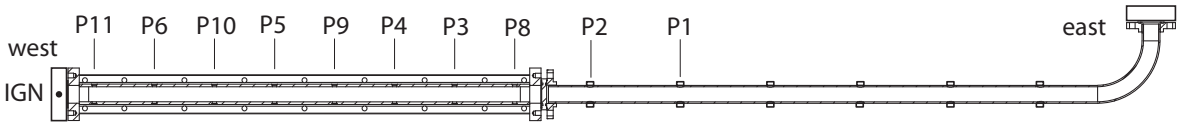

Figure 28: Location of sensors in shots 14 and 15.

In both tests, the flame accelerated, created a series of precursor shock waves, and transition to detonation occurred between gages P3 and P9. The shock waves leading up to and created by the transition event as well as the detonation propagating detonation downstream can be observed in the pressure histories in Figs. 29 and 30. Gage P2 shows a significant thermal artifact with a negative signal after 6.9 ms. The pressure histories for the two test are qualitatively and quantitatively quite similar except that the transition event occurs about 300 μ later in shot 15 than in shot 14. Video visualization was carried out with the self-luminosity of the combustion products, the parameters for both shots are given in Table 6.

The flame acceleration phase leading up to transition was clearly visualized in shot 14, a sequence of frames illustrating this in shown in Fig. 31. Transition in shot 14 occurs at 5.739 ms and a sequence of frames in Fig. 32 shows the generation of the "bubble" and waves propagating away from the event very close to the location of port 8B. Transition in shot 15 occurs at about 6.039 ms with a classical detonation "bubble" emerging from the lower surface of the channel, Fig. 33 several inches to the E of port 8B. Luminous fronts propagate upstream and downstream and then the details are lost due to the saturation of the camera.

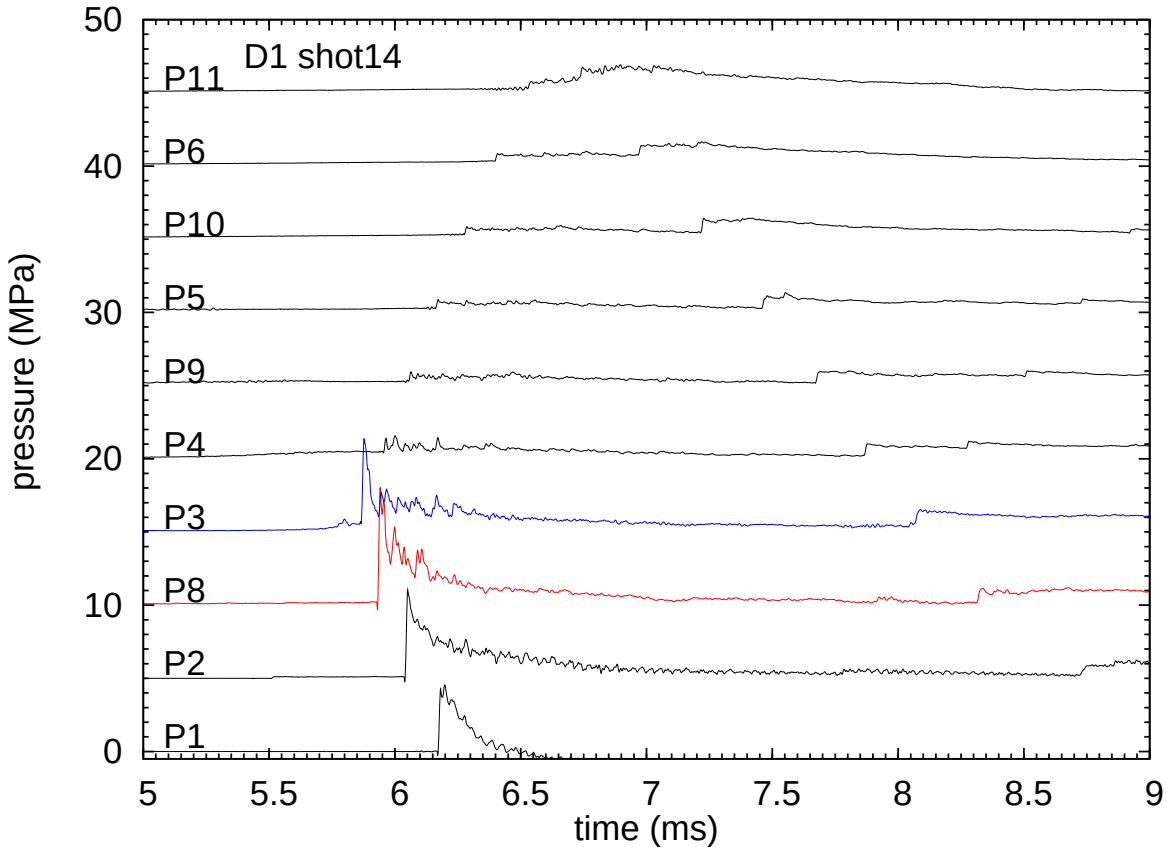

Figure 29: Shot 14 filtered and baseline corrected pressure-time histories showing DDT event.

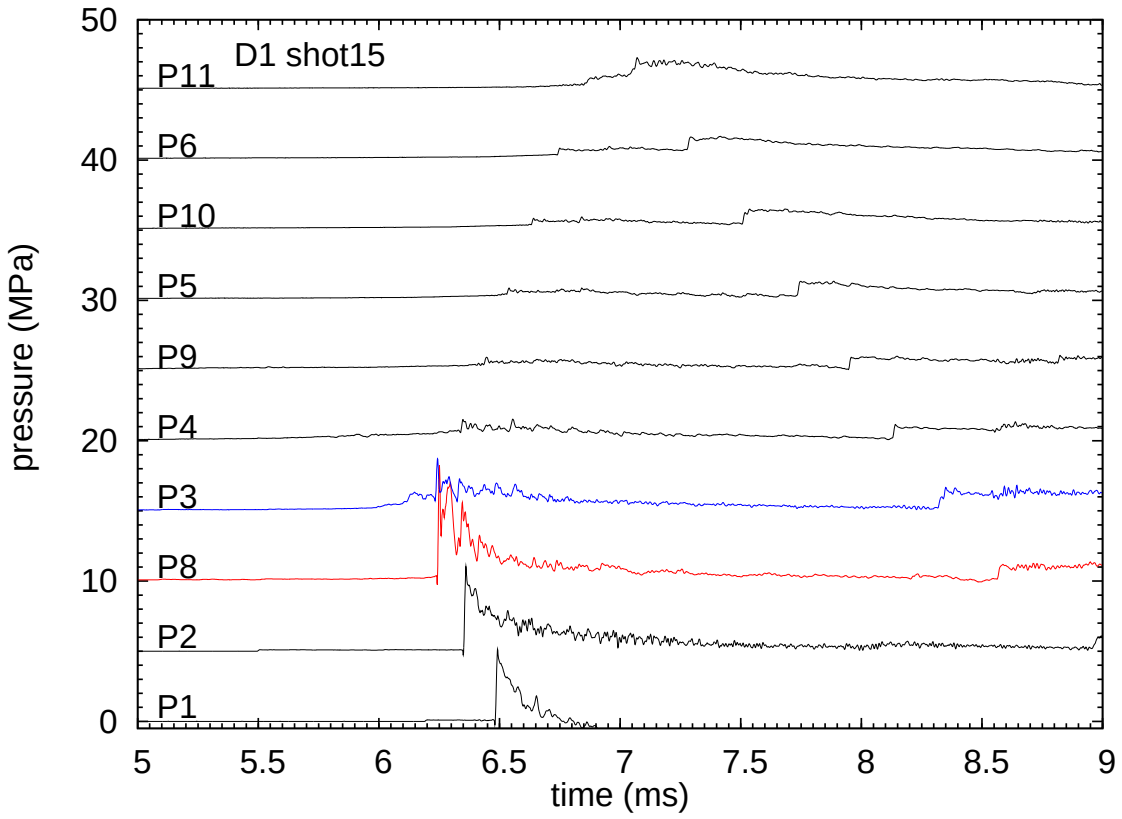

Figure 30: Shot 15 filtered and baseline corrected pressure-time histories showing DDT event.

Table 6: Video settings for shot 14 and 15

shot 14

horizontal field of view	63 in
exposure time	0.31 microsecond
interframe time	13.88 microsecond
DDT time	5.739 ms, 413 frame
	detonation bubble appears at bottom between P3 and P9
wave reaches end of channel	5.836 ms, 420 frame
	camera saturated
visible flame	2.012, ms 145 frame
	Flame visible propagating along bottom from ignition end
resolution	1232×80
Notes:	No back light - self-luminosity only

shot 15

horizontal field of view	63 in
exposure time	0.31 microsecond
interframe time	13.88 microsecond
DDT time	6.069 ms, 437 frame
	detonation bubble appears at bottom between P3 and P9
wave reaches end of channel	6.153 ms, 443 frame
	camera saturated
visible flame	3.084, ms 222 frame
	First appearance of strong luminosity at ignition end
resolution	1232×80
Notes:	No back light - self-luminosity only

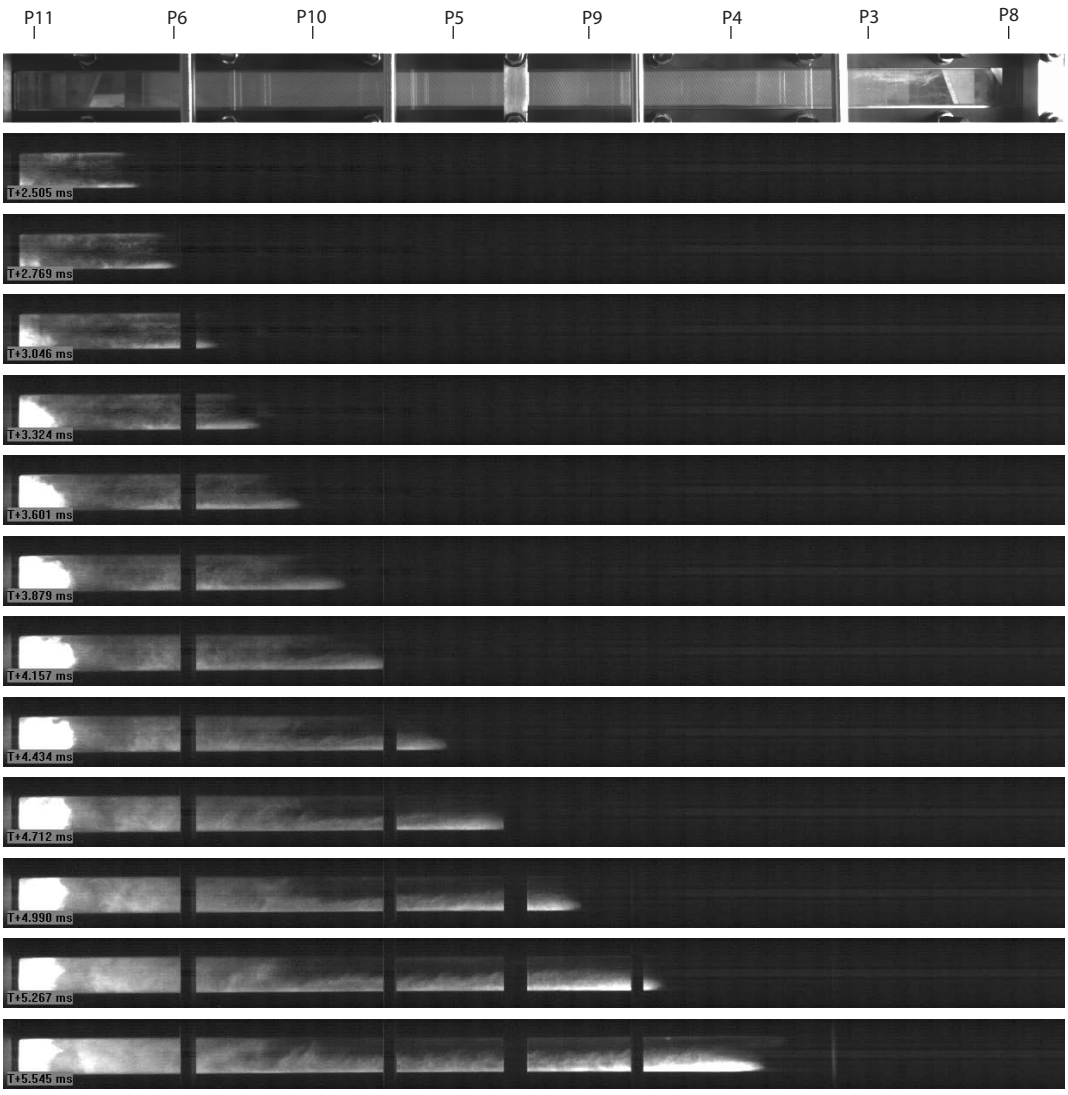

Figure 31: Every 20th frame between 2.505 and 5.545 ms from the visualization of shot 14. Time increases from top to bottom. The approximate sensor locations are shown above an image of the test section taken immediately prior to the shot.

Figure 32: Sequential frames between 5.670 and 5.892 ms from the visualization of shot 14. Time increases from top to bottom. The approximate sensor locations are shown above an image of the test section taken immediately prior to the shot.

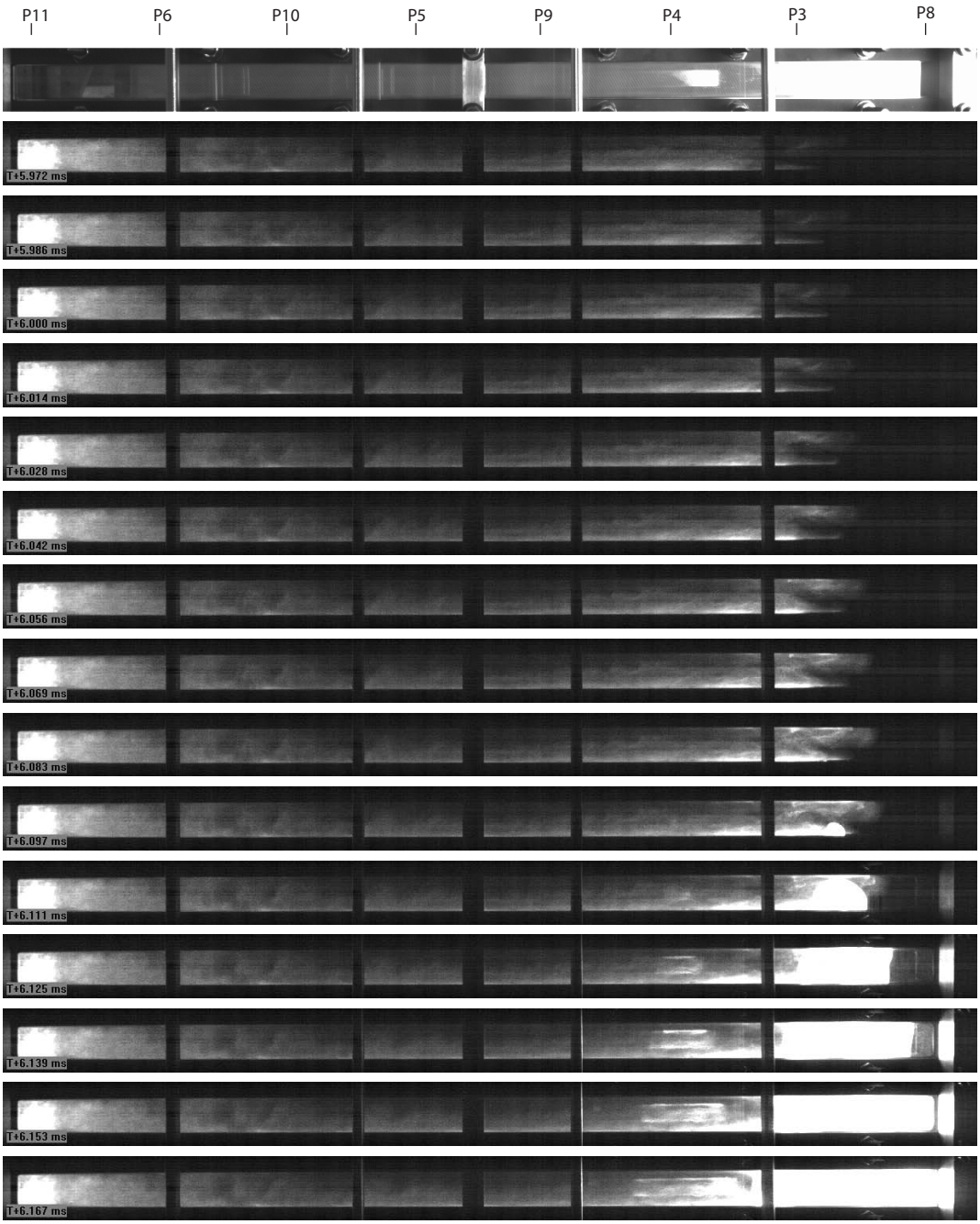

Figure 33: Sequential frames between 5.972 and 6.167 ms from the visualization of shot 15. Time increases from top to bottom. The approximate sensor locations are shown above an image of the test section taken immediately prior to the shot.

3.3 Discussion of D1 testing

Shots 1-6 These tests demonstrated the repeatability of the testing procedure and the effect of the blockage on the detonation propagation. Arrival time data for all 6 tests are plotted in Fig. 34 and it is apparent that the detonation propagates steadily in shots 1 and 2. As mentioned above, the small blockage element (midway - 0.5) has a relatively modest effect on the wave propagation in shots 3 and 4 but a substantial decrease in velocity and significant period of acceleration can be observed downstream of the larger blockage element (midway + 0.5) for shots 5 and 6. However, the peak pressures, Fig. 35, are essentially unaffected by the presence of the blockage element. The pressure arrival time data was analyzed using linear regression to obtain wave speeds and found to be within 1% of the nominal CJ speed (2088 m/s) for the shots 3 and 4, and within 0.4% for shots 1 and 2.

Table 7: Wave speeds determined by linear regression.

Shot	Speed	
1	2065	m/s
2	2059	m/s
3	2080	m/s
4	2080	m/s

Shots 7-13 These tests demonstrated that relatively thin water layers (0.25-0.50 in) and variations in the blockage ratio have a modest effect on the transition distance and peak pressures, Fig. 36. Shots 7, 8 and 9 used the smaller blockage ratio (midway - 0.5) and shots 10, 11, 12, and 13 used the larger blockage ratio (midway + 0.5). With the larger blockage ratio, the flow speed is higher upstream of the blockage during flame acceleration, which appears to result in greater turbulence and slightly earlier transition than in the case of the smaller blockage ratio. As a consequence, the peak pressure on gage P3 (1.55 m from ignition) is on the order of 13-15 MPa in shots 7-9 and on the order of 4-7 MPa for shots 11-13, shot 10 is an intermediate case for a peak pressure of 10 MPa. There does not appear to be a systematic effect of water on the acceleration process but the depths used are small and there are only a few shots.

Shots 14-15 These tests demonstrated that removing the blockage completely has a modest effect on the transition process and the pressures are comparable to those obtained in shots 11-13. The results were repeatable, probably because the transition location was near the connection between the visualization section and the piping section. The welded joint between the channels and flange had metal tabs that protruded into the flow and downstream there was a complex geometrical change from the rectangular to circular cross section. The peak pressure, Fig. 37, initially drops with increasing distance from the ignition source. The peak pressures in the initial part of the channel, 0-1.2 m, are actually associated with the reflected shock waves resulting from the retonation (backward propagating shock) from transition and reflection from the W end wall. After a minimum at 1 m, the peak pressure

increases with distance and transition occurs near P3, resulting in the peak pressure of 8 MPa, and subsequently the overdriven shock decays with decreasing pressure on P2 and P1.

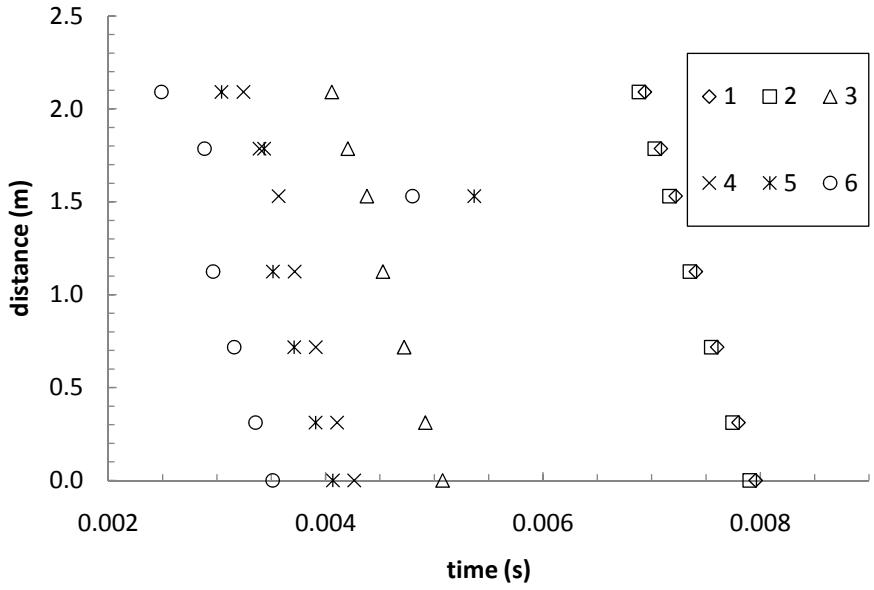

Figure 34: Arrival time vs. distance for shots 1-6 with detonation initiation via Shchelkin spiral and spark source at E end.

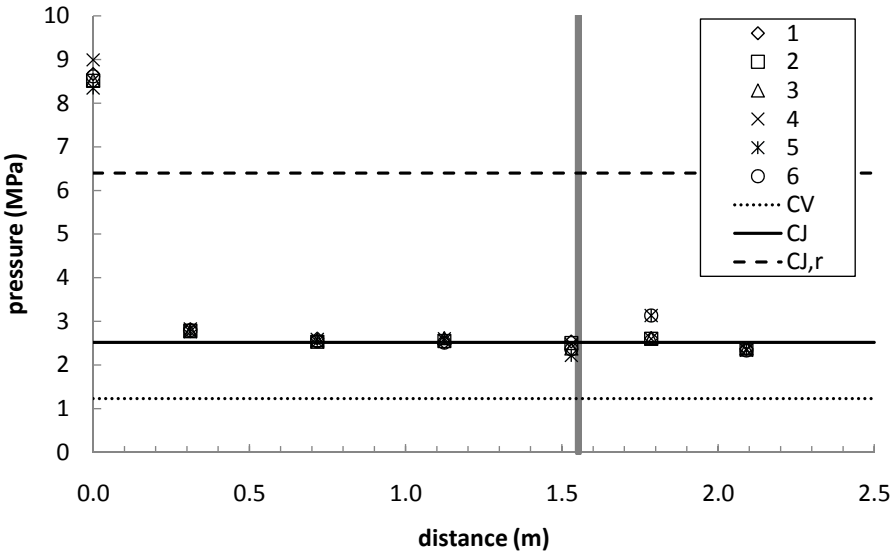

Figure 35: Peak pressures for shots 1-6 with detonation initiation via Shchelkin spiral and spark source at E end.

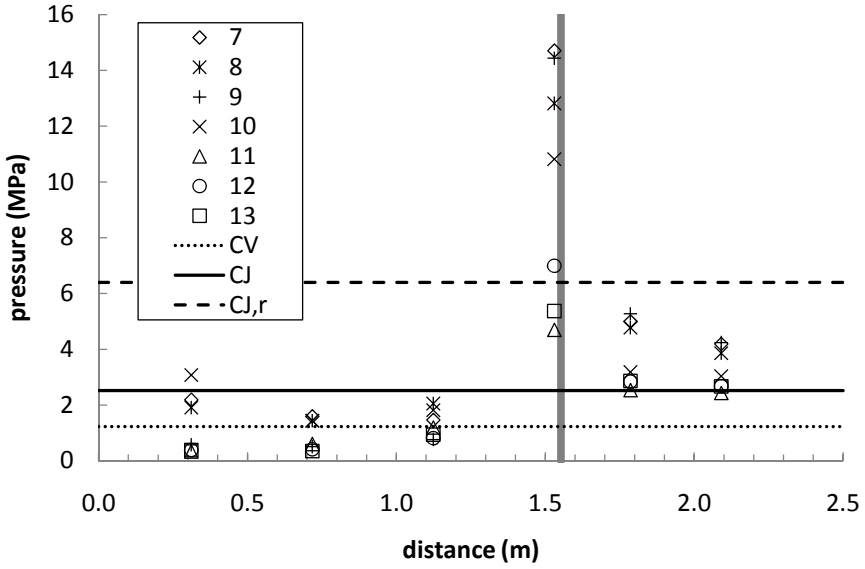

Figure 36: Peak pressures for shots 7-13 with detonation via DDT from flame started by a spark source at W end.

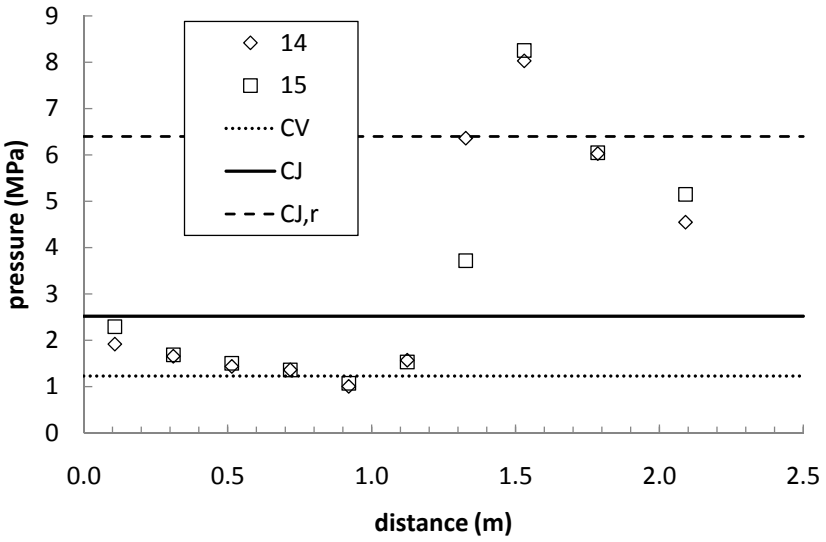

Figure 37: Peak pressures for shots 14-15 with detonation via DDT from flame started by a spark source at W end.

4 D2 Results

A series of 6 tests (shots 16-21) were carried out with the visualization section alone, Fig. 38. All of these tests were carried out with spark initiation and DDT occurred with in the visualization section alone. The visualization section has a rectangular interior of 2 in × 3 in and is approximately 63 in long. Engineering details are given in Appendix A. The top and bottom are constructed of C-channel, the channels are welded to plates at the ends, and the sides are sealed with clear polycarbonate sheets containing o-rings. Eight ports are located along each of the top and the bottom channels. These are used to hold the pressure transducers, thermocouple sensors (TC), liquid fill line (L), and in tests 17-21, the spark plug used as the igniter. Pressure transducers were mounted in the end flanges that were formed the fixture closure, the transducer surface and mounting plug is located approximately 0.75 outboard of the end plate.

In shots 18-21, a layer of water was present in the test section and back-lighting was used to observe the motion of the liquid surface. The location of the gages and labeling are shown in Fig. 38. Additional details about the transducer locations are tabulated and the raw data is plotted in Appendix G. In addition to the pressure gages, the events were visualized with

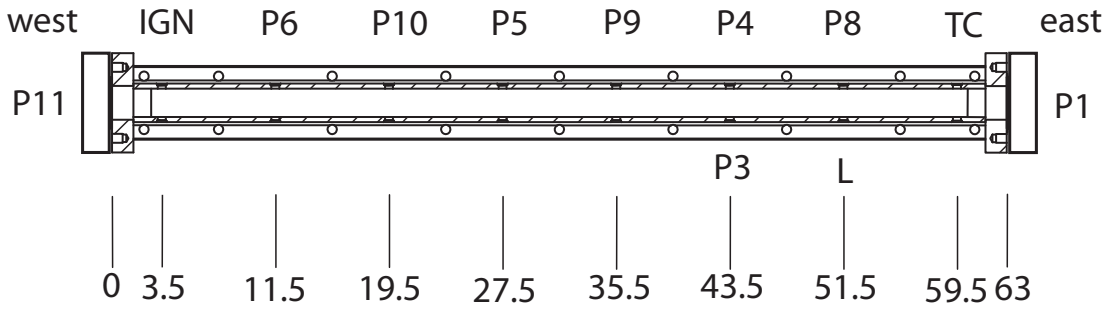

Figure 38: Instrument locations for the visualization section D2. Dimensions are given in inches from the east end plate; The pressure transducers in the end flanges are located 0.75 in outboard of this surface. The configuration shown in for shots 17-21. In shot 16, the locations of the igniter and P11 were exchanged.

high-speed video using a combination of self-light to visualize the combustion fronts and refraction or scattering to observe the liquid motion using back lighting from flashlamps.

4.1 Shot 16

This test was carried out with the spark plug mounted in the west flange and no water for a comparison with earlier tests in the D1 series (7, 8, 10, 14 and 15) that were carried out with this ignition location. This shot is an excellent example of detonation initiation occurring within shocked gas very close to the end wall at the opposite end of the tube from the ignition source. In Fig. 39, a series of precursor shock waves can be observed ahead of the main shock front, even more can be observed can be observed at earlier time in the raw data plot of Fig. 104. The video visualization used self-light (Table 8) and although the

camera was saturated after the DDT event, it is clear that the transition occurs in the last frame shown in Fig. 40 at about 6.578 ms, nearly coincidence with the pressure jump shown in Fig. 39. The approximate location of the pressure gages in indicated at the top of Fig. 40. Between P8 and the E flange, a luminous front can be seen accelerating as it propagates toward the E flange. The transition occurs between P8 and P1, 51.5–63.75 in (1.33–1.64 m) from the ignition location.

A distinct reflected shock wave can observed in Fig. 39 propagating from W to E and reflecting as a secondary shock at the ignition end, propagating E to W and reflecting again from the E end of the fixture. The peak pressure on the gage P1 is about 31.6 MPa, this is equal to the highest pressure that was observed in the ES1 DDT testing, 31.9 MPa in ES1 Shot 9. Note that the expected pressure for ideal reflection of Chapman-Jouguet detonation is $P_{CJ,r} = 6.4$ MPa.

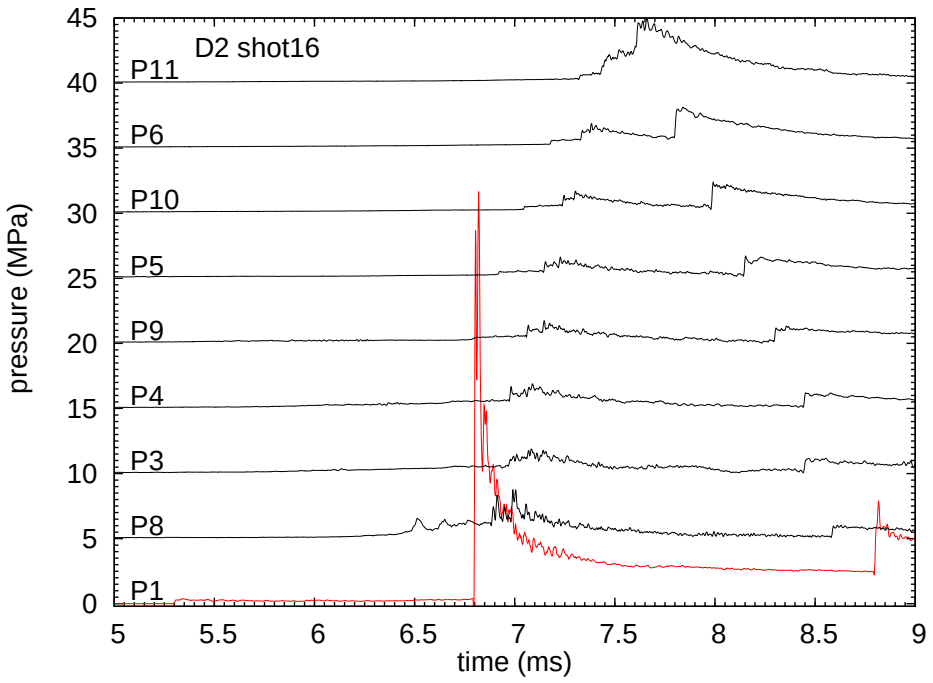

Figure 39: Shot 16 filtered and baseline corrected pressure-time histories showing DDT event. The pressure signals are arranged so that the top trace (P11) is closest to the ignition point and distance from ignition increases from top to bottom, with the lower trace corresponding to gage P1 located in end of the tube opposite ignition.

Table 8: Video settings for shot 16

horizontal field of view	63 in
exposure time	0.31 microsecond
interframe time	13.88 microsecond
DDT time	6.578 ms, 473 frame
	Event saturated camera - difficult to fix start time
Wave reaches end of channel	6.675 ms, 480 frame
visible flame	4.76 ms, 343 frame
resolution	1232×80
Notes:	No back lighting - self-luminosity only
	Strobe light decays before DDT event

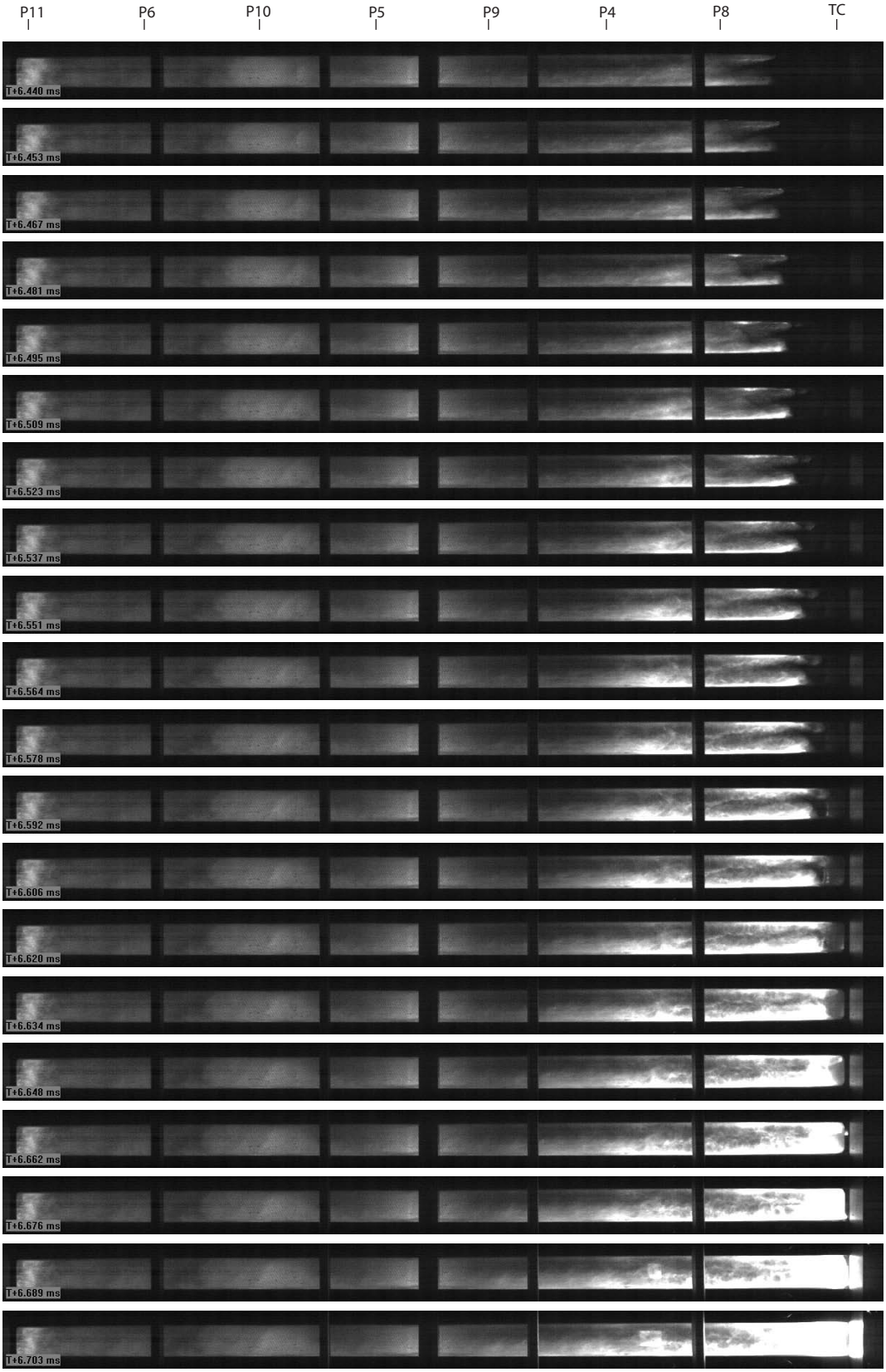

Figure 40: Sequential frames between 6.440 and 6.703 ms from the visualization of shot 16. Time increases from top to bottom in increments of 13.88 μs.

4.2 Shot 17

In preparation for the water tests, the ignition location was moved to port 14T on top of the test section. A miniature spark plug (Rimfire[1] model Macro Viper Z3, 6MM Hex, 10-40 thread type, see Fig. 41) was mounted onto the test-section. Shot 17 was used to verify the operation in this visualization test without a water layer and can be compared to shot 16 as well as subsequent tests. Moving the ignition source resulting the transition to detonation

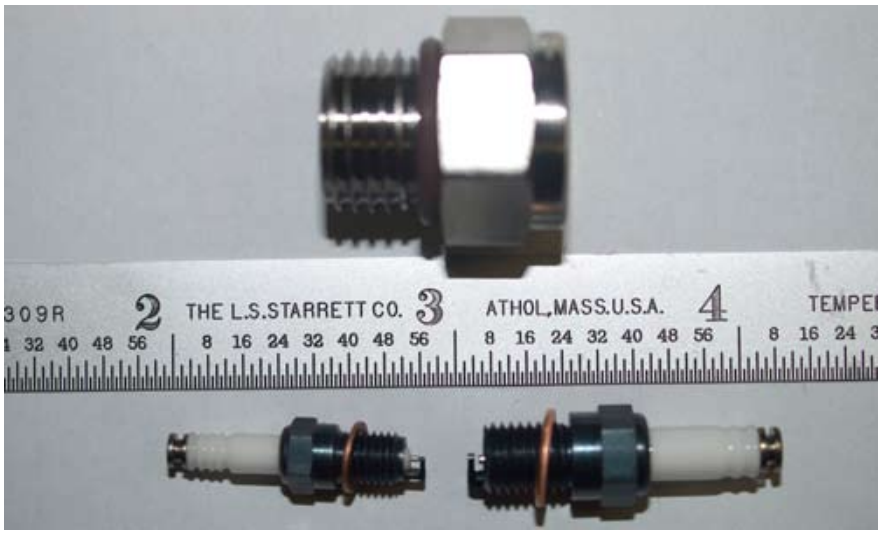

Figure 41: Small spark plugs of the type used for testing with water layers. The SAE J1926 pipe plug fitting that was machined to hold the spark plug is shown above the spark plugs for comparison.

occurring earlier, well before the end of the chamber. The pressure histories, Fig. 42, show an event near gages P3/P4 that generates shock waves propagating in both directions. This can be clearly observed as two luminous fronts in Fig. 43 that originate near the location of gage P8, 48 in (1.22 m) from the ignition source at a time of 5.09 ms. An annotated photo of the test section before the shot is shown at the top of Fig. 43 to indicate the approximate position of the gages and the location of the reinforcing bars and C-clamps that are in the field of view. The front propagating to the right is the detonation and that propagating to the left is the "retonation", a strong shock wave in the combustion products.

The only difference in shot 16 and 17 is the location of the igniter. Apparently moving the ignition from the W flange to the 8T position has the effect of generating more turbulence and accelerating the flame. This results in a decrease in the

[1]Available from Roland M Morrison, P.O. Box 555, Benton City, WA 99320, http://sparkplugs.morrisonandmarvin.com

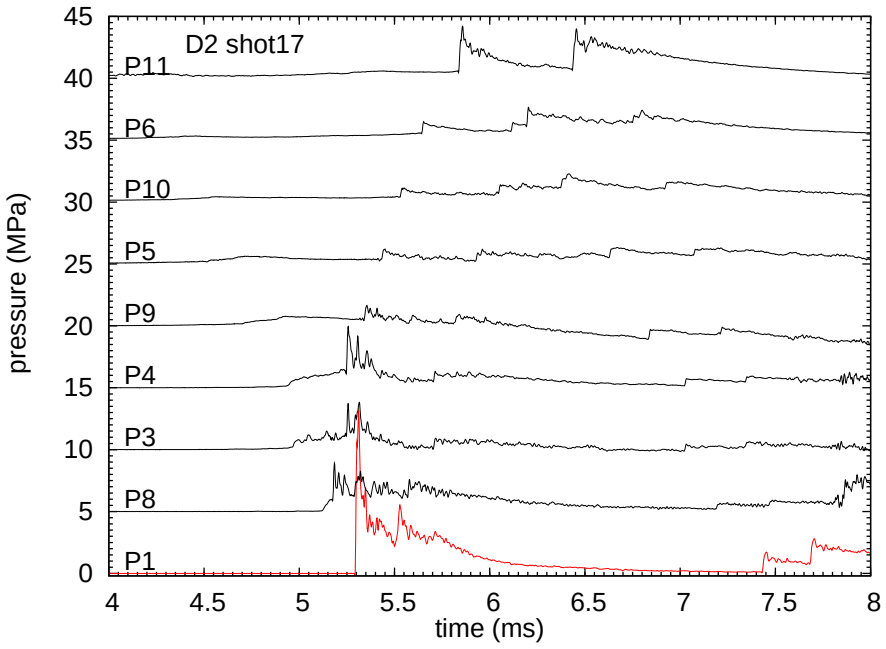

Figure 42: Shot 17 filtered and baseline corrected pressure-time histories showing DDT event.

Table 9: Video settings for shot 17

horizontal field of view	63 in
exposure time	2 microsecond
interframe time	13.88 microsecond
DDT time	5.049 ms , 363 frame
Wave reaches end of channel	5.16 ms, 371 frame
visible flame	4.563 ms, 330 frame
resolution	1200 × 80
Notes:	no back lighting - self-luminosity only

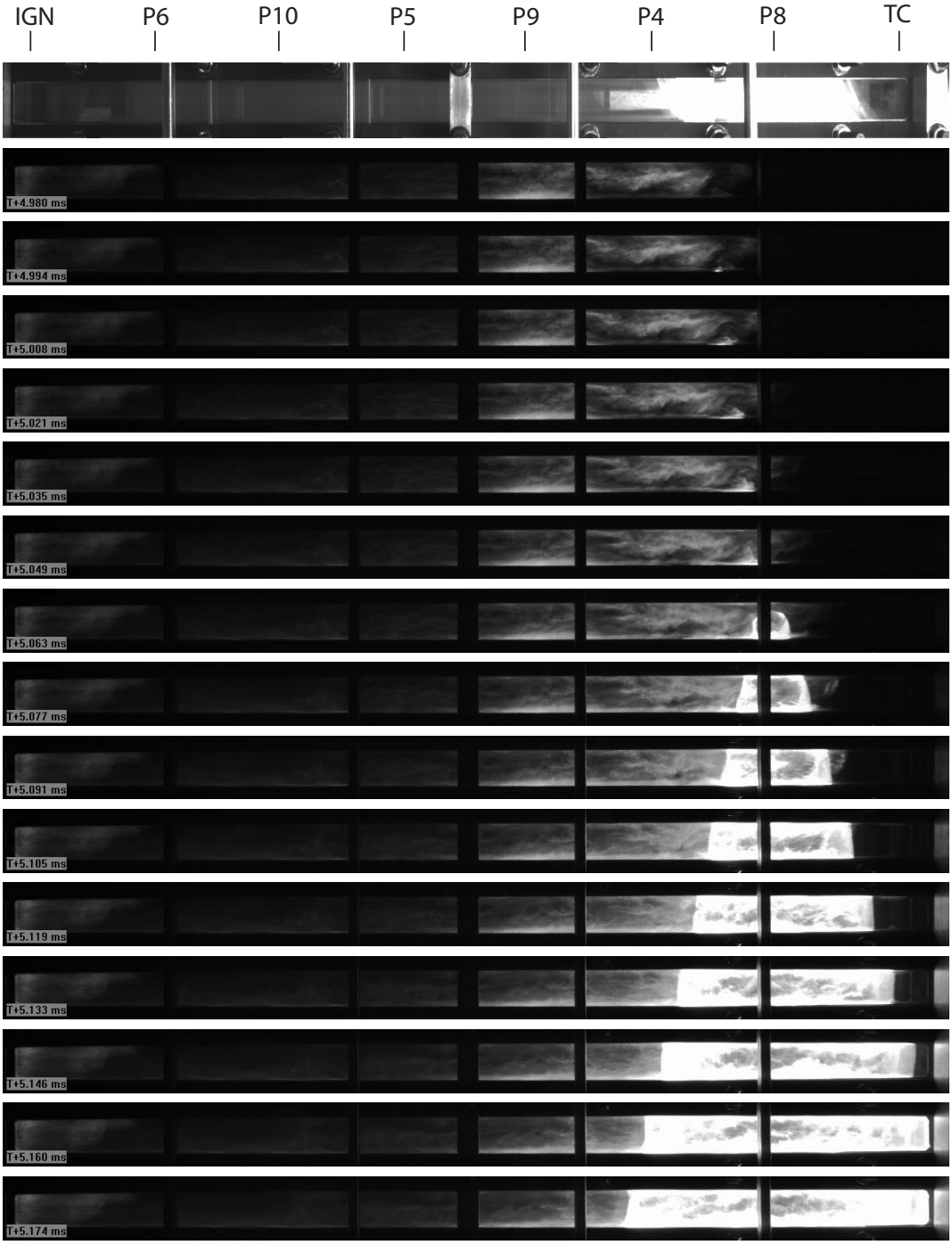

Figure 43: Sequential frames between 4.980 and 5.174 ms from the visualization of shot 17. Time increases from top to bottom in increments of 13.88 μs.

4.3 Shot 18

This test was carried out a with water depth of about 1.35-1.375 in (gas layer of 0.625-0.65 in) and ignition with the miniature spark plug in port 8T. A range of values for the water depth is quoted because there is some parallax in measurements taken from the photographs and also the top and bottom of test section were not completely flat and level.

DDT was observed in the last half of the test section, between the location of gages P4/P3 and P8, 40–48 in (1.02–1.22 m) from ignition, at about 4.038 ms. Fig. 44 shows a strong spike in pressure on gages P3/P4 just after this time, and a strong shock wave is observed on P8 at the same time. As was observed in shot 17, there are two luminosity fronts emerging from the event, a detonation propagating to the right and a shock moving to the left. The luminosity is not as high as in shot 17 since the gas does not fill the channel but the similarity between the two events is striking. The peak pressures on P8 and P1 are lower in shot 18 than 17. However, both P1 and P3 are below the surface of the water in shot 18 while completely exposed in 17. Introducing the layer of water had the effect of shortening the transition distance and reducing the peak pressures.

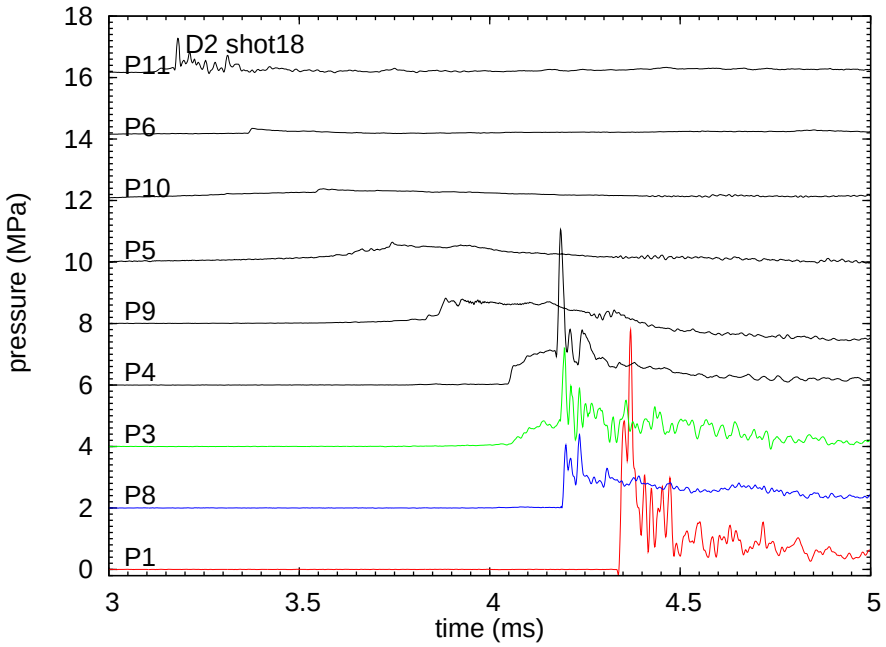

Figure 44: Shot 18 filtered and baseline corrected pressure-time histories showing DDT event.

Table 10: Video settings for shot 18

horizontal field of view	63 in
exposure time	3.31 microsecond
interframe time	13.88 microsecond
DDT time	4.010 ms, 288 frame
	Detonation bubble visible in 291
wave reaches end of channel	4.204 ms, 302 frame
visible flame	3.649 ms, 261 frame
resolution	1200×80
Notes:	back lighting with diagonal striped screen

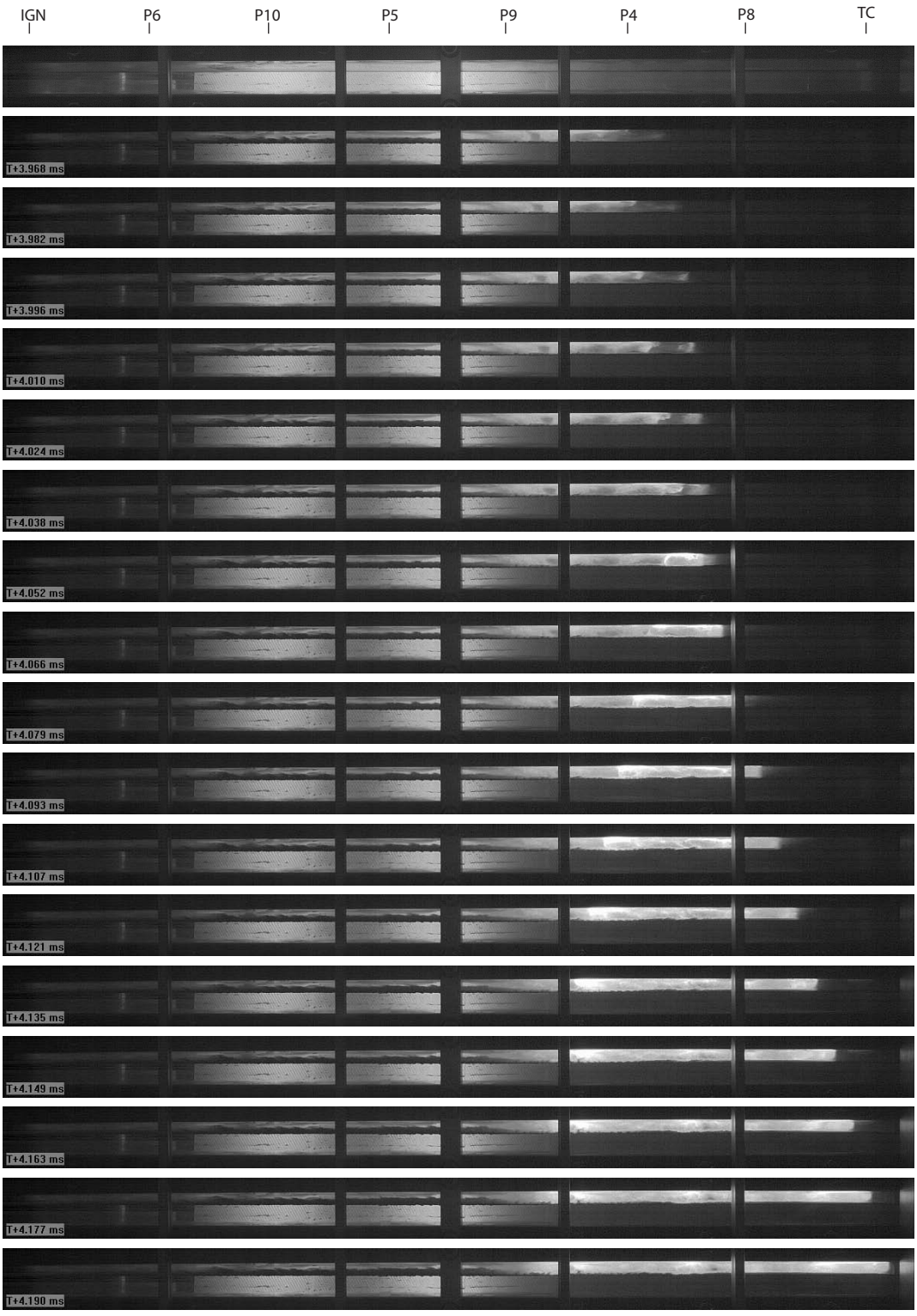

Figure 45: Sequential frames between 3.954 and 4.190 ms from the visualization of shot 18. Time increases from top to bottom in increments of 13.88 μs. Top image is test section with water before the shot.

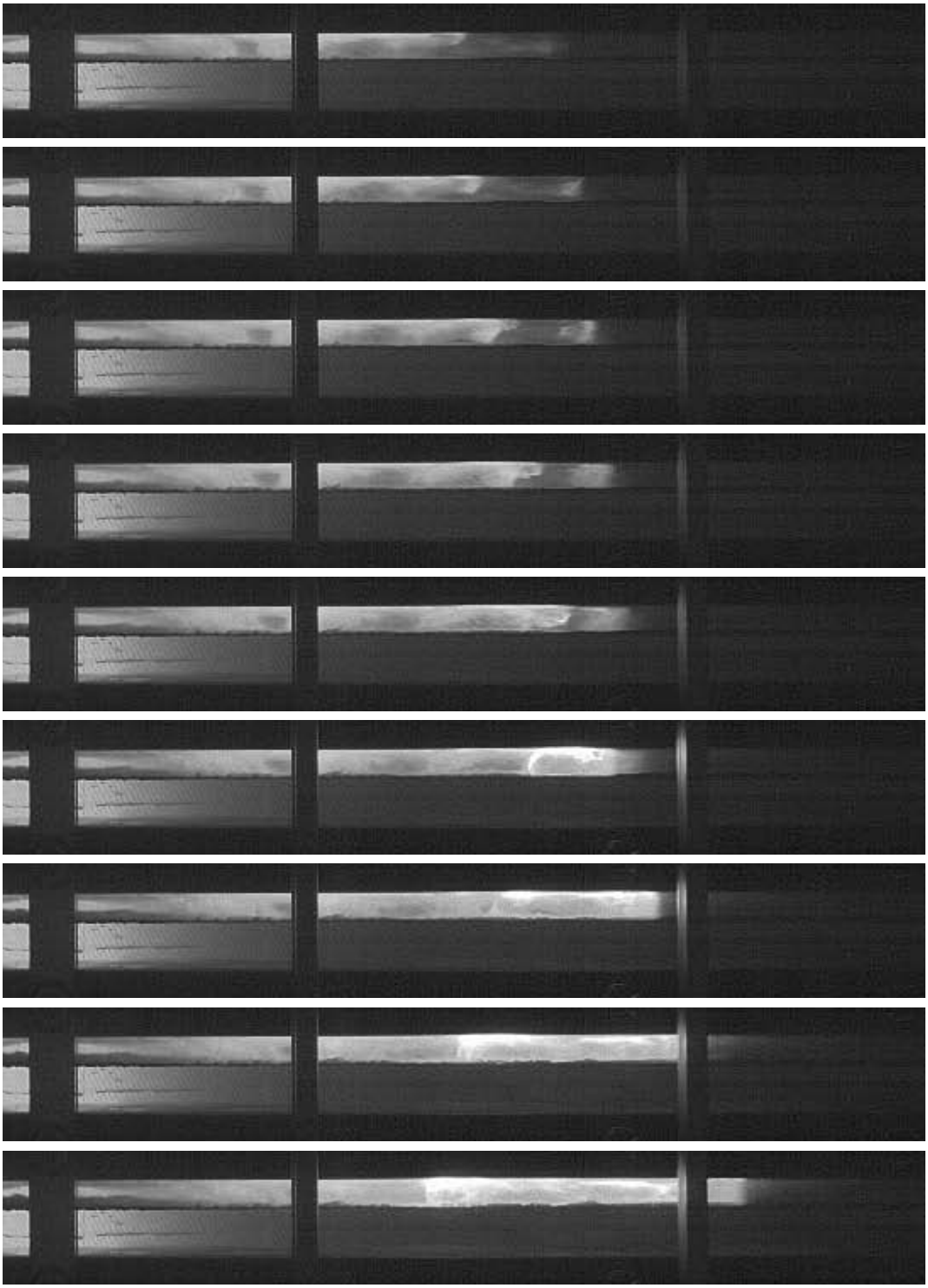

Figure 46: Sequential frames showing enlarged view between 3.982 and 4.093 ms from the visualization of shot 18. The DDT event occurs between 4.038 and 4.053 ms. Time increases from top to bottom in increments of 13.88 μs.

4.4 Shot 19

This test was carried out a with water depth of about 1.55–1.65 in (gas layer of 0.35-0.45 in) and ignition with the miniature spark plug in port 8T. Pressure transducers P1, P3, and P11 were located beneath the water layer. The pair P3 and P4 are at the same axial location below and above the water. From the pressure histories, Fig. 47, transition to detonation appears to occur at 3.316 ms, between transducer P9 and P4, 32–40 in (0.81–1.02 m) from the ignition location. The is slightly sooner than in shot 18, consistent with transition location scaling proportional to the gas layer height.

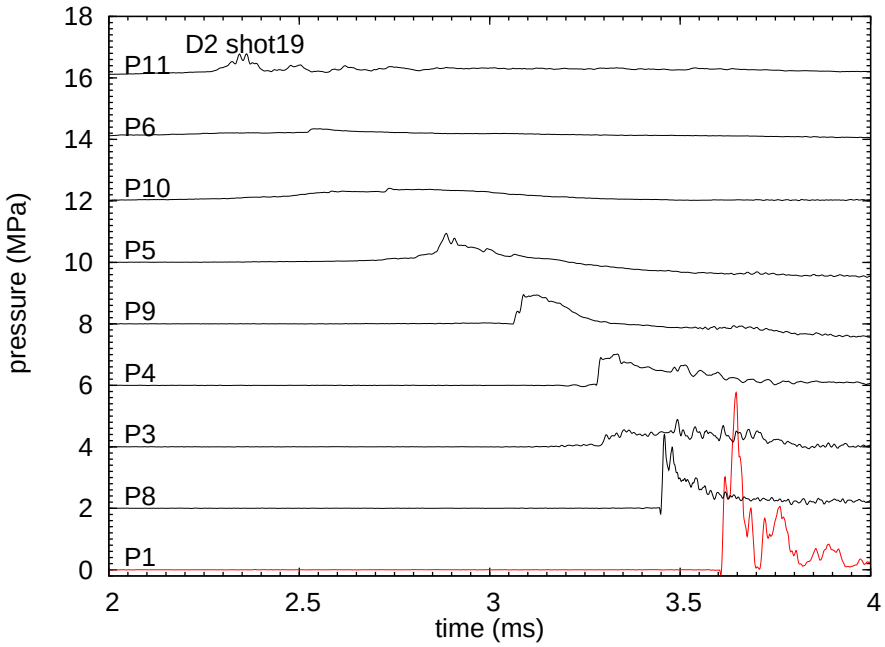

Figure 47: Shot 19 filtered and baseline corrected pressure-time histories showing DDT event.

Table 11: Video settings for shot 19

horizontal field of view	63 in
exposure time	2 microsecond
interframe time	13.88 microsecond
DDT time	3.303 ms , 237 frame
wave reaches end of channel	3.469 ms, 249 frame
visible flame	3.192 ms, 229 frame
resolution	1200 × 80
Notes:	back lighting with diagonal striped screen

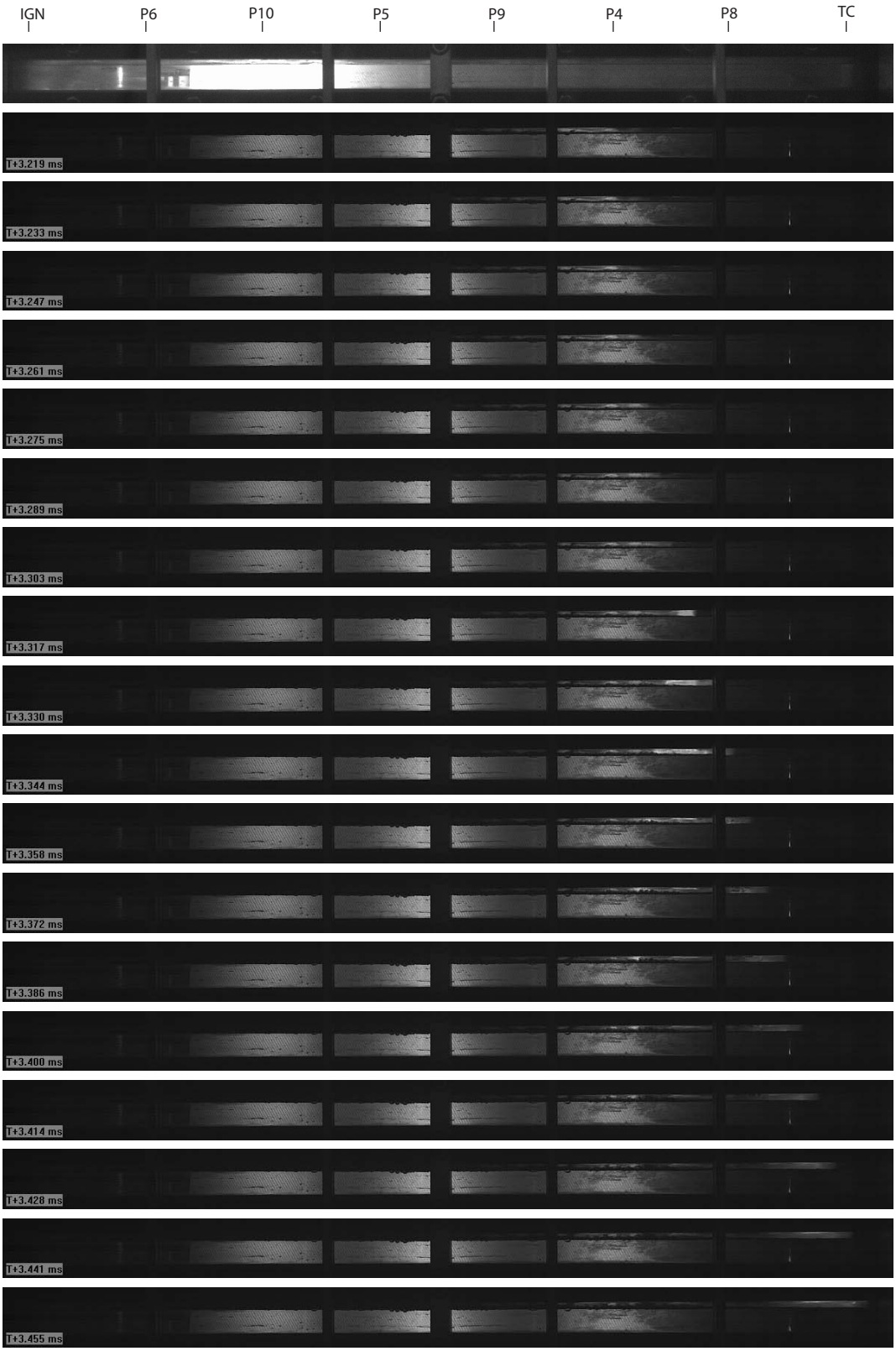

Figure 48: Sequential frames between 3.205 and 4.455 ms from the visualization of shot 19. Time increases from top to bottom in increments of 13.88 μs.

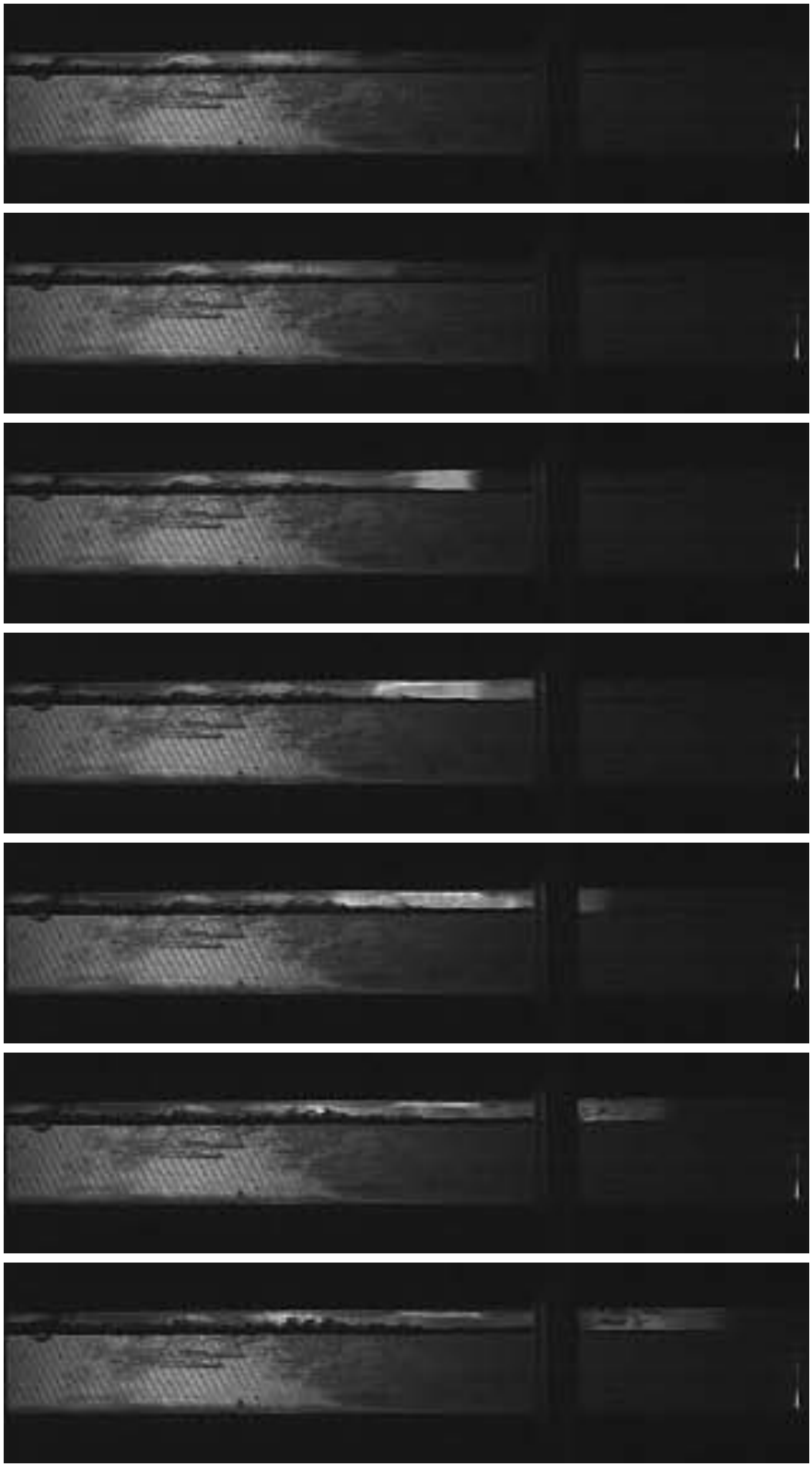

Figure 49: Sequential frames showing enlarged view between 3.219 and 3.455 ms from the visualization of shot 19. The DDT event occurs at about 3.303 to 3.316 ms. Time increases from top to bottom in increments of 13.88 μs. The top image was taken after water filling but prior to ignition.

4.5 Shot 20

This test was carried out a with water depth of about 1.85–1.90 in (gas layer height of 0.10-0.15 in) and ignition with the miniature spark plug in port 8T. This was the thinnest gas layer that was tested. Pressure transducers P1, P3, and P11 were located beneath the water layer. The pair P3 and P4 are at the same axial location below and above the water. From the pressure histories, Fig. 50, transition to detonation may occur between transducer P9 and P4, 32–40 in (0.81–1.0 m) from the ignition location, however the onset is not as distinct as in shot 19. In fact, it is not clear if DDT actually took place and the combustion wave in the latter half of the chamber appears to be a high-speed flame or quasi-detonation.

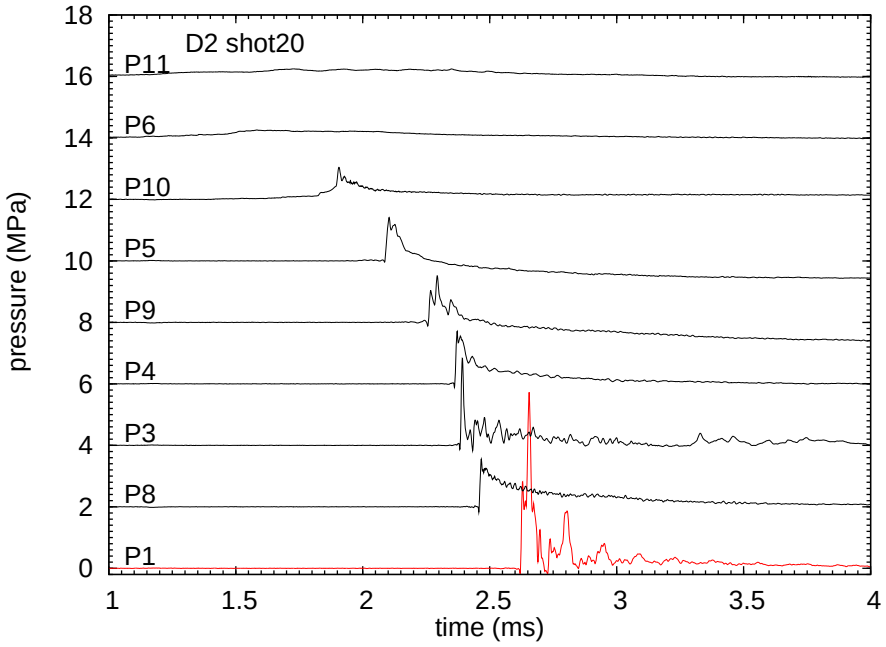

Figure 50: Shot 20 filtered and baseline corrected pressure-time histories showing DDT event.

A 25 mm wide-angle lens and back lighting with flash lamps was used with the high-speed video camera to obtain a visualization of the entire DDT process. The field of view of the camera was the entire test section length, 63 in. The rectangular obstruction at the center of the field of view is a reinforcing bar located at 31.5 in. Additional smaller vertical obstructions correspond to the C-clamps restraining the top and bottom of the channel. The time period covered by these frames is 2.184 to 2.448 ms. During this time, the luminous front appears to propagate at a speed of about 1600 m/s.

Table 12: Video settings for shot 20

horizontal field of view	63 in
exposure time	2 microsecond
interframe time	13.88 microsecond
DDT time	2.198 ms, 158 frame
	not a sharp transition, more like gradual acceleration
	unclear if DDT actually took place.
wave reaches end of channel	2.475 ms, 178 frame
visible flame	1.906 ms, 137 frame
resolution	1200×80
Notes:	back lighting with diagonal stripe screen
	oblique waves visible in water
	wave speed constant over last half of channel

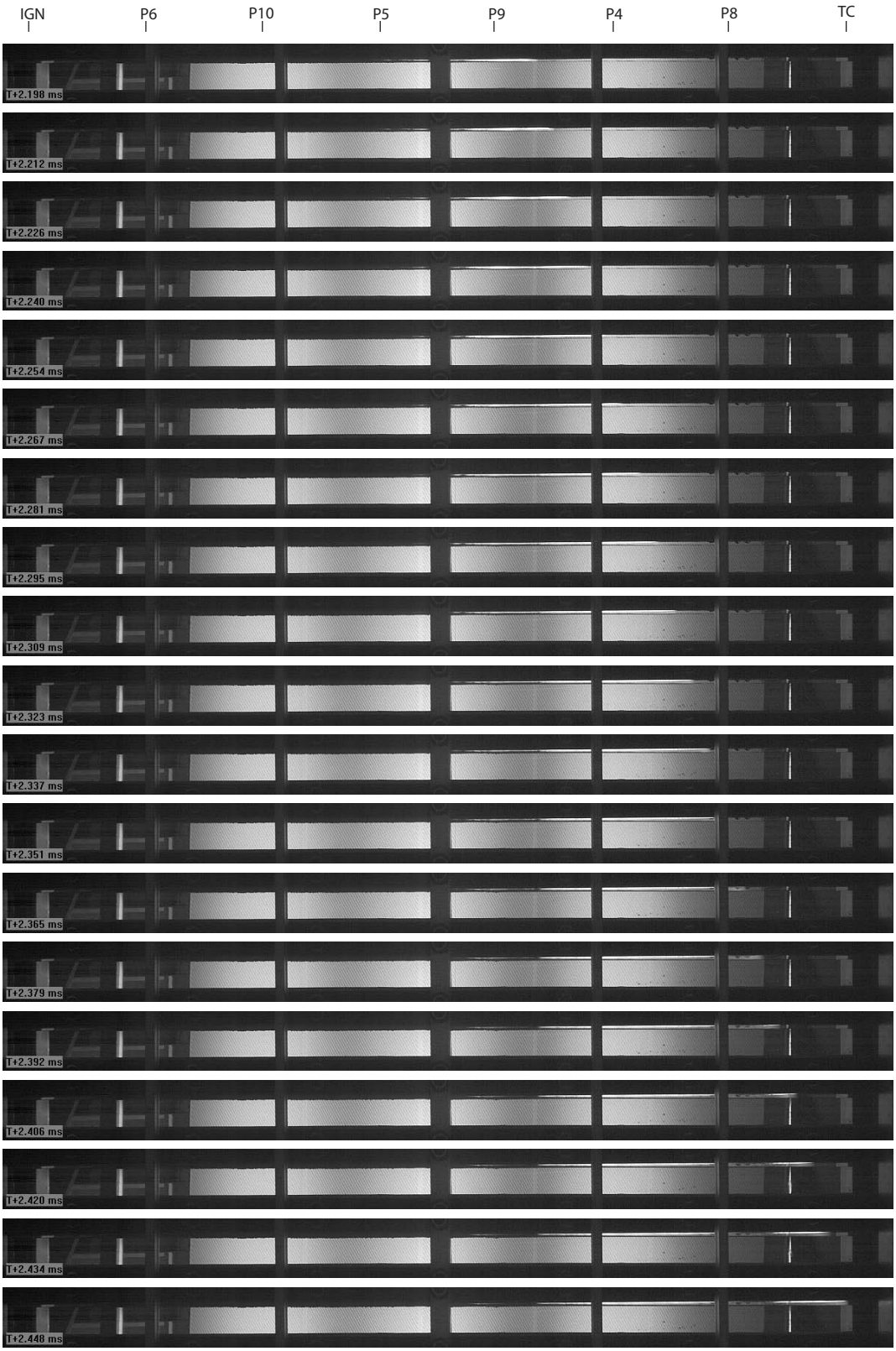

Figure 51: Sequential frames between 2.198 and 2.448 ms from the visualization of shot 20. Time increases from top to bottom.

4.6 Shot 21

This test was carried out a with water depth of about 1.70-1.75 in (gas layer height of 0.25–0.30 in) and ignition with the miniature spark plug in port 8T. The water depth was reduced slightly from that of shot 20 in order to assure that DDT would take place.

An 85 mm telephoto lens on the high-speed video camera was used to capture a close up of the transition event. Pressure transducers P1, P3, and P11 were located beneath the water layer. The pair P3 and P4 are at the same axial location below and above the water. From the pressure histories, Fig. 52, transition to detonation appears to occur between transducer P9 and P4, 32–40 in (0.81–1.02 m) from the ignition location, similar to shot 19.

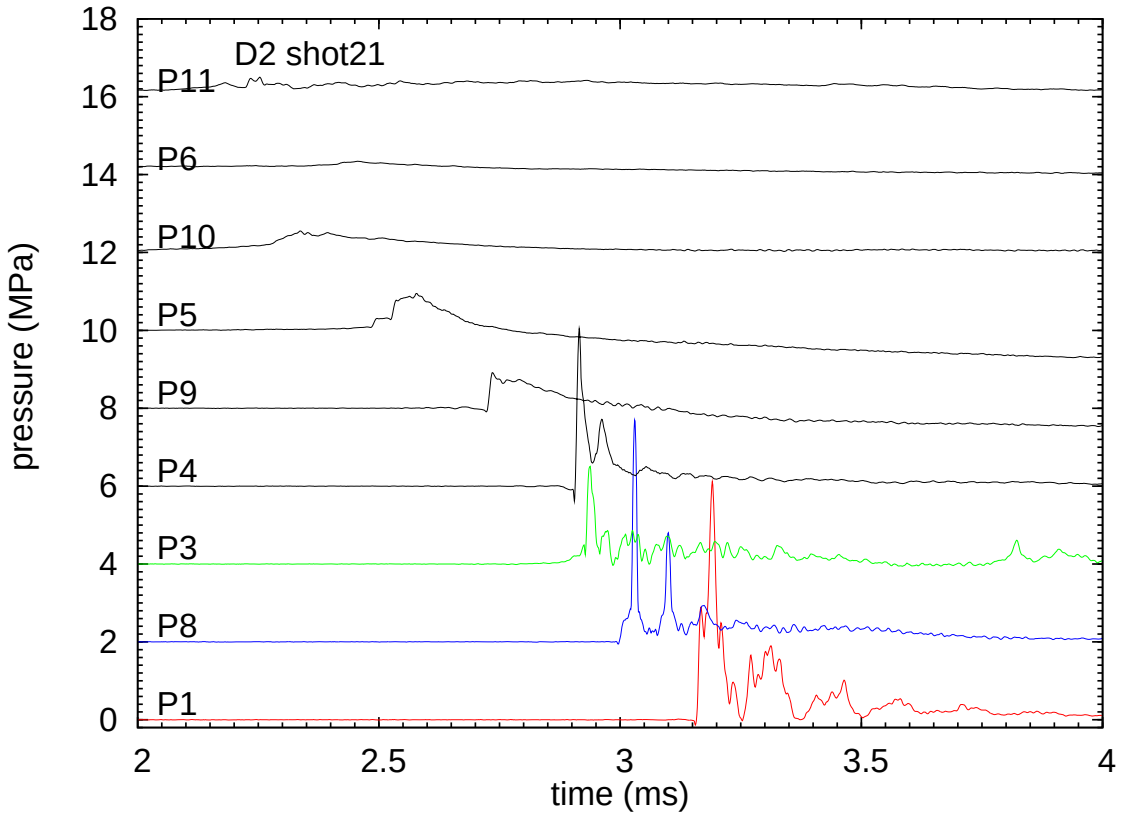

Figure 52: Shot 21 filtered and baseline corrected pressure-time histories showing DDT event.

A close-up view of the transition event was obtained using the high-speed video with 15.38 μs between frames and an exposure time of 0.31 μs. The test section was back lit using flashlamps and a transparent screen with diagonal ruling was used to aid in visualizing weak disturbances in the water. Selected frames are shown in Fig. 53. These frames span a time from 2.683 to 2.990 ms (outlined in red in Fig. 52) with a field of view that is just slightly higher than the 2-in height of the transparent area of the test section and a width of about 8.5 in. The gas layer is at the top of the frame and the leading edge of the combustion wave or shock front enters from the left-hand (west) side and travels to the right (east).

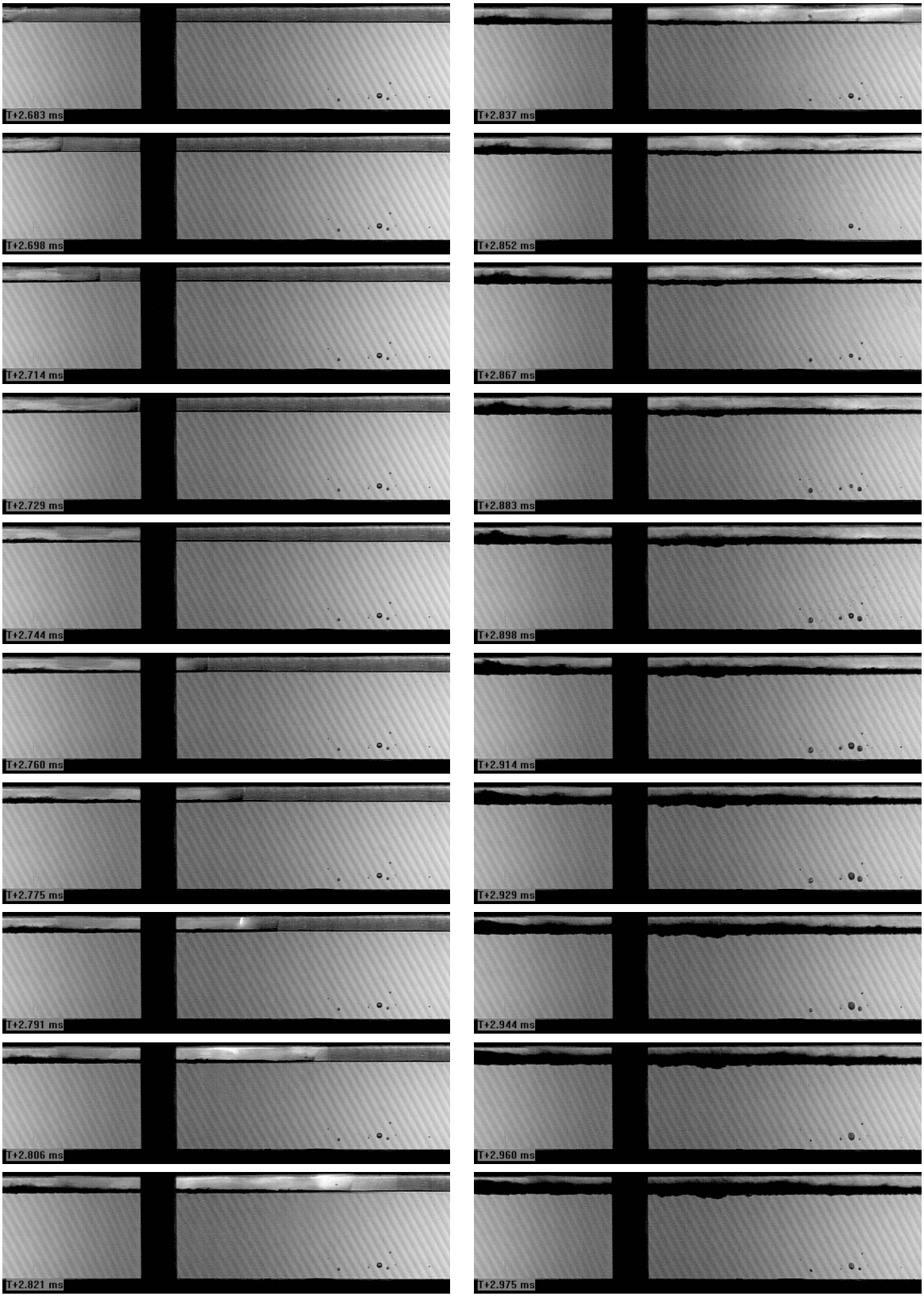

Figure 53: Sequential frames from 2.683 to 2.975 ms for the visualization of shot 21. Time increases from top to bottom, and left to right, 15.38 μs interval between frames.

The leading edge of this disturbance appears to propagate at speed of about 1400 m/s until transition starts with a localized high-luminosity event at 2.791 ms. For reference, a shock wave traveling at 1400 m/s will produce a pressure jump of about 2 MPa. A wave traveling at 1400 m/s is slightly subsonic so that the pressure waves in the water will be moving slightly faster than the wave in the gas. The actual magnitude of the leading shock wave at P9 is about 1 MPa and increases to almost 10 MPa at P9. After the transition, the leading front accelerates and rapidly runs out ahead of the luminous region with a speed between 1800-2400 m/s and is gone out of the field of view by 2.852 ms. At 2.821 ms, a oblique shock is clearly visible extending into the water from the leading front, an enlarged view of this is shown in Fig. 54. The shock wave makes an angle of 40° with respect to the water surface, which as discussed below corresponds to the shock speed of about 2330 m/s, about 11% higher than the CJ speed of 2088 m/s. This is a typical result of a DDT event (Ciccarelli and Dorofeev, 2008), an overdriven detonation that decays as it moves into the undisturbed reactants.

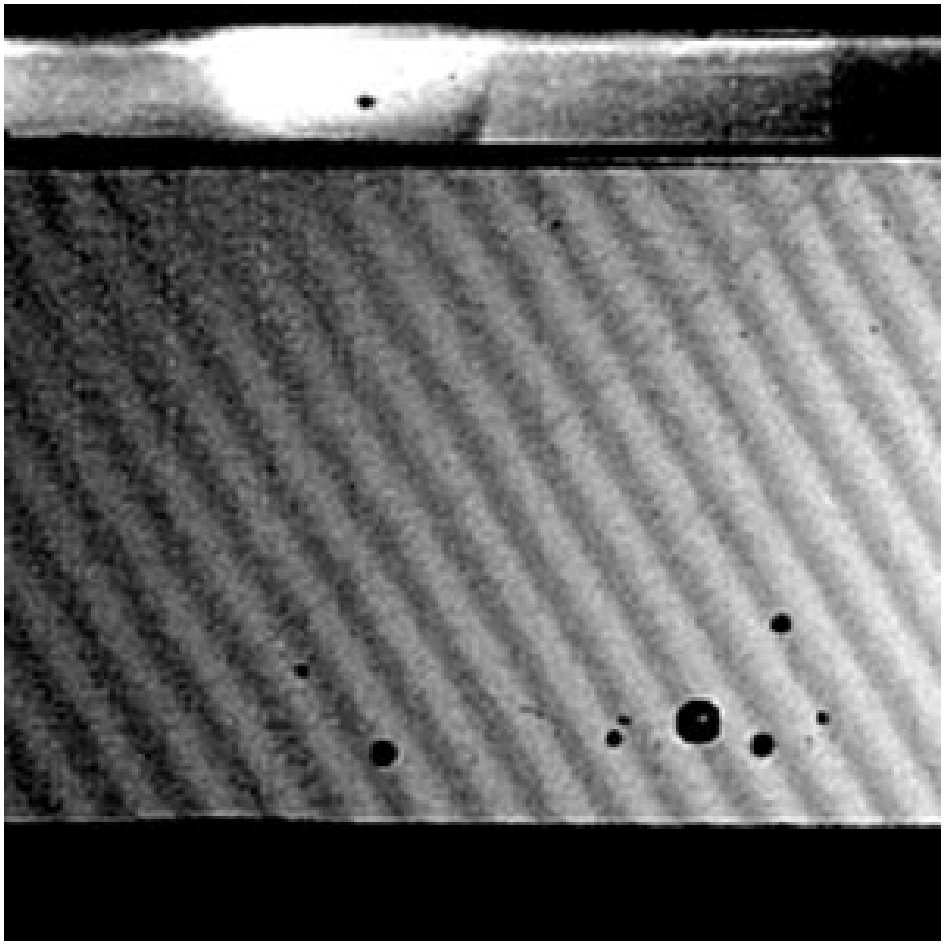

Figure 54: Close-up of frame at 2.821 ms showing oblique shock wave in water.

Based on these observations and the physics of wave interactions, a simplified picture (Fig. 55) of the wave pattern can be deduced for a constant speed shock or detonation front

in the gaseous layer. A nearly planar shock or detonation wave D propagates through the gas layer, creating an oblique shock T in the water which reflects as a shock R from the bottom of the channel, propagates as an oblique wave back to the free surface where it reflects as an expansion E_1 and returns as an oblique wave to the bottom of the channel, reflecting to form another oblique expansion E_2. If the reflection is sufficiently strong and enough tension is created in the liquid, then cavitation may occur on either the free surface or at the bottom of the channel. The wave angle can be computed with the Huygens' construction to obtain $\theta = \sin^{-1}(c/U)$. For a detonation with $U = 2088$ m/s and $c = 1500$ m/s, $\theta = 45.9°$.

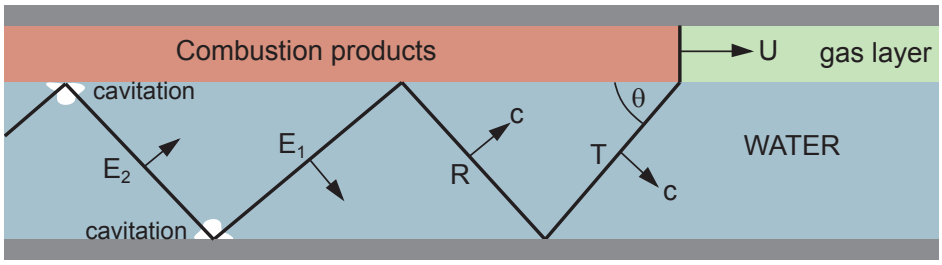

Figure 55: Idealized wave pattern resulting from shock or detonation wave moving at speed $U > c$, the sound speed in water.

A wedge-shaped darkened region is visibly growing at the free surface of the water after the wave has passed. This is water that has been lofted into the gas layer in the form of fine droplets and strongly scatters light. The lower surface of this wedge appears to coincide with the original free surface of the water for some distance (25-50 mm) behind the wave front. The height of the dispersed water layer has grown to about 0.15 in (3.8 mm) about 300 μs (200 mm) after the wave has passed by. However, immediately behind the wave, for at least 10–30 mm, there is little or no dispersed water visible. Since the thickness of the flame or detonation is less than 0.1 mm, the dispersion is too slow to directly affect the combustion process by heat transfer.

Heat transfer to the water from the hot combustion products may indirectly influence the combustion wave propagation but this will happen far downstream of the front. Heat transfer will cool the combustion products making them more dense and vaporization of the water will also occur, adding mass to the gas layer. These two competing effects will result either creating expansion or compression waves in the burned gas downstream of the front. These waves can catch up to the combustion wave and possibly influence the propagation rate. At sufficiently long times, Fig. 56, cavitation is observed within the water, this appears to take place on the polycarbonate windows and the bottom of the test section. The windows and test section are quite flexible so that the motion of these components may contribute to the cavitation along with the wave processes in the water and gas.

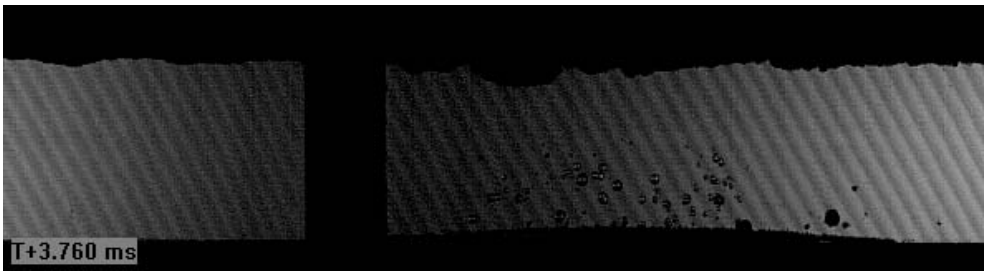

Figure 56: Close-up of frame at 3.760 ms showing cavitation on the side walls, on the bottom channel, as well as the highly disturbed water surface with dispersed water filling the original gas layer.

Table 13: Video settings for shot 21

horizontal field of view	8.5 in
exposure time	0.31 microsecond
interframe time	15.38 microsecond
DDT time	2.790 ms, 181 frame
	Bright spot, followed by "bubble' in next frame
wave reaches end	2.837 ms, 184 frame
	detonation (?) followed by luminous region
visible flame	2.683 ms , 174 frame
	Enters at left
resolution	592×160
Notes:	back lighting with diagonal stripe screen
	oblique waves visible in water
	wave speed constant over last half of channel

4.7 Discussion of D2 Testing

Tests without water Testing without a water layer (shots 16 and 17) demonstrated that DDT could take place in a 2 × 3 in channel 60 in long. When the igniter was located centrally at the W end of the channel, a strong "pressure piling" effect[2] was observed with DDT occurring in compressed gas adjacent to the end of the tube opposite the igniter. The resulting pressure peak was 5 times higher than the ideal shock pressure from a reflected CJ detonation. Moving the igniter 4.25 in from the end of the channel to the top resulted in a 25% decrease in the run-up distance and substantially reduced the pressure piling effect. The consequences of pressure-piling and the peak pressures due to DDT events are clearly quite sensitive to the details of the explosion process.

Tests with water Introducing a layer of water into the channel did not quench the combustion process or prevent flame acceleration even with gas layers as thin as 0.10–0.15 in (2.5–3.8 mm). Transition to detonation either did not occur or was very marginal with the thinnest layer (shot 20) of gas. This is reasonable since the layer thickness was comparable to the detonation cell width (3-6 mm) in that case. In the cases with thicker gas layers, shots 18, 19, and 21, transition to detonation was observed. The water layer had the the effect of moving the transition point closer to the igniter but the peak pressures were decreased in comparison to the shot 17 without water.

Dispersion The water is dispersed in the form of a mist or fine droplets and fills a 0.25 in (6 mm) gas layer within 0.3–04 ms after the wave passes. However, immediately behind the wave, for at least 10–30 mm, there is little or no dispersed water visible. Since the thickness of the flame or detonation is less than 0.1 mm, the dispersion is too slow to directly affect the combustion process within the flame or detonation by heat transfer. This does not mean that there is no influence of the water free surface, just that it is more subtle than direct quenching of the combustion process. Evaporation behind the flame or detonation will produce pressure waves that may catch up to and influence the combustion front, momentum transfer to the dispersed water and propagation of acoustic waves in the water layer will also create fluid motion that can affect the front. The dispersed water does appear to significantly attenuate the shock waves created by DDT or detonation reflection from the ends of the test chamber. The result is that in the tests with a water layer, the peak pressures observed upstream of the ignition event in a tube without water are substantially reduced or eliminated in the tests with a water layer.

Peak pressures Peak pressures in the tests with a water layer are comparable (Fig. 57) to those in tests without a layer *except* for regions near the end of the tube. Without a water layer, the pressure at the end opposite ignition was between 2–5 $P_{CJ,r}$ in shots 16 and 17. With a water layer, the peak pressure was on the order of $P_{CJ,r}$ in shots 18, 19, 20, and 21. A strong reflected shock wave $P_{CJ} < \Delta P < P_{CJ,r}$ was observed near the ignition end in tests 16 and 17 but were absent in the tests with water.

[2]Referred to as the PRC-DDT situation in the HPAV analysis community Lachmann and Minichiello (2010).

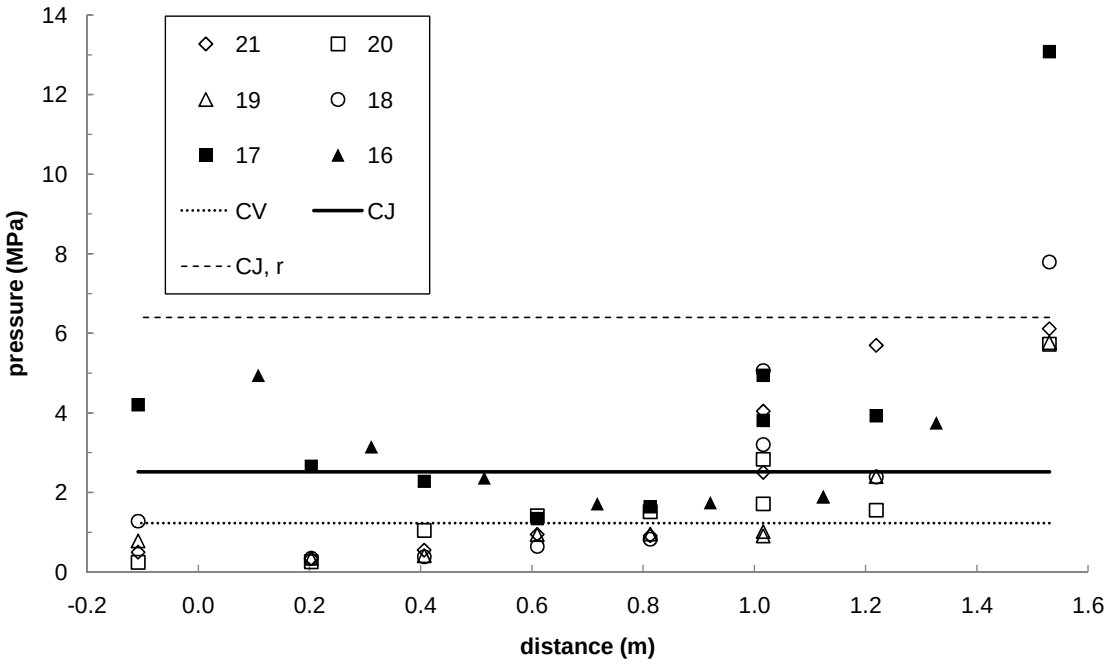

Figure 57: Peak pressures ΔP_{max} as a function of distance from the igniter for shots 16-21. The peak pressure at P1 transducer was 32 MPa and is not shown on this plot.

5 D4 Results

Three tests were carried out in a horizontal segment of 2-in diameter Schedule 40 pipe which was constructed by cutting a segment from the SS1-3 piping (See Shepherd and Akbar, 2009b) to create a 60-in long specimen with ports for instruments and other fittings, see Fig. 59, the detail drawings in Appendix A, and Table 24 in Appendix H. The specimen had 9 bonded strain gages (Vishay CEA09250UN-350/P2) mounted at three axial locations as shown in Fig. 59 and oriented to measure hoop strain. A photograph of the test section installed in the test cell is shown in Fig. 58.

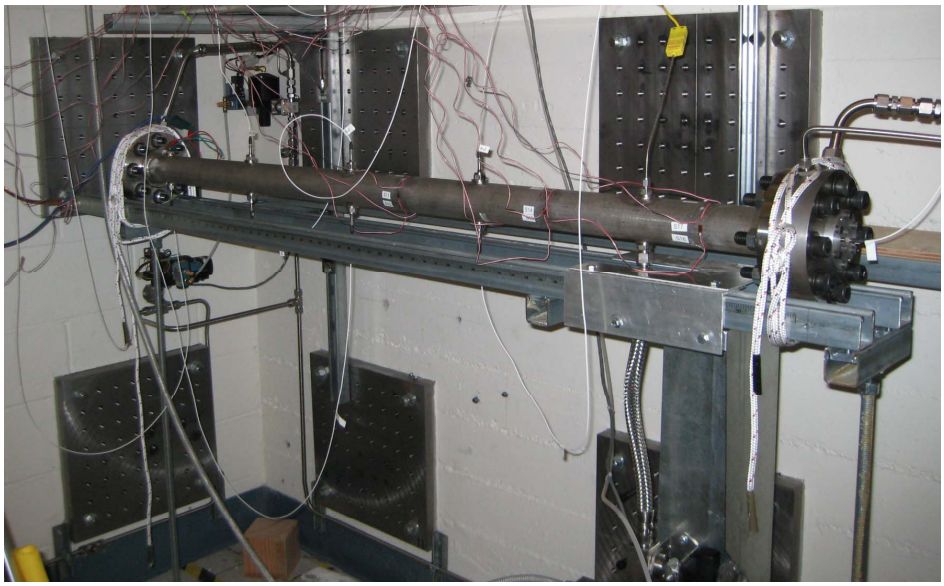

Figure 58: Photograph of D4 specimen as installed in test cell; west end is on left, east on right.

The gages were connected to Vishay 2310B amplifiers operated with the wide-band setting (150 kHz 3-db point) and digitized through main data acquisition system. The strain gages were mounted on the top, side and bottom of the pipe; 0, 90 and 180 deg measuring clockwise from the top of the pipe and looking from east to west. Piezotronics 133B22 piezoelectric pressure gages were mounted in end flanges and in 7 ports on the top and bottom of the tube as shown in Fig. 59. The signals were processed through Piezotronics 481A signal conditioners and digitized by the main data acquisition system. Typically 100 ms of data were recorded with a 1 MHz sampling rate. Trigger for spark discharge was 100 μs after $t = 0$. The first 15 ms of raw data for each shot are presented in Appendix H.

Water was introduced through the port "L" after the gas mixture was prepared and mixed within the pipe. The gas mixture was at a lower pressure than ambient and the water was located in a carboy about 4 ft about the pipe. When the valve V10 isolating the carboy from the pipe was opened, water was pulled into the bottom of the pipe. The pressure in the gas was monitored during the filling process and the valve V10 was closed when the desired final pressure of 1 atm (760 Torr) was reached. The amount of water used in shots 23 and 24 was determined by the method of measuring the initial P_i and final (after water addition)

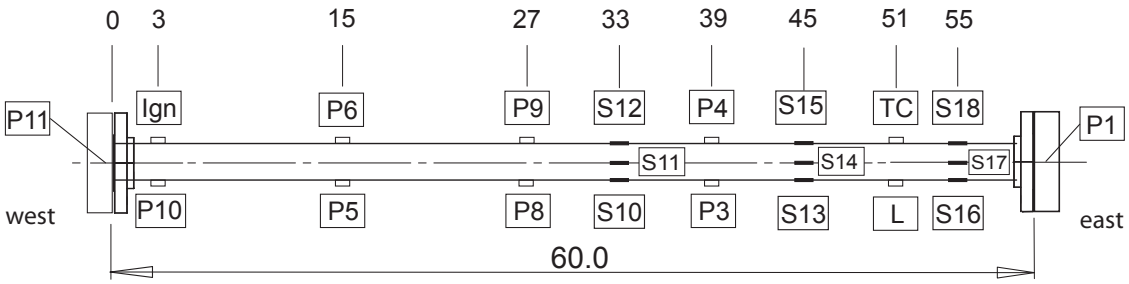

Figure 59: Port assignments and locations for D4 testing. Dimensions are given in inches from the reference location of the pipe flange surface on the W end.

P_f gas pressure and using the gas law $PV = nRT$ together with analytic geometry to find the final gas volume V_2' given the initial volume V_2 of the test chamber pipe.

$$V_2' = \frac{P_i}{P_f}\left(V_1 + V_2 + V_3\right) - V_3 \tag{1}$$

In doing so, the volume of the water filling lines V_1 and gas lines V_3 has to be accounted for since these contribute to the initial gas volume. The gas filling lines are connected at the top of the flanges at each end of the pipe so these will also contribute to the final gas volume. The nominal free volume V_2 of the piping segment is determined by the distance L_2 = 61.625 between the pressure transducer mounting plugs inner surface for P1 and P11. This is slightly longer than the 60 in pipe length since the pressure transducers are recessed within the gas handling flanges attached to the ends of the pipe. The nominal inside diameter of the pipe is $2R = 2.03$ in. The volume $V_2 = \pi R^2 L_2 = 199$ in^3 or 3268 cc.

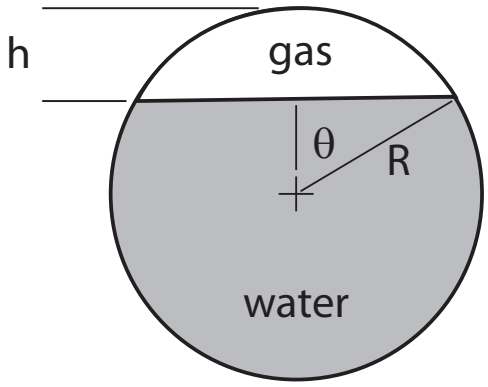

Figure 60: Geometry used for liquid filling computation in D4 shots 23 and 24.

The geometry of Fig.60 can be used to compute the cross-sectional area of the gas volume

$$A_2' = R^2\left(\theta - \cos\theta \sin\theta\right) \ , \tag{2}$$

and the height of the gas layer.

$$h = R\,(1 - \cos\theta) \tag{3}$$

The hydraulic diameter of the gas volume is

$$d_h = 2R\left[\frac{\theta - \cos\theta\sin\theta}{\theta + \sin\theta}\right] \ . \tag{4}$$

The volume V_2' is computed from (1), the measured pressures. and estimated volumes V_1 and V_3. The area ratio

$$A_2'/A_2 = V_2'/V_2 \tag{5}$$

$$= \left[\frac{\theta - \cos\theta\sin\theta}{\pi}\right] \tag{6}$$

is found using the SOLVER in Excel to find θ in order to compute h and d_h. The ratio $h/2R$ is for a wide range of area ratios, nearly a linearly function as shown in in Fig. 61.

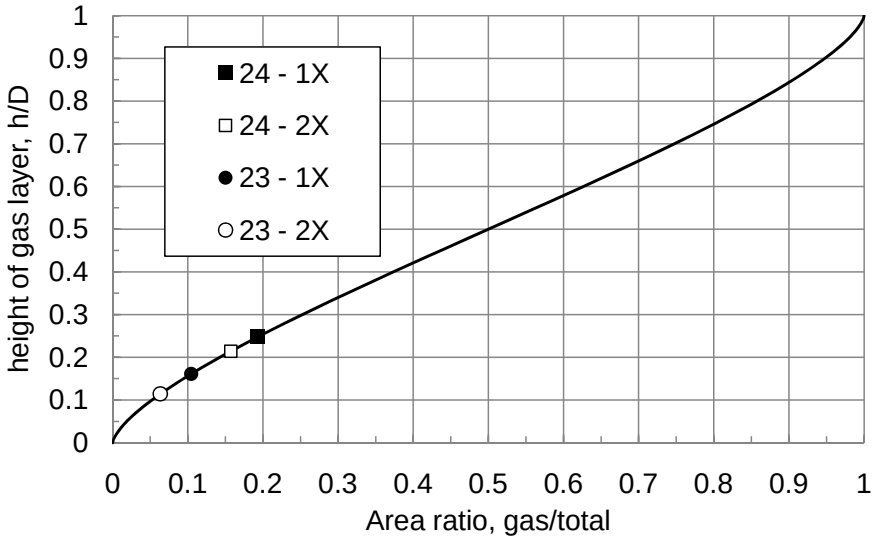

Figure 61: Normalized gas layer height as a function of cross-section area ratio (gas-to-total) in the pipe.

Sources of uncertainty include absorption of the N_2O by water (it is highly soluble) and underestimation of volumes of the water and gas filling lines. Although the Henry's Law coefficient is quite high for N_2O in water, the exposure time of the water to the gas is small (less then 5 min) before the shot and no noticeable drop in gas pressure was observed during this time so this effect is neglected. The line volume estimates, V_1 = 2.76 in^3 (45.2 cc), V_3 = 10.0 in^3 (165 cc), are particularly uncertain since these contain sections of bellows tubing which has a larger but unknown volume compared to hard tubing of the same nominal diam-

eter To bound the height of the water, computations were performed with both the nominal line volume (case 1X) and twice (case 2X) that value. The results of the computations are shown in Fig. 61 and in Table 14.

Table 14: Analysis of water levels for shots 23 and 24.

Case	θ (rad)	h (in)	h/D	A_2'/A_2	d_h (in)	V_{water} (cc)
	Shot 23 $P_i = 111$ Torr $P_f = 763$ Torr					
1X	0.826	0.327	0.161	0.104	0.426	2971
2X	0.690	0.232	0.114	0.0633	0.304	3151
	Shot 24 $P_i = 174$ Torr $P_f = 761$ Torr					
1X	1.042	0.503	0.248	0.193	0.646	2682
2x	0.963	0.435	0.214	0.157	0.562	2844

5.1 Shot 22

Shot 22 was carried out with no water inside the tube as a reference for shots 23 and 24. Ignition was from the miniature spark plug in the top port at the west end of the chamber as indicated by the "I" in Fig. 59. The pressure and strain data during the DDT event are shown in Fig. 62. The traces are arranged so that the instruments closest to the ignition point (E end) are at the top and distance from ignition increases from top to bottom (W end). The RTV coating on gage P11 had deteriorated at this point in the testing and the pressure signal shows a negative drift superposed on a series of shock waves created by the DDT event; all other signals show no signs of thermal or vibration artifacts.

As indicated by both the pressure and strain traces, DDT occurs between 24 and 31 inches (610-788 mm) from the ignition point. This corresponds to a scaled transition distance of 12 $\ell < \ell/D < 16$, roughly midway between the ends of the pipe. By comparison, the DDT testing in the 5.7 m long ES1 specimen (Shepherd and Akbar, 2009b) showed that the transition distance for this mixture was between 1300 and 2000 mm, and Bollinger et al. (1962) found an average transition distance of 1900 mm in a 79 mm diameter, 10 m long smooth tube. In this case, decreasing the length of the pipe to 1.5 m resulted in decreasing the DDT distance by a factor of 2–3 over the long pipe results. This effect is probably due to the increase of flame surface area associated with the formation of "tulip" shaped flames and shock-wave flame interaction, as discussed by Ciccarelli and Dorofeev (2008).

The pressure signal pairs P5-P6, P8-P9, P3-P4 show that the transition process results in similar pressure waves on the top and bottom of the pipe. The shock waves propagating E to W and preceding the DDT event are clearly visible on P5-P6 and P8-P9 as is the reflected shock wave propagating from W to E. The hoop strain shows the characteristic breathing

mode oscillation on all the strain gages. The peak amplitude is over 500 μstrain closest to the transition point and 300 μstrain downstream, consistent with the observations in the ES1 DDT testing Shepherd and Akbar (2009b).

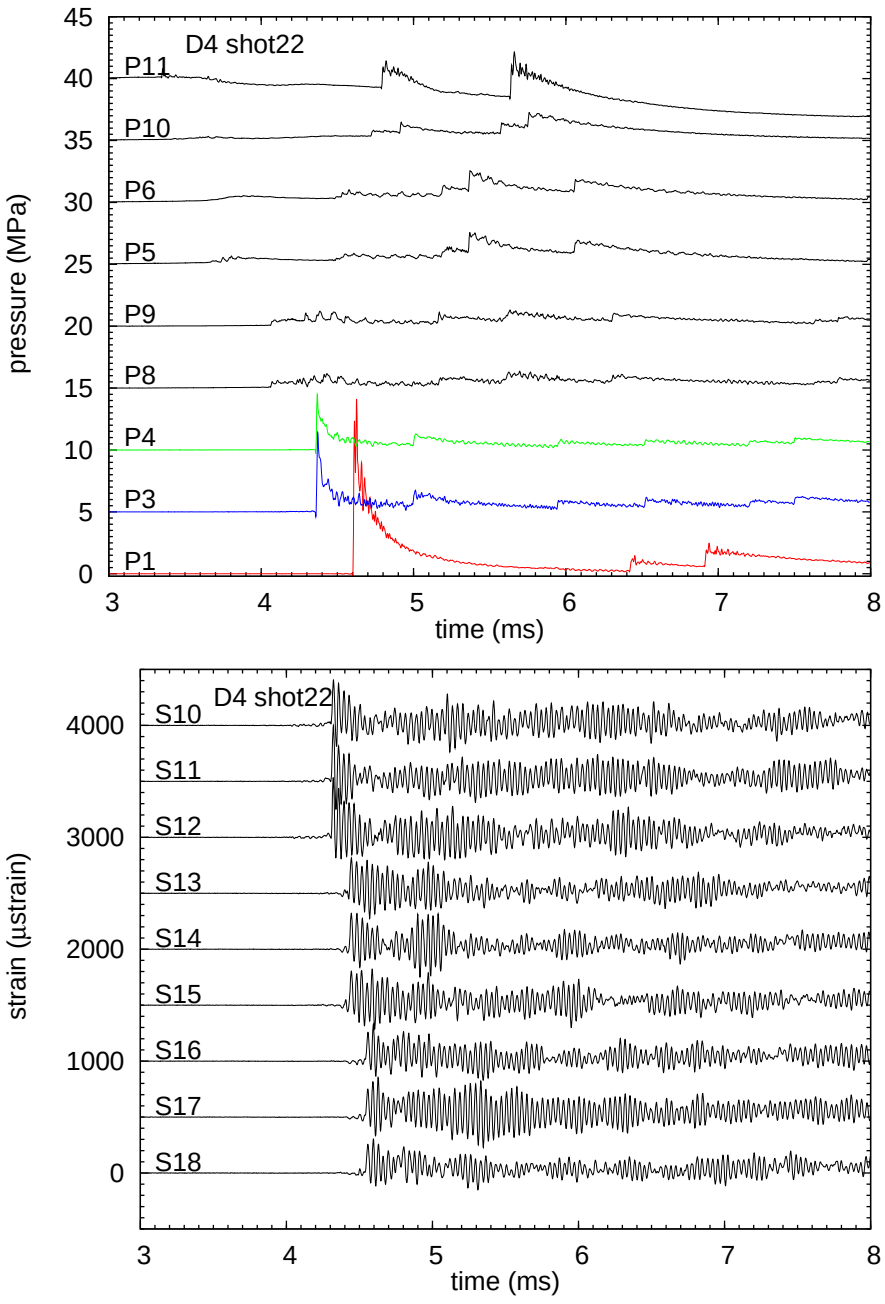

Figure 62: Enlarged view of pressure and strain data from shot 22. Filtered to remove noise about 50 kHz, baseline corrected, and removed ignition transient artifact from strain signals.

5.2 Shot 23

In this shot, the initial pressure of the H_2-N_2O mixture was set at 111 Torr before water addition and 763 Torr afterwards. According to the bounding computations described in the introduction to this, this resulted in a gas layer height of $0.23 < h < 0.33$ inch, slightly smaller than the target of 0.375 inch. A check on the water addition was performed by capturing the water removed from the chamber after the shot, a total of 3100 cc was recovered which is bounded by the 1X and 2X case values of 2971 – 3151 cc.

The pressure and strain signals (Fig. 63 show that although combustion took place and a substantial compression wave developed by gage location P3-P4, transition to detonation did not take place. The peak strains were 33–90 μstrain, which are between the CV and CJ reference values for a dynamic load factor of 1. These strains are a factor of 5 to 10 smaller than obtained in shot 22 in which DDT did occur. The strain gages S10, S13, and S16 were at the bottom of the pipe, S11, S14, and S17 were on the side, and S12, S15, and S18 were on the top. There does not appear to be a significant systematic difference between the peak values depending on the location relative to the water surface.

Pressure gages P10, P5, P8, and P3 were at the bottom of the pipe and submerged in the water, as were the two gages on the end P1 and P11. Shock waves in the gas (P8, P9, P4) have sharp fronts that lag behind a more diffuse pressure wave in the water that runs ahead of the gas shock. This is visible when comparing gages P8 and P9 as well as P3 and P4 On all gages except P1, the peak pressures are between 0.4–1.4 MPa, comparable to or less than the CV explosion pressure rise of 1.23 MPa. At these pressures, the waves in the water are acoustic and nonlinearity is relatively unimportant so that smooth compression waves will not steepen into shocks. However, in the gas, the pressures are high enough that nonlinearity is important and compressions will steepen into shocks, this is what is observed.

5.3 Shot 24

This shot was a repeat of shot 23 with a smaller amount of water in order to obtain conditions more favorable for DDT. In this shot, the initial pressure of the H_2-N_2O mixture was set at 174 Torr before water addition and 761 Torr afterwards. According to the bounding computations described in the introduction to this, this resulted in a gas layer height of $0.43 < h < 0.50$ inch, almost twice as large as in shot 23. A check on the water addition was performed by capturing the water removed from the chamber after the shot, a total of 2825 cc was recovered which is bounded by the 1X and 2X case values of 2682 – 2844 cc. Note that in both shot 23 and 24, the recovered amount of water is consistent with the 2X case.

The pressure and strain signals (Fig. 63 show that transition apparently occurred after the compression wave reflected from the E end of the pipe, resulting in a peak pressure over 7 MPa on P1. Although shock wave precursors can be observed on P5-P6 and P8-P9, there is no significant signal due to a reflected shock wave propagating from W to E. In addition, the strain signals show a peak amplitude of between 23 and 92 μstrain with only S18 showing significant hoop oscillations. This indicates that the detonation was within a small gas volume close to the E end and the resulting shock wave rapidly decayed due to the small extent of the high pressure region.

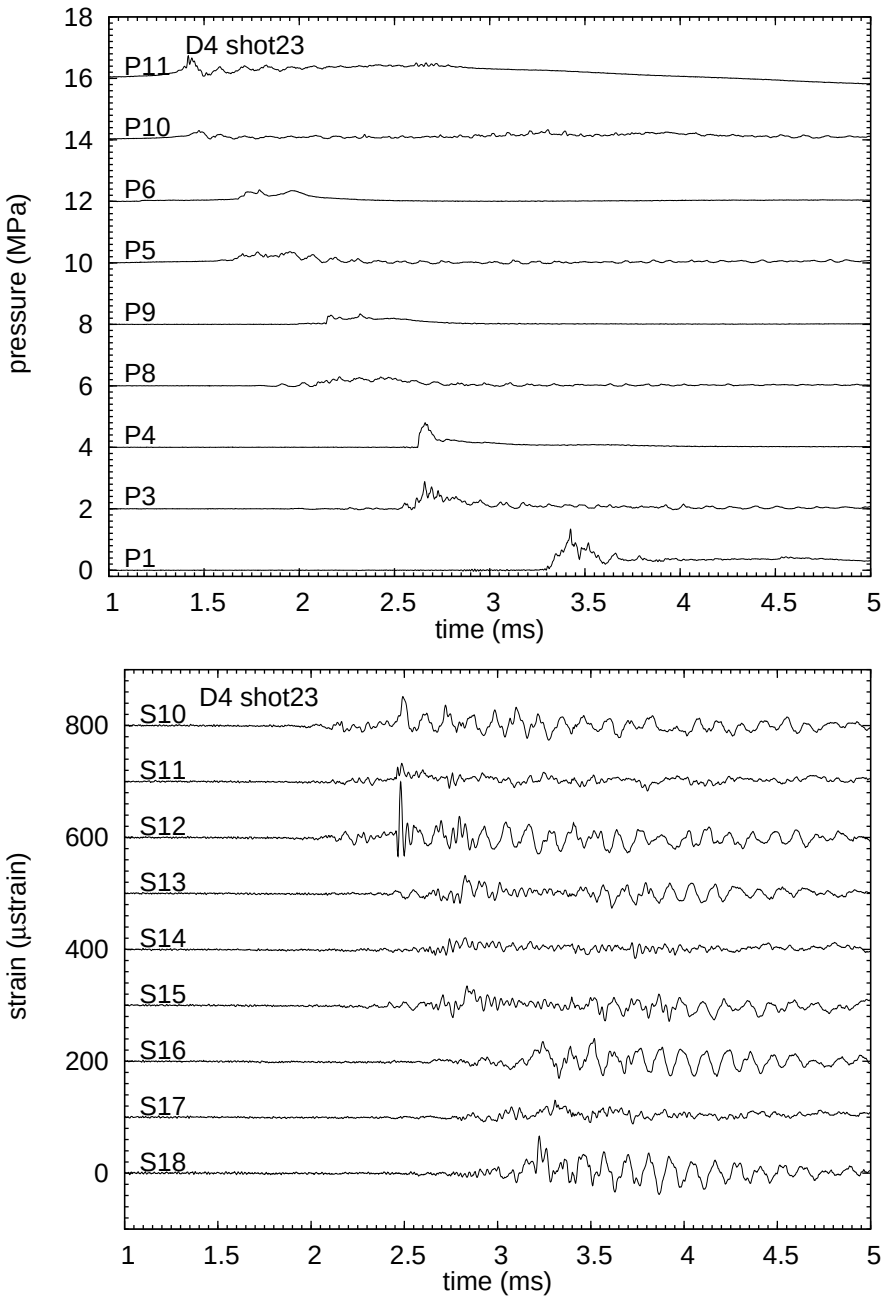

Figure 63: Enlarged view of pressure and strain data from shot 23. Filtered to remove noise about 50 kHz, baseline corrected, and removed ignition transient artifact from strain signals.

5.4 Peak Pressure and Strain

The data from all three shots were analyzed to obtain the peak values of strain and pressure. This was done using the filtered data to eliminate the effects of the initial signal offset and the ignition transient in the strain signals. The pressure data are compared with reference

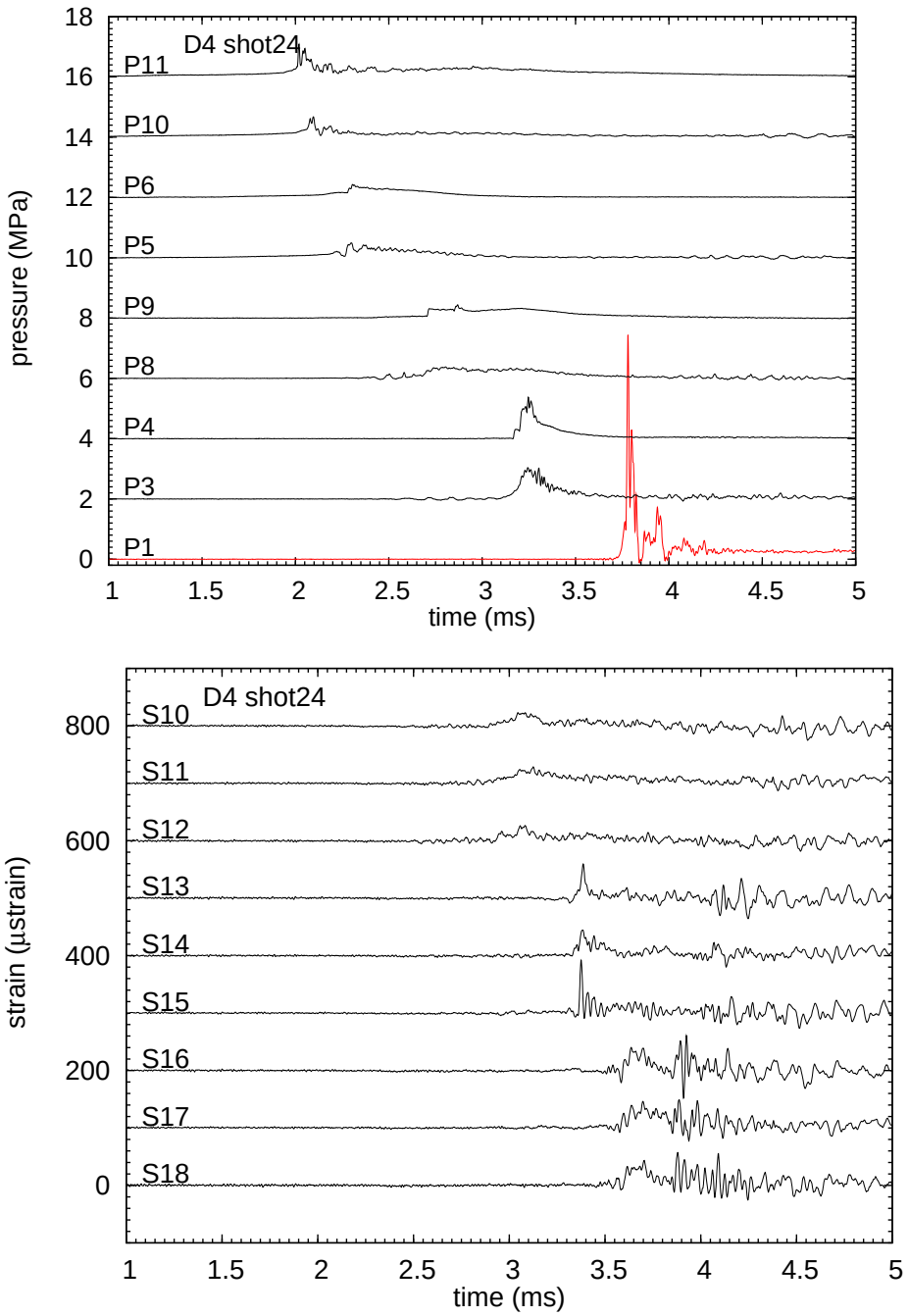

Figure 64: Enlarged view of pressure and strain data from shot 24. Filtered to remove noise about 50 kHz, baseline corrected, and removed ignition transient artifact from strain signals.

values computed from thermochemical equilibrium (Browne et al., 2004) for constant-volume (CV) explosion, Chapman-Jouguet (CJ) detonation, and reflection of CJ detonation (CJ,r). The strain data are computed from the reference pressures and the single-degree-of-freedom

model for static hoop response

$$\epsilon = \frac{\Delta P}{E}\frac{R}{h} \, . \tag{7}$$

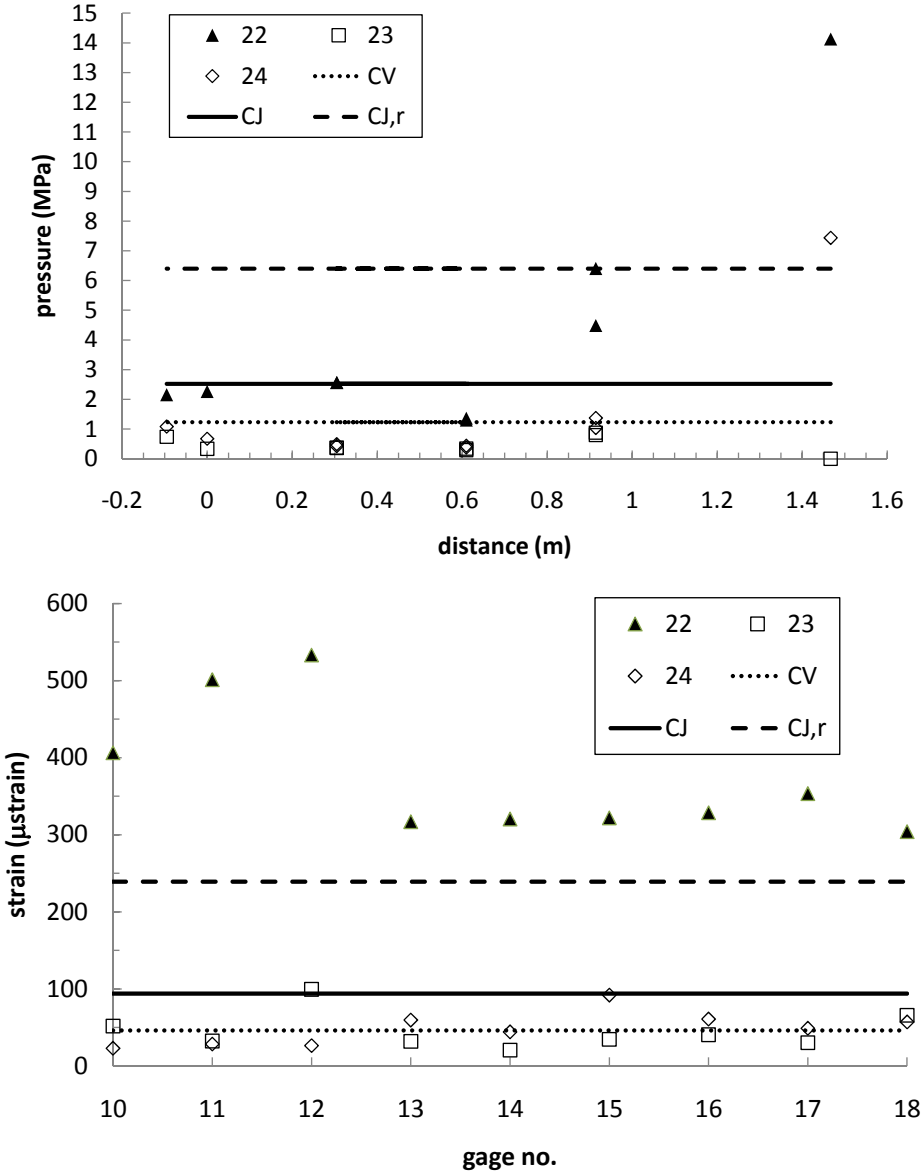

Figure 65: Peak pressure and strain for shots 22-24 as a function of gage location. Peak values were determined by analyzing filtered data.

The peak values for test 22 are consistent with the results for the DDT tests carried out in ES1 as documented in Shepherd and Akbar (2009b). The peak values for shots 23 and 24 are consistent with deflagrations moving at except for the transducer P1. The peak pressure on P1 is consistent with the formation of a strong shock due to an explosion or detonation of a small volume at the end of the pipe.

5.5 Precursor Shocks and Flame Speeds

The rapid flame propagation leads up to detonation in shot 22 and persists throughout the combustion event in shots 23 and 24. The volume displacement of the flame results in flow ahead of the flame and shock waves, which are visible in the the pressure plots. This are more obvious if we focus on one pair of pressure gages and examine the signals on an enlarged pressure and time scale. The results for the pressure gage pair P8/P9 and strain gage triple S10/S11/S12 are shown in Fig. 66. In shot 22, there is no water layer and the signals on the upper (P9) and lower (P8) gages are almost identical even in the rapid fluctuations of pressure. This indicates that the shock waves are moving along the tube axis and are relatively planar so that the situation is nearly one-dimensional. The strain signals are almost identical on all three gages, which supports the conclusion that the shock wave loading that creates these motions is approximately axi-symmetric. The shock waves or detonation arrive at the strain gages slightly later in time since they are located downstream of the pressures transducers P8/P9.

In shots 23 and 24, the signal on the lower gage arrives before the upper gage and the initial signal is oscillatory, with three to four discrete pulses spaced about 100 μs apart. Based on the observations of waves in the D2 test series, we proposed that these correspond to reflections of the acoustic waves in the water between the free surface and the lower surface of the pipe. By contrast, the signal on upper transducer P9 shows a slow compression followed by a sharp jump that corresponds to the precursor shock wave in the gas layer. The strain signals also show the asymmetry induced by the water layer and the characteristic signature of rapid onset of the hoop oscillation observed in shot 22 is not observed in shots 23 or 24. The signal in shot 23 has a much lower amplitude at this location than the signals in shot 24, but larger amplitudes are observed on the gages in the downstream locations, see Fig. 64.

These features can be explained by considering the differences in wave propagation processes in the water and gas layers. In the water, the compression waves propagate close to the sound speed, which is about 1500 m/s at 27°C, see Table 18. The shock waves in the gas travel more slowly, at a speed between 1 and 3 times the initial mixture sound speed of 321 m/s, based on using the observed pressure jumps ΔP to compute the shock Mach number M_s from the jump condition as discussed subsequently. For example, a peak pressure of ΔP = 0.9 MPa corresponds to a M_s = 3.0 and the shock wave will move at 963 m/s. However, the detonation waves travel supersonically with respect to the water since $U_{CJ} \approx$ 2090 m/s, see Tables 20 and 19. As a consequence, we expect that the pressure waves in the water run out ahead of the deflagrations and precursor shock waves but lag behind the detonation fronts.

The flame speed and turbulent burning speed can be back calculated from the shock wave strength using the idealized flow model for low-speed deflagration (Phase I) as discussed in Krok (1991) and illustrated in Fig. 67. The analysis proceeds by using the shock pressure to back calculate the shock Mach number

$$M_s = \left[\frac{\gamma + 1}{2\gamma} \frac{\Delta P}{P} + 1 \right]^{1/2} , \tag{8}$$

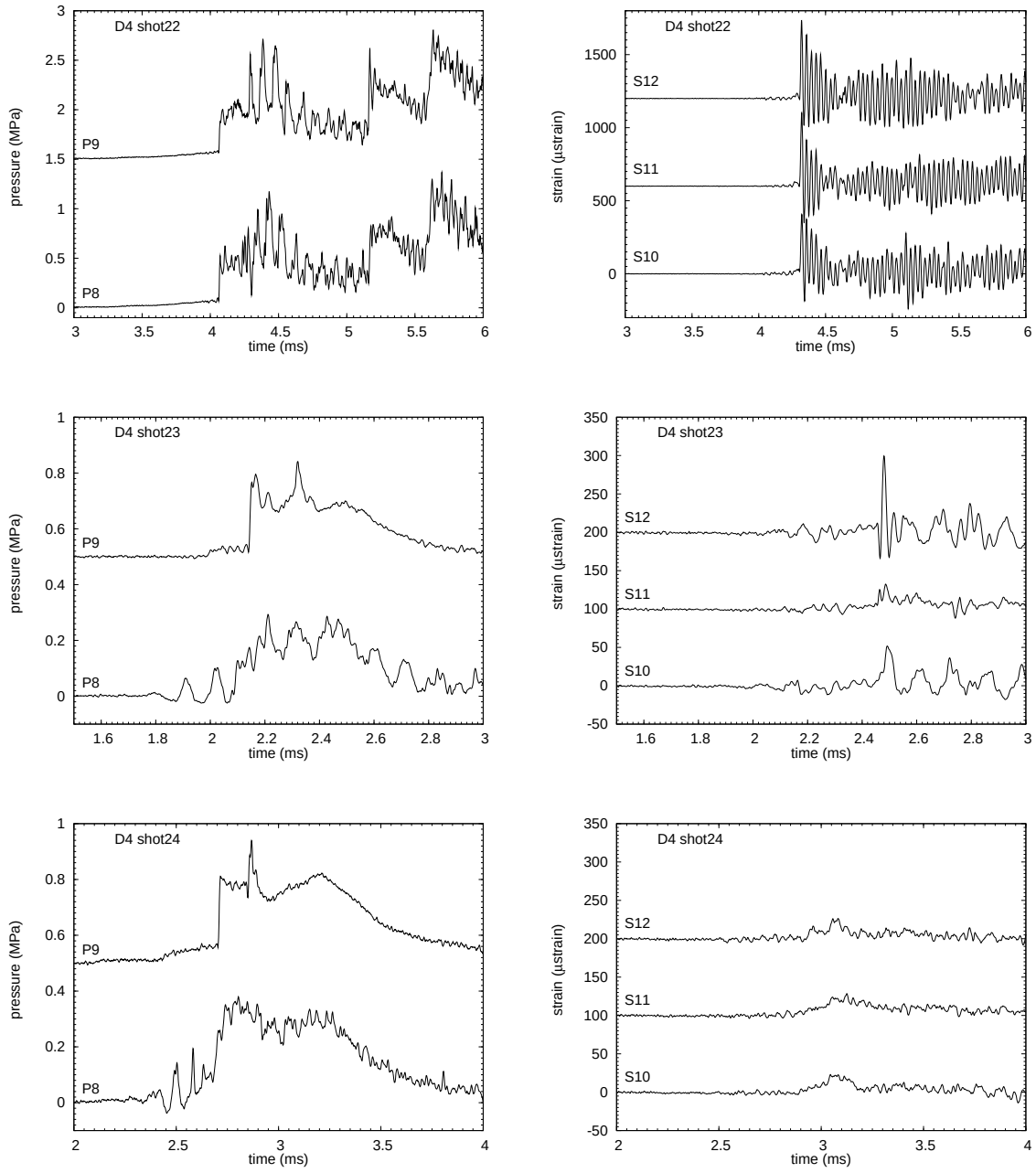

Figure 66: Close-up of pressure and strain signals for shots 22-23. P8 is below the water layer and P9 is above in shots 23 and 24. The strain gages are located slightly (6 in) downstream from the pressure transducers; S10 is at the bottom, S11 on the side, and S12 at the top of the pipe.

where $\gamma = 1.3$ for the unburned gas mixture. The velocity of the shock is

$$U_s = a_1 M_s \ , \tag{9}$$

where $a_1 = 321$ m/s for the reference mixture discussed in Table 19. The flow velocity behind the shock can be computed with the aid of the density ratio from the shock jump conditions

$$\frac{\rho_2}{\rho_1} = \frac{\gamma + 1}{\gamma - 1 + 2/M_s^2} \ , \tag{10}$$

and mass conservation across the shock wave

$$u_2 = U_s \left(1 - \frac{\rho_1}{\rho_2} \right) \ . \tag{11}$$

The flame speed can be computed by assuming that the gas is stationary between the flame and the end of the tube (region 3) and using conservation of mass across the flame with the known expansion ratio $\sigma = \rho_2/\rho_3 = 11.2$ for the reference mixture.

$$V_f = \frac{\sigma u_2}{\sigma - 1} \tag{12}$$

The burning speed is just the velocity of the flow relative to the flame

$$S_f = V_f - u_2 \tag{13}$$

$$= \frac{V_f}{\sigma} \tag{14}$$

The results for the leading shock waves in shots 22 and 23/24 are given in Table 15. This analysis results as estimates of turbulent burning speed $S_f \sim$ 38-54 m/s. The turbulent burning speed can be compared with the laminar deflagration speed, measurements of the laminar burning speed are reviewed by Rodriguez (2008). For a 30/70 H_2/N_2O mixture, the laminar burning speed is estimated to be 1.2–2 m/s. The burning speed S_f is actually the *effective turbulent burning speed* which includes both the large-scale turbulent effects (on the order of the tube dimension) due to the mean flow in region 2 and the smaller scale effects (down to the flame thickness) due to turbulence.

Typically, maximum turbulent burning speeds observed in DDT are on the order of 10–20 times the laminar burning speed (Ciccarelli and Dorofeev, 2008) but there is an additional multiplier since the flame is not a planar surface but substantially tilted with respect to the tube axis. The present results are on the upper end of the range but there is a substantial amount of uncertainly in the laminar flame speed in these mixtures and the model relating shock wave strength to flame speed is highly idealized.

5.6 Discussion of Shots 22-24

Shot 22 demonstrated that decreasing the length of the tube decreased the DDT run-up distance for a mixture of 30/70 H_2/N_2O. The peak pressures and strains were comparable to that observed in previous tests with longer tube and DDT events that occurred away from the tube end.

DDT did not appear to occur in shots 23 and 24, although there was a rapid explosion

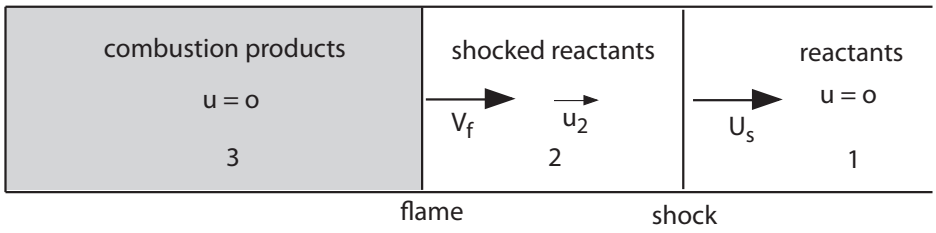

Figure 67: Schematic of idealized one-dimensional flame and shock wave configuration, based on Phase 1 model of low speed deflagration described in Krok (1991).

Table 15: Results of idealized analysis of precursor shock waves in shots 22-24.

Shot	ΔP (MPa)	M_s	U_s (m/s)	ρ_2/ρ_1	u_2 (m/s)	V_f (m/s)	S_f (m/s)
22	0.50	2.33	750	3.8	553	607	54
23-24	0.30	1.91	614	2.7	387	425	38

at the end of the tube in shot 24. The depth of the water was approximately 6 mm (0.23 in) in shot 23 and 10 mm (0.42 in) in shot 24. Based on these values and the measured cell size (Pfahl et al., 1998) of λ = 3-5 mm, the situation is marginal for DDT since the conventional wisdom is that the layer height $h > \lambda$ for DDT to occur. We conclude that for these two tests there does appear to be a significant effect of gas layer height or water free surface on the mode of combustion and consequently the peak pressures and strains.

There are two potential effects that were not controlled in these experiments. As discussed in Appendix B, some fraction of N_2O in gas layer may have been absorbed into the water layer. Estimates of the solubility and diffusivity indicate that less 10% of the gaseous N_2O may have gone into solution although that it is possible that up to 75% could be dissolved over a long period of time. In addition, there may have also been vaporization of the water with up to 4 kPa partial pressure being present if the humidity was 100% at 30°C. The actual extent of absorption and evaporation can be bounded using the pressure measurements during the filling process. The measured pressure changes were less than 0.5% following the filling process, indicating that these effects are not expected to significantly influence either the thermodynamic parameters or detonation sensitivity.

The peak pressures and strains in shots 23 and 24 are consistent with rapid deflagration and the values are bounded by the CV and CJ estimates based on reference thermochemical computations. The magnitude of the precursor shock waves indicates that the flame speeds are on the order of 400-600 m/s and the turbulent burning velocities were 40-50 m/s. The leading compression waves measured under the water layer are more diffuse and travel ahead ahead of the leading gas phase shock waves in the latter half of the tube. This is a consequence of the difference in sound speed a and compressibility ρa^2 of the gas and water.

6 Summary

The test results have provided some insights into the behavior of gaseous explosions over horizontal liquid layer. These results have not resolved all the issues but can serve as a guide to future studies. The two key findings of the present study are:

1. The implications of our results are that the combustion process during both deflagration and detonation occurs much more quickly than lofting and heat transfer to the liquid spray from the combustion products above a horizontal liquid layer

2. Flame acceleration resulting in transition to detonation (DDT) is possible with a 60-in segment of 2-in pipe or a 2 × 3 in rectangular channel filled with a 30/70 H_2-N_2O gas mixture.

3. High speed explosions and shock waves are possible within 30/70 H_2-N−2O gas layer greater than 1/4-in in height above water in a horizontal 2-in Schedule 40 piping section less than 60-in long.

4. A very limited amount of dispersion of the water ahead of and immediately behind the combustion front was observed. Based on this, we speculate that our results will be valid not only for waste with water-like rheology but for more viscous waste with non-zero yield stress.

5. The strains created by the explosion of a 9-10 mm layer of gas above a water layer in a 2-in pipe were up to a factor of 4 smaller than those observed in a pipe completely filled with the same gas mixture. Both the change in explosion mode and dynamics of the gas-liquid interaction appeared to be factors.

Discussion of combustion events The key results of the present experiments are summarized in Table 16.

Although combustion clearly occurred in even the thinnest layers within both the rectangular channel and pipe, there were important differences between the results for the rectangular channel and the pipe. Some type of transition in the combustion mode that can be described as DDT was observed in all shots the rectangular channel with a water layer. However, a clear cut transition event was not observed in the two pipe tests with water. Analysis of the pressure arrival data from shots 23 and 24 indicates that the shock waves were still accelerating and at the end of the pipe and transition had clearly not occurred in shot 23 but may have been marginal in 24. The maximum peak pressures in shot 24 was comparable to that obtained in detonation testing but the usual pressure and strain signatures of DDT were not observed on any of the gages.

One consideration is that within the pipe, the gas layer height is not constant. The lenticular shape of the gas volume may place much greater constraints on the DDT limits than for a rectangular volume. Only the central portion of the gas volume can actually detonate. This may be one reason why DDT was obtained in the rectangular channel tests for gas layers of nominally smaller thickness than in the pipe cases. Another consideration is that although the water does not quench the combustion, it does interact with the combustion

Table 16: Summary of pressure wave and DDT observations.

Shot	Water Depth (in)	X_{DDT} (m)	$P1_{max}$ (Mpa)	$P_{i,max}$ (Mpa)	Notes on DDT and explosion mode
7	0	1.33	-	14.7	ion gage triggered DDT, smaller blockage ratio (Midway - 0.5)
8	0	1.58	-	12.8	smaller blockage ratio (Midway - 0.5)
9	0.375-0.5	1.58	-	14.4	smaller blockage ratio (Midway - 0.5)
10	0	1.40	-	10.8	Larger blockage ratio (Midway + 0.5)
11	0.375-0.5	1.39	-	4.7	Larger blockage ratio (Midway + 0.5)
13	0.375-0.5	1.43	-	5.4	Larger blockage ratio (Midway + 0.5)
14	0	1.29	-	8.03	E end open to SS1-2
15	0	1.36	-	8.25	E end open to SS1-2
16	0	1.6	30	3.75	Classical pressure piling, multiple reflected shock waves, igntion on W end.
17	0	1.2	13	4.95	Average wave speed over last 1/4 of test section was 2694 m/s. Pressure piling, multiple reflected shock waves, ignition location changed for 17 and later.
18	1.3-1.375	1.1	7.8	5	Precursor shock moving at 1268 m/s, detonation wave travels at 2248 m/s according to video.
19	1.55-1.65	0.9	5.8	2.4	Precursor shock at 1185 m/s, detonation 2210 m/s
20	1.85-1.9	0.8	5.7	1.7	Starting at P10, a sharp shock wave precursor appears. The precursor shock accelerates from 600 to 1100 m/s then there is a clear transition in speed at 0.8 m, resulting in a detonation traveling at 1964 m/s from pressure and 1973 from video
21	1.7-1.75	0.9	6.1	5.7	Precursor shock moving at 1003 m/s, detonation wave travels at 1934 m/s.
23	1.7-1.8	>1.6	1.34	0.8	Shock waves accelerate from 600 to 800 m/s, no transition
24	1.53-1.6	>1.6	7.5	1.4	shock waves accelerate from 400 to 1200 m/s, transition right at end?

products and can remove heat and momentum from the flow. This can produce acoustic waves and fluid motion that can propagate up to the combustion front and influence the propagation speed.

The transition distance appears to decrease with increasing water depth, i.e., decreasing gas layer height until a minimum distance of 0.9 m is reached in shot 20. This is consistent with previous studies, summarized in Ciccarelli and Dorofeev (2008), that transition distance

is proportional to the thickness of the gas layer or in the case of gas-filled pipe or channel, the pipe diameter or channel height. DDT testing Liang and Shepherd (2007) with H_2-O_2 mixtures in thin planar layers have demonstrated this effect and shown that DDT is possible in layers as thin as 1.3 mm at 100 kPa initial pressure. Below this thickness, heat and momentum transfer to the confining walls prevents sustained propagation of a detonation.

Discussion of strains The effect of water on peak strains is inconclusive. The measured peak strains in shots 23 and 24 are substantially lower than shot 22 but the comparison is spoiled by not getting a clear-cut DDT event in either shot 23 or 24. One reason that the peak strains are lower in shots 23 and 24 as compared to 22 is that the peak pressures are lower since the combustion mode is not a classical detonation.

It is likely that the waste layer will influence both the explosion mode and the coupling of the explosion to the piping. Either of these will have the effect of reducing the peak strains but for different reasons. In order to resolve the influence of the water on the coupling of the explosion to the tube, numerical simulation would be quite valuable since the mode of explosion can be artificially controlled so that the fluid-structure interactions aspects can be independently studied.

6.1 Implications for HPAV Safety Assessment

1. Combustion of a gas layer above a horizontal layer of waste is a credible event.
2. The assessment of explosions of gas layers over liquid waste should include an evaluation of deflagration-to-detonation transition.
3. Transition to detonation can occur in gas layers that are 60-in long and and 0.5-in high.

6.2 Further Work

The results of the present study are preliminary and further work is needed to resolve the following issues:

1. Dependence of explosion parameters (peak pressure and wave speed) on the gas layer height.
2. Effect of viscosity and yield stress of the waste on the explosion mode.

   Attempts to carry out experiments with non-newtonian waste simulant (Laponite) were unsuccessful. The material was very difficult to distribute evenly and we were not able to obtain a layer of material that provided a useful initial condition for explosion experiments. The experiment will need to be redesigned in order to successfully include high yield-stress materials.
3. Role of the relative height of the gas and liquid layers on the peak strains in the piping.

   This will require further experiments and numerical simulation to isolate the various effects of the liquid layer. In order to carry out definitive experiments, the explosion

mode will have to be controlled independently of the water depth. This can probably only be done in the case of detonation.

7 Acknowledgments

The sponsor of this work was the US Department of Energy, Office of River Protection (ORP) of Richland, WA under Contract DE-AC27-09-RV 15086. The contract monitor at the ORP was Greg Jones. Hales Manufacturing, and the staff of the Aeronautics and Physics machine shops contributed to fabricating the specimens and many fixtures used in these tests. Expert Swagelok plumbing and mounting of fixtures was provided by Steve Ballard. Alexandra Katsas was responsible for administrative support and helping with the QA program documentation. Dominion Engineering provided samples and characterization of waste simulant material.

Bibliography

R. Akbar, M. Kaneshige, E. Schultz, and J.E. Shepherd. Detonations in H_2-N_2O-CH_4-NH_3-O_2-N_2 mixtures. Technical Report FM97-3, GALCIT, July 1997. 122, 123

A. Akgerman and J. L. Gainer. Predicting gas-liquid diffusivities. *Journal of Chemical and Engineering Data*, 17(2):372–377, 1972. 120

L. E. Bollinger, J. A. Laughrey, and R. Edse. Experimental detonation velocities and induction distances in hydrogen-nitrous oxide mixtures. *American Rocket Society Journal*, 32: 81–82, January 1962. 83

S. Browne, J. Ziegler, and J. E. Shepherd. Numerical solution methods for shock and detonation jump conditions. Technical Report FM2006.006, GALCIT, 2004. 87, 122, 123

G. Ciccarelli and S. Dorofeev. Flame acceleration and transition to detonation in ducts. *Progress Energy Combust Sci*, 2008. doi:10.1016/j.pecs.2007.11.002. 75, 83, 91, 94

V. A. Del Grosso and C. W. Mader. Speed of sound in pure water. *J. Acoustical Society of America*, 52(5):1442–1446, 1972. 10, 121

K. Denbigh. *The Principles of Chemical Equilibrium*. Cambridge University Press, fourth edition, 1981. 119

P. Hildebrant and F. McCoy. WTP – control of hazards associated with hydrogen accumulation in piping and ancillary vessels. Alternative evaluation and design approaches. Technical report, DOE - ORP, February 2009. Report of the HPAV Assessment Team. 11

J. Chris Krok. One-dimensional flame propagation mechanisms. Unpublished notes on the solution of ideal steady high-speed flames. RPI, Troy, NY, July 1991. 89, 92

S. Lachmann and J. Minichiello. Hpav engineering analysis methods and criteria. Technical Report 24590-WTP-RPT-ENG-07-011, Rev 3, Bechtel River Protect Project, Waste Treatment Plant, April 2010. 78

Z. Liang and J.E. Shepherd. Explosion testing of the nested can containment system. part I: Planar gap. part II. thick-walled tube. part III. 3013 outer can. Technical Report FM2007-001, Graduate Aeronautical Laboratory, California Institute of Technology, May 2007. 95

Z. Liang, J. Karnesky, and J.E. Shepherd. Delflagration-to-detonation transition tests in H_2-O_2-N_2-He mixtures. Technical Report FM2006-004, Graduate Aeronautical Laboratory, California Institute of Technology, August 2006. 11

David R. Lide, editor. *CRC Handbook of Chemistry and Physics*. Taylor and Francis, 90th edition, 2010. Internet Version 2010. 10, 121

U. Pfahl, E. Schultz, and J.E. Shepherd. Detonation cell width measurements for H_2-N_2O-O_2-CH_4-NH_3 mixtures. Technical Report FM98-5, GALCIT, April 1998. 92

E. A. Rodriguez. Pressure-time history for design of HPAV vessel and piping subjected to gaseous H2-N2O deflagrations. Technical Report GNNA-0-039, Gobal Nuclear Networks, LLC, December 2008. 91

J. E. Shepherd and R. Akbar. Forces due to detonation propagation in a bend. Technical Report FM2008-002, Graduate Aeronautical Laboratories California Institute of Technology, February 2009a. 11

J. E. Shepherd and R. Akbar. Piping system response to detonations. results of es1, ts1 and ss1 testing. Technical Report FM2009-001, Graduate Aeronautical Laboratories California Institute of Technology, April 2009b. Revised June 2010. 11, 13, 16, 19, 80, 83, 84, 88

SwRI. HPAV gaseous deflagration, detonation, and deflagration-to-detonation (DDT) test program. Technical Report SwRI Project 18-14165, Engineering Dynamics Department, Southwest Research Institute, 6220 Culebra Road, San Antonio, TX 78228-0510, March 2009. Final Report. 11

A Engineering Drawings

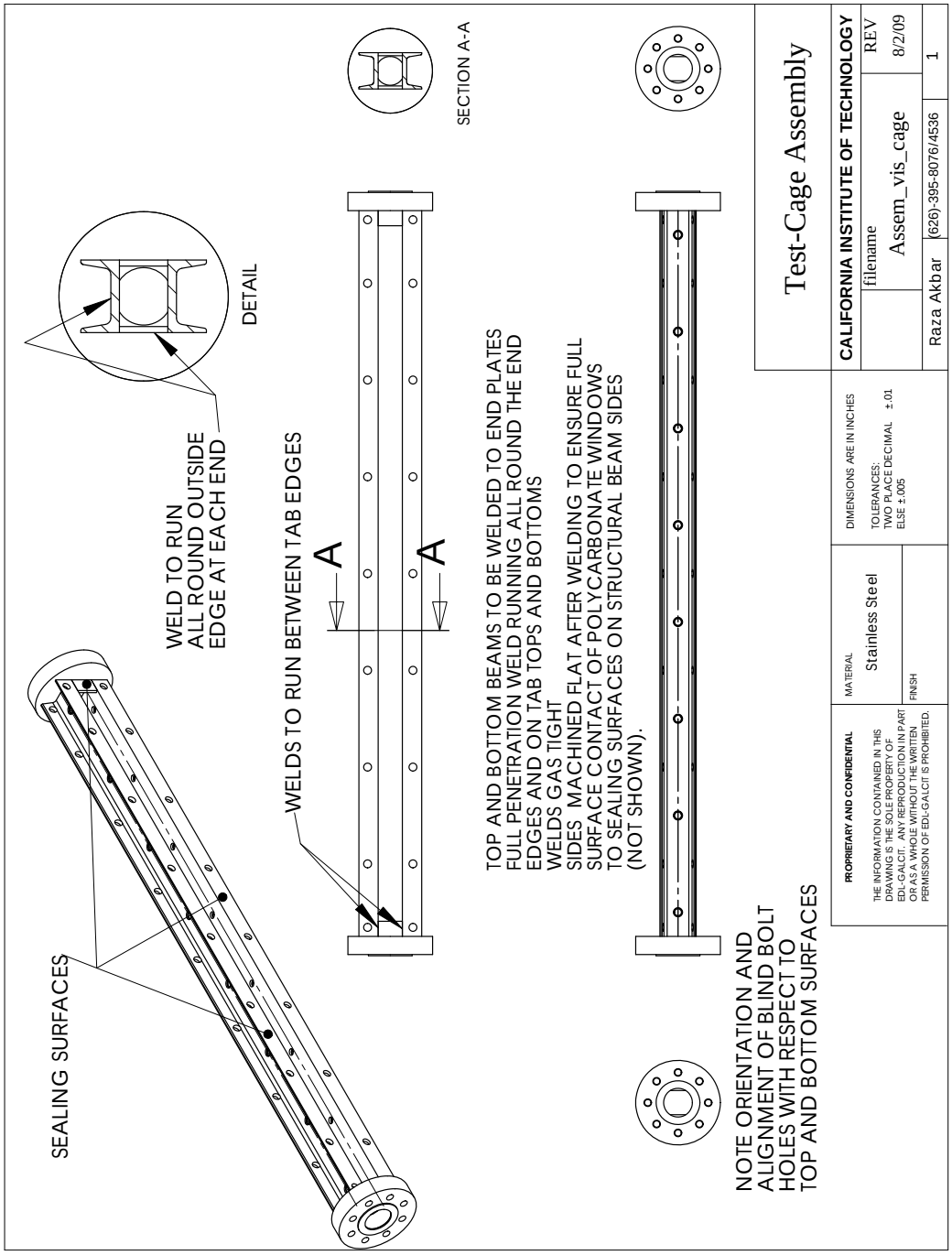

Figure 68: Visualization test section construction details.

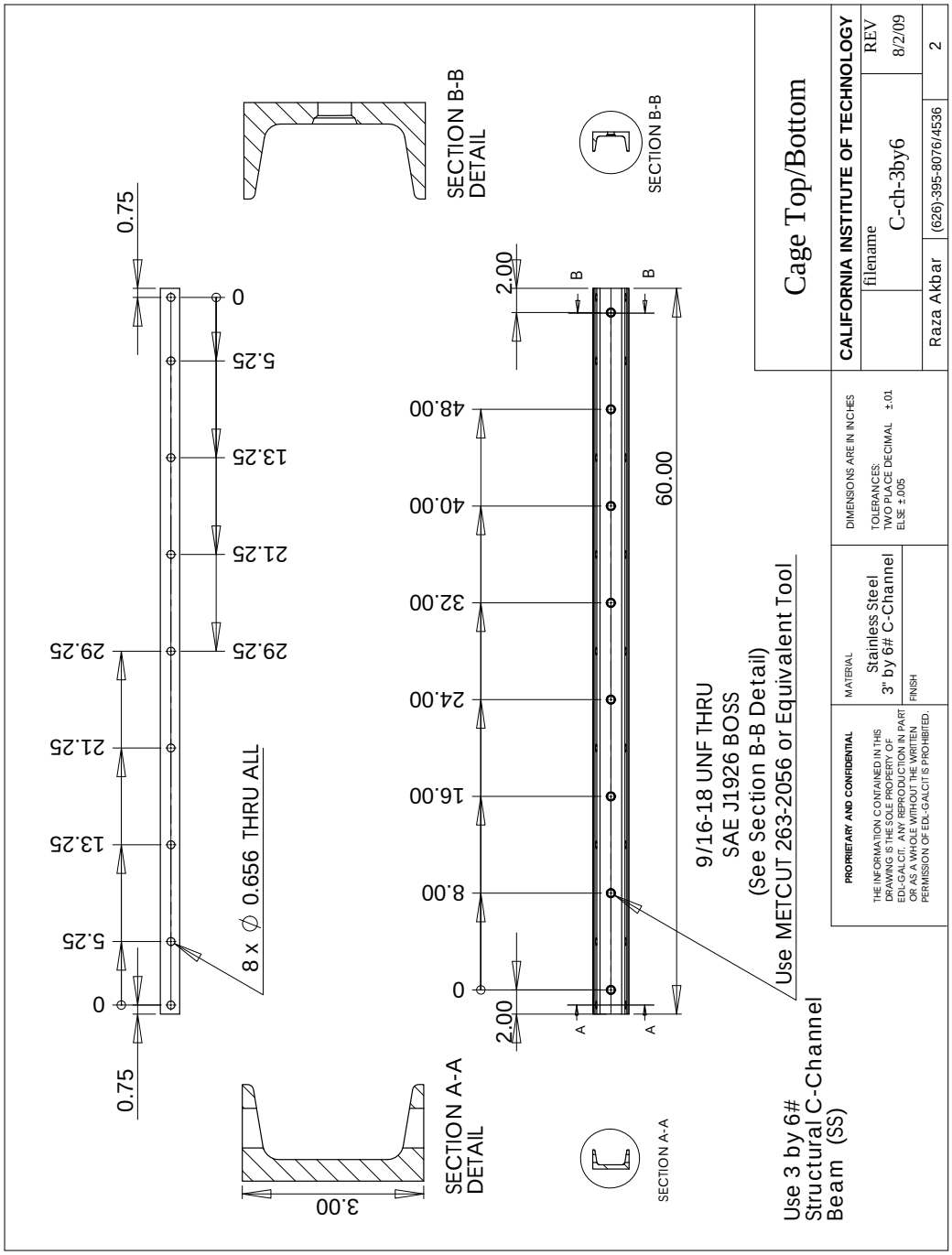

Figure 69: Visualization test section channel component.

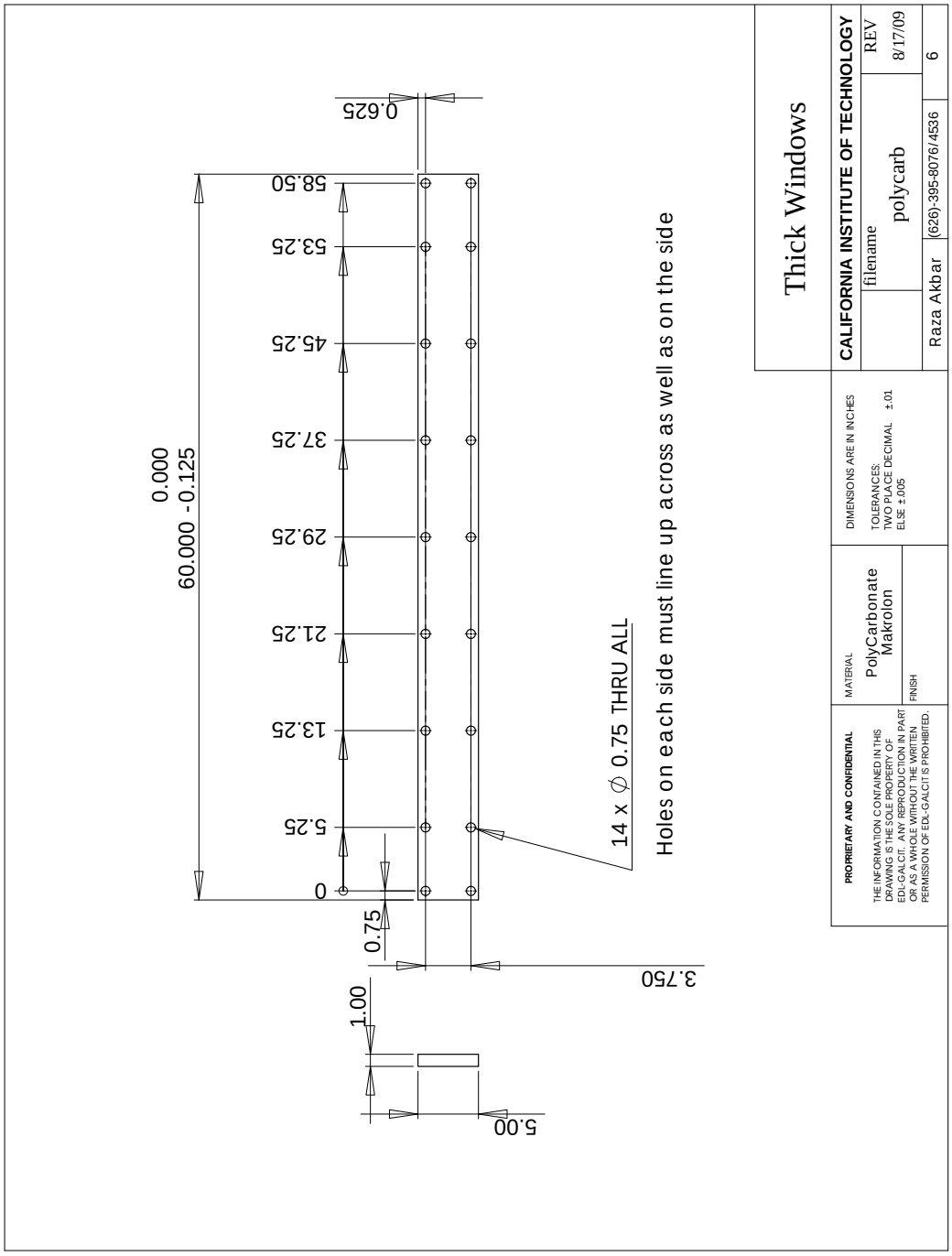

Figure 70: Visualization test section polycarbonate (Makrolon WG) window.

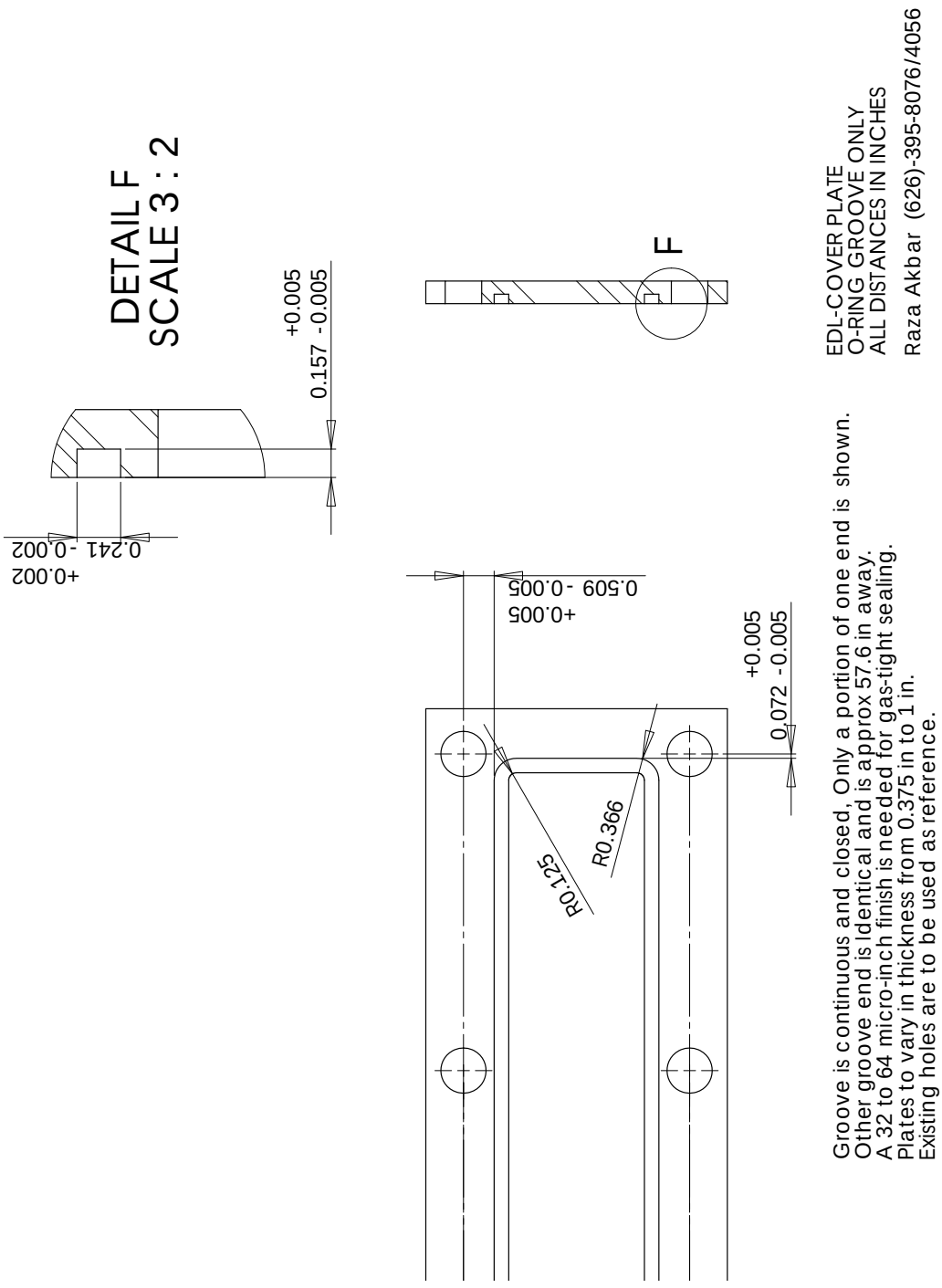

Figure 71: Visualization test section o-ring groove for window.

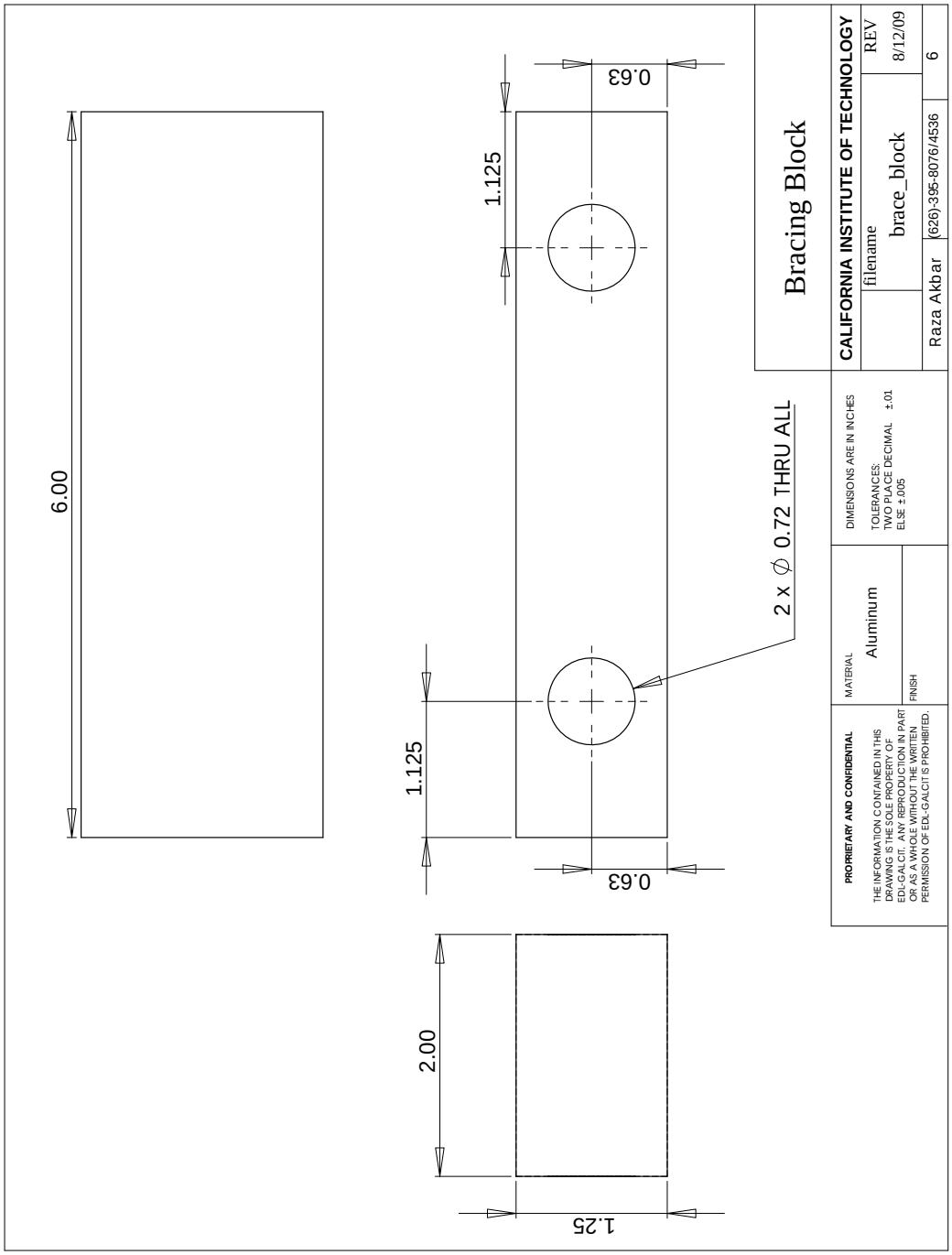

Figure 72: Visualization test section bracing block used to reinforce window.

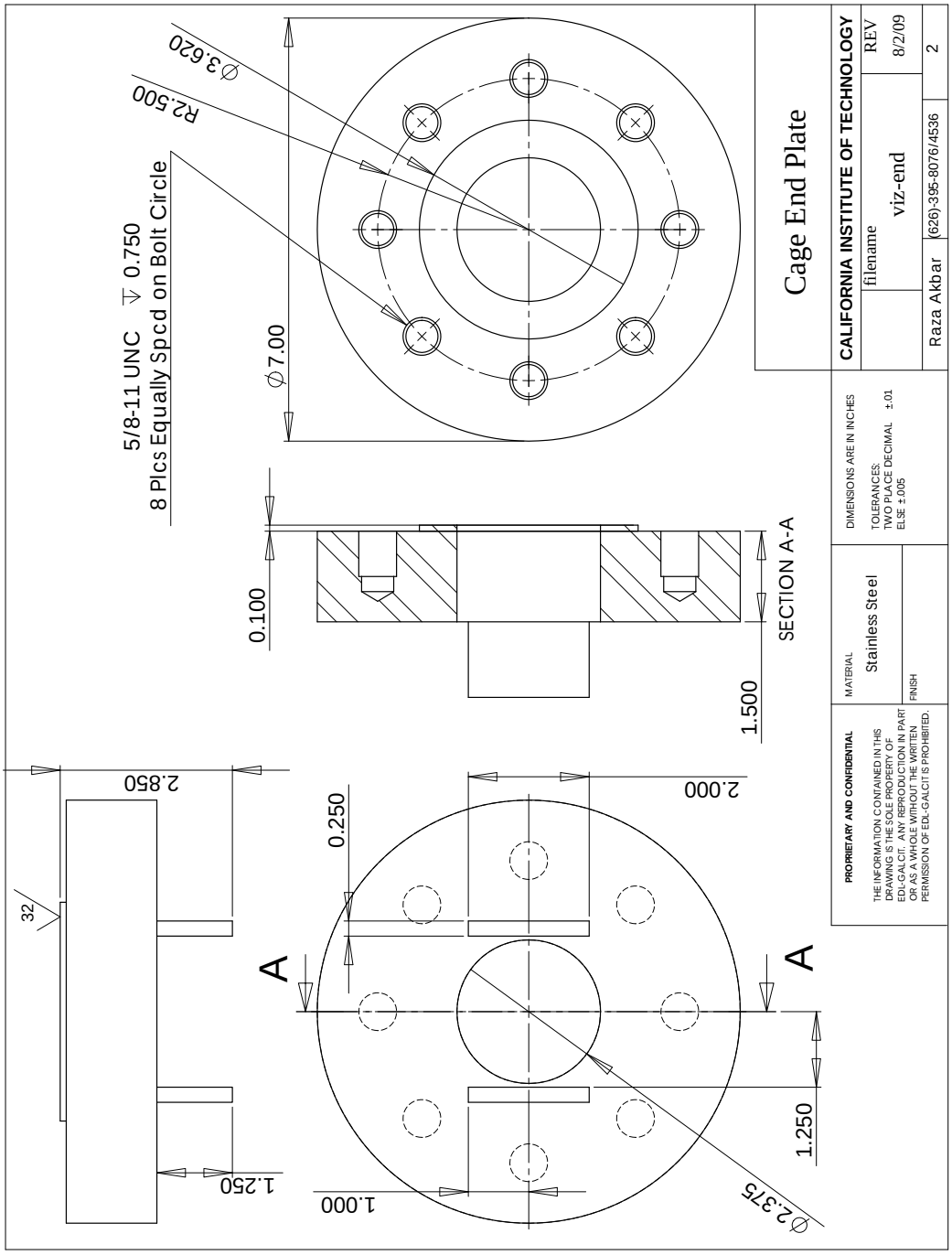

Figure 73: Visualization test section end plate.

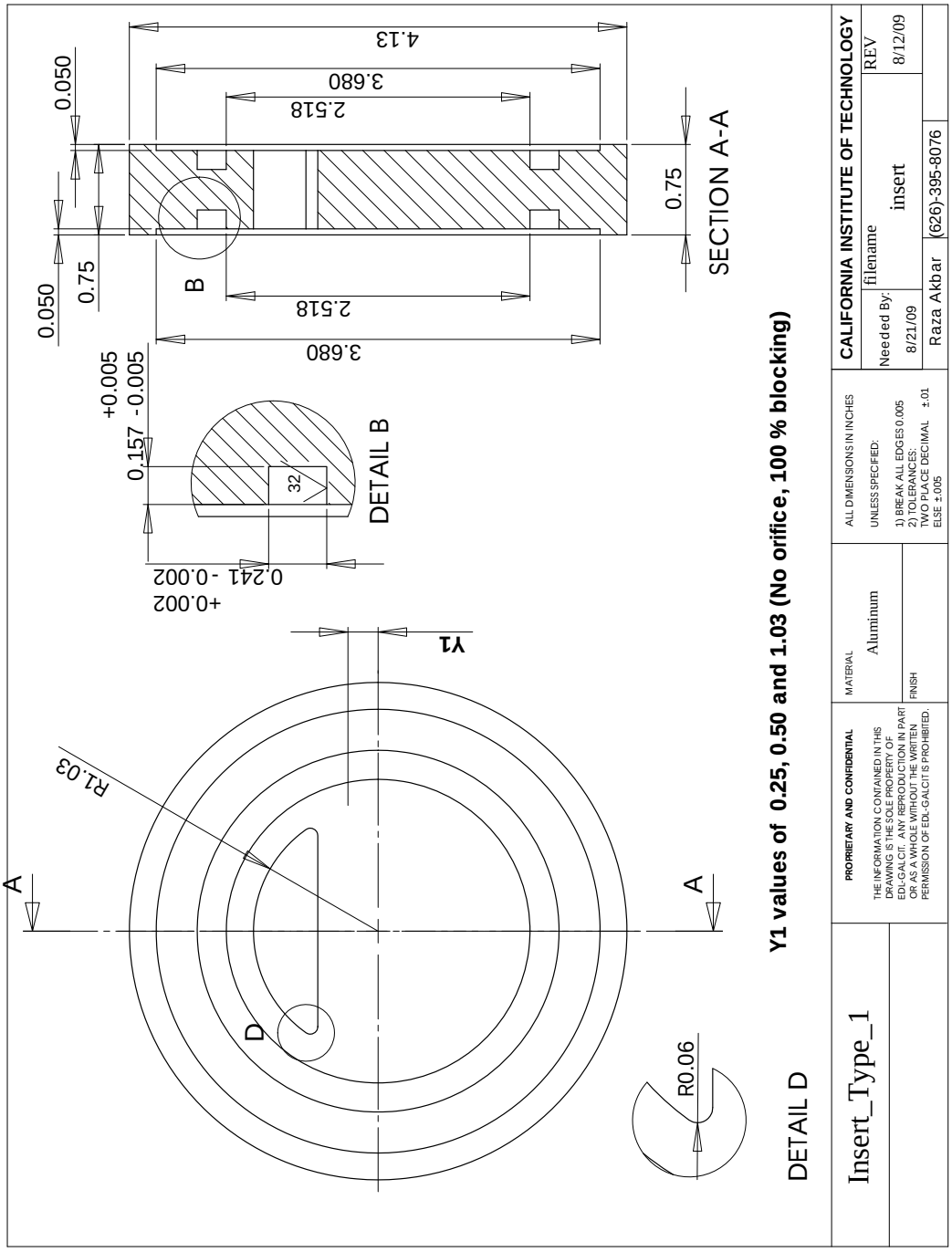

Figure 74: Visualization test section coupling insert.

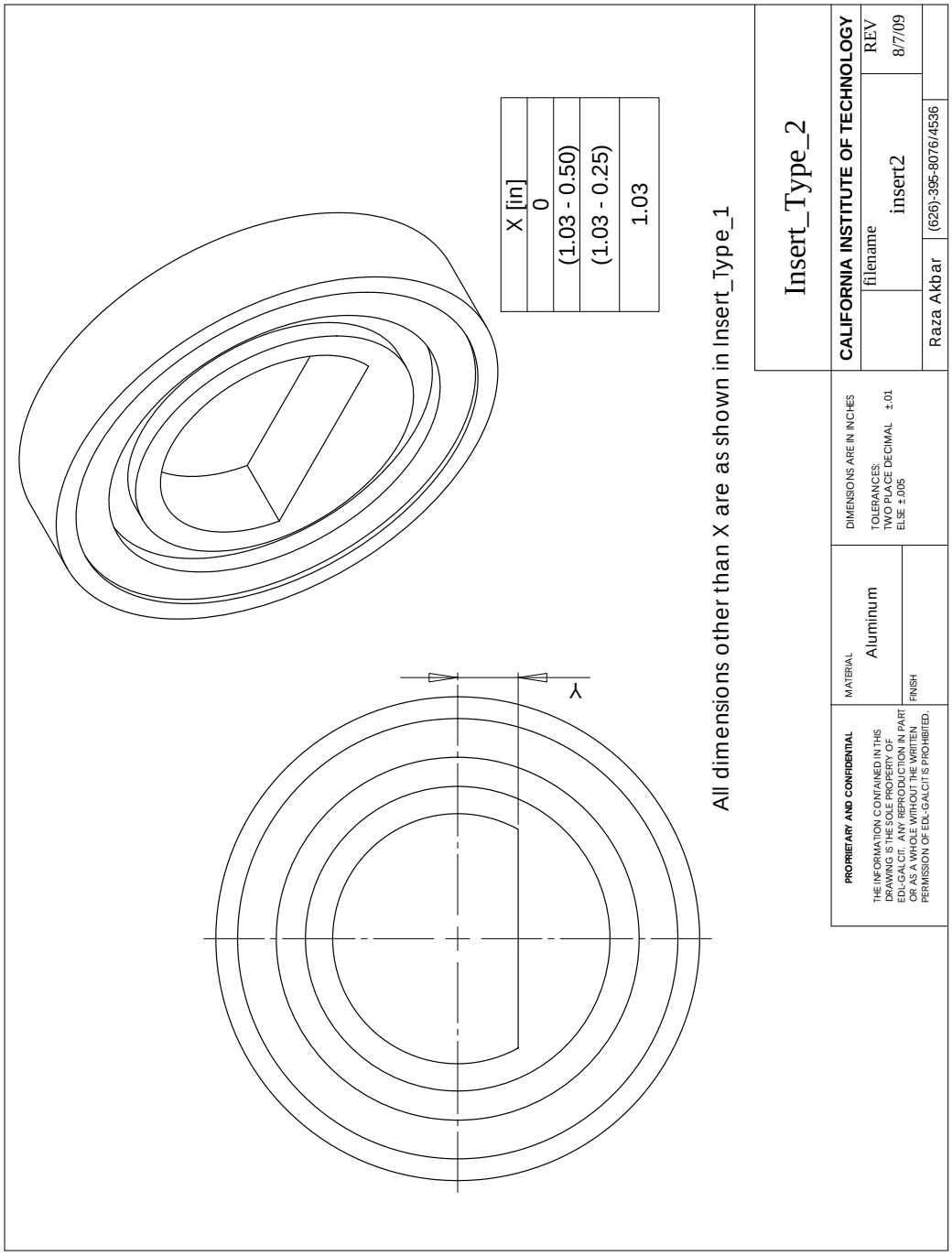

Figure 75: Visualization test section coupling insert perspective view.

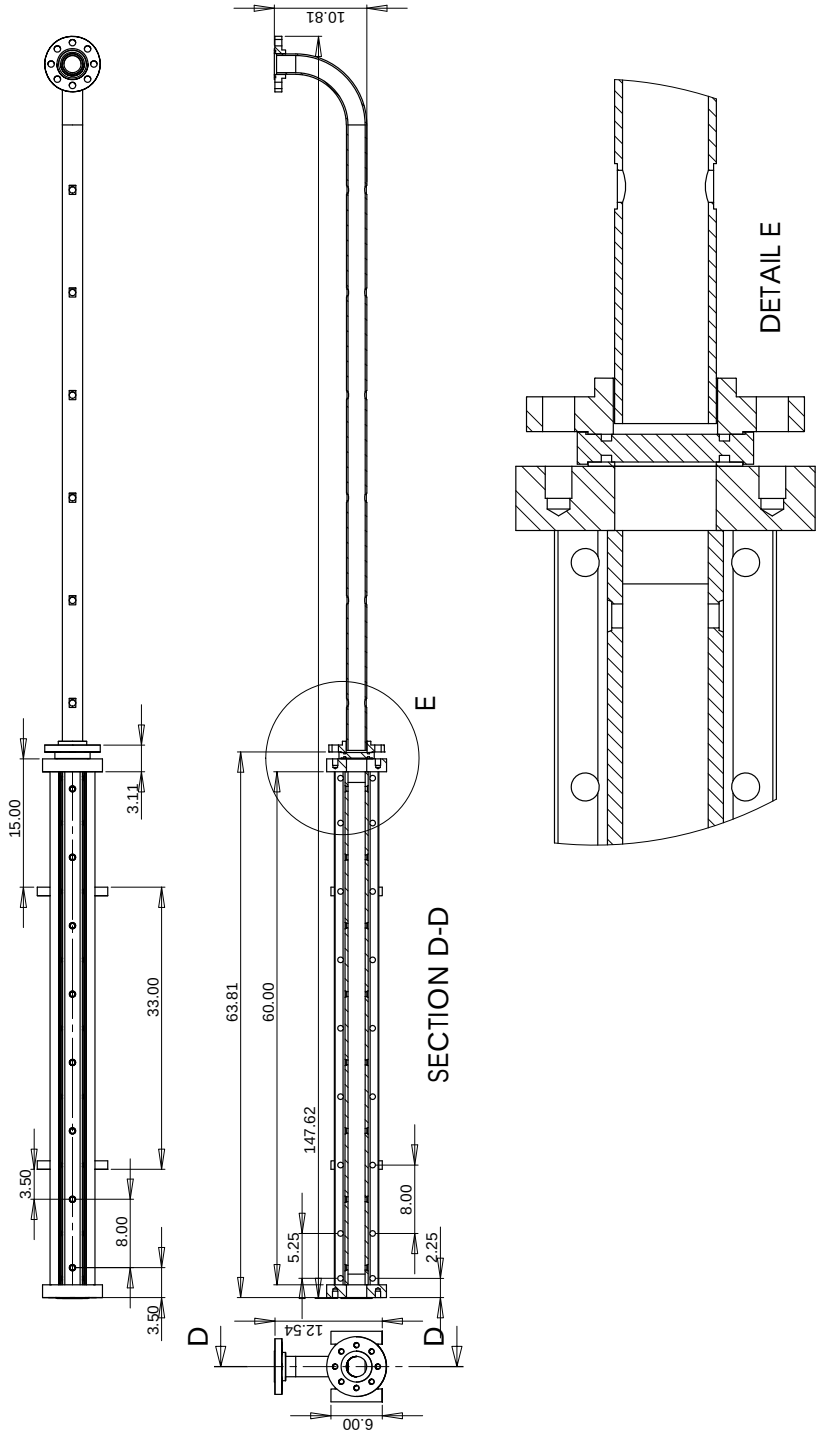

Figure 76: Visualization test section assembly dimensions.

Figure 77: Assembly of modified SS1-3 pipe sections for D4 testing.

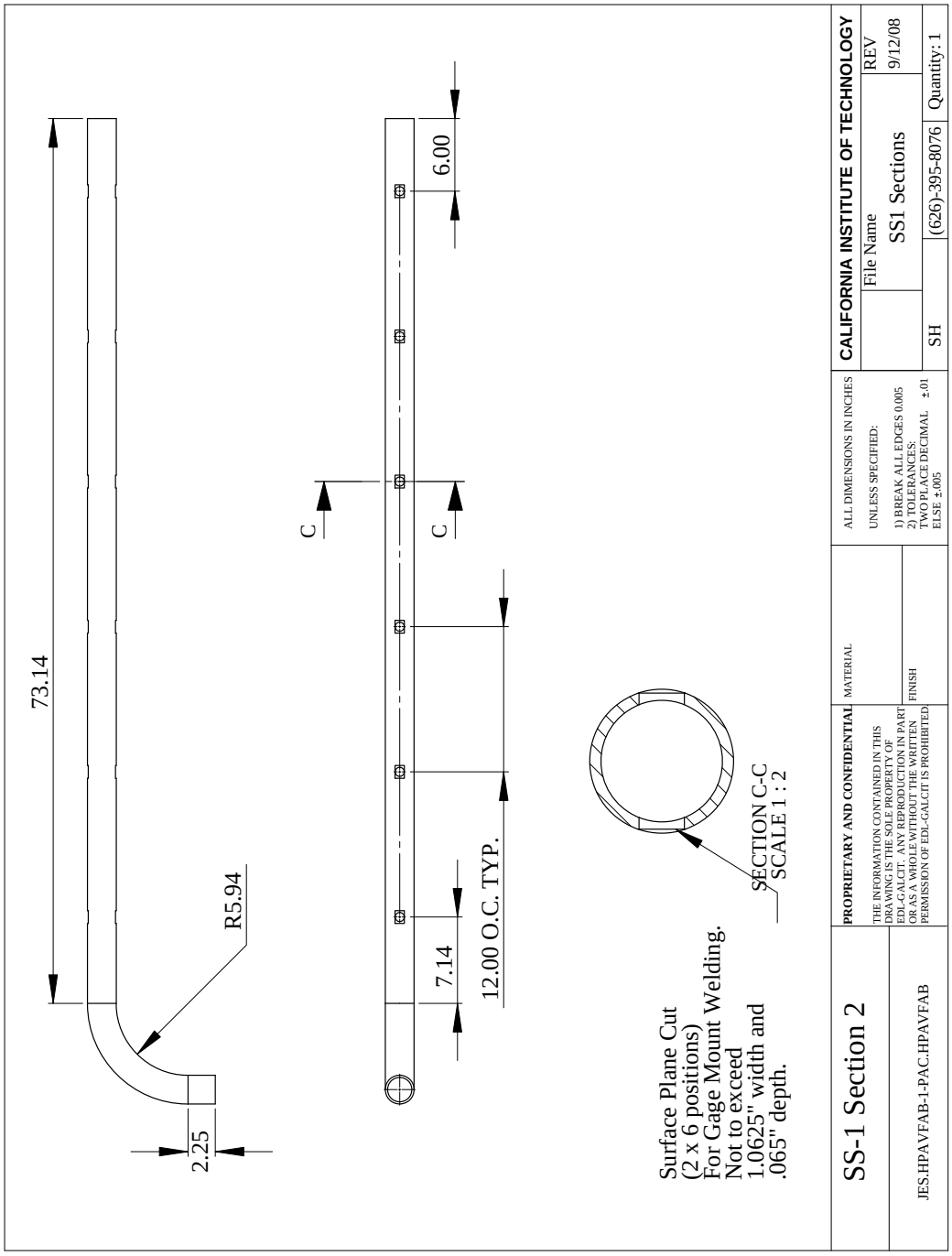

Figure 78: SS1-2 pipe section used for D1 testing.

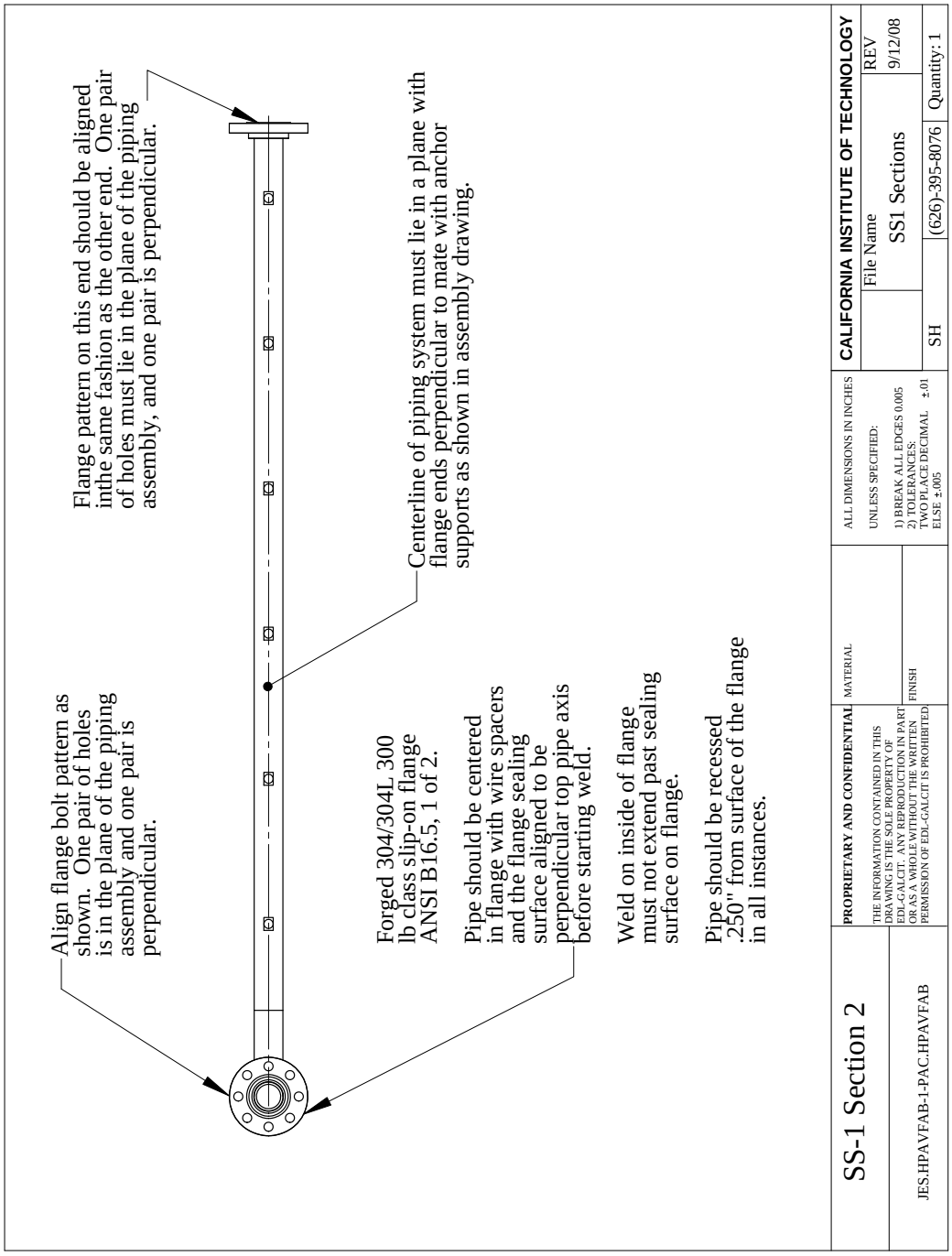

Figure 79: SS1-2 pipe section used for D1 testing.

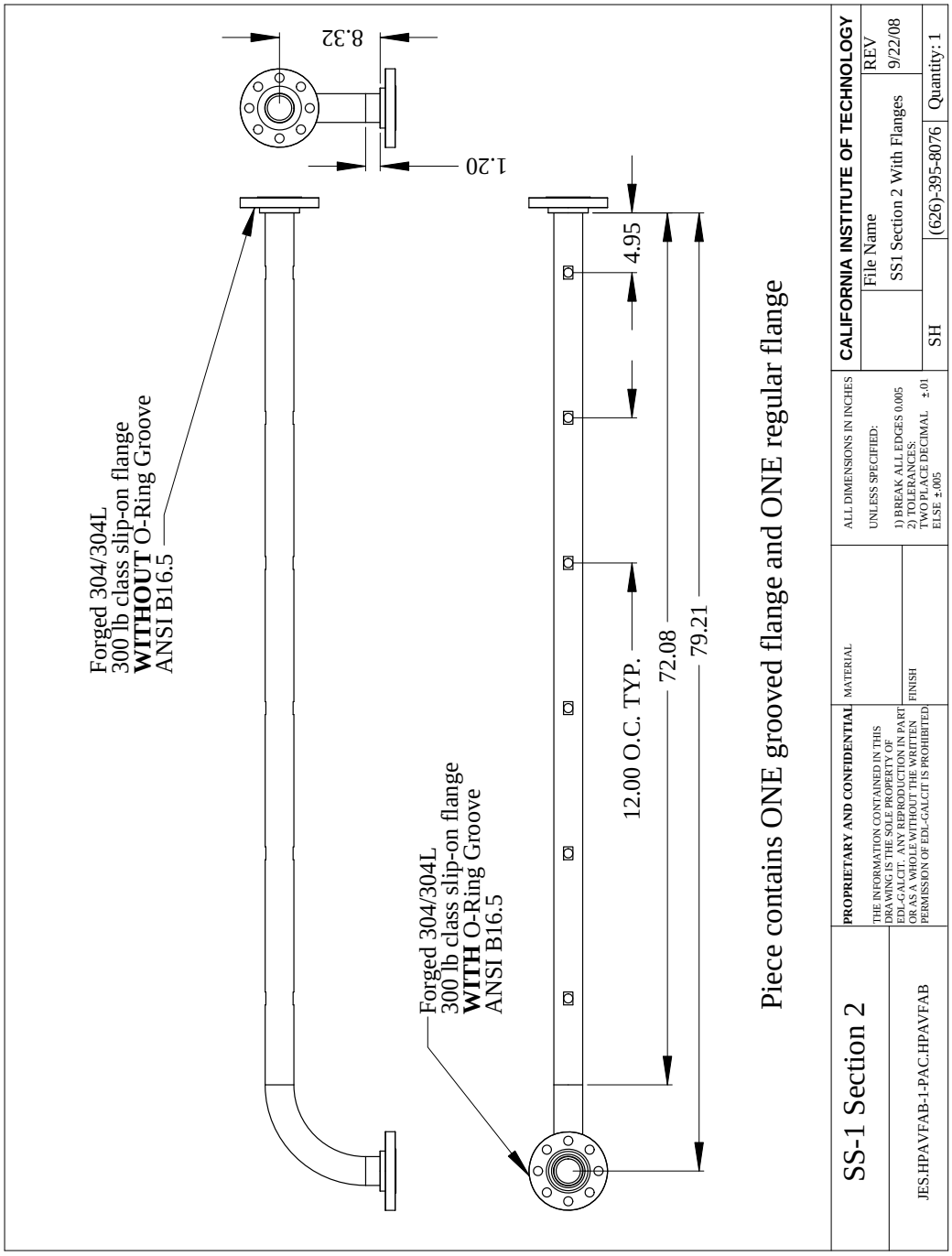

Figure 80: SS1-2 pipe section used for D1 testing.

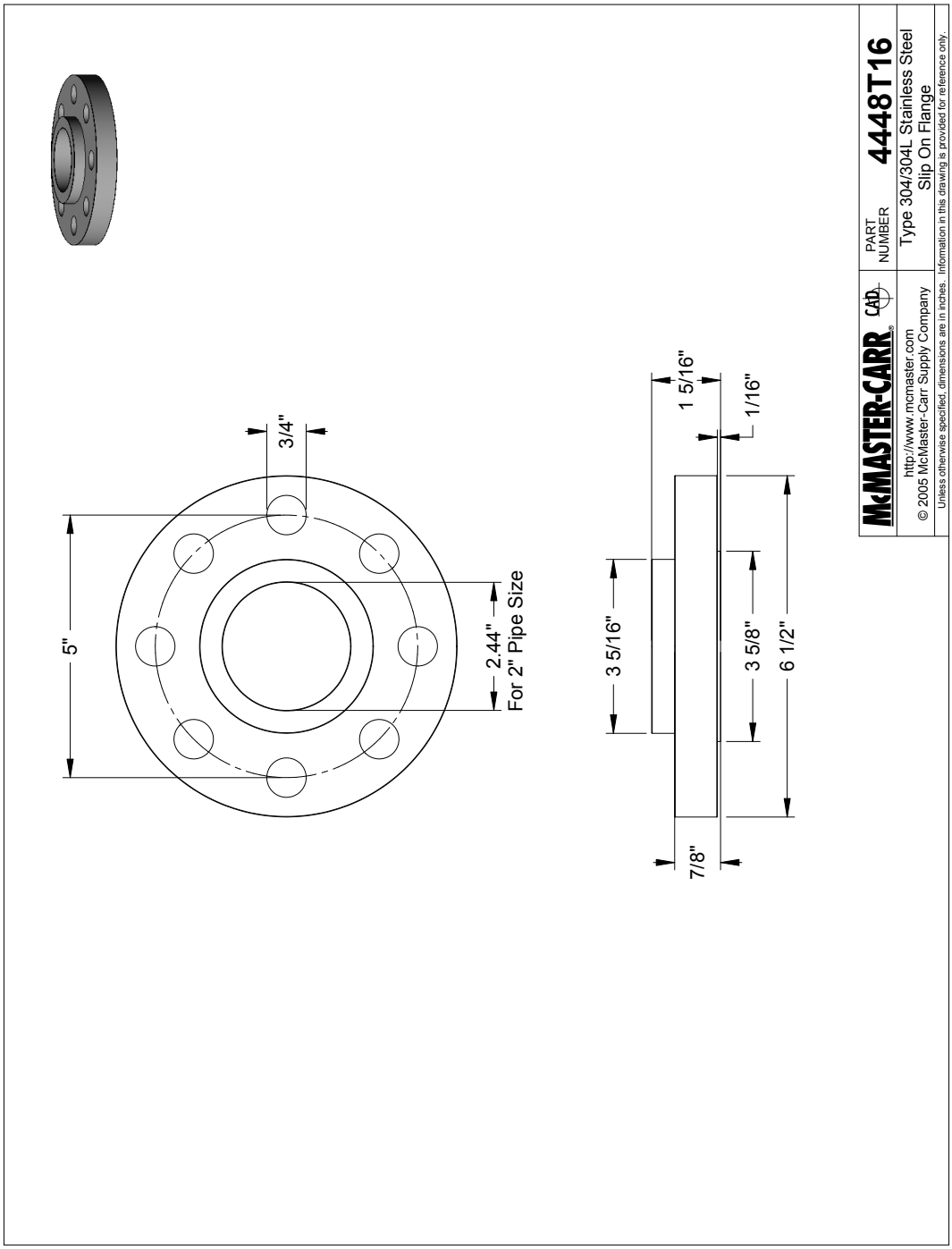

Figure 81: Slip-on flanges for pipe sections.

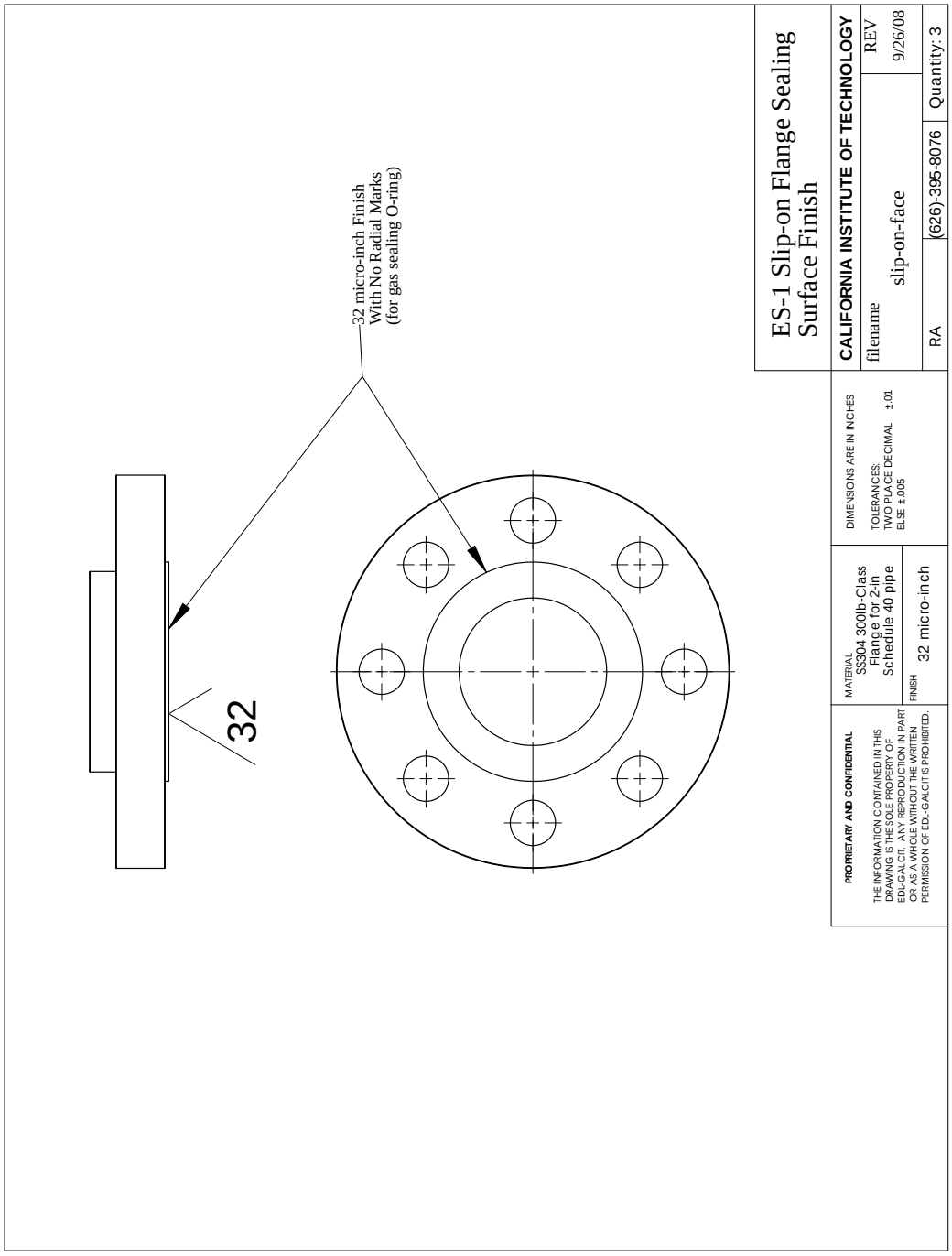

Figure 82: Modification of slip-on flanges for pipe sections.

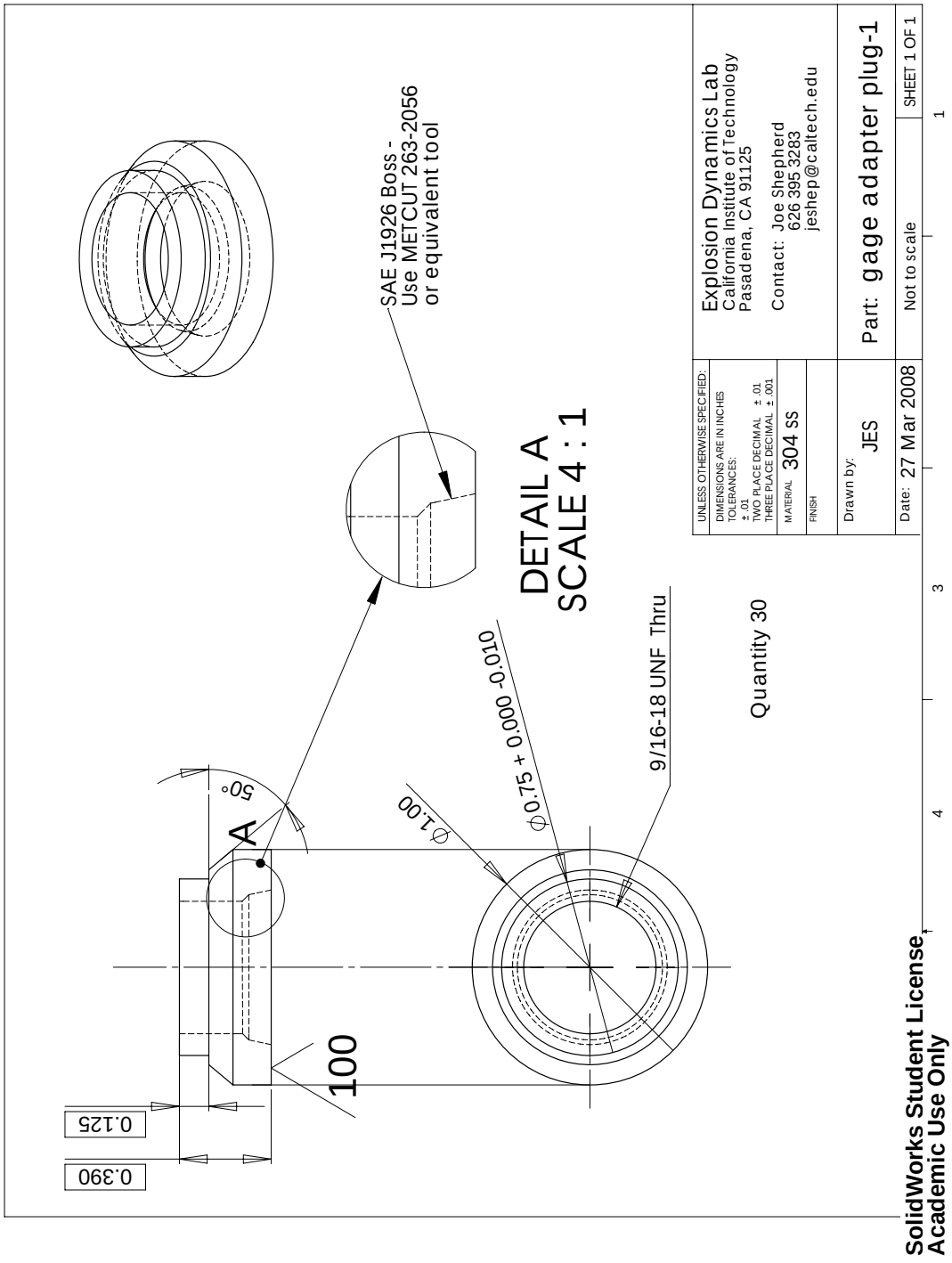

Figure 83: Ports for pipe sections.

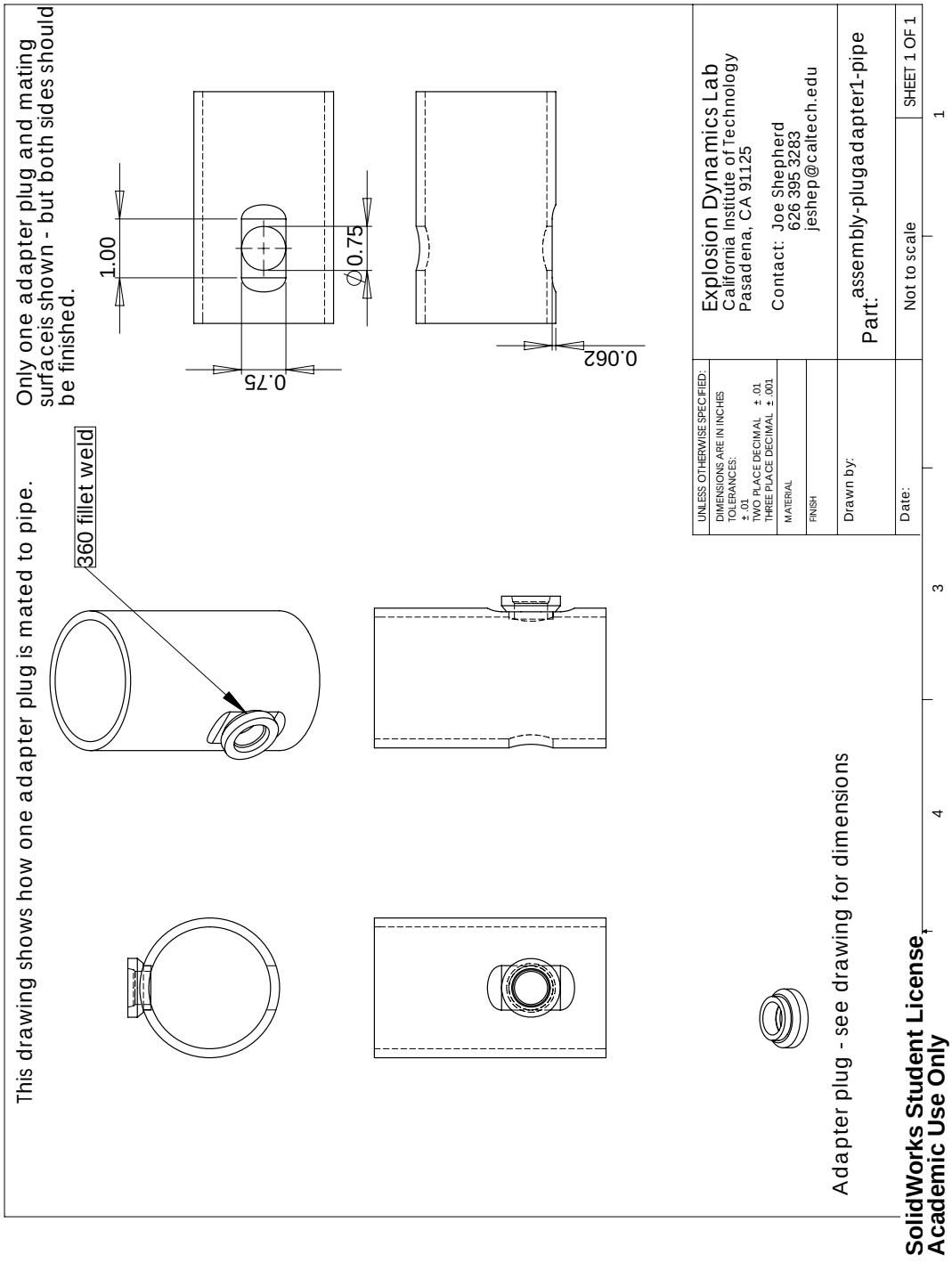

Figure 84: Port assembly to pipe sections.

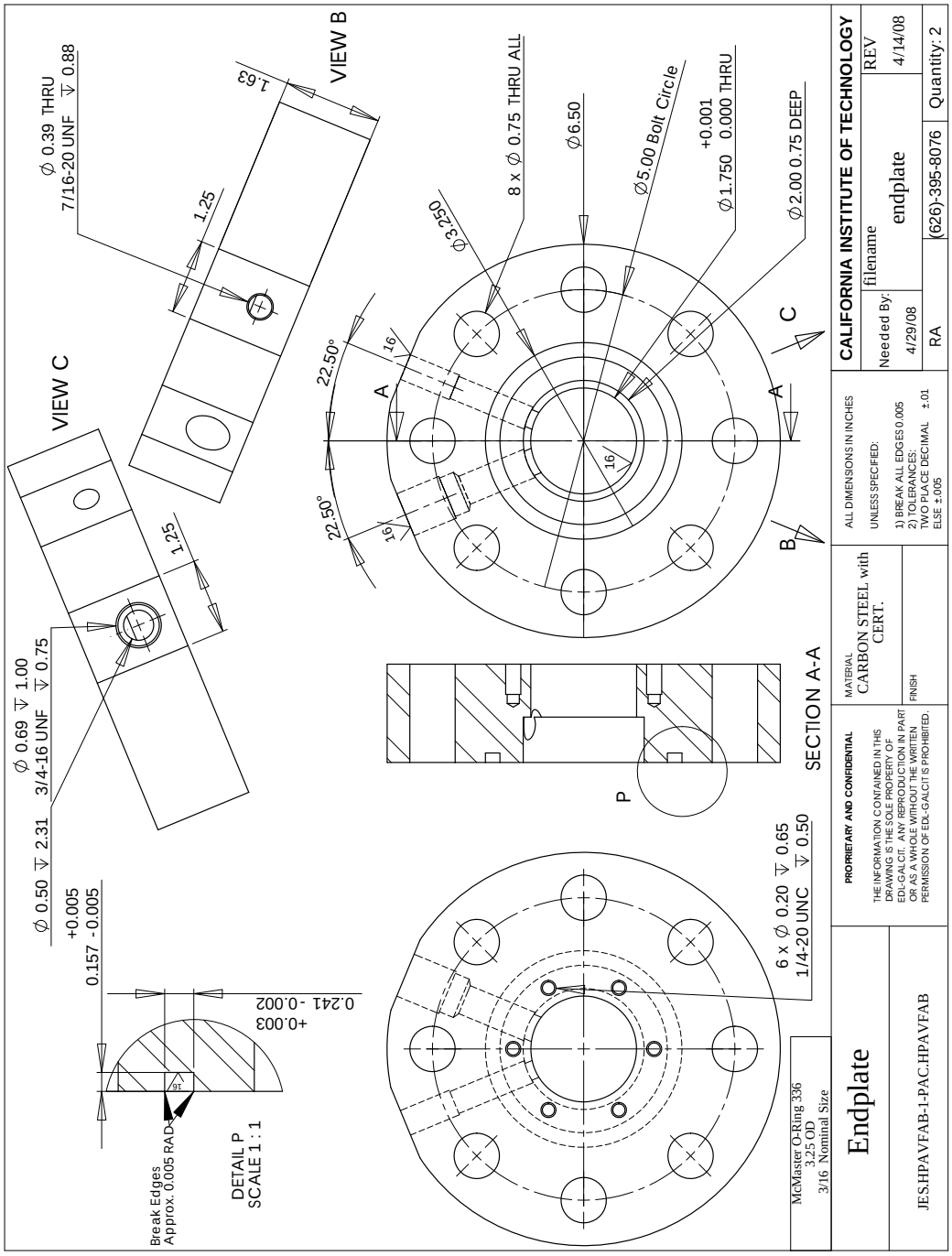

Figure 85: Gas handling flange.

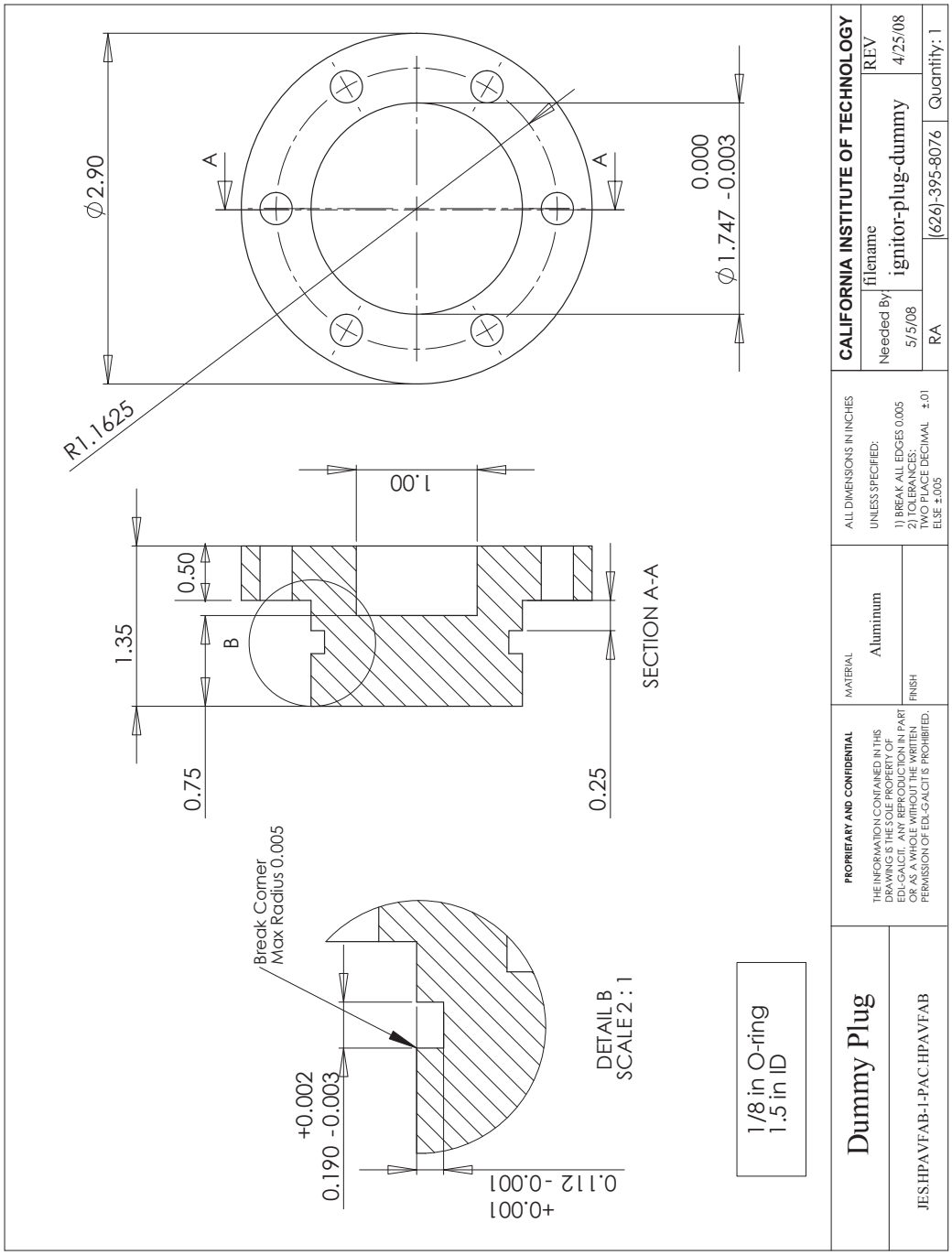

Figure 86: Plug used to mount PCB transducer in gas handling flange.

B Solubility of gases in water

In the present experiments, a layer of water was introduced beneath a gas mixture of N_2O and H_2 and there was a period of contact (up to 10 minutes) before the explosion was initiated. This raises the possibility that some of the gas was absorbed by the water with different components having different solubility, thereby changing the composition of the gas and lowering the initial pressure. There was no evidence of this effect but in order to be thorough, this possibility was examined by estimating the possible extent of dissolved gas.

The solubility of gases in liquids is conventionally expressed in terms of Henry's Law (Denbigh, 1981, p. 225)

$$[i] = k_H P_i \tag{15}$$

where $[i]$ is the molar concentration (mol/kg) of species i dissolved in the liquid and P_i is the partial pressure of the gas species i. The value of k_H depends strongly on temperature and is usually fitted to an Arrhenius expression

$$k_H = k_H^\circ exp(A/T - A/T^\circ) \tag{16}$$

where $T^\circ = 298.15$ K. The constants in this expression are given for the gases of interest in the NIST Webbook http://webbook.nist.gov/ and are listed in Table 17 At standard

Table 17: Solubility parameters for four gases in water. NIST webbook

Gas	W (g/mol)	k_H° (mol·kg^{-1}·bar^{-1})	A (K)
N_2O	44.01	2.5×10^{-2}	2600.
N_2	28.01	6.0×10^{-4}	1300.
O_2	32.00	1.3×10^{-3}	1700.
H_2	2.016	7.8×10^{-4}	500.

temperature, the equilibrium dissolved gas concentrations in the water below a mixture with $P_{N_2O} = 0.7$ bar and $P_{H_2} = 0.3$ bar are $[N_2O] = 1.75\times10^{-2}$ mol·kg^{-1} and $[H_2] = 2.34\times10^{-4}$ mol·kg^{-1}. Using the molar mass W to convert these to mass fractions Y, we find that $Y_{N_2O} = 0.77$ g·kg^{-1} and $Y_{H_2} = 4.7\times10^{-4}$ g·kg^{-1}. In the case 2X for shot 24, the conditions in the pipe were about 2.75 liter water and 0.5 liter gas. For these nominal conditions, the mass of the gas components before absorption into the water can be computed from the ideal gas law $P_i V_g = m_i\ R_i\ T$, these initial amounts are $m^o_{N_2O} = 0.65$ g and $m^o_{H_2} = 1.2\times10^{-2}$ g. The maximum amount of gas that can be dissolved into the water under these conditions can be estimated from the equilibrium mass fractions and we find that $m^\ell_{N_2O} = 2.1$ g and $m^\ell_{H_2} = 1.3\times10^{-3}$ g.

Based on these considerations we would expect that over a long time a substantial fraction of the N_2O in the gas will be absorbed into the water but only about 10% of the hydrogen will be absorbed. After absorption into the water, the remaining gas mixture will have a larger fraction of H_2 compared to the initial condition. In a closed system a substantial drop

in the pressure of the gas would occur so that this effect can be readily detected. A mass balance can be used to compute the expected equilibrium partial pressure of species i if the total volume, gas plus liquid, is constant. We find that for our example, the final partial pressure of N_2O will drop to 0.158 bar, with 67% of the original N_2O in the gas absorbed into the water. The final partial pressure of H_2 will drop to 0.27 bar, with 10% of the original H_2 absorbed into the water. The total pressure is predicted to drop from 1 bar to 0.43 bar. No such effect was observed in the present testing.

The explanation is straight forward. Although the solubility of N_2O is quite high, the rate of diffusion of gas into a stagnant water layer is quite low. The diffusivity N_2O into water is $D = 2.6{\times}10^{-5}$ cm^2·s^{-1} (Akgerman and Gainer, 1972). Using the conventional estimate of diffusion layer thickness, $\delta = \sqrt{Dt}$, we compute that after 10 min, the N_2O has only diffused about 1.4 mm into the water. This amounts to a total mass of approximately $7{\times}10^{-2}$ g or about 10% of the gas mass.[3] This would have resulted in a pressure drop of about 23 Torr, which would have been readily observable had this occurred. The other possibility is that some gas absorption occurred during the water filling process, we would have had no way to detect this.

The detonation parameters are relatively insensitive to the gas composition (see Table 20) in the range of $0.3 < X_{H2} < 0.5$ so that a slight increase in the H_2 fraction in the gas layer should not significantly affect the results. In fact, the mixture should be slightly more sensitive (small induction zone and cell width) with essential unchanged thermodynamic parameters. Evaporation of the water and dilution of gas mixture is estimated (Appendix D) is expected to have a larger and potentially compensating effect compared to any decrease in N_2O fraction. The largest pressure changes that we have observed are about .5% (< 4 Torr) between the introduction of the gas and the initiation of the explosion. The pressure actually tends to increase after filling due to thermal equilibrium of the gas and vaporization of the water. In the worse case, if the pressure increase due to water evaporation was the maximum (100% humidity at 30°C) amount of 4 kPa (30 Torr), then the compensating decrease in N_2O must have been comparable in magnitude. In this bounding situation, an estimate of the final composition would be 0.3 H_2, 0.66 N_2O and 0.04 H_2O. Such a mixture is estimated (Section D and E) to have similar thermodynamic properties and detonation sensitivity (reaction zone length or cell width) will be about 25% larger (see the last entry in Table 19) than that of the 0.3/0.7 mixture that was the target for the test condition.

These computations support our conclusions based on the experimental data that there was either negligible absorption of the gas mixture into the water on the time scale of the gas-water contact in the present experiments or absorption was compensated for by evaporation of water into the mixture. In either case, the effects of absorption and vaporization will have a modest effect on the mixture parameters.

[3] In making this estimate, we have assumed that the liquid is stagnant but the gas is well stirred so that the solution to the diffusion problem is approximately that for diffusion into a semi-infinite slab with a fixed boundary concentration equal to the equilibrium value.

C Water properties

Table 18: Thermophysical properties of water: vapor pressure Lide (2010), density Lide (2010), and sound speed Del Grosso and Mader (1972).

T °C	P_v kPa	ρ kg/m^3	a m/s
20	2.3393	998.2063	1482.343
22	2.6453	997.773	1488.319
24	2.9858	997.2994	1493.976
25	3.1699	997.0480	1496.687
26	3.3639	996.787	1499.323
28	3.7831	996.2371	1504.370
30	4.247	995.6511	1509.127
32	4.7596	995.0302	1513.603
34	5.3251	994.3756	1517.806
36	5.9479	993.6883	1521.745
38	6.6328	992.9695	1525.428
40	7.3849	992.2204	1528.863

D Effect of Humidity on Explosion Properties

Explosion parameters have been computed using realistic thermochemical properties (Browne et al., 2004) for 0.3 H_2 + 0.7N_2O mixtures saturated with water vapor. The total initial pressure $P_1 = 101.325$ kPa for all cases and the initial temperature T_1 range is 20–33°C. The initial partial pressures have set so that the ratio of $H_2/N_2O = 0.3/0.7$ is the same for all mixtures. The first entry is the reference condition with no water vapor and the subsequent entries have the partial pressure of water set equal to the saturation values of Table 18. The ratio of ZND reaction zone lengths, the last column, can be used as an estimator for the ratio of detonation cell widths (Akbar et al., 1997). The reference length $\Delta_o = 79$ μm.

Table 19: Computed explosion properties

P_{CV}	constant volume explosion pressure
σ	volume expansion ratio (burned/unburned) for constant pressure combustion
c_b	burned gas sound speed for constant pressure combustion
U_{CJ}	Chapman-Jouguet detonation speed
P_{CJ}	Chapman-Jouguet detonation pressure
$P_{CJ,r}$	Reflected shock pressure due to normal incidence of CJ detonation
Δ/Δ_o	ratio of ZND reaction zone lengths

T_1 (K)	P_{CV} (MPa)	σ	c_b (m/s)	U_{CJ} (m/s)	P_{CJ} (MPa)	$P_{CJ,r}$ (MPa)	Δ/Δ_o
Reference condition - no water vapor							
300.00	1.33	11.2	1011	2088.2	2.62	6.50	1.00
Saturated with water vapor							
293.15	1.34	11.3	1007	2079.3	2.63	6.52	1.17
295.15	1.33	11.2	1007	2077.8	2.61	6.47	1.19
297.15	1.31	11.1	1007	2076.3	2.59	6.41	1.21
298.15	1.31	11.0	1006	2075.4	2.57	6.37	1.23
299.15	1.30	11.0	1006	2074.5	2.56	6.35	1.25
301.15	1.29	10.9	1006	2072.7	2.54	6.29	1.28
303.15	1.28	10.8	1005	2070.6	2.51	6.24	1.32
305.15	1.26	10.7	1005	2068.3	2.48	6.15	1.37
0.30 H_2, 0.66 N_2O and 0.04 H_2O							
300.	1.29	10.9	1013	2088.6	2.54	6.29	1.24

E Effect of Mixture Composition

Explosion parameters have been computed using realistic thermochemical properties (Browne et al., 2004) for dry X H_2 + (1-X)N_2O mixtures. The total initial pressure $P_1 = 101.325$ kPa for all cases and the initial temperature T_1 range was 300 K (26.85 °C.) The ratio of ZND reaction zone lengths, the last column, can be used as an estimator for the ratio of detonation cell widths (Akbar et al., 1997). The condition at 0.3 H_2 was used as the reference datum.

Table 20: Computed explosion properties as a function of hydrogen fraction.

X_{H_2} (K)	P_{CV} (MPa)	σ	c_b (m/s)	U_{CJ} (m/s)	P_{CJ} (MPa)	$P_{CJ,r}$ (MPa)	Δ/Δ_o
0.20	1.32	11.0	952.7	1956.0	2.59	6.41	1.78
0.25	1.33	11.1	981.1	2021.1	2.61	6.48	1.27
0.30	1.33	11.2	1010.7	2088.2	2.62	6.50	1.00
0.35	1.33	11.2	1042.0	2158.2	2.63	6.53	0.85
0.40	1.32	11.2	1075.6	2231.8	2.61	6.47	0.77
0.45	1.31	11.0	1111.7	2309.3	2.58	6.40	0.73
0.50	1.29	10.9	1150.7	2391.1	2.57	6.44	0.75
0.55	1.26	10.6	1193.1	2476.4	2.47	6.13	0.83
0.60	1.21	10.2	1239.5	2566.0	2.39	5.91	1.00

F D1 Data Plots

Table 21: Sensor locations in D1 testing.

Sensor	Port	Location	Distance (in)
		Shots 14-15	
P1	5T	81.56	
P2	6T	top	69.56
P8	7T	bottom	59.50
P3	8T	bottom	51.50
P4	9T	top	43.50
P9	10T	top	35.50
P5	11T	top	27.50
P10	12T	top	19.50
P6	13T	top	11.50
P11	14T	top	3.50
IGN	W	west flange	-0.75
		Shots 12-13	
P1	5T	81.56	
P2	6T	top	69.56
P3	8T	bottom	51.50
P4	9T	top	43.50
P5	11T	top	27.50
P6	13T	top	11.50
IGN	W	west flange	-0.75
S11		window	45.5
S12		Channel - vertical	45.5
S13		Channel - horizontal	45.5
		Shots 13 only	
S14		window	43.5
S15		window	51.50

Table 22: Sensor locations in D1 testing, shots 1–11.

Sensor	Port	Location	Distance (in)
		Shots 7-11	
P1	5T	top	81.56
P2	6T	top	69.56
P3	7T	top	59.50
P4	9T	top	43.50
P5	11T	top	27.50
P6	13T	top	11.50
IGN	W	west flange	-0.75
		Shots 1-6	
IGN	E	East flange	
P1	5T	top	81.56
P2	6T	top	69.56
P3	7T	top	59.50
P4	9T	top	43.50
P5	11T	top	27.50
P6	13T	top	11.50
P7	W	west flange	-0.75

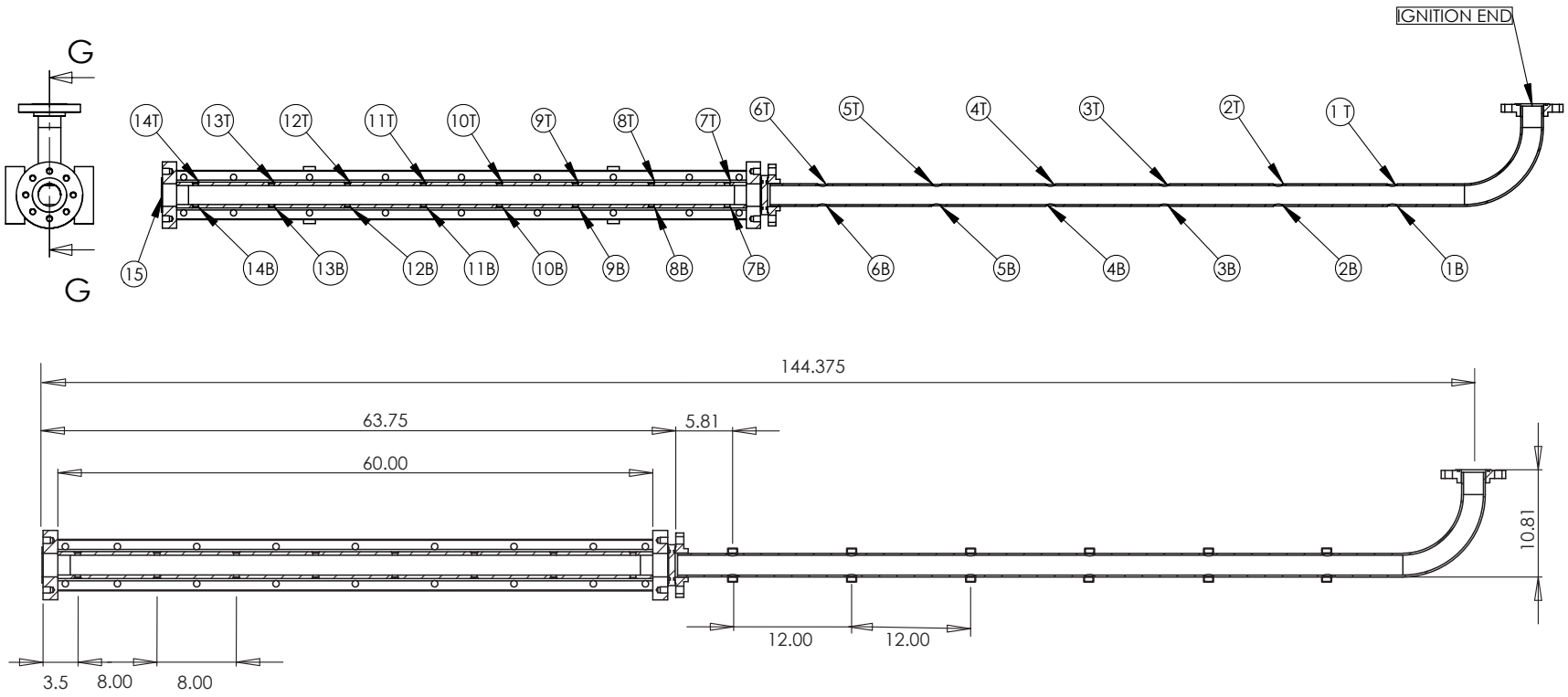

Figure 87: Port labeling and locations for D1 testing. Dimensions are given in inches from the east end of the visualization section. The spacing of the instruments ports is 8 in within the visualization section and 12 in within SS1-2.

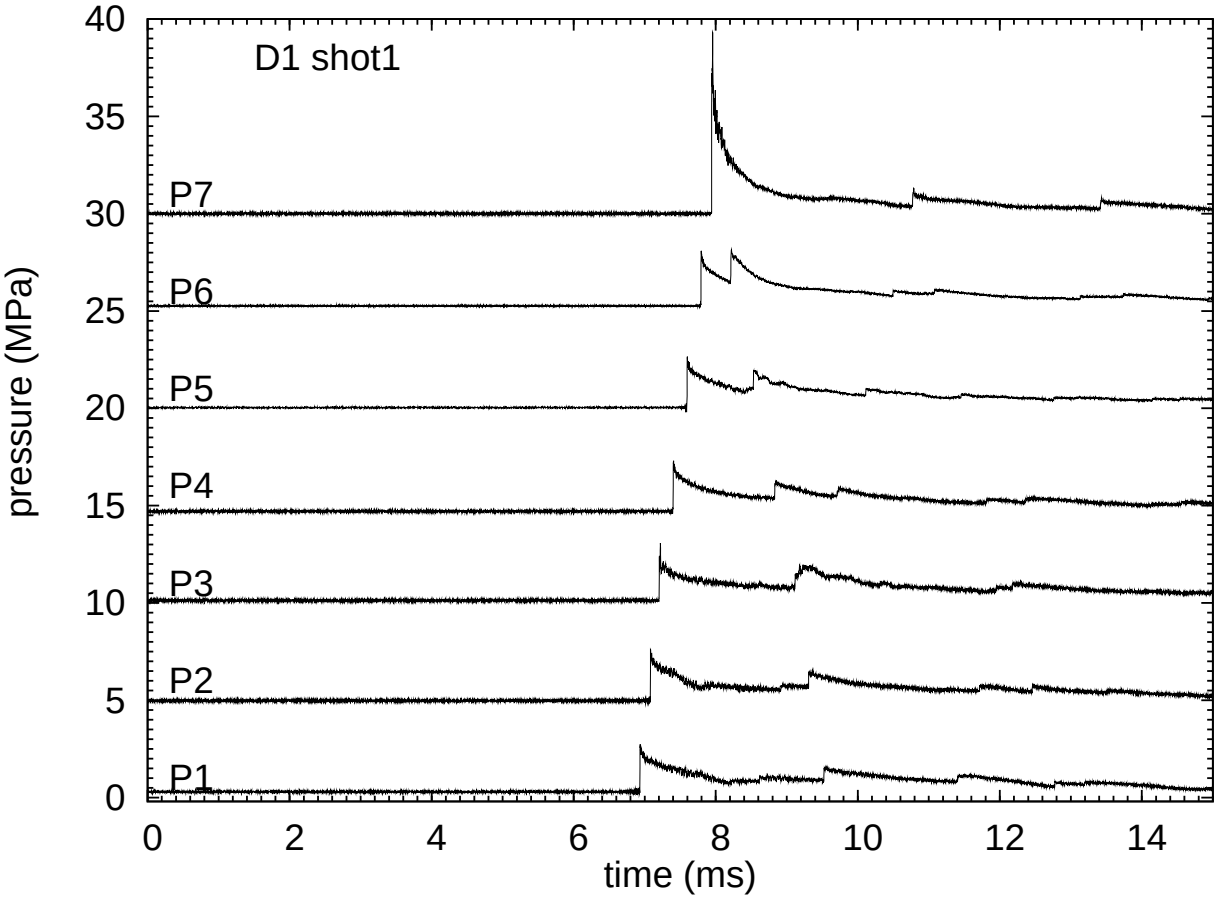

Figure 88: Pressure data from shot 1. Raw data without baseline correction. Trigger for spark discharge was 100 μs after $t = 0$.

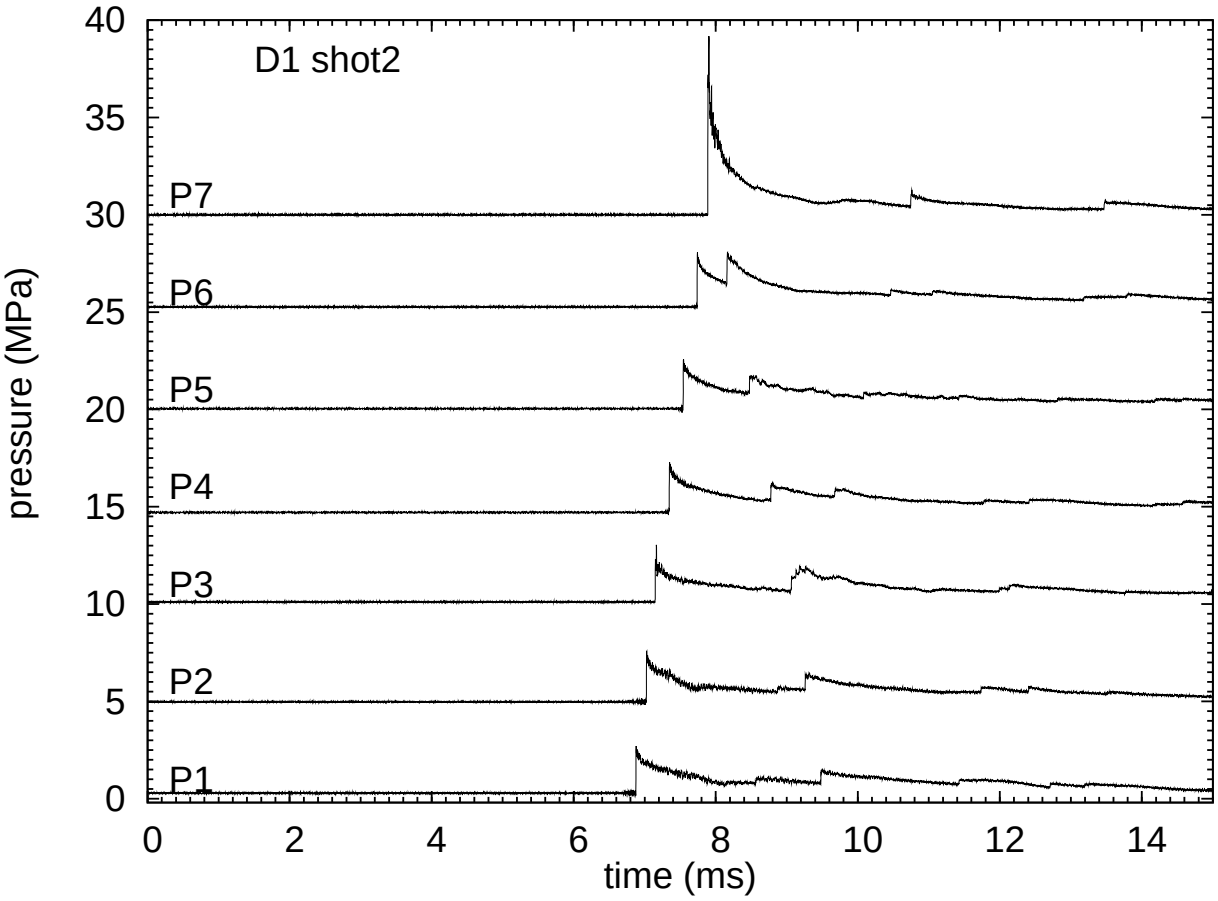

Figure 89: Pressure data from shot 2. Raw data without baseline correction. Trigger for spark discharge was 100 μs after $t = 0$.

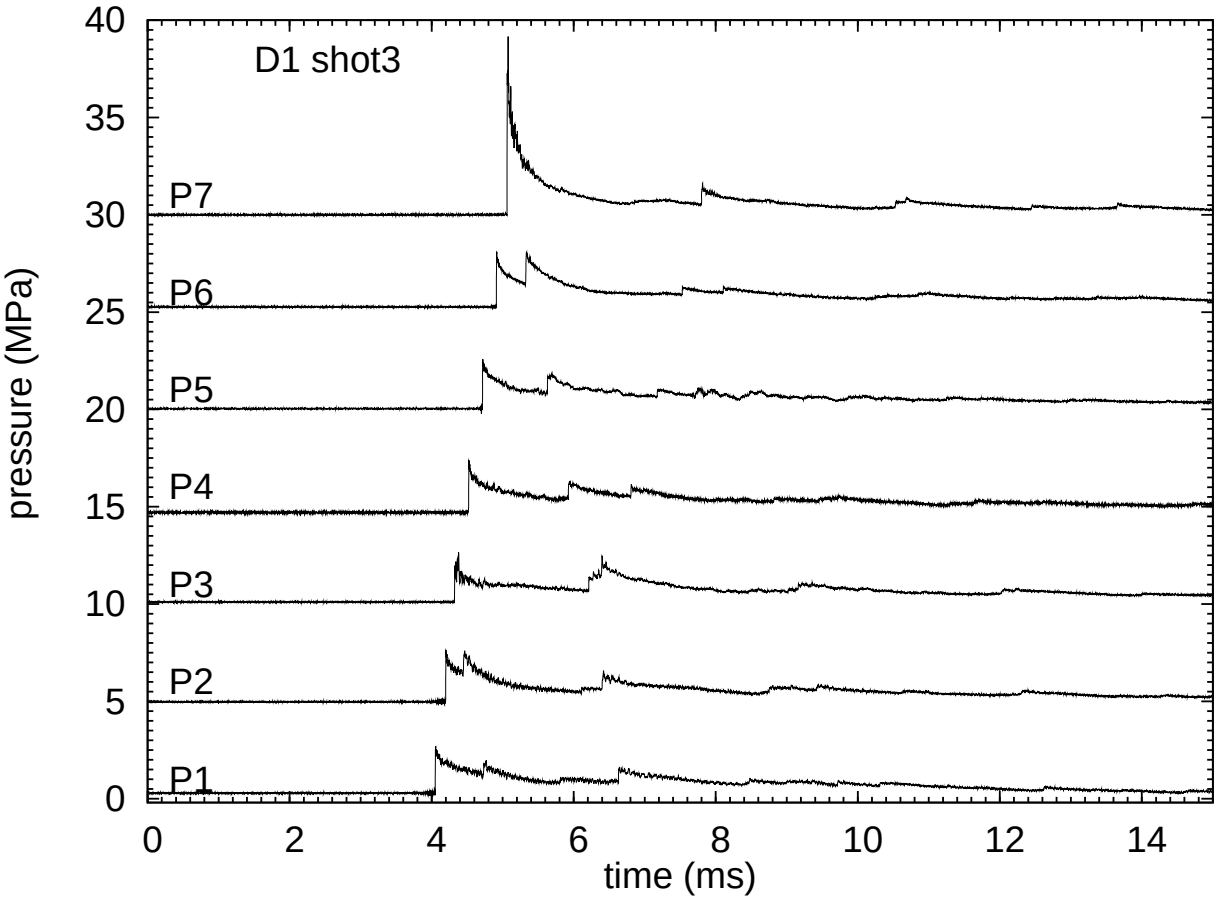

Figure 90: Pressure data from shot 3. Raw data without baseline correction. Trigger for spark discharge was 100 μs after $t = 0$.

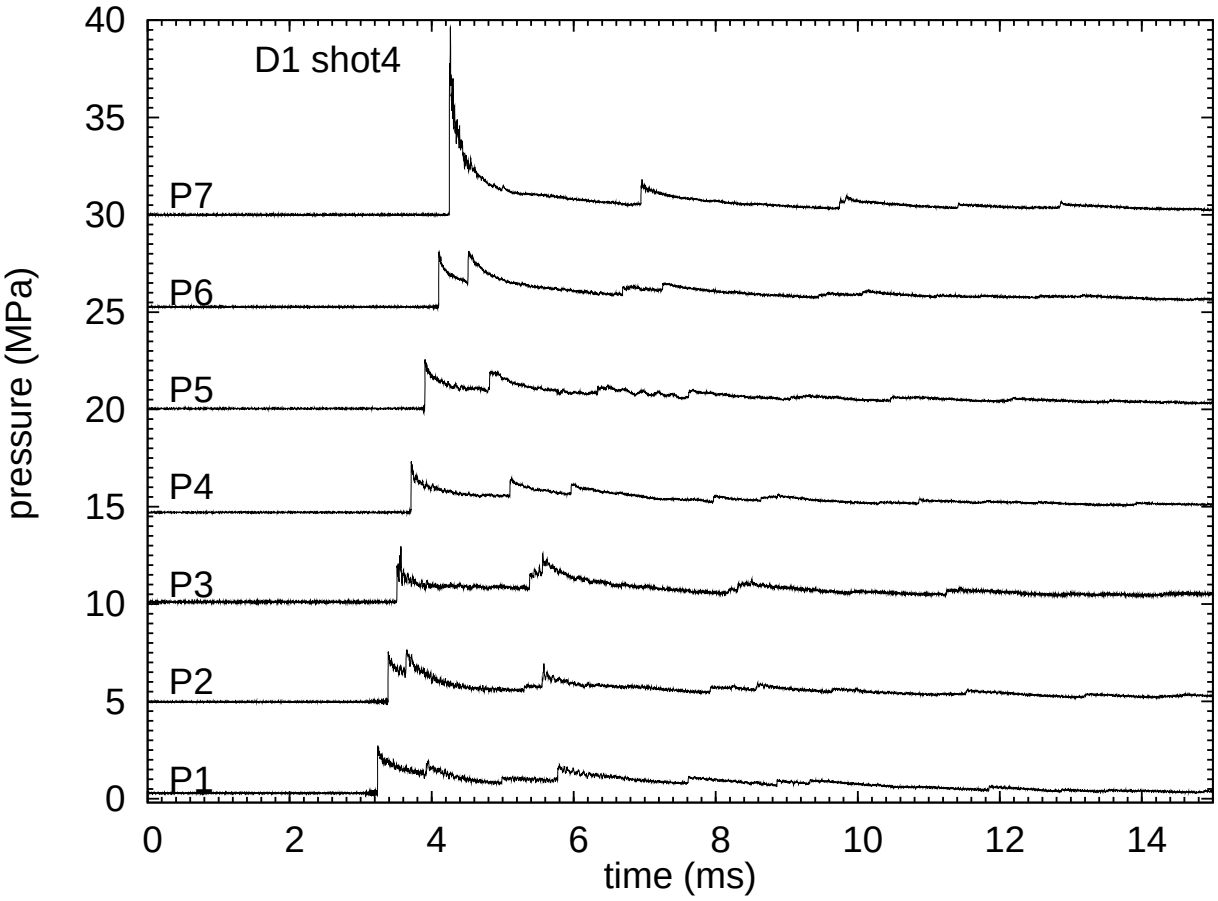

Figure 91: Pressure data from shot 4. Raw data without baseline correction. Trigger for spark discharge was 100 μs after $t = 0$.

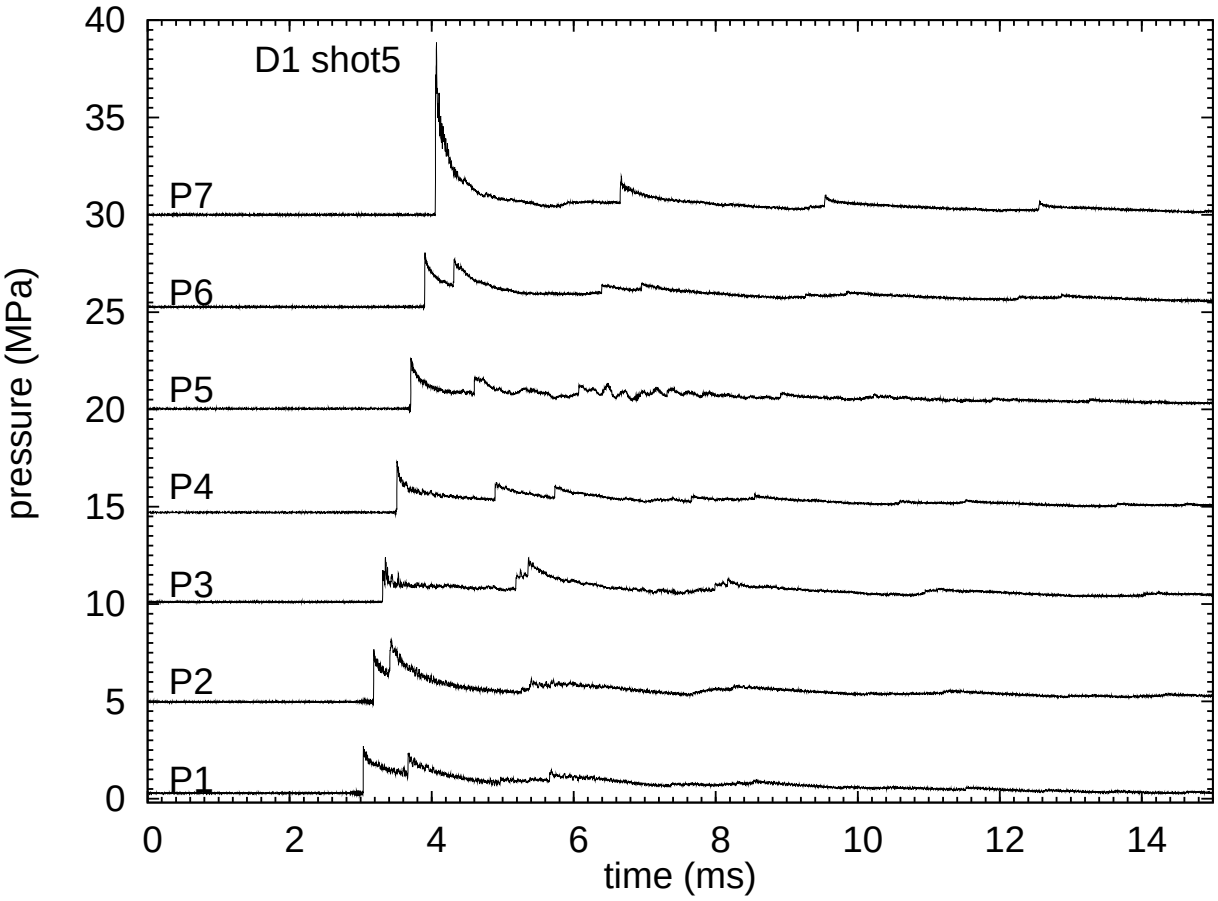

Figure 92: Pressure data from shot 5. Raw data without baseline correction. Trigger for spark discharge was 100 μs after $t = 0$.

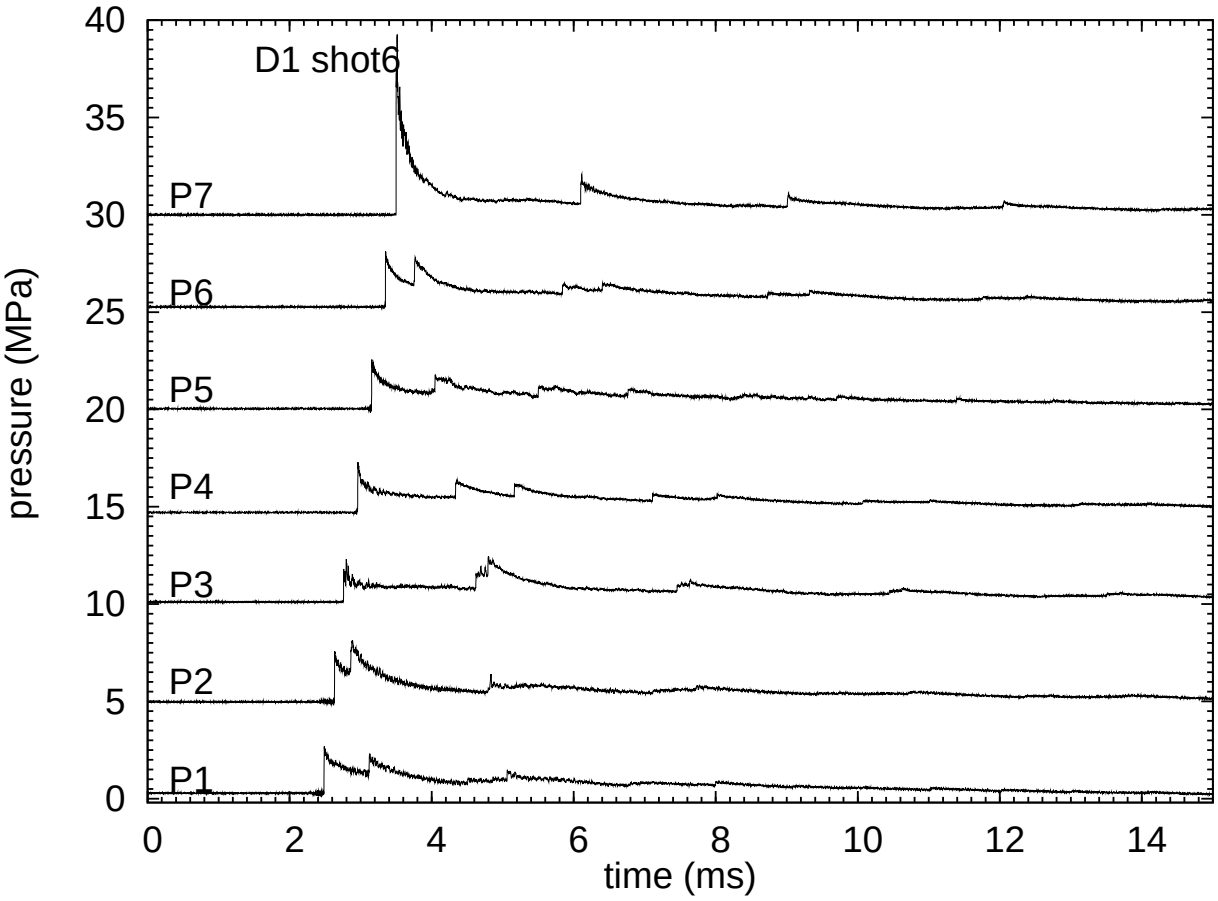

Figure 93: Pressure data from shot 6. Raw data without baseline correction. Trigger for spark discharge was 100 μs after $t = 0$.

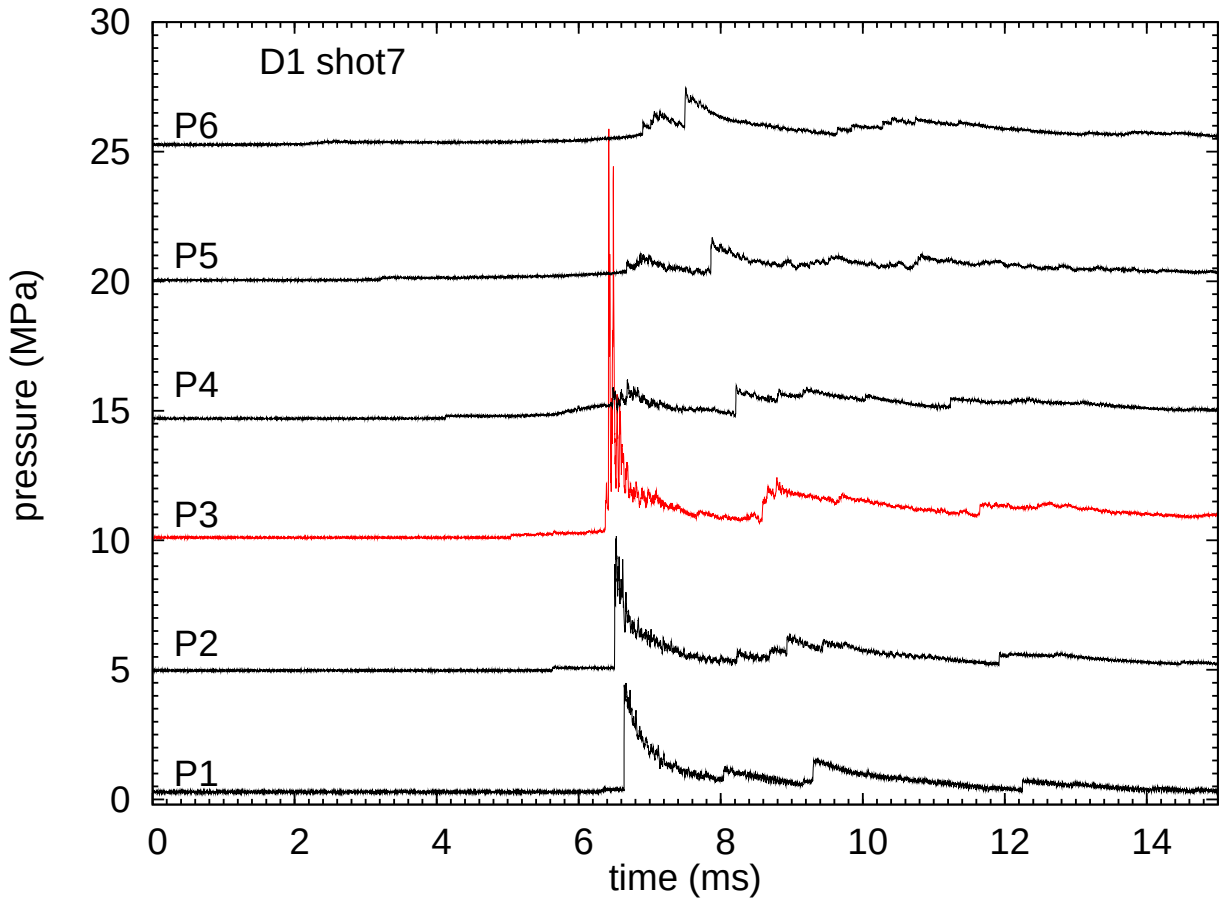

Figure 94: Pressure data from shot 7. Raw data without baseline correction. Trigger for spark discharge was 100 μs after $t = 0$.

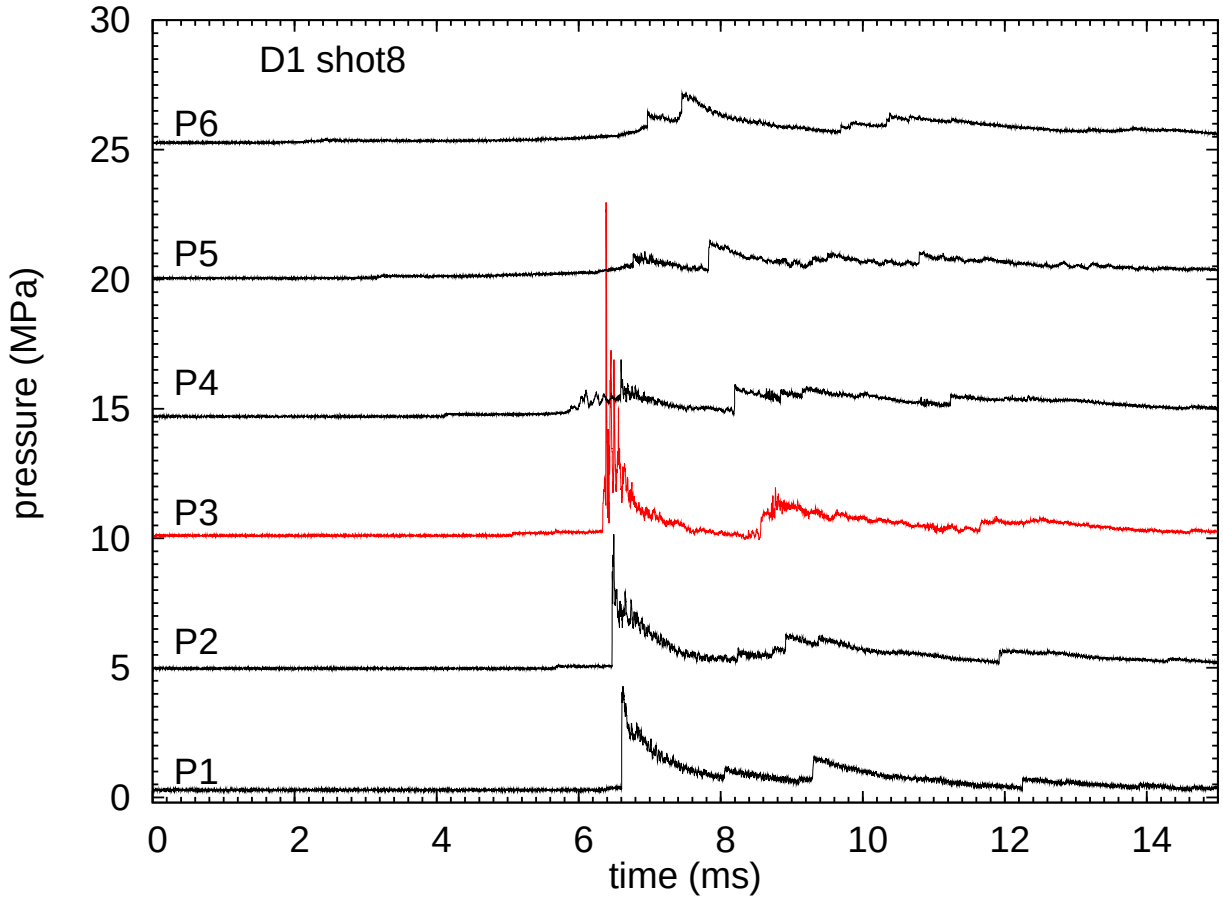

Figure 95: Pressure data from shot 8. Raw data without baseline correction. Trigger for spark discharge was 100 μs after $t = 0$.

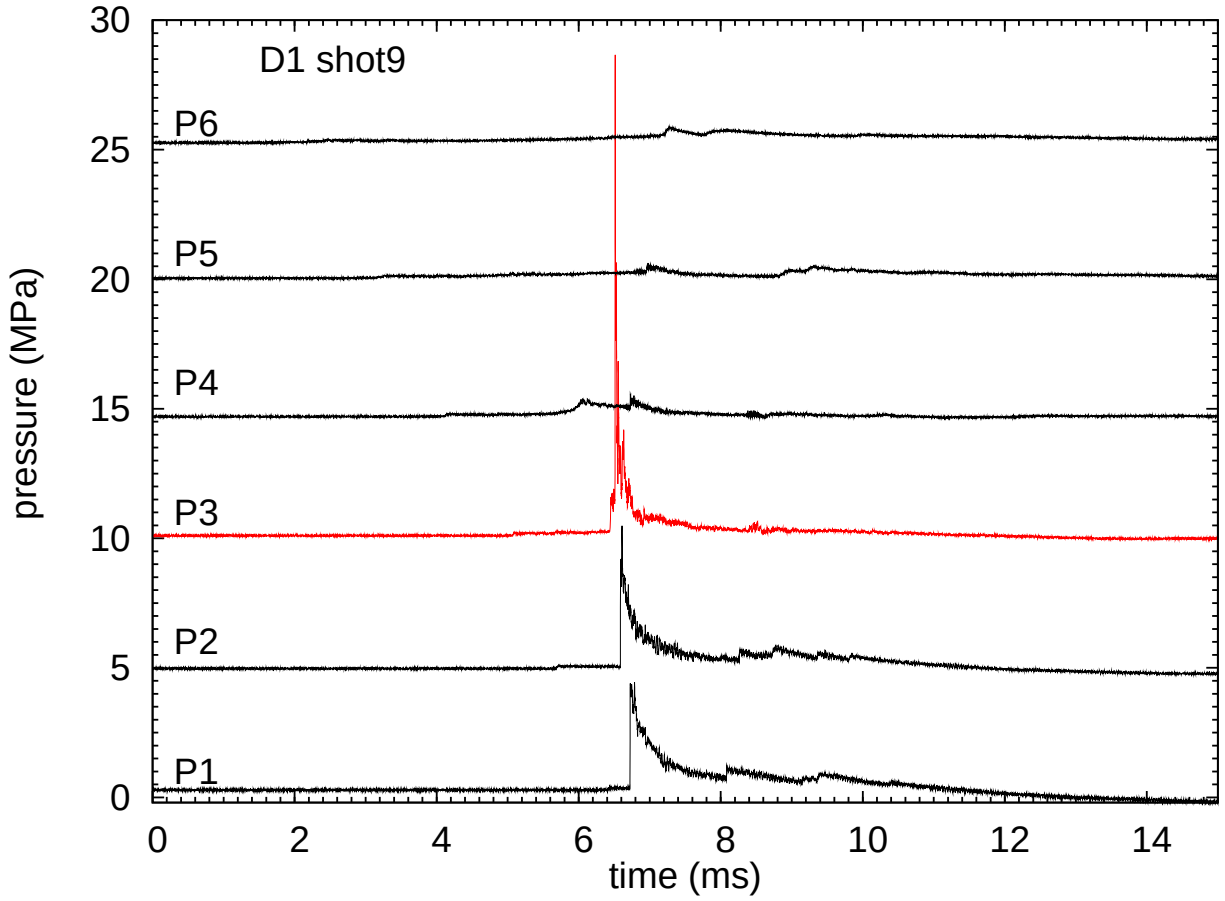

Figure 96: Pressure data from shot 9. Raw data without baseline correction. Trigger for spark discharge was 100 μs after $t = 0$.

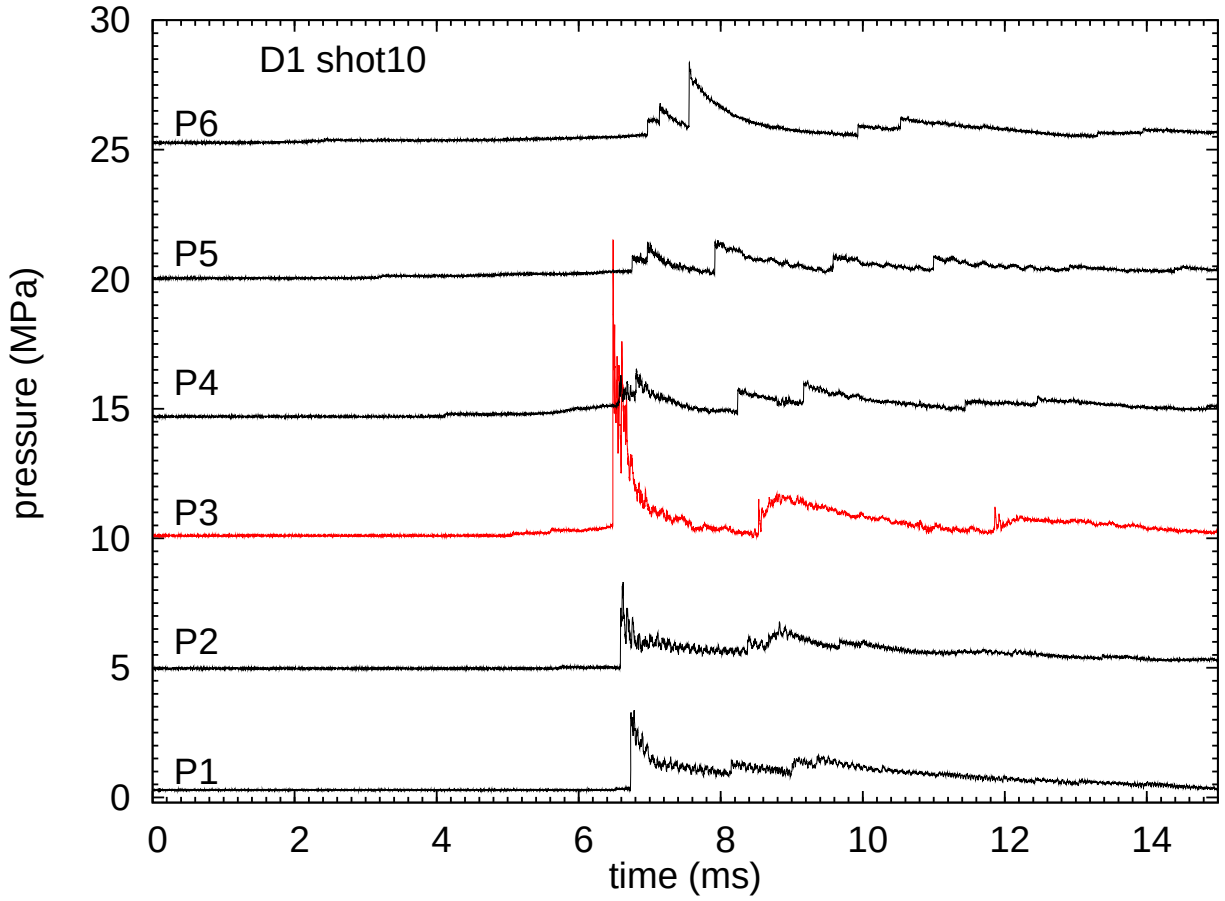

Figure 97: Pressure data from shot 10. Raw data without baseline correction. Trigger for spark discharge was 100 μs after $t = 0$.

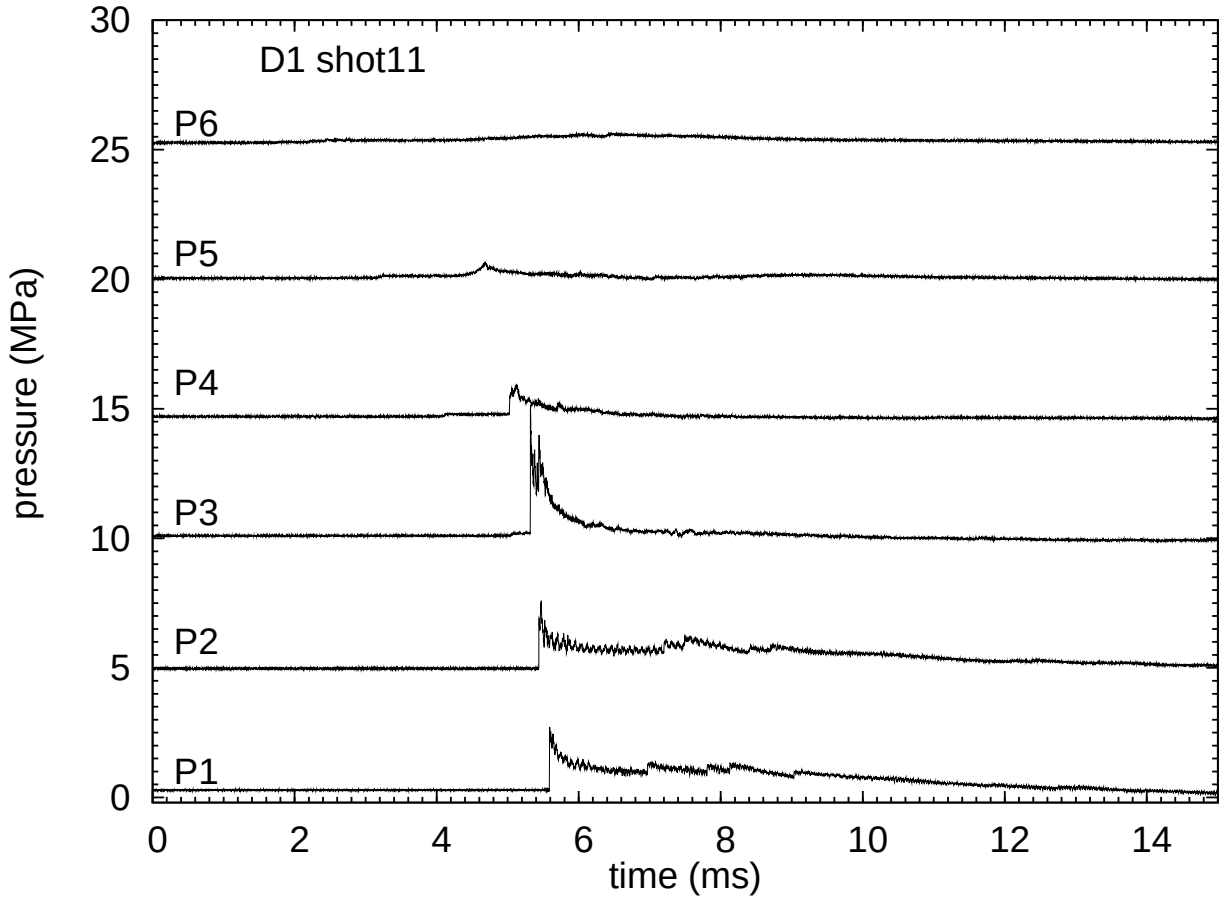

Figure 98: Pressure data from shot 11. Raw data without baseline correction. Trigger for spark discharge was 100 μs after $t = 0$.

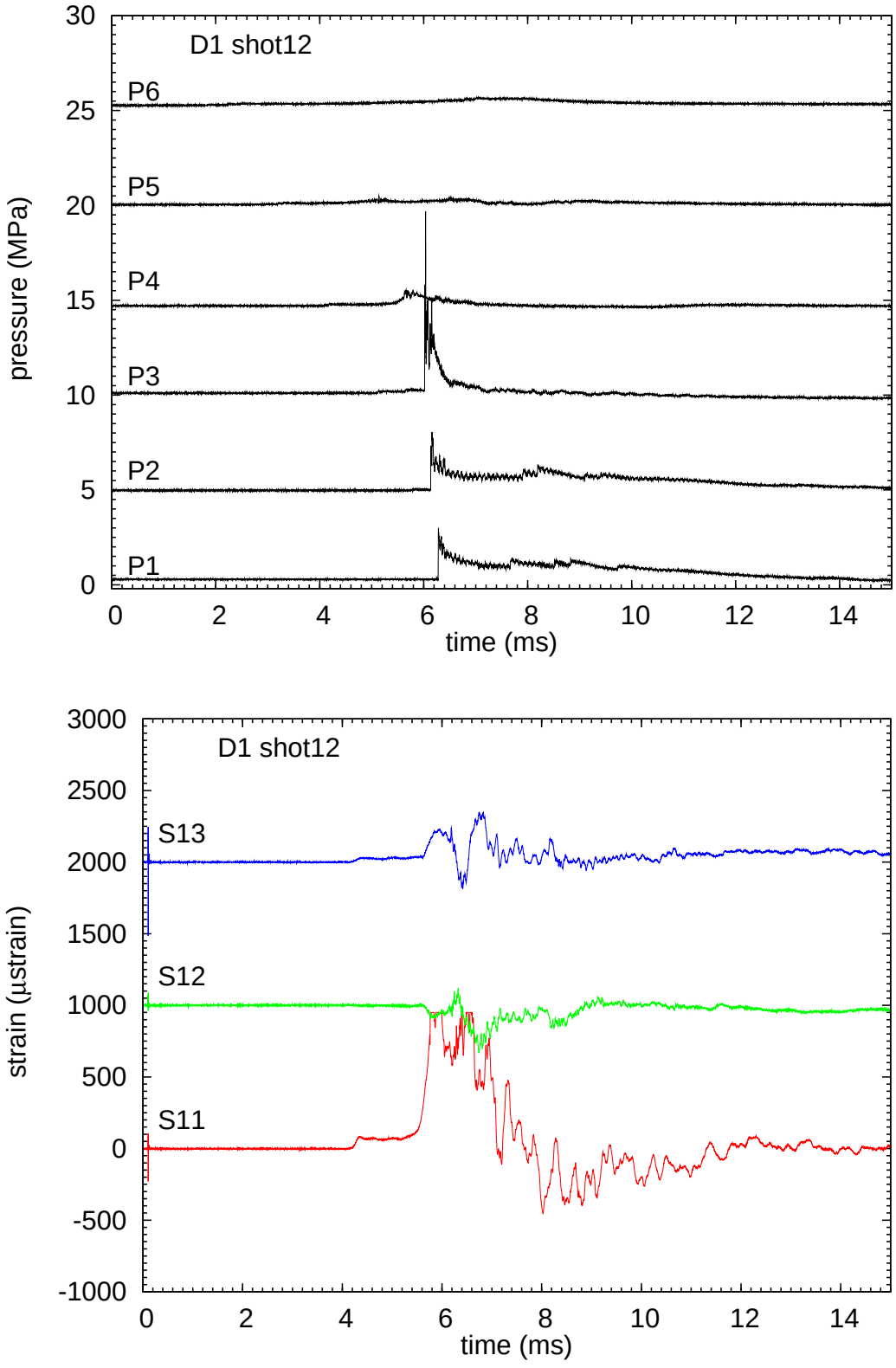

Figure 99: Pressure and strain data from shot 12. Raw data without baseline correction or removal of ignition transient artifact from strain signals. Trigger for spark discharge was 100 μs after $t = 0$.

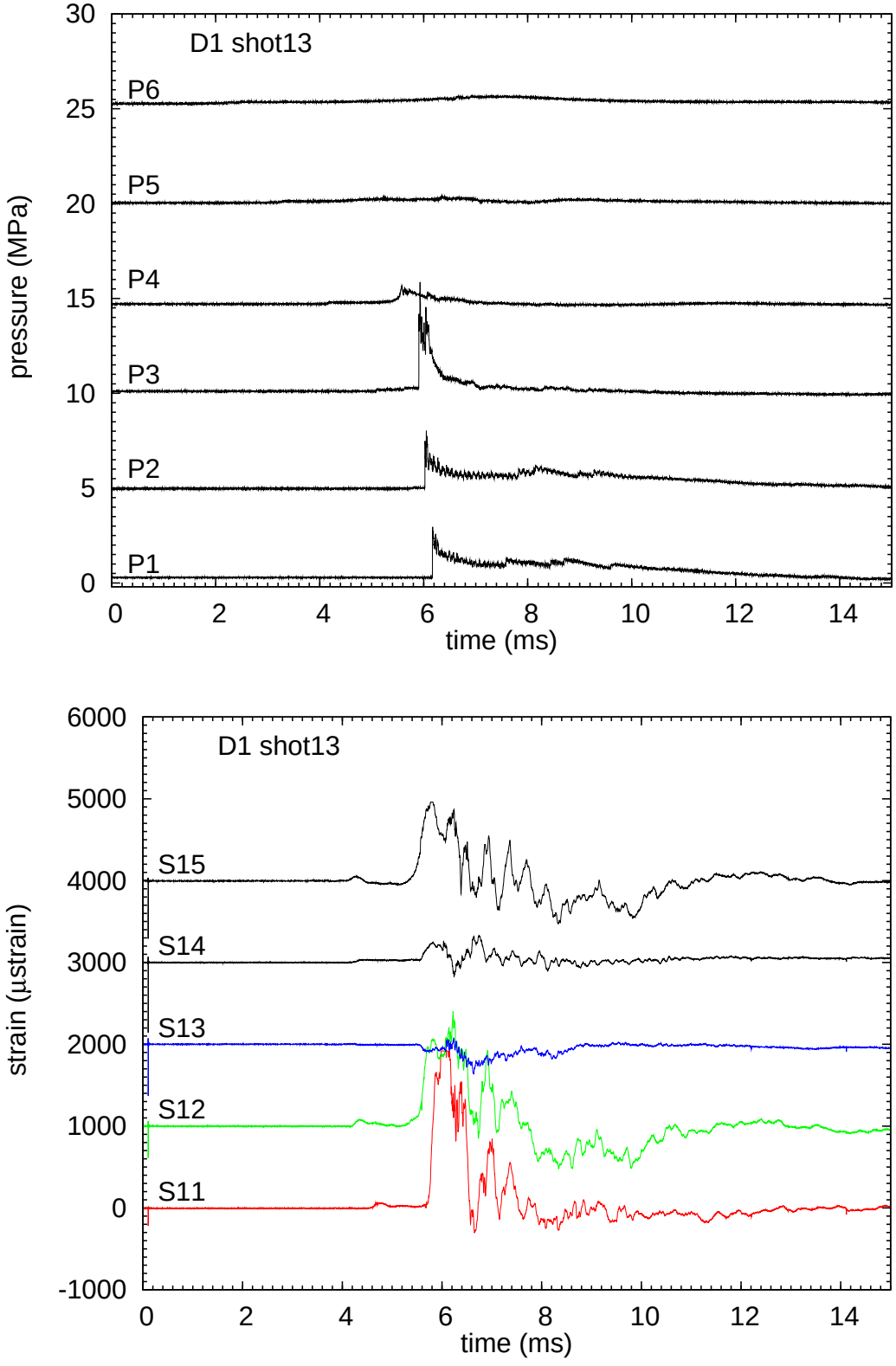

Figure 100: Pressure and strain data from shot 13. Raw data without baseline correction or removal of ignition transient artifact from strain signals. Trigger for spark discharge was 100 μs after $t = 0$.

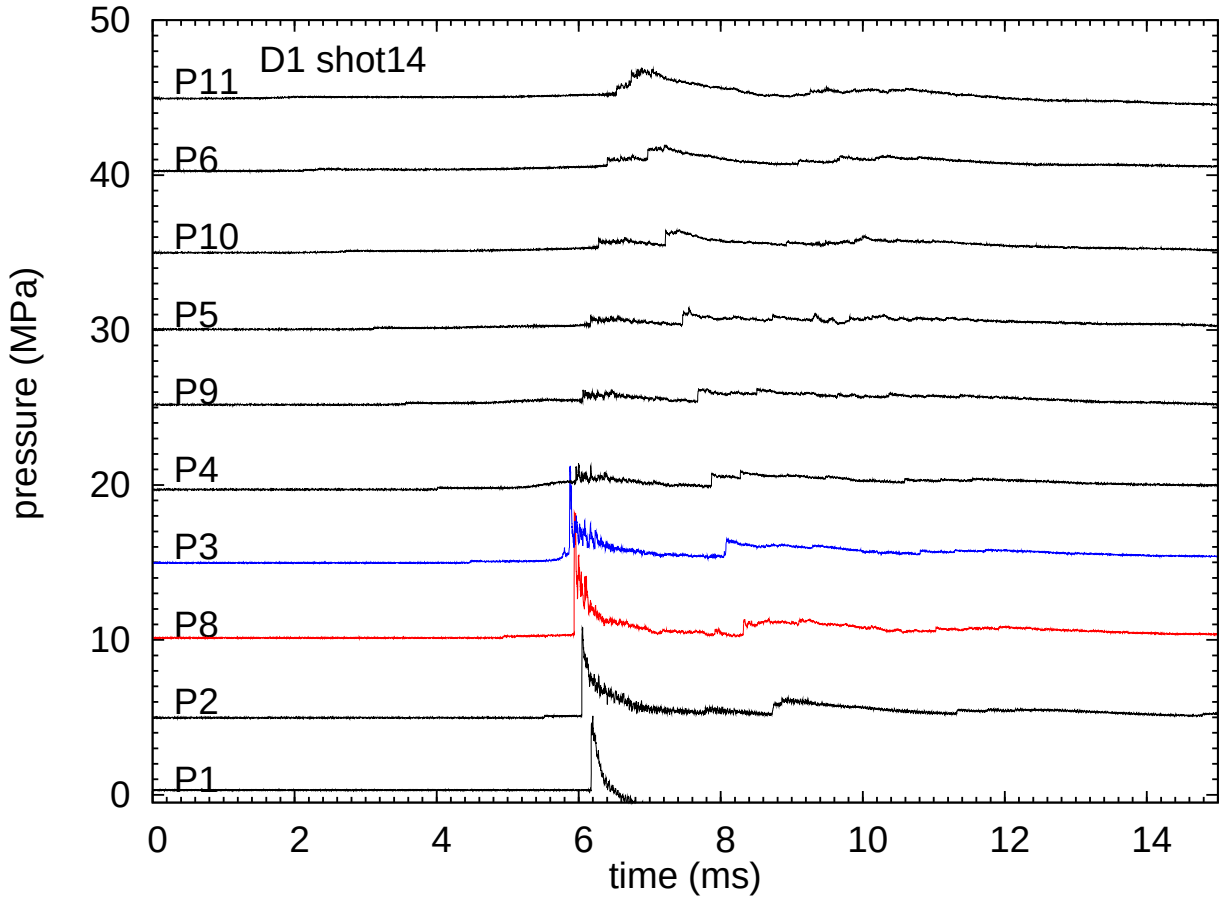

Figure 101: Pressure data from shot 14. Raw data without baseline correction. Trigger for spark discharge was 100 μs after $t = 0$.

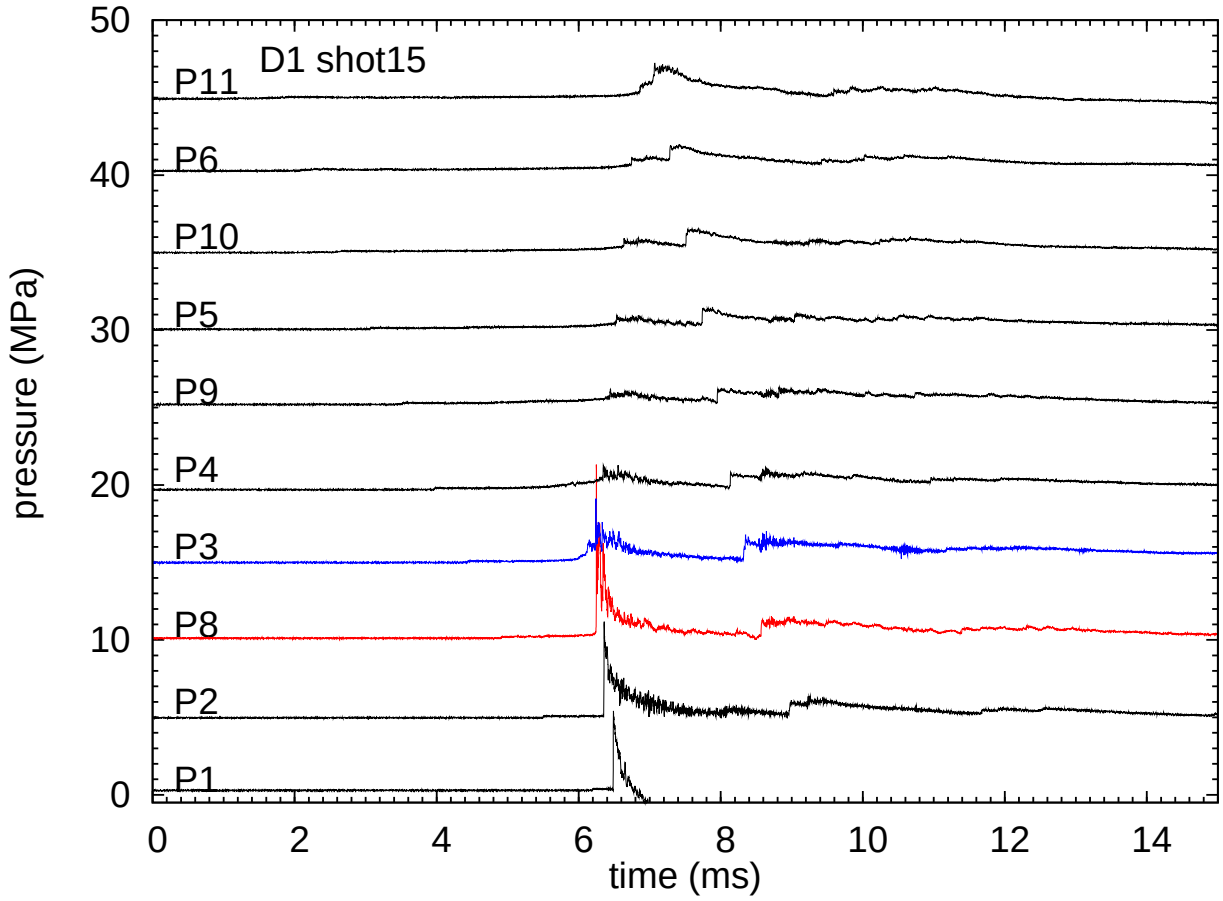

Figure 102: Pressure data from shot 15. Raw data without baseline correction. Trigger for spark discharge was 100 μs after $t = 0$.

G D2 Data Plots

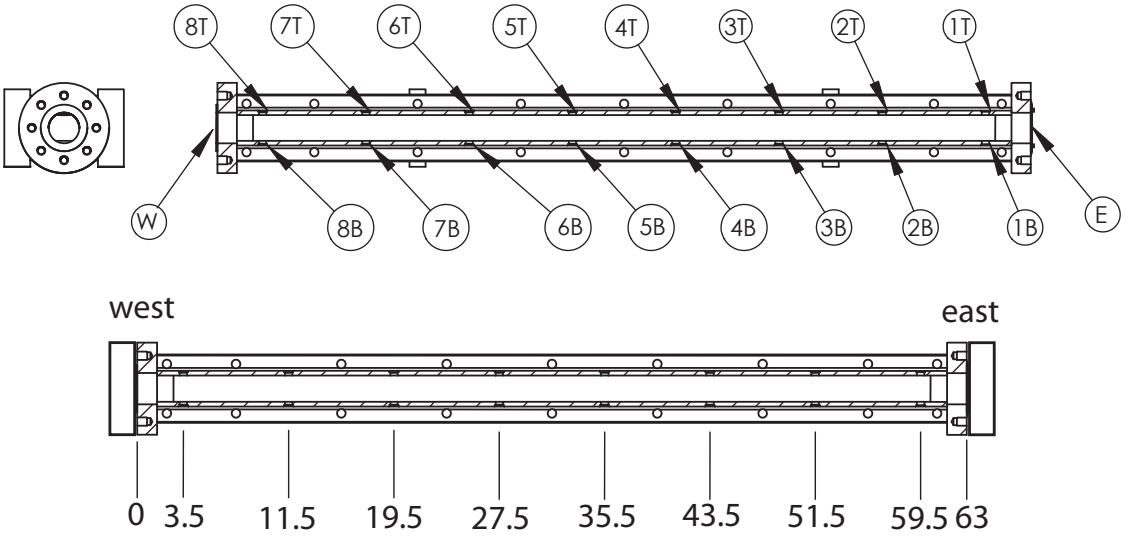

Figure 103: Port labeling and locations for the visualization section D2. Dimensions are given in inches from the east end plate; The pressure transducers in the end flanges are located 0.75 in outboard of this surface.

Table 23: Sensor locations in D2 testing.

Sensor	Port	Location	Distance (in)
		Shots 17-21	
P1	E	east flange	63.75
TC	1T	top	59.50
P8	2T	top	51.50
L	2B	bottom	51.50
P3	3B	bottom	43.50
P4	3T	top	43.50
P9	4T	top	35.50
P5	5T	top	27.50
P10	6T	top	19.50
P6	7T	top	11.50
IGN	8T	top	3.50
P11	W	west flange	-0.75
		Shot 16, P11 and IGN locations were exchanged	
P11	8T	top	3.50
IGN	W	west flange	-0.75

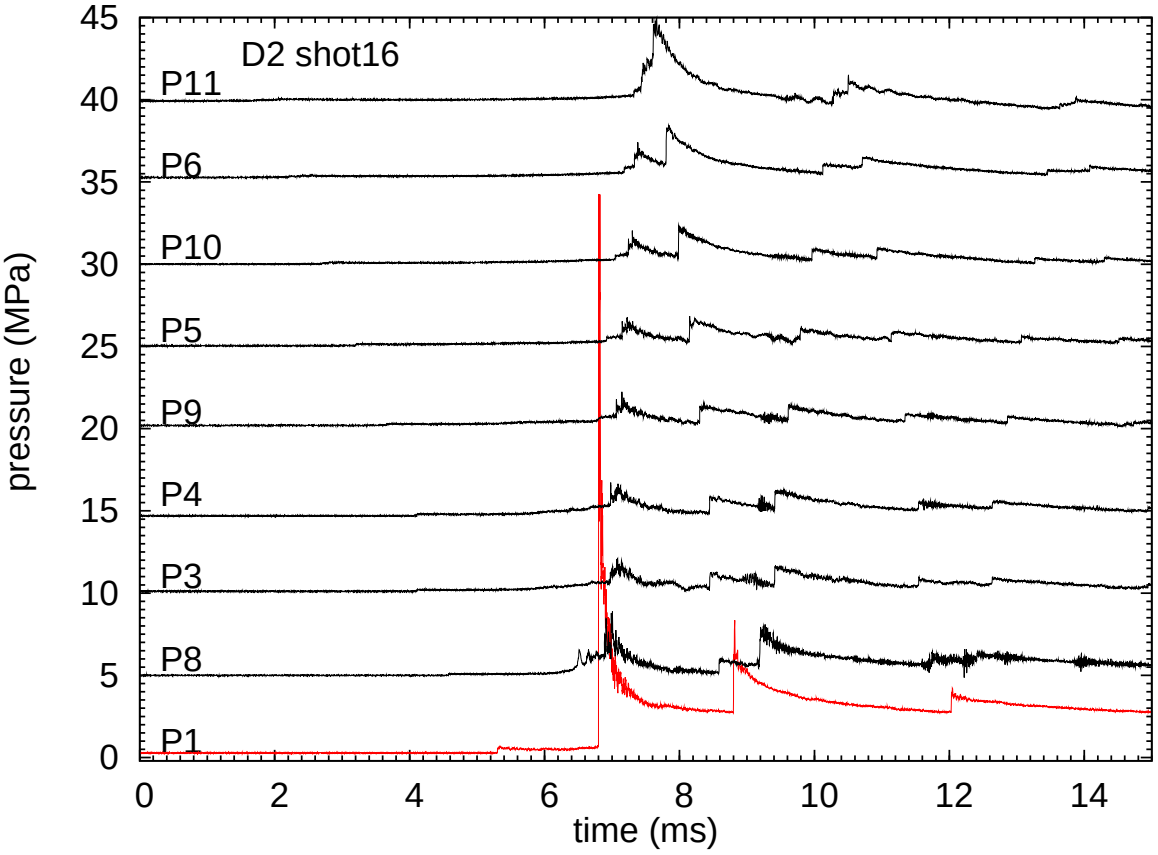

Figure 104: Pressure data from shot 16. Raw data without baseline correction. Trigger for spark discharge was 100 μs after $t = 0$.

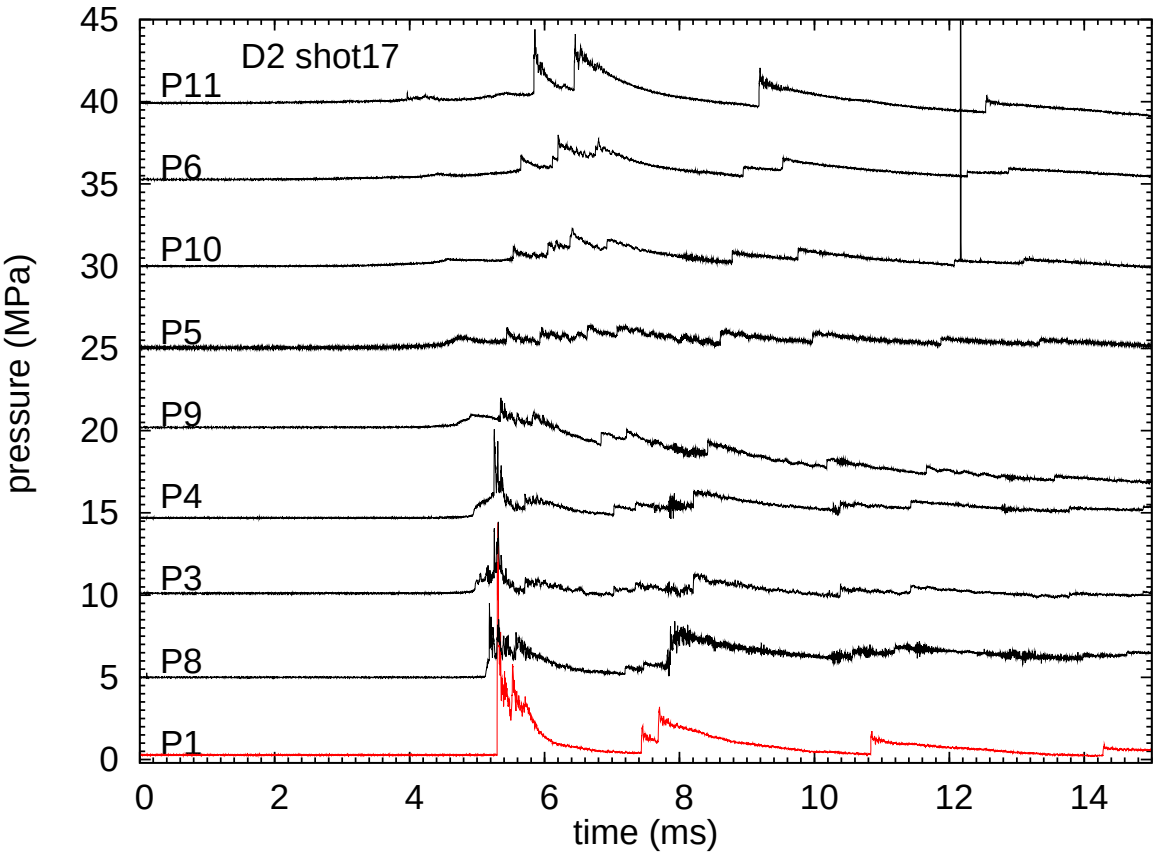

Figure 105: Pressure data from shot 17. Raw data without baseline correction. Trigger for spark discharge was 100 μs after $t = 0$.

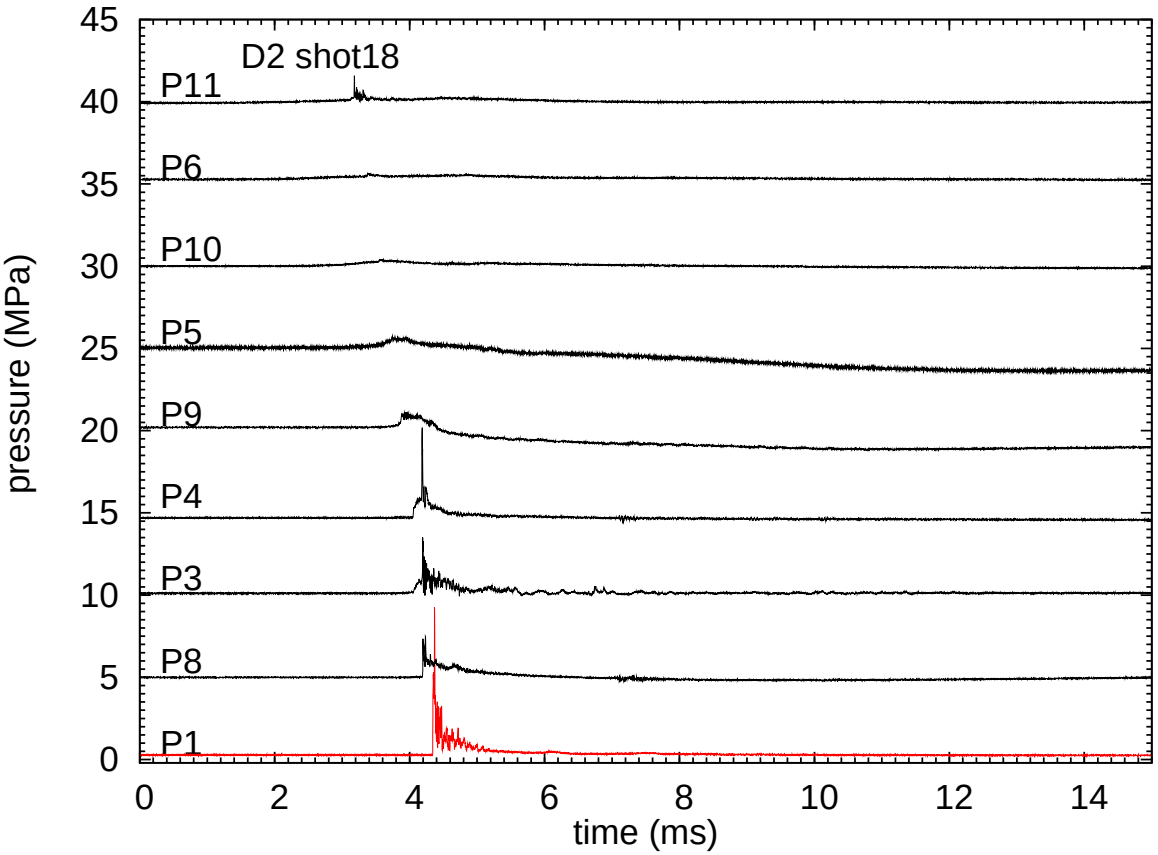

Figure 106: Pressure data from shot 18. Raw data without baseline correction. Trigger for spark discharge was 100 μs after $t = 0$.

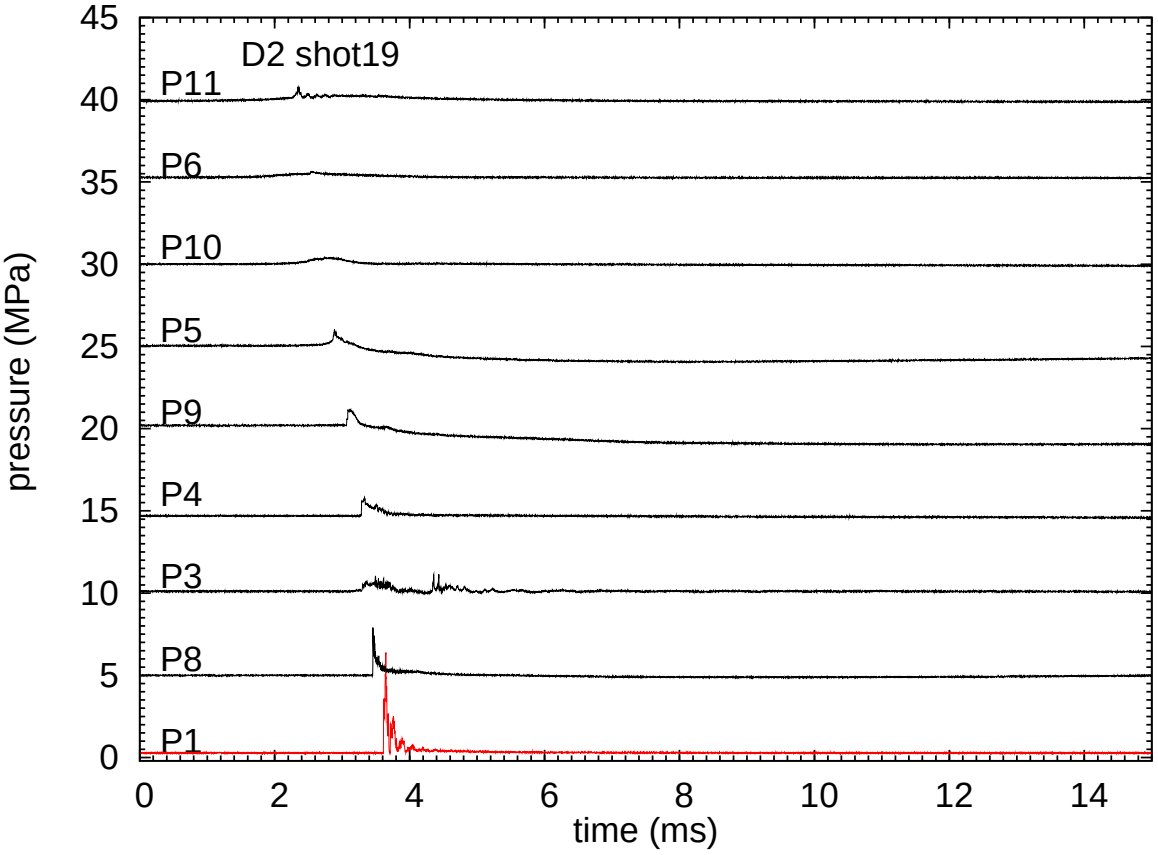

Figure 107: Pressure data from shot 19. Raw data without baseline correction. Trigger for spark discharge was 100 μs after $t = 0$.

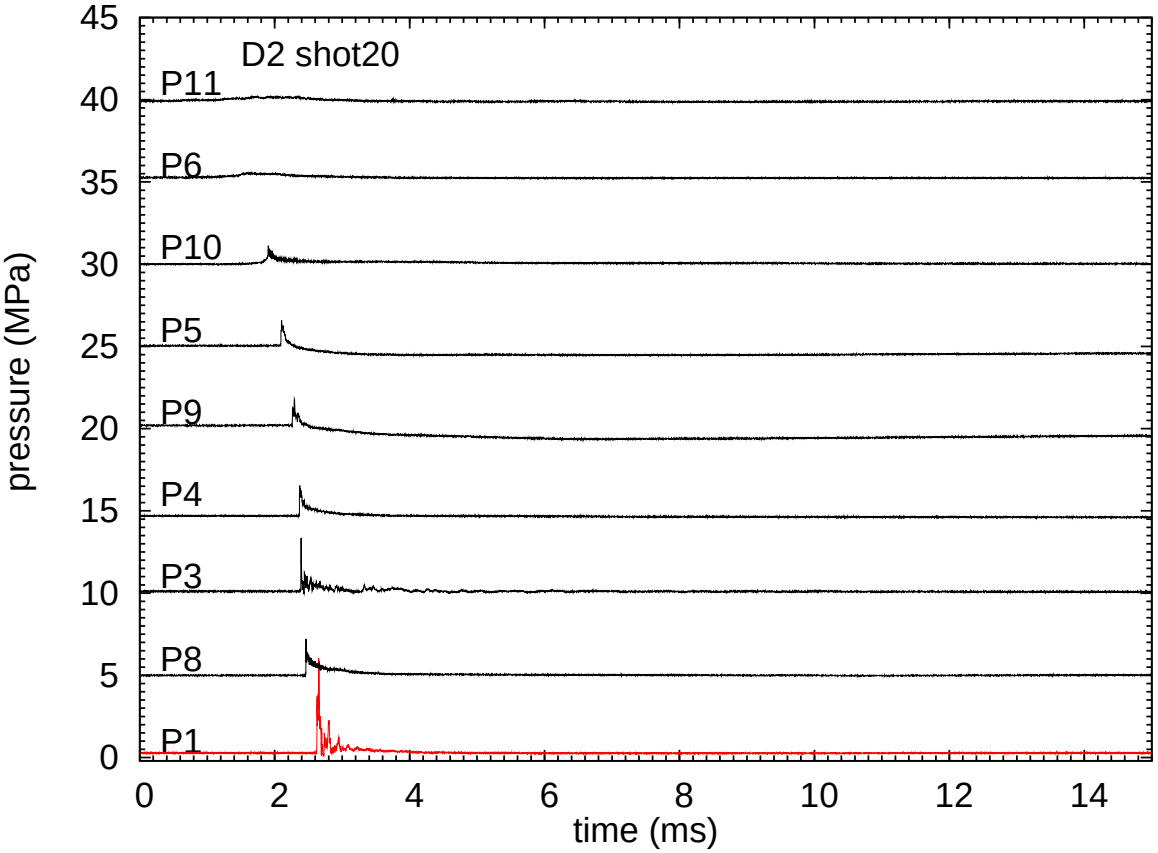

Figure 108: Pressure data from shot 20. Raw data without baseline correction. Trigger for spark discharge was 100 μs after $t = 0$.

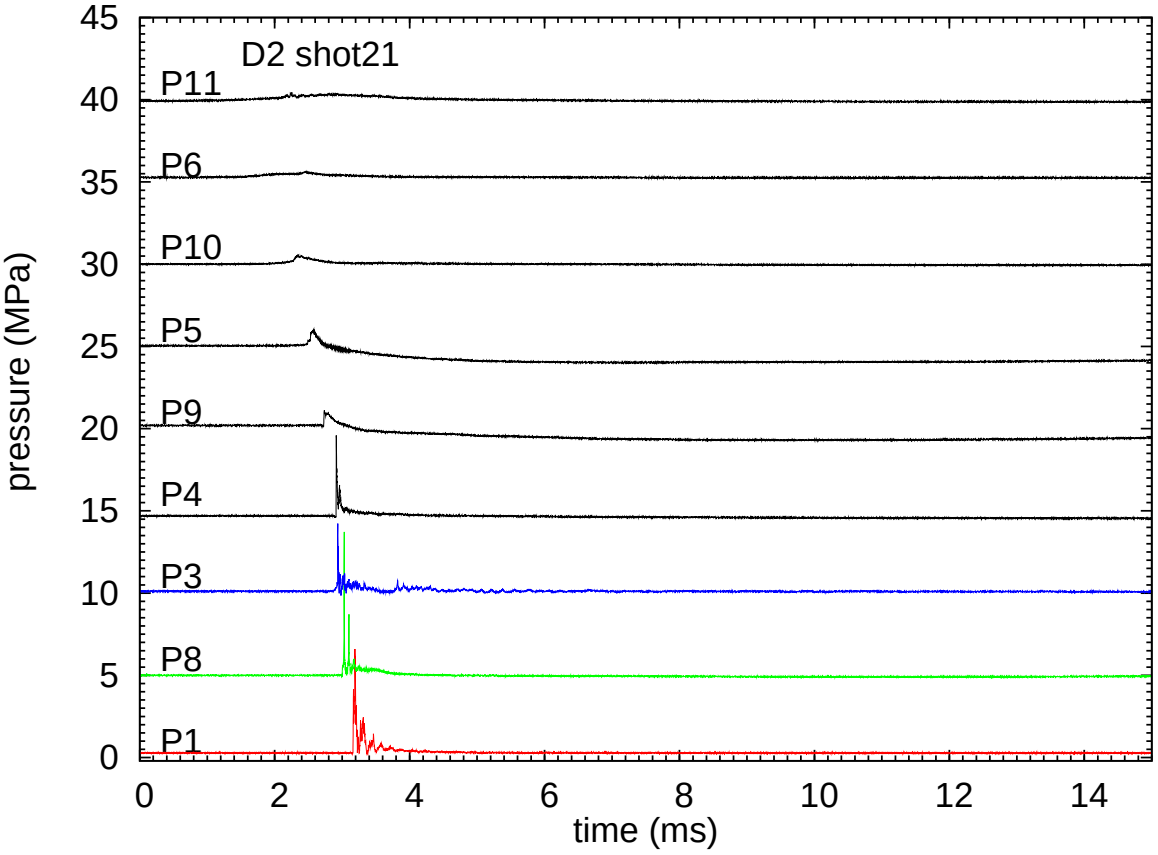

Figure 109: Pressure data from shot 21. Raw data without baseline correction. Trigger for spark discharge was 100 μs after $t = 0$.

H D4 Data Plots

Table 24: Sensor locations in D4

Sensor	Distance (in)	Port location
P11	-0.75	centerline, W flange
-	0.0	W flange outer surface
IGN	3.0	
P10	3.0	bottom
P6	15.0	top
P5	15.0	bottom
P9	27.0	top
P8	27.0	bottom
P4	39.0	top
P3	39.0	bottom
TC	51.0	top
Liquid fill	51.0	bottom
-	60.0	E flange outer surface
P1	60.75	centerline, E flange
S10	33.0	bottom
S11	33.0	middle
S12	33.0	top
S13	45.0	bottom
S14	45.0	middle
S15	45.0	top
S16	55.0	bottom
S17	55.0	middle
S18	55.0	top

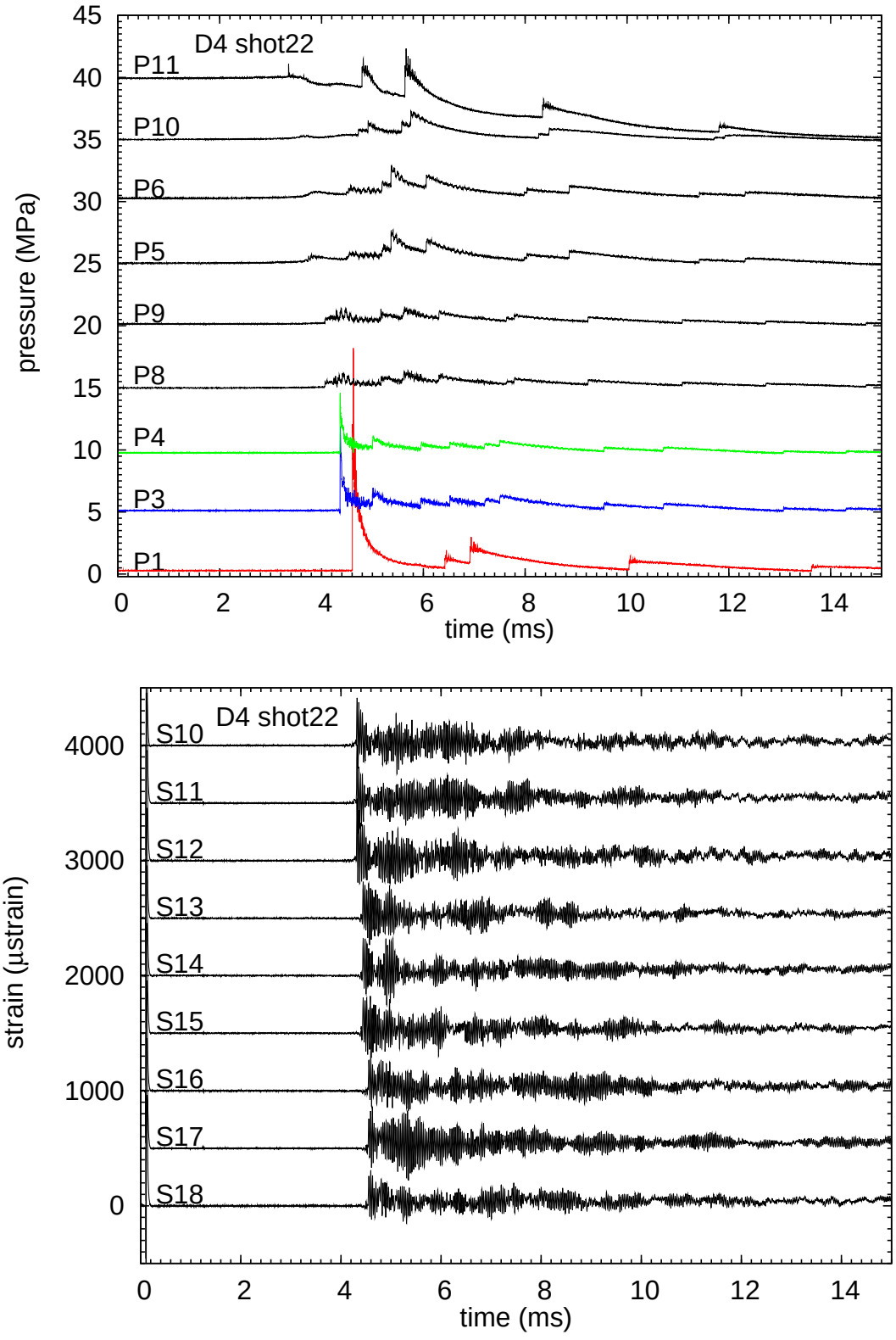

Figure 110: Pressure and strain data from shot 22. Raw data without baseline correction or removal of ignition transient artifact from strain signals. Trigger for spark discharge was 100 μs after $t = 0$.

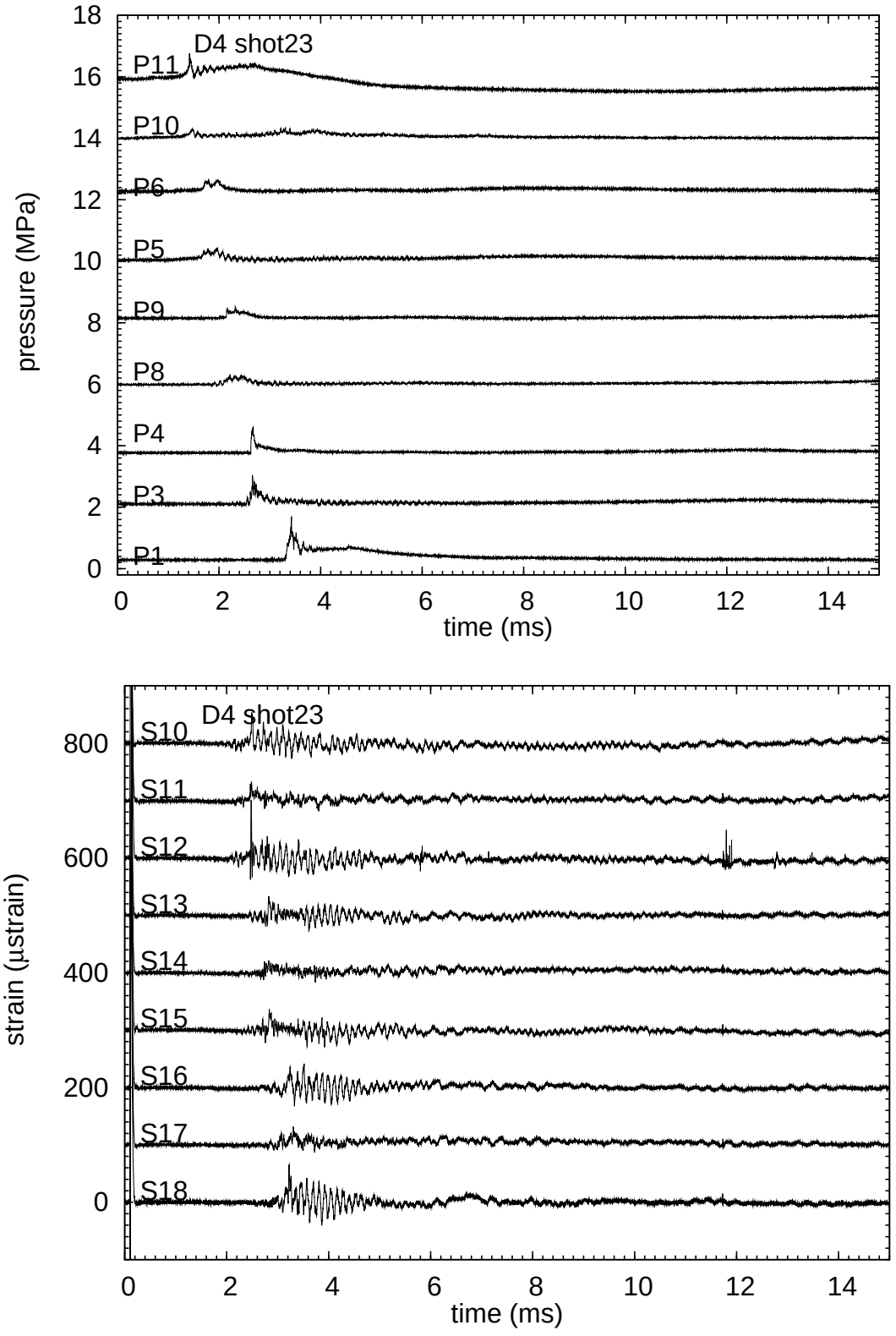

Figure 111: Pressure and strain data from shot 23. Raw data without baseline correction or removal of ignition transient artifact from strain signals. Trigger for spark discharge was 100 μs after $t = 0$.

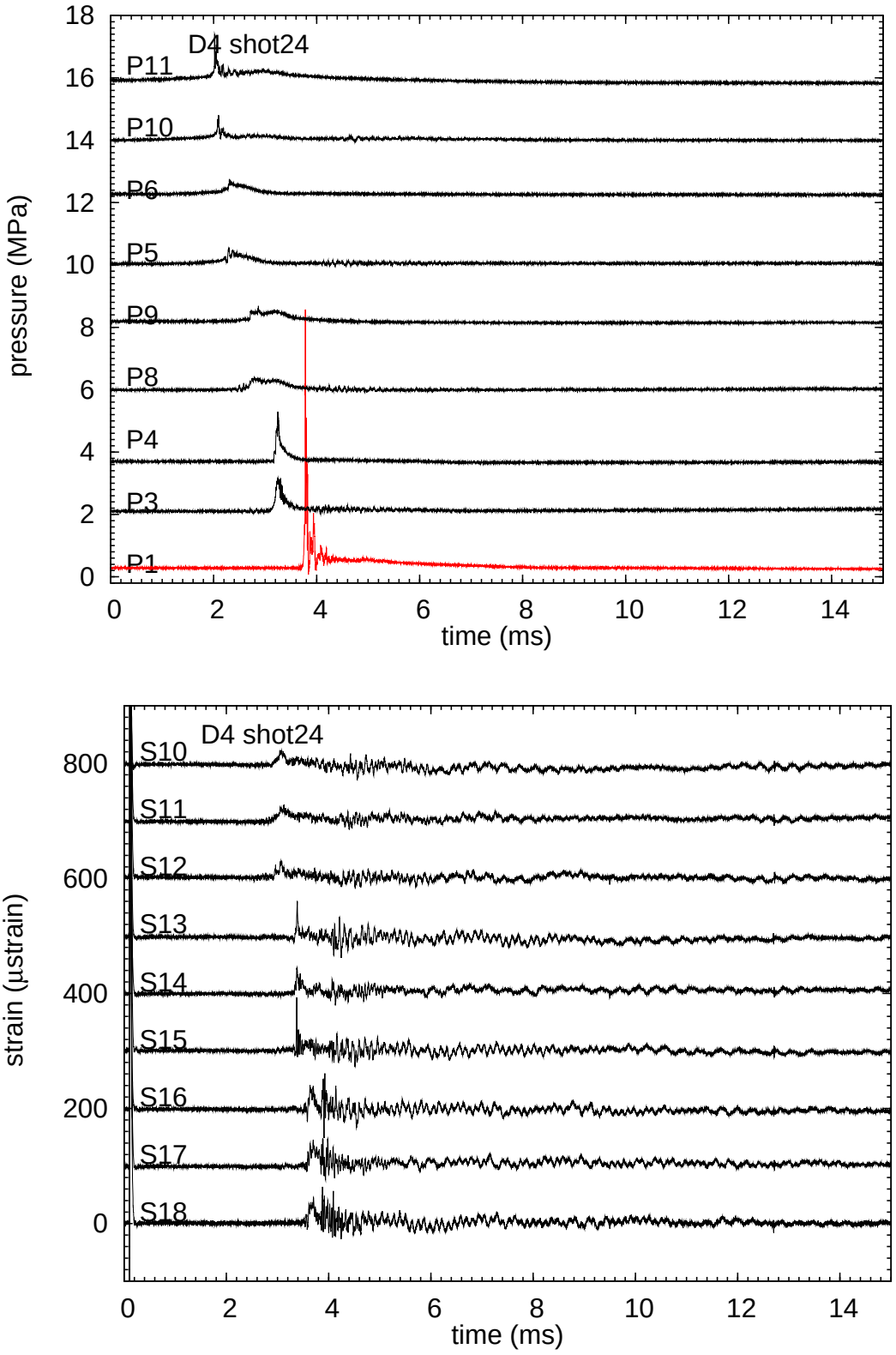

Figure 112: Pressure and strain data from shot 24. Raw data without baseline correction or removal of ignition transient artifact from strain signals. Trigger for spark discharge was 100 μs after $t = 0$.

I Quality Assurance Surveillance Report

OPERATIONAL AWARENESS DATABASE ENTRY 11025
CAL TECH SURVEILLANCE
November 11-13, 2009

SURVEILLANCE
CALTECH
RESEARCH AND DEVELOPMENT
QUALITY ASSURANCE PROGRAM

Purpose:

On November 10 through 13, 2009, the U.S. Department of Energy (DOE), Office of River Protection (ORP) conducted a surveillance of the California Institute of Technology's (Caltech) implementation of its Quality Assurance (QA) program for a Research and Development (R&D) activity.

Scope:

The Caltech R&D QA program surveillance scope included document reviews, personnel interviews and observation of activities at the testing facility. The surveillance lines of inquiry were based on ANSI/ASQ Z1.13-1999, *American National Standard for Quality Guidelines for Research.* By previous assessment, ORP determined that ANSI/ASQ Z1.13-1999 meets the expectations of NQA-1, Subpart 4.2, *Guidance on Graded Application of Quality Assurance (QA) for Nuclear-Related Research and Development,* as implemented by Caltech's Project Proposal and Quality Assurance Program documents.

The DOE assessors evaluated applicable procedures, examined records, and interviewed staff members who manage and implement the program, and performed field observations to determine the adequacy and effectiveness of the QA Program. Initial discussions were held with the Principle Investigator (PI) on November 11 and 12, 2009, with a review of the laboratory work area.

Criteria:

The assessment utilized lines of inquiry to conduct fieldwork. Lines of inquiry were developed from:

- regulatory and procedural requirements,

Lines of inquiry are detailed in Attachment 1.

Results:

The observance of the protocols and processes for gathering qualified data in the Guggenheim Laboratory was found to be in compliance with ANSI/ASQ Z1.13-1999, *American National Standard for Quality Guidelines for Research.*

OPERATIONAL AWARENESS DATABASE ENTRY 11025
CAL TECH SURVEILLANCE
November 11-13, 2009

Team Member:

Gregory L. Jones Lead Assessor, Director, Nuclear Safety Division (NSD)

Pertinent Documents:

1. ANSI/ASQ Z1.13-1999, *American National Standard for Quality Guidelines for Research*

2. NQA-1, Subpart 4.2, *Guidance on Graded Application of Quality Assurance (QA)for Nuclear-Related Research and Development*

3. Caltech Project Proposal and QA Program Documents

4. Data Sheets

   A. PCB Piezotronics Model 113B22 Dynamic Pressure Sensor Manual
   B. RM19 Visualization Combustion Test #5 Checklist
   C. Instrumentation Setup Spreadsheet (setup.xls)
   D. Visualization Configuration
   E. Phantom Camera Operation Procedure

Attachments:

Attachment A – Model S113B22 ICP Dynamic Pressure Sensor Installation and Operating Manual

Attachment B – Phantom Camera Operation Procedure

Attachment C – RM19 Visualization Combustion Test Checklist (Non-Flashbulb) Test #5

Attachment 1
Lines of Inquiry

Item	Requirement	Results
1	(601.3 – Organization) The relationship of those performing specific tasks in applied research should be defined to ensure task objectives are met individually and collectively. • Observe work activity to verify defined task responsibility is implemented as discussed in the QAP Sections Section 2.1 and 4.1.	Reviewed the Caltech Research and QA Plans and compared individuals listed with those actually performing work and activities specified. No issues were identified. Dr. Shepherd (Principle Investigator) is active in the management and performance of the research program. Discussed specific testing program activities with a Research Engineer (RE) who is performing activities under the guidance of the PI to satisfy the identified tasks. The RE was knowledgeable of the testing activity and QA expectations.
2	(602.3 – QA Program) Applied research should be accompanied by more documentation than basic research. • Evaluate the use of lab notebooks, associated electronic files, and test result log sheets with supporting electronic files. • Evaluate the processes by which data integrity will be insured. Consider laboratory practices, documentation of test procedures, instrument calibration procedures including documentation, and fixture specifications.	The research activity documentation is being maintained by multiple media. Hard copy laboratory notebooks are maintained by the PI and RE. The hard copy pages are scanned into a computer system and stored as electronic media. The offices housing the computer and laboratory notebooks are locked when not occupied by assigned research personnel. Instrument calibration procedures and documentation are provided by the instrument manufacture. Test documentation and procedures contain relevant specifications. (Attachment A) Computer files are prepared documenting sensor location, manufacturer, and verified prior to a specific test. • Recalibration rule of thumb is « one year ». Need for earlier calibration or replacement judged by - Spurious signals - Substantially different o Time of arrival o Amplitude and trace shape • Physical inspect of sensors used to

		determine failure. • Return to manufacturer for inspection and recalibration. • Sensors are replaced if determined to be beyond repair. Failure of an instrument is determined by the absence of data from a detector/gage.
3	(603.1 – Design Control) As the applied research matures, design control, commensurate with that activity (using a graded approach), should be used to support subsequent development. • Has Caltech established the fixture expectations for the test prior to conduct of the test IAW the Project Proposal?	Caltech has established the physical layout of the test piping to meet the expectations of the request for proposal. Physical layout was consistent with the test plan for the current level of testing. See attached layout diagram of test specimen (Attachment B).
4	(605.3 – Instructions, Procedures, and Drawings) Are the test procedures contained in the lab notebook and test log sheets?	The instructions, procedures, drawings, and test data sheets are contained in the lab notebooks which are CIT QA records. Several lab notebooks are used to file documents setting up and documenting the results of the test program.
5	(606. – Document Control) As a minimum, laboratory notebooks should be subject to document control procedures. • Verify that test set-up and test result information is documented in accordance with the QAP Section 4.3 and 4.4. • Verify that test results are archived in accordance with QAP, Section 4.4.7	The test protocol was observed for Visualization test 5 (Attachment C) and found to follow CIT QAP standards and requirements.
6	(609.3 – Control of Processes) Process control is minimal and is largely contingent upon the complexity of the research and the ability to duplicate the research if data were lost. Process control instructions are documented in the QAP, Sections 4.3 and 4.4. Verify:	The process of gathering data to support

	• Test matrix – electronic record of test conditions, test numbers, parameters and associated data files for each test. • Parameter acceptance range for pre-test conditions – there will be pre-determined parameter ranges for maximum vacuum and pressure leak rates, number of operational channels, and maximum vacuum and pressure leak rates, etc. • Test procedure. Test procedure will be noted in the lab notebook and test log sheets. • Checklist control of experiments will serve as a safety process and also help insure correctness of the experimental procedure. • Post-test documentation for all aspects of testing including fixtures, procedures, specimens, data assessment, and analysis.	the test program is set up to document the below information. All required preliminary information was listed in the lab notebooks. Testing was documented and followed procedure in attached checklist for Visualization Test 5 (Attachment C). System was evacuated until specified pressure was reached and leak rate was checked. Post-test analysis carried out by PI, see attached data plots (Attachment C).
7	(611.3 – Test Control), review the test plan to verify it is appropriate for the activity and is being implemented by the testers.	The test plan meets the request for proposal. Testing activities were performed and were test plan was implemented satisfactorily.
8	(612.3 – Control of Measuring and Test Equipment) Standard M&TE procedures should be followed. • Verify that all instruments are calibrated in accordance with the Caltech QAP, Section 4.2.	Standard M &TE requirements of the manufacturer are being followed by the lab. Additionally, the initial calibration is performed by the manufacturer. The calibration documentation is maintained in the lab notebooks. Example of Dynamic Pressure Sensor calibration information provided in Attachment A.
9	(616.3 – Corrective Actions) Verify that a corrective action plan has been implemented IAW the QAP, Section 4.4.6.	A corrective action plan is in place regarding unexpected results, misfiring of a test, etc. Misfire is handled by a special checklist procedure (Attachment

		C at end of procedure).
10	(617 – Quality Assurance Records) In many cases, the notebook or journal of the researcher is the QA record. Controls are needed for these documents, e.g., maintain copies of critical pages or access-controlled (locked door to lab) filing when not in use to preserve process repeatability and the QA record. Electronic media may be used to record data and should be subject to appropriate administrative controls for handling and storage of data. • Verify all records are maintained IAW QAP, Section 4.4.	The process to manage the quality and integrity of the laboratory notebooks is satisfactory as discussed in item 2, 4, and 5 above. The data is recorded on the hard drive of the data acquisition computer and recorded to CD-Rom for individual tests. Access to room is controlled by door lock. All records are maintained in accordance with CIT QAP.
11	(618 – Audits) Verify that an assessment process has been implemented by the testing organization IAW the QAP, Section 4.5.	Initial assessment was performed by Bill Smoot's surveillance on June 16th, 2008 This Surveillance/Audit was performed on 1/26/2009-1/27/2009 and again by this surveillance.

ATTACHMENT 14

PRESSURE DIVISION

Model S113B22

ICP® Dynamic Pressure Sensor

Installation and Operating Manual

For assistance with the operation of this product , contact the Division of PCB Piezotronics, Inc.

Division toll-free 888-684-0015
24-hour SensorLineSM 716-684-0001
Fax 716-686-9129
E-mail pressure@pcb.com

PCB PIEZOTRONICS INC.
PRESSURE DIVISION

Materials Authorization (RMA) Number. This RMA number should be clearly marked on the outside of all package(s) and on the packing list(s) accompanying the shipment. A detailed account of the nature of the problem(s) being experienced with the equipment should also be included inside the package(s) containing any returned materials.

A Purchase Order, included with the returned materials, will expedite the turn-around of serviced equipment. It is recommended to include authorization on the Purchase Order for PCB to proceed with any repairs, as long as they do not exceed 50% of the replacement cost of the returned item(s). PCB will provide a price quotation or replacement recommendation for any item whose repair costs would exceed 50% of replacement cost, or any item that is not economically feasible to repair. For routine calibration services, the Purchase Order should include authorization to proceed and return at current pricing, which can be obtained from a factory customer service representative.

Warranty – All equipment and repair services provided by PCB Piezotronics, Inc. are covered by a limited warranty against defective material and workmanship for a period of one year from date of original purchase. Contact PCB for a complete statement of our warranty. Expendable items, such as batteries and mounting hardware, are not covered by warranty. Mechanical damage to equipment due to improper use is not covered by warranty. Electronic circuitry failure caused by the introduction of unregulated or improper excitation power or electrostatic discharge is not covered by warranty.

Contact Information – International customers should direct all inquiries to their local distributor or sales office. A complete list of distributors and offices can be found at www.pcb.com. Customers within the United States may contact their local sales representative or a factory customer service representative. A complete list of sales representatives can be found at www.pcb.com. Toll-free telephone numbers for a factory customer service representative, in the division responsible for this product, can be found on the title page at the front of this manual. Our ship to address and general contact numbers are:

PCB Piezotronics, Inc.
3425 Walden Ave.
Depew, NY 14043 USA
Toll-free: (800) 828-8840
24-hour SensorLine℠: (716) 684-0001
Website: www.pcb.com
E-mail: info@pcb.com

DOCUMENT NUMBER: 21354
DOCUMENT REVISION: B
ECN: 17900

OPERATION MANUAL FOR
QUARTZ PRESSURE SENSORS
MODELS 102A, A03, A04, A06, A12, A15, A21, A22
MODELS 113A21, A22, A23, A24, A26, A27, A28
MODELS 113A31, A32, A33, A34, A36, A37, A38
MODELS 113B51, B52, B53
MODELS 113B31, B32, B33, B34, B36, B37, B38

The Model 102A12 utilizes the same inner probe design as the above two designs but in a 3/8-24 threaded adaptor with floating clamp nut to allow adjustment of diaphragm mounting depth where it is necessary to adapt to various wall thicknesses. These models are supplied only as low-pressure (250 psi and 100 psi) sensors and are also "off ground".

Models 102A21 and 102A22 are high-temperature ICP® versions to 400 °F (204 °C), with a 3/8-24 straight threads adaptor and 1/8-27 NPT adaptor, respectively.

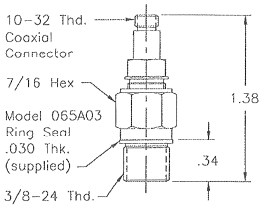

Series 102: Thread Mount Design, Ground-Isolated Sensor

3.0 INSTALLATION

This manual contains outline and installation information for your specific model.

Prepare mounting ports ' in accordance with instructions given in specific installation drawings, paying particular attention to sealing surfaces. These surfaces must be smooth and free from chatter marks, nicks and other irregularities which could preclude a pressure tight seal.

To fully realize the high-frequency response capabilities of this sensor series, flush mounting of the diaphragm must be used.

In some cases, where flash temperatures such as those generated by blasts and shock fronts are present, it may be necessary to thermally insulate the diaphragm to minimize signals generated by these effects.

Drawing Number: 21075
Revision: A
ECN Number: 21871

Common black vinyl electrical tape has been found to be an effective insulating material in many cases. One or more layers may be used across the end of diaphragm and adaptor.

A silicone rubber coating approximately .010" thick has also been proven effective in many applications. General Electric RTV type 106 is recommended. Apply the rubber coating to the surface of the diaphragm and allow it to cure in accordance with the manufacturer's instructions. (If you have ordered the ablative coated models, further protection will not be necessary.)

Although ICP® sensors have low-output impedance and in general are not affected by moisture, in extreme environments it is good practice to protect cable connections with shrink tubing.

It is not necessary to use low-noise cable with this sensor series. In fact, an optional Model 070A09 Solder Connector Adaptor allows the use of ordinary two-wire cable if desired.

4.0 OPERATION

It is only necessary to supply the sensor with a 2 to 20 mA constant current at +20 to +30 VDC through a current-regulating diode or equivalent circuit. (See guide G-0001B for powering and signal utilization information pertaining to all ICP® instrumentation).

Most of the signal conditioners manufactured by PCB have an adjustable current feature allowing a choice of input currents from 2 to 20 mA. In general, for lowest noise (best resolution), choose the lower current ranges. For driving long cables (to several thousand feet), use higher current, up to 20 mA maximum.

To operate system using a PCB signal conditioner:

1. Switch power on.

2. Wait several minutes for the IC amplifier to turn on and stabilize.

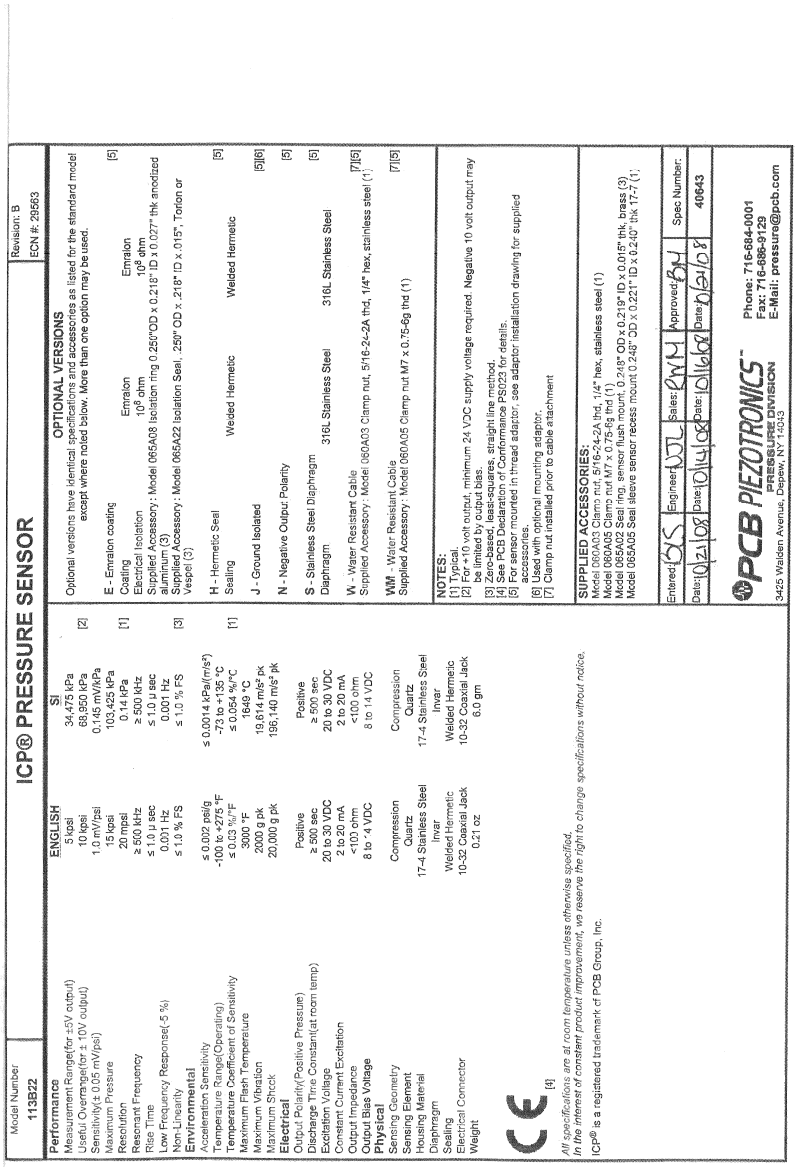

Model Number: 113B22

ICP® PRESSURE SENSOR

Revision: B
ECN #: 29563

Performance	ENGLISH	SI	
Measurement Range(for ±5V output)	5 kpsi	34,475 kPa	
Useful Overrange(for ± 10V output)	10 kpsi	68,950 kPa	[2]
Sensitivity(± 0.05 mV/psi)	1.0 mV/psi	0.145 mV/kPa	
Maximum Pressure	15 kpsi	103,425 kPa	
Resolution	20 mpsi	0.14 kPa	[1]
Resonant Frequency	≥ 500 kHz	≥ 500 kHz	
Rise Time	≤ 1.0 µ sec	≤ 1.0 µ sec	
Low Frequency Response(-5 %)	0.001 Hz	0.001 Hz	
Non-Linearity	≤ 1.0 % FS	≤ 1.0 % FS	[3]
Environmental			
Acceleration Sensitivity	≤ 0.002 psi/g	≤ 0.0014 kPa/(m/s²)	
Temperature Range(Operating)	-100 to +275 °F	-73 to +135 °C	
Temperature Coefficient of Sensitivity	≤ 0.03 %/°F	≤ 0.054 %/°C	[1]
Maximum Flash Temperature	3000 °F	1649 °C	
Maximum Vibration	2000 g pk	19,614 m/s² pk	
Maximum Shock	20,000 g pk	196,140 m/s² pk	
Electrical			
Output Polarity(Positive Pressure)	Positive	Positive	
Discharge Time Constant(at room temp)	≥ 500 sec	≥ 500 sec	
Excitation Voltage	20 to 30 VDC	20 to 30 VDC	
Constant Current Excitation	2 to 20 mA	2 to 20 mA	
Output Impedance	<100 ohm	<100 ohm	
Output Bias Voltage	8 to 14 VDC	8 to 14 VDC	
Physical			
Sensing Geometry	Compression	Compression	
Sensing Element	Quartz	Quartz	
Housing Material	17-4 Stainless Steel	17-4 Stainless Steel	
Diaphragm	Invar	Invar	
Sealing	Welded Hermetic	Welded Hermetic	
Electrical Connector	10-32 Coaxial Jack	10-32 Coaxial Jack	
Weight	0.21 oz	6.0 gm	

CE [4]

All specifications are at room temperature unless otherwise specified.
In the interest of constant product improvement, we reserve the right to change specifications without notice.
ICP® is a registered trademark of PCB Group, Inc.

OPTIONAL VERSIONS

Optional versions have identical specifications and performance as listed for the standard model except where noted below. More than one option may be used.

E - Emralon coating

	Emralon	
Coating	Emralon	[5]
Electrical Isolation	10^8 ohm	

Supplied Accessory: Model 065A08 isolation ring 0.250"OD x 0.218" ID x 0.027" thk anodized aluminum (3)

H - Hermetic Seal

	Welded Hermetic	
Sealing	Welded Hermetic	[5]

J - Ground Isolated [5][6]

N - Negative Output Polarity [5]

S - Stainless Steel Diaphragm

	316L Stainless Steel	
Diaphragm	316L Stainless Steel	[5]

W - Water Resistant Cable [7][5]
Supplied Accessory: Model 060A03 Clamp nut, 5/16-24-2A thd, 1/4" hex, stainless steel (1)

WM - Water Resistant Cable [7][5]
Supplied Accessory: Model 060A05 Clamp nut M7 x 0.75-6g thd (1)

NOTES:
[1] Typical.
[2] For +10 volt output, minimum 24 VDC supply voltage required. Negative 10 volt output may be ordered (-10 output bias).
[3] Zero-based, least-squares, straight line method.
[4] See PCB Declaration of Conformance PS023 for details.
[5] For sensor mounted in thread adaptor: see adaptor installation drawing for supplied accessories.
[6] Used with optional mounting adaptor.
[7] Clamp nut installed prior to cable attachment

SUPPLIED ACCESSORIES:
Model 060A03 Clamp nut, 5/16-24-2A thd, 1/4" hex, stainless steel (1)
Model 060A05 Clamp nut M7 x 0.75-6g thd (1)
Model 065A02 Seal ring, sensor flush mount, 0.248" OD x 0.219" ID x 0.015" thk, brass (3)
Model 065A05 Seal sleeve sensor recess mount, 0.246" OD x 0.221" ID x 0.240" thk 17-7 (1)

Entered:	Engineer:	Sales:	Approved:	Spec Number:
Date: 10/21/08	Date: 10/14/08	Date: 10/16/08	Date: 10/29/08	40643

PCB PIEZOTRONICS
PRESSURE DIVISION
3425 Walden Avenue, Depew, NY 14043
Phone: 716-684-0001
Fax: 716-686-9129
E-Mail: pressure@pcb.com

CALIBRATION CERTIFICATE

Model:	S113B22		
Serial #:	19816	**Date:**	2/24/2009
Description:	Pressure Sensor	**By:**	Brian MacDonald, Cal. Tech.
Type:	ICP	**Station:**	Dead Weight #2 (Test Procedure AT601-2)
Sensitivity*:	1.010 mV/PSI 146.4 mV/MPa	**Temp:** **Humidity:**	70 deg F [21deg C] 30 %
Linearity*:	0.5% FS	**Cert #:**	320909
Uncertainty:**	+/- 1 %		

Bias: 8.9 VDC

* Zero based, least-squares straight line.

** Measurement uncertainty represented using a coverage factor of k=2 which provides a level of confidence of approximately 95 %.

Condition of Unit:
As Found: Not applicable
As Left: In tolerance, new unit

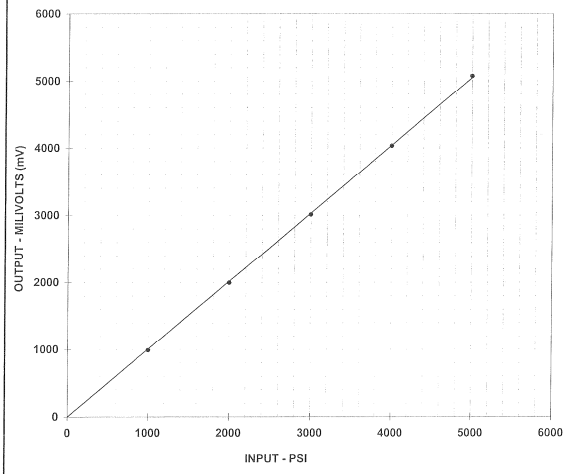

TEST DATA

INPUT (PSI)	OUTPUT (mV)
1000	991
2000	1996
3000	3011
4000	4033
5000	5076

Notes:
1 STATION #18
2 Calibration is traceable to NIST and is accredited to ISO 17025 and ANSI/NCSL Z540-1-1994.
3 NIST traceability through PCB control # CA348.
4 This certificate may not be reproduced, except in full, without written approval from PCB Piezotronics, Inc.

ACCREDITED
Cert. No. 1862.01

PCB PIEZOTRONICS

Page 1 of 1

Tel: 716-684-0001 Fax: 716-684-0987 Email: sales@pcb.com
3425 Walden Avenue, Depew NY 14043

ISO 9001 CERTIFIED

ATTACHMENT 5

Phantom Camera Operation Procedure

This procedure is to enable a user to operate the phantom using a dedicated controlling computer. It is simpler and more reliable.

It is assumed that the camera has been already been set-up correctly with
respect to the lighting and composition (object field).

Also, the camera should not be operated in an environment of dust, particulatea etc.

Sequential Setup Steps

1) Make sure the dedicated control computer has no ethernet cable plugged in and has
its address changed to 100.100.100.1, subnet 255.255.0.0.

2) Plug in all cables on the Phantom and make sure the lens cap remains on.

3) Turn on the camera, watch the lights come on and become steady- (this can be trouble-shooted
later if there are problems). Wait 2 min.

4) Plug in the camera into the dedicated control computer.

5) Click on the camera software icon to bring up the application.

6) Go to the acquisition menu and select setup and capture.

7) Click on the current session reference button to take a reference image.

8) Remove the lens cap.

9) Verify the lighting at this stage (not flash bulbs-they need separate triggering considerations).

10) Check the exposure and framing rate settings and record the time duration.

Arming and Capture Sequence

A) External trigger

1) Verify that the experiment duration and the total duration of capture are correct.

2) Make sure the trigger line is connected.

3) Arm by pressing Capture button- save or erase movie in memory- then press capture again to arm.

B) Software (Radio Button).

1) Verify that the experiment duration and the total duration of capture are correct.

2) Use the capture radio button to arm.

3) Press the trigger radio button to start recording.

After recording is complete, the cinefile created should be saved upto the point needed by
pressing escape to limit the saving. The saved portion can be played back.
Alternatively the relavent portion can be marked and saved.
Both these partial saves are necessary as the files are typically very big and contain the
experimental result in a small portion at the beginning.

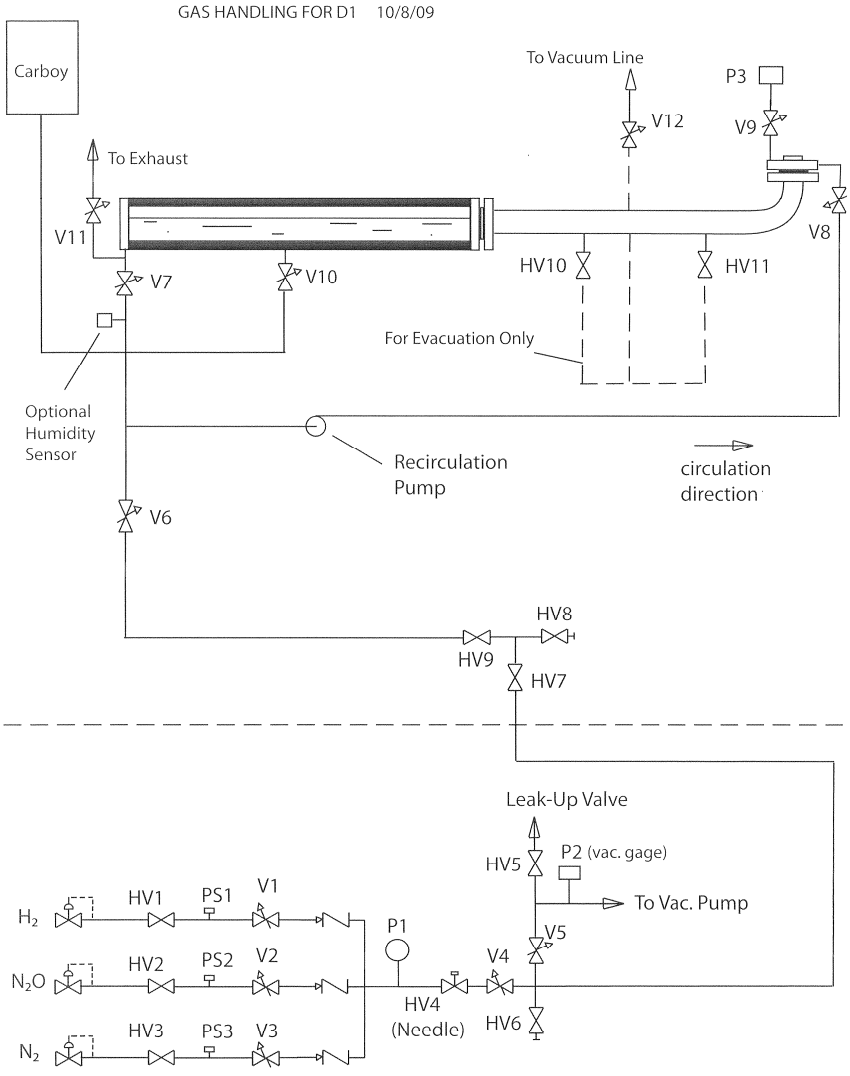
GAS HANDLING FOR D1 10/8/09
Carboy
To Vacuum Line
P3
V12
V9
To Exhaust
V11
V8
HV10
HV11
V7
V10
For Evacuation Only
Optional
Humidity
Sensor
Recirculation
Pump
circulation
direction
V6
HV8
HV9
HV7
Leak-Up Valve
HV5
P2 (vac. gage)
To Vac. Pump
V5
H2
HV1
PS1
V1
P1
V4
N2O
HV2
PS2
V2
HV4
(Needle)
HV6
N2
HV3
PS3
V3

Attachment C

JES.HPAV-1-PAC.HPAV 11/10/2009

RM19 Visualization Combustion Test Checklist (NON-FLASHBULB)

Test Number: 5.

Test Specimen or Series: _____ **D1**_____

Test Date: 11/11/09

Operator(s): RA.

Instrumentation layout file: D1_shot5.xls

Instrumentation setup file: template_D1.seq

Before starting a series of tests *without* the mixing chamber:

1. ✓ Turn on air supply to valves
2. ✓ Turn on control panel in Rm 19, check circuit breaker in panel LXX
3. Verify remote valve operation and hand valve positions
   - ✓ Close all valves on panel (All green lights on?)
   - ✓ HV7, HV8 open.
   - ✓ HV9 closed and capped off.
   - ✓ HV6 closed and capped off.
4. ✓ HV10 and HV 11 closed and locked.
5. ✓ Turn on gas bottle. Check bottle pressures, replace if below 200 psi.
   - ✓ Set regulators at 15-20 psi
   - ✓ Open hand valves at regulator and gas lines (HV1, HV2, HV3).
   - ✓ Verify pressure in lines. Pressure switch indicator lights green?
6. ✓ Close vacuum valve HV5 and V5. Turn on vacuum pump in closet, note hours since last oil change, and change if needed.
7. ✓ Turn on TC vacuum gage P2. Pressure after pumping for 5 minutes 30 millitorr.
8. ✓ Turn on video camera, vcr, and monitor, adjust video camera tripod and focus.
9. ✓ Take dark field reference for camera and take lens cap off after.
10. ✓ Switch on strobe or other light and ion gage power.
11. ✓ Verify operation of gas leak detectors.
12. ✓ Verify power switch is on at spark box
13. ✓ Verify circulation pump operation

Prepared By: JES & Raza Akbar 1

JES.HPAV-1-PAC.HPAV 11/10/2009

14. __L__ Verify operation of interlocks. Close vent, door, warning light on, reset gas detectors if needed, check for green light on fireset control panel
15. ___ Check fireset operation with dummy sparkplug. Remove key, safe fireset. Re-attach cable to sparkplug on SPECIMEN.

For each explosion test:

Calculate composition target and estimate CJ parameters

Gas	Target Fraction	Target Partial P (Torr)	Target Fill P (Torr)	Actual Fill P (Torr)
Starting pressure				
H2	0.3	228	227.5	227.4
N2O	0.7	532	759.5	759.4
Final preshot pressure (Torr)		756.9 Torr		
Final preshot temperature (°C)		26.8 °C		
CJ wave speed (m/s)				
CJ pressure (MPa)				

1. ___ Computer, DAQ and instrumentation amplifiers turned on and warmed up.
   ___ Verify all signal cables and interconnect cables are in place.
   ___ Tighten PCB Microdot connectors at gage!
   ___ PCB signal conditioner gains set per setup sheet.
   N/A Displacement gage power supply turned on. Verify gage operation.
   ___ Check camera and strobe/light operation (NOT FLASH BULB)
   ___ Turn on MKS pressure gage P3 and omega thermocouple readout T1
2. Evacuate lines and test specimen.
   ___ Open vent in 19A.
   ___ Open V5, V6. V7, V8, V9 (V10) (V12) HV10 and HV11
3. ___ Note ultimate pressure after pump down of ___ minutes
   -0.5 Pressure P3
   304 Pressure P2
4. **Leak check.**
   ___ Close V6, (V12) HV10 (and lock) , HV11 (and lock) and V5 and wait 5 minutes. Pressure P3 -0.5
5. **Flush lines from bottles.**
   ___ Verify V6 , (V12) are closed and HV10, HV 11 are closed and locked
   ___ Activate key in gas panel

Prepared By: JES & Raza Akbar 2

___ Set HV4 2-1/2 turns from closed and open V5.
___ Activate V4 and each of V1, V2, V3 for 2 s

FROM HERE ON V12 is to remain closed and not be used until after the shot.

6. **Evacuate fill lines.**
___ Close HV1, HV2, HV3.
___ Open V4 until P2 is stable.
7. ___ Open V6, V7, V8, V9 and evacuate specimen (if needed)
8. ___ Close V5. Verify HV10 and HV11 are closed.
9. ___ Close door to 19A (check for green light)
10. ___ Warning light on
11. ___ Ear protection on.
12. ___ Verify V12 (large vacuum valve) is closed.
13. **Fuel fill**
___ Open HV1.
14. ___ Open V1, and V4 to fill fuel to target pressure at P3.
15. Evacuate lines.
___ Close V6 and HV1.
___ Open V4, HV4, V5. Evacuate until P2 is stable.
16. **Oxidizer fill.**
___ Close V5 and open HV2.
17. ___ Open V2 and V4 to charge oxidizer line unit P1 is stable.
18. ___ Open V6. Fill by opening V4 and V2, adjust flow rate with HV4.
19. ___ Close V6, HV2
20. ___ Run circulation pump for 5 minutes. Turn pump off. **(THE TIME IS BEING VERIFIED).**
21. ___ Record final pressure and temperature
22. ___ Close V7, V8, V9.
23. ___ Open V6 and V5, pump until P2 is stable.
24. ___ Close V6 and V5
25. **Arming and Firing**
26. ___ Close vent in 19A
27. ___ Arm Camera
28. ___ Verify interlock green (Check door switch if not)
29. ___ start video recording
30. ___ Arm the DAS
31. ___ Turn on power to fireset panel with key
32. ___ ARM FIRESET BY HOLDING ARM SWITCH ON FOR 3 s.
33. ___ KEEPING ARM SWITCH ON, PRESS FIRE BUTTON.
34. ___ Remove key from fireset, put back into gas panel.

35. ___ End video recording . _____ Video End time
36. ____ Save data from DAS- make archive copies on CD-ROM.
Shot Time: 3:44 pm

37. **Cool down, Pump Out and Cold Trap Ops.**
___ Monitor temperature gage T1, when this drops below 40C, open V9
___ Record final pressure on P-3 634.
___ Open vent in Rm 19A
___ Verify V5 is closed and then perform an N2 purge using V11, before proceeding with the next step.
38. ___ Charge cold-trap with liquid-nitrogen (repeat a few times until full).
___ Open V5, V6, V7, V8, V10 and V12
Evacuate until P2 is stable. Run circulation pump if needed.
39. ___ Close V6, V7, V8, V9, V5 and V12 Turn off circulation pump
40. ___ Turn off vacuum pump, open HV5
41. ___ Remove top of trap and place in bucket of water and leave it in there until all the L-N2 has evaporated.

OK
OK
RA.

42. **Shut down**
43. ___ Shut off gas bottles.
44. ___ Turn off displacement gage power, DAS, signal conditioners.
45. ____ Turn off P1, T1, P2
46. ____ Turn off Control Panel.

Misfire Checklist

Use the battery operated trigger signal generator to attempt ignition (by connecting it to the BNC connection the splits to F1 and the DAS). If that does not work, then complete the following dilution checklist.

DILUTION (9 steps)
1. _____ Check V9 is closed.
2. _____ Verify V5, V12 and H5 are closed.
3. _____ Make sure N2 pressure is higher than 16 psig.
4. _____ Verify V6 is open, but V8 and V10 are closed.
5. _____Using V3 and V4 and P1 (Dial Gage) charge the lines.
6. _____While V3 and V6 are open, open V8 and fill facility until no further flow takes place and P1 indicates a pressure of at least 12 psig (adjust HV4 if necessary).

7._____Close V3, V4 and V6.
8._____Open V7 and V10 and run the circulation pump for 5 min.
9._____Open V5 and cycle (on/off) V6 until the facility is pumped out to below 100 millitorr.

V2.6 10 Nov. 2009

U.S. Department of Energy
Office of River Protection
P.O. Box 450, MSIN H6-60
Richland, Washington 99352

10-NSD-038

MAY 0 6 2010

Mr. R. W. Bradford, Project Manager
Bechtel National, Inc.
2435 Stevens Center Place
Richland, Washington 99354

Dear Mr. Bradford:

CONTRACT NO. DE-AC27-01RV14136 – BECHTEL NATIONAL, INC. (BNI) USAGE OF CALIFORNIA INSTITUTE OF TECHNOLOGY (CIT) DATA GENERATED IN SUPPORT OF HYDROGEN IN PIPING AND ANCILLARY VESSELS (HPAV)

References:
1. Office of River Protection Operational Awareness Data Base, "Surveillance of CalTech QA Program," Report 3766, July 3, 2008.
2. ORP letter G. L. Jones to file, "In Process Surveillance of California Institute of Technology (CIT) Testing Program in support of Hydrogen in Piping and Ancillary Vessels," 09-NSD-023, March 25, 2009.
3. Office of River Protection Operational Awareness Data Base, "Surveillance of California Institute of Technology (CIT) Hydrogen in Piping and Ancillary Vessels," Report 10417, dated May 6, 2010.

This letter authorizes BNI to utilize published data by CIT provided under the U.S. Department of Energy, Office of River Protection (ORP) contracts for use in supporting development of methods and criteria by which HPAV is evaluated. The data is controlled by CIT and is located on the CIT/Explosion Dynamics Laboratory (EDL) website.

ORP and BNI contracted testing in support of HPAV criteria and methods for evaluating hydrogen hazards in 2008 and 2009 to CIT and Southwest Research Institute. This letter is specific to the CIT contracts data collected in 2008 and 2009 and summarized by the following scopes of work:

2008 contract DE-AB27-03RV14546:

1. Validation of structural response modeling of piping systems. EDL at CIT will provide test data that can be used to validate models for forces and structural response predictions by Finite Element Models and BNI structural response code ME101.
2. EDL will provide fundamental test data on peak forces and strains for high-speed deflagrations and transition from deflagration-to-detonation.

3. EDL will provide fundamental data on the propagation of shock waves in tubes partially filled with liquid and liquid-solid suspensions.

2009 Contract DE-AC27-09-RV15086:

1. Conduct a quantification of minimum detonable geometries of gas pockets using 2 inch pipes.

2. Conduct visualization tests in a rectangular channel to determine the actual dispersion of the liquids simulating the Waste Treatment and Immobilization Plant waste with high speed video imaging.

3. Provide significant new data on flame and detonation propagation in pockets bounded by horizontal liquid layers.

4. Work with BNI and subcontractors to provide information and editorial comments for a review of the propagation above liquid levels.

Both of these contracts have the following statement regarding the data quality under Environmental, Health, Safety, and Quality Requirements necessary:

> *"The Contractor will comply with DOE Order 414.1C, "Quality Assurance," requirements as implemented through the NQA-1-2000, Subpart 4.2, "Guidance on Graded Application of Quality Assurance for Nuclear-related Research and Development," or demonstrated compliance with this Subpart 4.2 based on implementation of the ANSI/ASQ Z1.13 consensus standard."*

The testing at CIT was managed as "Applied Research" defined in NQA-1, Subpart 4.2, Section 103.2. Both contracts have Quality Assurance Plans (QAP). The QAP was initially approved in March 2008 with supporting surveillances by ORP Quality Assurance (QA) and follow-up surveillances performed by Nuclear Safety Division. An initial surveillance by ORP QA (Reference 1) concluded that:

> *"By separate assessment, ORP has determined that ANSI/ASQ Z1.13-1999 meets the expectations of NQA-1, Subpart 4.2...as implemented by CalTECHs Project Proposal and Quality Assurance Program documents."*

Separate follow-up surveillance (Reference 2 and 3) determined that CIT continued to adequately implement the requirements of the contract.

Therefore, the data generated by CIT and published on the CIT website can be used by BNI in support of the methods and criteria for evaluating HPAV hazards.

This letter is not considered to constitute a change to the Contract. In the event the Contractor disagrees with this interpretation, it must immediately notify the Contracting Officer orally, and otherwise comply with the requirements of the Contract clause entitled 52.243-7, "Notification of Changes."

If you have any questions, please contact me, or your staff may contact Victor L. Callahan, Director, Nuclear Safety Division, (509) 373-9880.

Sincerely,

Guy A. Girard, Acting Assistant Manager
Waste Treatment and Immobilization Plant

NSD:GLJ

cc: Gregory R. Ashley, BNI
David J. Jantosik, BNI
Mike G. Wentink, BNI
BNI Correspondence